UNIVERSIDADE DE LISBOA

FACULDADE DE CIÊNCIAS
DEPARTAMENTO DE QUÍMICA E BIOQUÍMICA

Genetic Screens in *C. elegans* for New Modulators of Protein Homeostasis with Relevance for Conformational Diseases

María Catarina Telo Baptista Lima da Silva

Doutoramento em Bioquímica
(Especialidade: Genética Molecular)

Tese orientada por
Professora Doutora Margarida D. Amaral
e Professor Doutor Richard I. Morimoto

2011

De acordo com o disposto no ponto 1 do artigo nº41 do Regulamento de Estudos Pós-Graduados da Universidade de Lisboa, deliberação nº 93/2006, publicada em Diário da República – II Série nº 153 – 5 de Julho de 2003, a Autora desta dissertação declara que participou na concepção e execução do trabalho experimental, interpretação dos resultados obtidos e redacção dos artigos incluídos nesta dissertação:

- **M. Catarina Silva**, Susan Fox, Monica Beam, Happy Thakkar, Margarida D. Amaral, and Richard I. Morimoto (2011) A Genetic Screening Strategy Identifies Novel Global Regulators of the Proteostasis Network. *PLoS Genetics, In Press*

- Barbara Calamini, **M. Catarina Silva**, Franck Madoux, Darren M. Hutt, Shilpi Khanna, Monica A. Chalfant, Sanjay A. Saldanha, Peter Hodder, Bradley D. Tait, Dan Garza, William E. Balch, and Richard I. Morimoto (2011) Small Molecule Proteostasis Regulators for Protein Conformational Diseases. *Nature Chemical Biology, In Press*

- **M. Catarina Silva**, Margarida D. Amaral, and Richard I. Morimoto (2011) Modulation of Synaptic Activity Restores Proteostasis in Muscle Cells Through HSF-1 Activation. (Submitted and Reviewed)

- Monica Beam, **M. Catarina Silva**, Margarida D. Amaral, and Richard I. Morimoto (2011) Dynamic Imaging of Polyglutamine Aggregation States by Fluorescence Correlation Spectroscopy (Submitted)

Referenciado mas não incluído:

- Susana M. Garcia, M. Olivia Casanueva, **M. Catarina Silva**, Margarida D. Amaral, and Richard I. Morimoto (2007) Neuronal signaling modulates protein homeostasis in *Caenorhabditis elegans* postsynaptic muscle cells. *Genes and Development* 21:3006-3016.

PREFACE

Protein folding is an essential molecular process for cellular function, and protein misfolding is associated with a large and increasing number of human diseases. A hallmark of many protein conformational disorders is the appearance of insoluble protein aggregates or inclusions, also referred to as amyloid, as occurs in Alzheimer's disease, Parkinson's disease, Huntington's diseases, amyotrophic lateral sclerosis and ataxias. Although the initiating aggregation-prone protein for each disease differs in sequence, function and expression pattern, the appearance of aggregates represents an early event associated with an imbalance in protein homeostasis, or proteostasis, and cellular toxicity. Despite great advances in the genetic and patho-physiological characterization of these diseases, the cause of toxicity is still not entirely understood. In particular, whether protein aggregates are directly pathogenic, incidental, or protective has become a topic of great interest. While many studies have indicated a correlation between aggregates and toxicity, others have suggested that large inclusions correlate poorly with onset and severity of neurodegeneration and could have a protective function.

Upon protein misfolding, the strategy employed by the cell to restore balance invokes many processes to alter expression, concentration, conformation, activity, and localization of proteins, readjusting "the innate biology of the cell" through the activation of stress responses. Genetic screens performed in model organisms have identified a large number of modifier genes of protein aggregation, including molecular chaperones, proteasome subunits, components of the autophagy machinery, and the stress-induced regulators DAF-16 and HSF-1. Nearly all studies to date have focused on genetic modifiers that enhance aggregation, leading to the discovery of processes that maintain protein homeostasis. Rather than focusing on the cause of toxicity for a specific disease, or on the cellular components responsible for protein folding and clearance, the studies presented in this thesis took a distinct and novel approach. The tractable genetic model organism *Caenorhabditis elegans*, expressing aggregation-prone YFP-tagged polyglutamines (polyQ), was employed to perform a genome-wide RNA interference (RNAi) screen for suppression of protein aggregation. The purpose of this screen was to identify genes that, when knocked down by RNAi, enhanced the cellular capacity for protein folding, leading to suppression of aggregation and toxicity.

In Chapter I, an overview of the literature relevant for these studies is described, including a description of the quality control machinery and stress response pathways employed by the cell to combat protein misfolding and toxicity. An introduction to diseases of protein misfolding and aggregation, model organisms used in the study of disease, and genetic screens for modifiers of protein homeostasis, are also included. Finally, a brief commentary on the current advances in the field of genetics and chemical biology for the development of therapeutics is presented.

Chapter II describes the genome-wide RNAi screen performed in *C. elegans* for suppression of polyglutamine aggregation, to identify new modulators of proteostasis. The results revealed that aggregation suppression could be genetically uncoupled from the effect on toxicity. A set of secondary

screens was then strategically carried out to identify the genes that represented the most robust modifiers of homeostasis maintenance. That is, genes that when downregulated activate protective cellular processes that enhance the capacity for folding and suppress misfolding, aggregation and toxicity, of both heterologous proteins, as well as endogenous metastable proteins. The gene-modifiers identified, not previously linked to quality control, revealed new genetic mechanisms to restore cellular proteostasis.

Chapter III introduces one of the genes identified in the screen, encoding GEI-11. This work explored the relevance of neuronal signaling on post-synaptic protein homeostasis, in particular how cholinergic signaling can be modulated to produce opposite effects on post-synaptic muscle protein folding. This study demonstrated that within a defined range of signaling modulation, increase in neuronal cholinergic stimulation of muscle cells can activate the transcription factor HSF-1 and expression of chaperones, through a calcium-dependent mechanism, restoring folding and muscle function. The neuronal cell non-autonomous regulation of proteostasis is relevant for many diseases of neuro-muscular dysfunction.

Chapter IV integrates the results described in the previous chapters, and also results presented in the appendices. It is also discussed how the approach taken and the results obtained contribute to the understanding of the cellular processes that maintain proteostasis and that can be modulated/targeted in disease scenarios. Finally, it is discussed how the combination of genetic and chemical (small molecules) modifiers of proteostasis and stress responses is relevant for the development of therapeutics.

The appendices included in this thesis describe (I) the development of fluorescence correlation spectroscopy tools to analyze the biophysical properties of soluble oligomeric and insoluble aggregated protein species formed *in vivo*; (II) the new proteostasis modulator LET-607, a new modifier of ER and cytosolic stress responses; and (III) a small molecule screen for proteostasis regulators, validated in cell and animal models of diseases of protein conformation.

ACKNOWLEDGEMENTS/AGRADECIMENTOS

I would like to acknowledge and thank all that contributed in some way to my doctoral work and dissertation. I would like to begin by thanking Professor Margarida Amaral and Professor Rick Morimoto, my PhD advisers, for providing me with the opportunity and environment to learn and become a scientist. To Professor Margarida, for introducing me to Rick Morimoto, for the support, advice and mentorship throughout graduate school, for sharing her enthusiasm for science, and for the guidance over future decisions. To Professor Rick Morimoto, for welcoming me in his lab and offering me a rich scientific environment, for always challenging me to work hard and to do my best, for trusting my capabilities. Thank you for the lab environment you have created, and for the critical and animated lab meetings that have kept me on track and excited about science.

Ao Ministério da Ciência, Tecnologia e Ensino Superior e Fundação para a Ciência e Tecnologia (FCT) em Portugal, por ter possibilitado o meu doutoramento e investigação na Northwestern University (EUA) ao me atribuir a bolsa de doutoramento de 2007 a 2010 (SFRH/BD/28461/2006). À Faculdade de Ciências da Universidade de Lisboa (FCUL), por me aceitar como estudante de doutoramento e permitir a realização do trabalho de investigação nos EUA.

To my first bench mentor, Professor Carlos Farinha at FCUL, thank you for welcoming me in the lab and training me as an undergraduate student. To Susana Garcia, the Portuguese that welcomed me in the Morimoto lab from day one. Thank you for your mentorship, friendship, energetic good mood, and for setting up the standards.

To all my colleagues and friends in the Morimoto lab, past and present. Thank you Sue Fox, for being all that you are and for all that you do for us in the lab (and out). For welcoming me in and for being like a big sister away from home. To Daniel Czyz, the best lab, desk and bench mate, thank you for your joy, commitment and friendship. To Mário Neto, Andreia Castro and again Susana Garcia, my Portuguese "team" in "Morimoto-land", for your support and friendship. Mário, thank you for the fun you provide and for all the espresso moments. To Finola Moore, Tali Gidalevitz, Cindy Voisine and Anan Yo, for your friendship, kindness, advice and support. To Carmen Krammer, Barbara Calamini, Chris Brzezinski, Elizabeth Miller, Tanuja Devaraj, James West and Heather Brignull. A special word to Happy Thakkar, my student and colleague, for being truthful to your name. To Georgette Pliml, thank you for the friendliness and assistance finding solutions for

the bureaucratic problems. A special thank you to Diane Korling, for welcoming me in my first home abroad, for her strong support and care.

A very (very) special thank you to my best friends Tom Krupinski and Taneli Helenius: for your friendship, care and patience. For teaching me so much, for making grad school a better experience, for the fun we have together and for your "life coaching".

O agradecimento mais especial para a minha Mãe, Pai e Irmã. À minha Mãe e Pai, por apoiarem a minha partida para os EUA e por sempre apoiarem as minhas decisões e me incentivarem a não desistir. Por todo o apoio, amor, carinho, sacrificios e presença constantes na minha vida, por tudo mais que estas palavras não possam descrever. À minha Irmã Luisa, a minha cara-metade que toma conta de mim sempre, obrigada pelo teu amor, amizade, apoio e força.

Contents

CHAPTER IV

APPENDICES

APPENDIX I

APPENDIX II

APPENDIX III

REFERENCES

‘Genetic Screens in *C. elegans* for New Modulators of Protein Homeostasis, with Relevance for Conformational Diseases’

SUMMARY

Protein folding is an essential cellular process, required for proper molecular and cellular function. The cell has evolved as a sophisticated machinery that ensures the quality and stability of the proteome. The network of cellular processes that coordinates protein synthesis, folding, trafficking and clearance, and determines the fate of proteins that do not acquire a native conformation, is responsible for maintaining protein homeostasis (proteostasis) and is referred to as “the proteostasis network” (PN). The key components of the quality control system are molecular chaperones that ensure proper folding under physiological and stress conditions. To restore homeostasis, the PN also relies on stress sensors and inducible pathways, such as the heat shock response (HSR), the unfolded protein response (UPR) and the oxidative stress response. How a protein folds and acquires its native conformation is a matter of high medical relevance since a large number of human diseases are associated with protein misfolding. These conditions are broadly classified as conformational disorders, and they are caused either by genetic mutations that cause protein misfolding and premature degradation (e.g. Cystic Fibrosis and Gaucher’s disease); or by the accumulation of misfolded, aggregated and/or fibrillar protein inclusions that are toxic to the cell. In particular, the phenomenon of protein aggregation is a hallmark of a large number of neurodegenerative diseases (*e.g.* Alzheimer’s, Parkinson’s and Huntington's diseases and several ataxias), muscular dystrophies, metabolic disorders and certain types of cancer. Considerable efforts have been directed at dissecting of the mechanisms of protein aggregation and toxicity, but the full extent of events leading to cell dysfunction is still unclear (Chapter I). The unifying aspect of conformational disorders is, however, the inability of the PN to respond efficiently to misfolded and aggregation-prone proteins so as to prevent cellular toxicity. Therefore, it is urgent and relevant to multiple diseases to identify genetic modifiers that enhance proteostasis function and consequently prevent protein aggregation and toxicity. Research has benefited from powerful model systems that recapitulate important aspects of the human disease. In particular, the nematode *Caenorhabditis elegans* (*C. elegans*) is a tractable genetic model organism that combines sufficient complexity so as to allow research on both cellular and organismal (including behavioral) phenotypes, with simplicity that facilitates rapid, high-throughput testing of hypotheses (Chapter I). Genetic screens performed to date have identified the network’s protective components which, when knocked down or deleted, lead to enhanced aggregation and/or toxicity. These

include molecular chaperones, proteasome subunits, components of the autophagy machinery, and the stress-induced transcriptional regulators FOXO/DAF-16 and HSF-1.

The work described in this thesis is novel as it focuses on the opposite side of the PN, *i.e*., the pathways that when down-regulated lead to enhanced folding capacity. We established a screening strategy in *C. elegans* using RNA interference (RNAi) to identify genetic modifiers that suppress protein aggregation and toxicity of multiple disease-related proteins (Chapter II). Our goal was to identify genes that, when downregulated, enhanced the functional properties of the proteostasis network and restored the folding environment. We thus identified 63 genetic modifiers that suppressed both polyglutamine (polyQ) and mutant superoxide dismutase I (SOD1) aggregation, of which only 23 also suppressed the toxicity phenotype associated with aggregation. This was an important finding as it demonstrated that aggregation and toxicity can be genetically uncoupled. From the initial hits, 9 modifiers systematically reduced the misfolding of endogenous metastable mutant proteins, suggesting a general improvement of the folding environment. We postulated that this effect could be a consequence of activation of the heat shock stress response and chaperone expression by the modifiers. Although, we found that 5 improved folding in a HSF-1/chaperone dependent manner, the remaining modifiers improved folding by altering metabolism and RNA processing functions. Overall, this study introduced new genetic modifiers that promote alternate cellular folding environments broadly protective against misfolding events.

We then characterized further the genetic modifier *gei-11*, a negative regulator of the L-type acetylcholine receptor (AChR) at the neuromuscular junction, to determine the mechanism of proteostasis enhancement (Chapter III). Downregulation of *gei-11* increased cholinergic signaling and calcium flux into the cytoplasm of muscle cells, via activation of the voltage-gated calcium channel, EGL-19, and the sarcoplasmic reticulum ryanodine receptor, UNC-68. This resulted in selective activation of HSF-1 and up-regulation of cytosolic chaperones that restored the post-synaptic folding environment. Earlier work had identified a loss-of-function deletion mutation in *unc-30* that regulates GABA expression in *C. elegans* neurons, and resulting in enhanced polyQ aggregation in post-synaptic muscle cells (Garcia *et al.* 2007). Notably, enhanced aggregation occurs when GABAergic signaling is completely inhibited, resulting in maximum cholinergic overstimulation of muscle cells, whereas suppression of aggregation results from a moderate increase in cholinergic signaling. The effects of increased AChR expression are not the same as complete inhibition of GABA signaling, in part because the signaling response (and degree of stimulation) occurs at an intermediate level through a titrated response and waves of Ca^{2+} release. Therefore, the effect on post-synaptic protein aggregation is a consequence of the degree of imbalance generated between ACh and GABA, with an apparent range for folding improvement by cholinergic signaling. We propose that altogether these studies underscore the importance of the balance between cholinergic and GABAergic signaling as a mechanism for non-autonomous neuronal regulation of proteostasis in post-synaptic cells, and provide compelling evidence that will lead to a better understanding of the control of stress responses through tissue signaling events, which is very relevant for a number of neuromuscular disorders.

We have also initiated the characterization of the hit gene *let-607* (Appendix II). This gene is predicted to encode the *C. elegans* ortholog of CREBh, an ER regulated transmembrane protein (RIP)

bZIP transcription factor that maintains sterol homeostasis in the liver and mediates UPR. Downregulation of *let-607* in *C. elegans* led to an improvement of proteostasis function through activation of the HSR, up-regulation of molecular chaperones and consequent suppression of protein misfolding, in an HSF-1- and XBP-1-dependent manner. UPR induction was found to be epistatic and required for HSR activation by *let-607* RNAi. This is not observed for other UPR inducers, revealing specificity of "crosstalk" between the two stress responses through *let-607*. Currently, we are further characterizing the role of *let-607* on UPR and the mechanism involved in UPR-mediated activation of the cytosolic HSR.

The studies presented in this thesis emphasize the value of genetic screens and model organisms for the identification of genes and pathways that maintain protein homeostasis and are compromised in disease. Our screening strategy and triage hypotheses revealed novel genes/pathways that can be modulated to improve the PN capacity and help resolving the issue of protein aggregation-toxicity. Even greater value is offered by complementation of these genetic studies with small molecule screens to ultimately identify the suitable targets for therapeutics. This is highlighted in the work on "Chaperone Therapeutics: Small Molecule Proteostasis Regulators of the Heat Shock Response for Protein Conformational Diseases" (Appendix III). In this work we describe the results of a ~900,000 small molecule screen that identified small molecule proteostasis regulator compounds (PRs) that induce HSF-1-dependent chaperone expression and restore protein folding in multiple conformational disease models. The enhancement of proteome stability by the PRs is mediated by HSF-1, DAF-16/FOXO, SKN-1/Nrf2 and the chaperone machinery, through mechanisms that are distinct from current known small molecule activators of the HSR. Together, genetic and chemical modulation of the PN reveal new candidates and new mechanisms to be targeted by PRs, establishing promising therapeutic approaches for a variety of protein conformational diseases.

KEY WORDS:
Protein Misfolding; Neurodegenerative Diseases; Proteostasis; Stress Response; Chaperones

‘Genetic Screens in *C. elegans* for New Modulators of Protein Homeostasis, with Relevance for Conformational Diseases’

RESUMO

O *folding* proteico, processo pelo qual proteínas adquirem a sua conformação correcta, é essencial para o bom funcionamento molecular e celular. Assim, as células possuem um sofisticado mecanismo de controlo de qualidade do proteoma (i.e., a totalidade das proteínas da célula num dado instante). O conjunto de vias celulares que coordena a síntese, o *folding*, o tráfego e a degradação de proteínas, e que determina o destino de proteínas que não adquirem a conformação correcta, é responsável por promover e manter a homeostase proteica celular ("*proteostasis network*" ou PN). Os componentes principais deste sistema de controlo de qualidade são os chaperones moleculares, responsáveis pelo *folding* de proteínas quer em condições fisiológicas quer sob stress. A PN utiliza sensores e vias induzidas por stress para restabelecer a homeostase, como é o caso da *heat shock response* (HSR), da *unfolded protein response* (UPR) e a resposta ao stress oxidativo. O processo de *folding*, e o modo como cada proteína adquire a sua conformação nativa funcional tem uma enorme relevância clínica uma vez que existe um elevado número de doenças provocadas por *misfolding* proteico. Estas patologias são genericamente designadas por ‘doenças de conformação proteica’, e podem ser causadas por mutações que impedem uma dada proteína de adquirir a conformação correcta, o que leva à sua degradação prematura (ex: Fibrose Quística e doença de Gaucher); ou então podem ser a consequência da acumulação e agregação de proteínas na forma de inclusões ou fibras amilóides que são altamente tóxicas para a célula. O fenómeno de agregação proteica é característico de doenças neuro-degenerativas (ex: doenças de Alzheimer, Parkinson e Huntington e várias ataxias), distrofias musculares, doenças metabólicas e certos tipos de cancro. Têm sido desenvolvidos esforços consideráveis na investigação dos mecanismos responsáveis pela agregação, toxicidade e sintomas clínicos destas doenças, no entanto ainda existem muitas questões em aberto (Capítulo I). O aspecto comum entre as doenças de conformação proteica é, no entanto, a incapacidade das células ou da PN de resposta eficiente face à presença de proteínas com tendência para agregar, de modo a evitar a respectiva toxicidade. Assim, uma alternativa para fins terapêuticos à identificação da causa de toxicidade em cada doença em particular, poderá ser a identificação de moduladores genéticos que alteram e principalmente que melhoram a capacidade funcional da PN, consequentemente prevenindo agregação e toxicidade. Este tipo de trabalho tem tido imenso sucesso através da utilização de organismos modelo que

apresentam fenótipos relevantes para estas patologias. Particularmente, o nemátode *Caenorhabditis elegans* (*C. elegans*) oferece inúmeras vantagens em termos de facilidade de manipulação genética, estudo de fenótipos celulares e organismais (incluindo comportamentais), e possibilidade de ser usado em *high-throughput screens* genéticos (Capítulo I). Os *screens* genéticos executados até a data identificaram já os principais componentes da PN com função protectora os quais, aquando se reduz a sua expressão, levam ao aumento de *misfolding* e agregação proteícos e/ou toxicidade. Tais componentes da PN incluem chaperones, componentes das vias de degradação, como o proteasoma e autofagia, e os factores de transcrição FOXO/DAF-16 e HSF-1 que participam na resposta a *stress* celular.

O trabalho descrito nesta tese é inovador pois foca numa outra vertente da PN, ou seja, os componentes cuja redução da expressão leva a uma melhoria do *folding* global. Assim, foi estabelecida uma estratégia de *screening* em *C. elegans*, utilizando RNA de interferência (RNAi) para identificar moduladores genéticos que reduzem a formação de agregados e a toxicidade de múltiplas proteínas (Capítulo II). O objectivo deste trabalho foi identificar novos factores que, quando negativamente regulados por RNAi, melhoram a função da PN e consequentemente aumentam o *folding*. Foram inicialmente identificados 63 moduladores/RNAi que reduziram o fenótipo de agregação no modelo de expressão de poliglutaminas (polyQ) e da superóxido dismutase 1 mutante (SOD1). Destes, apenas 23 moduladores genéticos reduziram o fenótipo de toxicidade. Este resultado demonstra que os processos de agregação e toxicidade não têm de estar necessariamente acoplados. Por último, pusemos em evidência que 9 destes moduladores corrigiram dum modo consistente o *folding* de várias proteínas mutantes endógenas, extremamente susceptíveis a *misfolding*, sugerindo que os genes identificados são moduladores gerais do *folding* proteíco. Propusémos então que este efeito seja uma consequência da expressão de chaperones e outros componentes do controlo de qualidade celular que promovem *folding*.
De facto, o efeito de 5 destes genes parece ser dependente do factor de transcrição HSF-1 e do aumento da expressão de chaperones. Os restantes parecem afectar o *folding* através de alterações metabólicas e de processamento de RNA. Em conclusão, este trabalho identificou novos moduladores de homeostase proteica, os quais actuam de forma a promover um novo "ambiente celular" que propicia uma maior capacidade de *folding*.

De seguida, caracterizou-se o mecanismo pelo qual o modulador genético *gei-11* melhora a capacidade de *folding* (Capítulo III). Mostrámos que a redução da expressão do gene *gei-11*, descrito como sendo um regulador negativo do receptor de acetilcolina tipo-L (L-AChR) na junção neuro-muscular de *C. elegans*, aumenta o sinal colinérgico nas células musculares, activando os canais de cálcio na membrana (EGL-19) e o influxo do cálcio para o citoplasma através do retículo sarcoplásmico. Subsequentemente, verificou-se que ocorria a activação da HSF-1 e a expressão de chaperones que, por sua vez, assistem o *folding* de proteínas e minimizam agregação. Por ouro lado, tinha já sido descrito que a deleção do gene *unc-30*, que regula a via de síntese e secreção de GABA em células neuronais de *C. elegans*, intensifica a agregação de poliQ nas células musculares (Apêndice II). De notar, é o facto do aumento da agregação ocorrer apenas quando o sinal GABAergico é completamente eliminado, o que resulta em estimulação colinérgica máxima das células musculares. Por outro lado, a redução no número de agregados resulta dum "aumento intermédio" de actividade colinérgica. O aumento de expressão de

AChR através do *gei-11*/RNAi não é assim equivalente à total inibição do sinal GABAérgico, uma vez que no primeiro caso o efeito é de nível intermédio e com oscilação nos níveis de cálcio. Assim, a alteração dos níveis de agregação e uma consequência do grau de desequilíbrio entre ACh e GABA, com um aparente limite para efeito positivo no *folding* proporcionado por ACh. Deste modo, s duas componentes deste trabalho revelam que o equilíbrio entre o *input* neuronal GABAérgico e colinérgico é essencial para regulação da proteostase no músculo, e aparentemente revelam um limiar para a melhoria do folding por parte da sinalização colinérgica. Estes resultados também revelam assim duma forma clara as vias de comunicação entre o sistema nervoso e muscular, que se reveste de extrema relevância para um conjunto de doenças neuromusculares.

No Apêndice III são também brevemente descritos os resultados da caracterização do modulador genético *let-607*. Prevê-se que este gene codifique o ortólogo do gene humano CREBh, um factor de transcrição associado à membrana do retículo endoplasmático (RE) e responsável pela regulação dos níveis de esteróis no fígado, bem como pela regulação da UPR. Observou-se que a redução da expressão de *let-607* conduz à activação da UPR e da HSR, à expressão de chaperones dependentes de HSF-1 e XBP-1, e consequentemente uma melhoria do *folding* proteico. De notar que a UPR ocorre de forma epistatica relativamente à HSR, sob a acção do RNAi contra o gene *let-607*. Os resultados sugerem uma especificidade de comunicação ("*crosstalk"*) entre as duas vias de *stress* UPR e HSR, que é regulada pelos níveis de *let-607*. Presentemente, a função do *let*-607 na UPR e o mecanismo de activação da HSR pela UPR estão a ser caracterizados.

O trabalho apresentado nesta tese sublinha o valor dos *screens* genéticos em organismos modelo para a identificação de novos factores e vias que contribuem para a homeostase celular. A estratégia de *screening* e o método de triagem aqui aplicados revelaram componentes específicos da PN que podem ser modificados com o objectivo de reduzir o fenótipo de agregação e toxicidade proteíca. Estes estudos genéticos podem ser complementados por *screens* de pequenas moléculas ("*small molecules*") para identificação de compostos que sirvam de base para o desenvolvimento de novas terapêuticas. Este é o foco do trabalho publicado no artigo "*Chaperone Therapeutics: Small Molecule Proteostasis Regulators of the Heat Shock Response for Protein Conformational Diseases*" (Appendix IV). Nele é descrito o resultado dum *screen* de ~900.000 moléculas, a partir do qual foram identificados novos reguladores de proteostase (PRs) que activam a HSF-1 e a expressão de chaperones. A exposição de modelos celulares e animais de doenças de conformação proteica a estes PRs reduziu o *misfolding* de múltiplas proteínas e as respectivas consequências fenotípicas. Verificou-se que o melhoramento da capacidade de *folding* é regulado por HSF-1, DAF-16/FOXO, SKN-1/Nrf-2 e chaperones. No seu conjunto, este estudo revelou novos moduladores genéticos e químicos das vias de proteostase, os quais apresentam potencial terapêutico (por exemplo, os PRs) para várias doenças causadas por proteínas com conformações prejudiciais à célula/organismo.

PALAVRAS-CHAVE:

Misfolding Proteico; Doenças Neurodegenerativas; Proteostase; *Stress Response*; Chaperones

ABBREVIATIONS

17-AAG, 17-N-Allylamino-17-demethoxygeldanamycin
Aβ, Amyloid-beta protein
AC, autocorrelation curve
ACh, acetylcholine
AChR, acetylcholine receptor
AD, Alzheimer's disease
AGE-1, ortholog of the phosphoinositide 3-kinase (PI3K)
ALS, Amyotrophic Lateral Sclerosis
Amp., ampicillin
APP, amyloid-beta precursor protein
ARE, antioxidant response element
BSA, bovine serum albumin
BWM, body-wall muscle
***C. elegans**, Caenorhabditis elegans*
CF, Cystic Fibrosis
CFTR, Cystic Fibrosis Transmembrane Conductance Regulator
GA, Geldanamycin
CGC, Caenorhabditis Genetic Center
ChIP, chromatin immuno-precipitation
4-CmC, 4-Chloro-m-Cresol
DAF-2, insulin/growth factor receptor
DAF-16, *C. elegans* FOXO/HNF3 family
DIC, differential contrast
DMSO, dimethyl sulfoxide
DS, dantrolene sodium
dsRNA, double stranded RNA
DTT, dithiothreitol
***E. coli**, Escherichia coli*
ER, endoplasmic reticulum
EV, empty vector (RNAi)
ΔF508, phenylalanine 508 deletion
FCS, Fluorescence Correlation Spectroscopy
FOXO, Forkhead box transcription factor
FRAP, Fluorescence Recovery After Photobleaching
fw, forward
GABA, γ-Aminobutyric acid
GFP, green fluorescent protein
HD, Huntington's disease
Htt, huntingtin
HS, heat shock
HSC, heat shock cognate
HSE, heat shock element
HSF-1, heat shock factor 1
Hsp, heat shock protein
HSR, heat shock response
HTS, high throughput system
IGF-1
ILS, insulin-like signaling
IPTG, isopropyl-beta-D-1-thiogalactopyranoside
LB, Luria Bertani medium
luc, luciferase
MEFs, mouse embryonic fibroblasts
Nem.A, Nemadipine A
NGM, nematode growth media
NMJ, neuromuscular junction
PCR, polymerase chain reaction
PD, Parkinson's disease
PN, proteostasis network
polyQ, polyglutamine
PrP, prion protein
PR(s), proteostasis regulators
qPCR, quantitative PCR
Rev, reverse
RNAi, RNA interference
rt-PCR, reverse transcriptase PCR
RYR, ryanodine receptor
Ryr, ryanodine compound
SDS, sodium dodecyl sulfate
PAGE, polyacrylamide gel electrophoresis
SD, standard deviation
SEM, standard error of the mean
sHSP, small heat shock protein
SKN-1, bZIP transcription factor NRF1
SOD1, superoxide dismutase I
τ, time interval
τ_D, (Tau_D) brightness distribution
TM, tunicamycin
TS, temperature sensitive
UPR, unfolded protein response
UPRE, UPR element
UPS, ubiquitin-proteasome system
VGCC, voltage-gated calcium channel
WT, wild-type
YFP, yellow fluorescent protein

Chapter I

General Introduction

General Introduction

1. Protein Folding

Proteins are conformationally complex and versatile macromolecules, responsible for the majority of cellular functions. It is therefore not surprising that cells have evolved an elaborate machinery to ensure the quality and proper function of the proteome. Protein folding is a multi-step physical process by which a polypeptide chain acquires its native and functional three-dimensional structure, according to the information contained in the amino acids sequence, and partly dictated by attractive and repulsive forces between neighboring amino acids [1-4]. The energy component of protein folding can be illustrated by a funnel-shaped landscape representing the multitude of conformations populated by a given protein *en route* to the native state, via intra-molecular interactions (Figure 1). The free energy decreases as the native folded state is acquired, towards a minimum global energy and higher thermodynamic stability [3]. There are multiple energetically accessible paths going downwards the folding funnel, some with local energy minima that can trap the protein in kinetically stable "off-pathway" conformations that can drive inter-molecular interactions and formation of amorphous aggregates, or instead, ordered cross-β-sheet fibrillar structures, called amyloid (Figure 1) [1-3,5-7]. To prevent these events, protective mechanisms are in place to assist in the proper folding or degrade misfolded proteins [1,8]. Together with the synthesis and clearance machinery, molecular chaperones are the central components of the cellular quality control (QC) system that preserves protein homeostasis under normal and stress conditions (Figure 2). How proteins fold into a native and functional structure is a matter of great medical relevance, as protein misfolding can lead to a growing number of human diseases. Likewise, the mechanism by which misfolded proteins are

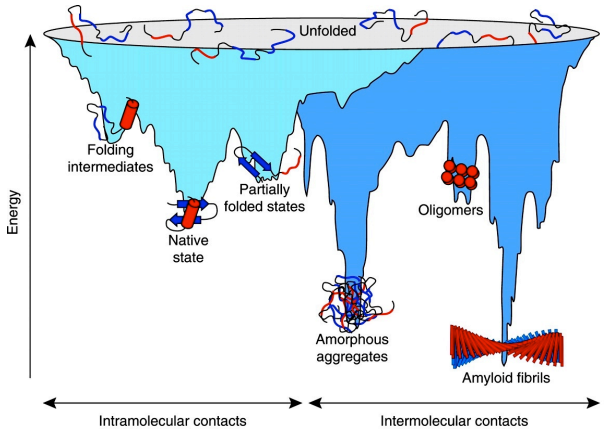

Figure 1: Energy landscape of protein folding and aggregation. A folding 'funnel' landscape depicts the number of energy pathways and intermediate conformations allowed to a given protein, *en route* to the lowest minimum energy and highest stability native state. Alternatively, due to aberrant but stable intermolecular interactions between unfolded intermediates, aggregation can occur. The width of the funnel represents entropy of molecular interactions, and the depth represents energy (adapted from [1]).

recognized, processed and ultimately degraded by the cell to avoid toxicity and disease are a topic of extensive research.

1.1. Quality Control Machinery

To ensure fidelity of gene expression at the post-translational level, the cell possesses a stringent QC system that ensures the coordination between gene transcription, protein synthesis, folding, trafficking and repair. To surpass all QC checkpoints, a protein must reach the correctly folded state. When proteins fail to attain their native conformation or damage occurs, a triage system comes into place to repair and refold proteins, or to promote degradation and avoid accumulation of misfolded and potentially toxic proteins (Figures 2 and 3). Furthermore, the cell employs folding sensors and enzymes that covalently tag proteins with molecules such as glucose, mannose or ubiquitin, for recognition by the folding and degradation machinery, respectively [9].

Cytosolic Molecular Chaperones

Surveillance of protein conformation is the primary function of molecular chaperones that ensure proper folding under normal physiological conditions and under cellular stress. Molecular chaperones are highly conserved proteins ubiquitously expressed in all cell types and cellular compartments that, by definition, interact with and assist a non-native protein to acquire its native conformation, without being present in the final functional structure (Figure 2). Notably, most molecular chaperones were first identified as genes induced by stresses that alter protein stability, such as exposure to elevated temperatures (heat shock), being therefore referred to as heat shock proteins (Hsps) [10]. Chaperones are grouped into families according to molecular mass (KDa) and sequence homology, and include Hsp100, Hsp90, Hsp70, Hsp60, Hsp40 and small Hsps (sHsp). Each chaperone family varies in size, substrate specificity, distribution into subcellular compartments, and cohort of co-chaperones that modulate chaperone-substrate specificity. Protein folding in the cytosol relies on a group of ribosome-associated chaperones that stabilize nascent polypeptide chains to initiate folding, the primary “control check-point”, and then on a second group of chaperones that complete the folding process [4,11]. **Ribosome-associated chaperones** include the bacterial trigger factor (TF), and the eukaryotic ribosome-associated complex (RAC) and nascent-chain associated complex (NAC) [1]. Other chaperones recognize and bind to the yet unfolded polypeptides to continue proper folding, assist in intracellular trafficking, or direct proteins to proteolytic degradation [1,10,11]. The **Hsp70** family members participate in protein co- and post-translational folding and translocation [1,10]. Hsp70 chaperones, both constitutive and stress-inducible, ensure proper folding through cycles of substrate binding and release in an ATP-dependent manner [1,10]. Co-chaperones and nucleotide exchange factors (NEFs) act in concert with the Hsp70 machinery to increase substrate-binding efficiency, specificity, and release, by modulating various steps of the ATPase cycle and interactions with other QC components [1]. **Hsp40**s are a family of chaperones with a signature J domain related to the *E. coli* DnaJ protein, that function as Hsp70 co-chaperones to stimulate ATP hydrolysis and stabilize Hsp70-

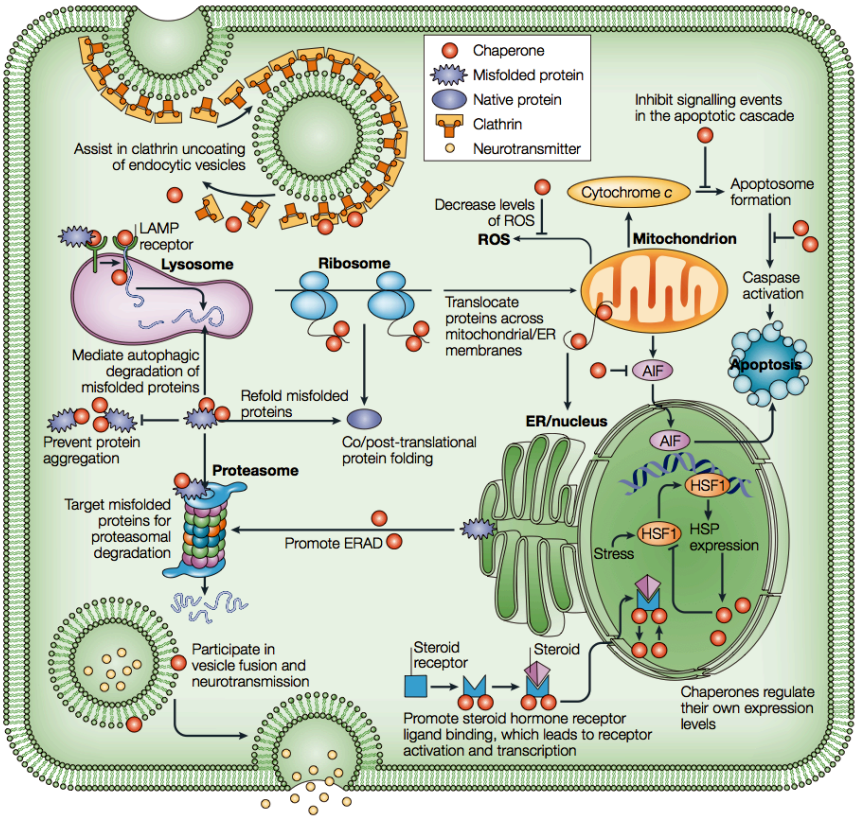

Figure 2: Molecular chaperones and the quality control machinery. Molecular chaperones facilitate protein folding and prevent misfolding. Chaperones are represented in all cellular organelles, and in addition to folding reactions, regulate other cellular processes, such as autophagy, vesicle fusion, signal transduction, apoptosis and proteasomal degradation. AIF, apoptosis-inducing factor; ER, endoplasmic reticulum; ERAD, endoplasmic reticulum-associated degradation; HSF1, heat shock transcription factor 1; HSP, heat shock protein; LAMP, lysosomal-associated membrane protein; ROS, reactive oxygen species. Figure from [308].

substrate binding. **Chaperonins,** such as Hsp60, the *E. coli* GroEL, and the eukaryotic TRiC (TCP-1 ring complex) or CCT (chaperonin containing TCP-1), are large double-ring multimeric complexes that encapsulate protein substrates (cage-like structure) to substantially accelerate the rate of folding through ATP-regulated cycles [1,4,10]. The **Hsp90** chaperone is fundamental for the structural maturation of specific client proteins involved in signaling processes (e.g. glucocorticoid receptor), transcription and cell cycle control [12]. The **Hsp100** family is a large family of ATPase Associated with diverse Activities (AAA+) chaperones, described to associate with proteases or with Hsp70, to assist in protein disaggregation and/ or degradation [10,13-15]. The **sHsp**s are chaperones of molecular masses ranging from 15 KDa to 40 KDa, with a conserved α-crystallin domain, that bind as dimers to misfolded proteins to prevent aggregation, without requiring ATP.

The Endoplasmic Reticulum Folding Environment

The endoplasmic reticulum (ER) has many functions, including lipid storage, calcium (Ca^{2+}) homeostasis, biogenesis of organelles, protein folding and QC, and protein degradation [9,16]. Chaperones operating at the ER have an essential role in the maturation of proteins destined for the

secretory pathway. The milieu of the ER differs from that of the cytosol in respect to ions, redox conditions, complement and concentration of chaperones and folding enzymes, providing an optimized environment for folding efficiency, disulphide bond formation and multi-domain protein assembly [9,16,17]. The ER chaperones include the Hsp70 family members BiP and Grp170 (Glucose-related protein); Hsp40 family members (ERdj1-5); one Hsp90 family member Grp94; and the lectin chaperones calnexin (CNX) in the ER membrane and calreticulin (CRT) in the ER lumen that assist the folding of proteins carrying monoglucosylated N-linked glycans. In addition, thiol-disulphide oxidoreductases and peptidyl-prolyl isomerases (PPIases) enzymes catalyze oxidation, isomerization and reduction of disulphide bonds [9,16,17]. The ER QC is a “retention-based system”. BiP, CNX and CRT, among other chaperones, serve as retention anchors, inhibiting the secretion of incompletely folded or misfolded proteins. If a protein is permanently misfolded or if it stays bound by chaperones for a prolonged time, it is targeted for ER-associated degradation (ERAD) and retro-translocated back into the cytosol for degradation by the 26S proteasome (Figure 2) [9,16-18]. This type of quality control is problematic when mutant, yet (partially) functional, proteins are retained and degraded because of (minor) structural defects, failing to reach their proper cellular location, leading to disease. Proteins that leave the ER enter vesicles for protein export into the Golgi complex and secretion. ER resident proteins that escape this secretory route contain an ER-retention signal at the C-terminus, such as the KDEL sequence (lysine-aspartate-glutamate-leucine).

Protein Clearance

The proteolytic machinery manages the clearance of misfolded, damaged and aberrant proteins. It also contributes to replenish the intracellular reserve of free amino acids to sustain protein synthesis (Figure 3) [8,19]. Protein degradation in eukaryotic cells is carried out by two major proteolytic systems: the ubiquitin-proteasome system (UPS) and the lysosomal system [19]. The proteolytic process occurs in a sequence of common steps: cargo selection and tagging, cargo recognition and delivery to the proteolytic entity, and degradation. Proteins destined for degradation by the UPS are first tagged by covalent conjugation of multiple molecules of ubiquitin (Figure 2) [20]. The conjugation of ubiquitin is orchestrated by the activity of three enzymes: E1, the ubiquitin-activating enzyme; E2, the ubiquitin-conjugating enzyme; and E3, the ubiquitin-ligase. E3 ligases can function in cooperation with the Hsp70 or Hsp90 chaperones to facilitate recognition of misfolded client proteins [8,19]. The 26S proteasome is a highly conserved multi-catalytic ATP-dependent protease complex with two main subunits: the catalytic 20S core particle (CP) and the regulatory particle (RP: 19S and 11S). Substrates are recognized via ubiquitin receptors, de-ubiquitinated by specific enzymes (DUBs), and then unfolded for threading through the narrow barrel-like proteolytic chamber [8,19].

Lysosomes are the main components of the autophagy proteolytic machinery. These single membrane vesicles contain a variety of proteases, lipases, glycases and nucleotidases in an acidic lumen environment that facilitates unfolding of proteins and proteolysis [8,19]. Macroautophagy participates in degradation of both cellular organelles and proteins, under basal or stress conditions. Cytosolic cargo is sequestered into autophagosome vesicles that fuse with lysosomes where degradation of the cargo occurs. In turn, microautophagy is characterized by direct sequestration of cytosolic cargo by the

lysosomes. Finally, chaperone-mediated autophagy (CMA) of cytosolic proteins requires the recognition of the target substrate by a cytosolic chaperone, complete unfolding and subsequent targeting to a surface receptor on the lysosome. CMA is mostly activated in response to stress.

The chronic expression of misfolded proteins, often associated with conformational disorders, leads to saturation of the QC and degradation machinery and results in accumulation of insoluble, aggregated and potentially toxic species (Figure 3). Aggregates of certain pathogenic proteins, although positive for ubiquitin and cargo recognition molecules, still fail to be recognized by the autophagy or proteasome machinery, which suggests failure in the clearance function as a possible contributor to pathogenesis [8,21]. In certain situations however, cells seem to recruit misfolded species into large protein inclusions as a protective mechanism against aberrant interactions with other cellular components, and to facilitate autophagy-mediated clearance [21-23]. The degradation of aggregated proteins by macroautophagy has been shown to be protective in cell and mouse models of Parkinson's and Huntington's diseases [19,21,24-27].

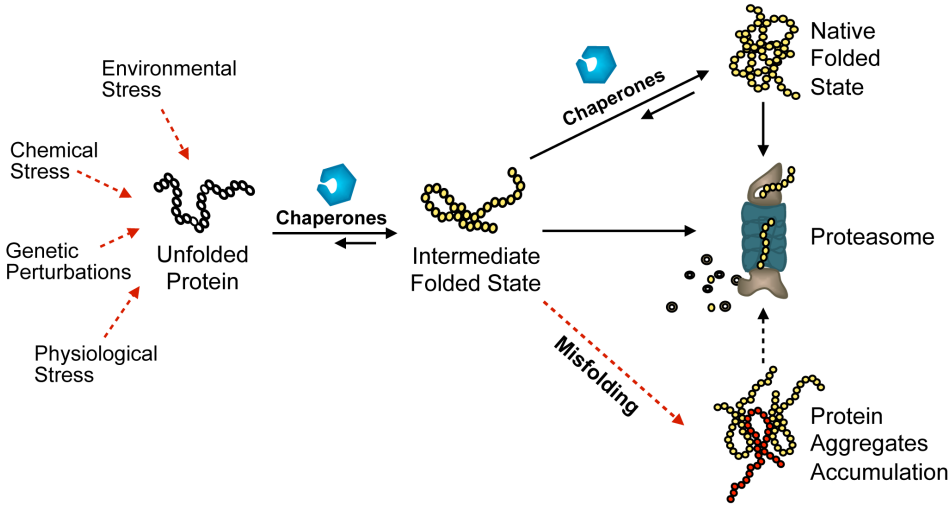

Figure 3: Protein folding homeostasis. Protein homeostasis is maintained by a delicate balance between proper folding of proteins and efficient removal of damaged proteins. Under certain conditions, proteins misfold and adopt alternate intermediate conformations. Molecular chaperones recognize non-native states and assist in (re-)folding. The proteasome system degrades both normal short-lived and abnormal misfolded proteins. Impairment in protein folding homeostasis, due to genetic mutations/perturbations or environmental stressors, leads to increase in misfolding events and accumulation of aggregates, leading to cellular toxicity. Adapted from [10].

1.2. Cell Stress Responses

'Stress' is defined as a noxious factor that causes harmful alterations in the cellular environment, triggers a series of molecular events and ultimately affects protein homeostasis. Acute forms of stress include environmental fluctuations in temperature (heat or cold shock), osmolarity, hydration and nutrient availability; chemical insults, such as oxygen free radicals and heavy metals; bacterial and viral infections, ischemia, or injury. Alternatively, protein homeostasis is perturbed by a chronic form of stress consisting of persistent expression of mutant, misfolded and/or aggregated proteins (Figure 3). Aging is also considered

a form of chronic stress that results from a gradual accumulation of deleterious modifications in nucleic acids, proteins, lipids and carbohydrates. The increase in Hsp levels during aging, without any other source of external stress, is an indication of intrinsic age-related stress [28]. Little is still known about the differences between molecular mechanisms that sense and respond to acute vs. chronic stress. In general, activated stress responses up-regulate chaperones for restoration of protein homeostasis, mainly by facilitating refolding, preventing accumulation of misfolded and toxic proteins, and by promoting degradation [1,21]. The folding environment is monitored within each compartment through specific pathways [29]. Whereas stress perturbation of the cytosolic folding environment selectively activates cytoplasmic chaperone expression, interference with ER or mitochondrial folding preferentially activates expression of ER- and mitochondria-localized chaperones, respectively.

The Cytosolic Heat Shock Response

The heat shock response (HSR) was discovered in 1962 by Ferruccio Ritossa, who reported a puffing pattern in polytene chromosomes of the fruit fly *Drosophila buschii* upon heat shock [30]. A decade later it was established that this pattern corresponded to the activation of genes encoding heat shock proteins [30]. The heat shock family (HSF) of transcription factors mediate both basal and stress-induced expression of chaperones. Whereas *S. cerevisiae*, *D. melanogaster* and *C. elegans* have one HSF, vertebrates have multiple and, in particular, humans have three: HSF1, HSF2 and HSF4 [31-34]. HSF family members are comprised of an amino-terminal helix-turn-helix DNA-binding domain (DBD), an adjacent coiled-coil trimerization domain responsible for activation-induced trimerization, and a regulatory domain (RD) that together with the transactivating domain is essential for responsiveness to stress [34,35]. HSF1 is constitutively expressed in most tissues and cell types, is the main transcriptional regulator of chaperone expression and the only HSF known to be active during stress [31,36,37]. Transcriptional activation of human HSF1 has been well characterized (Figure 4). Briefly, under physiological conditions HSF1 is predominantly localized in the cytoplasm in a monomeric inactive form, and interaction with Hsp70 and Hsp90 has been proposed to maintain HSF1 in a repressed state [38-40]. Upon stress stimuli, Hsp70 and Hsp90 are recruited to interact with misfolded proteins, releasing HSF1. Then a rapid cascade of events takes place, starting with HSF1 translocation to the nucleus, trimerization and binding to consensus sequences named heat shock elements (HSE) in heat shock gene promoter regions, and transcriptional activation of chaperone expression to combat protein misfolding (Figure 4) [34,35,41-43]. In mammalian cells, post-translational modifications of HSF1 are a determinant for transactivating potency and later repression of HSF1 activity, and include acetylation, phosphorylation and sumoylation (Figure 4). HSFs also participate in development, differentiation and growth [35]. The non-stress related roles of HSF1 include maintaining the stability of the proteome during cell cycle, embryonic development, cellular differentiation, cell growth, and spermatogenesis (reviewed in [34]). Of particular interest is that elevated levels of HSF1 have been detected in several types of human cancer, such as breast cancer and prostate cancer, probably as a consequence of high proteotoxicity and and demand for chaperone function in these cells [35]. Moreover, the stress response may also be somewhat cell-type specific, as studies have identified disparate sequence of events leading to activation of HSF1, specifically in neurons. Levels of

HSF1 expression, activity, and Hsp expression are reduced in certain neurons in comparison to other cell types, which may be related to the apparent susceptibility of neurons to the expression of aggregation-prone proteins and neurodegenerative disease incidence [10,44].

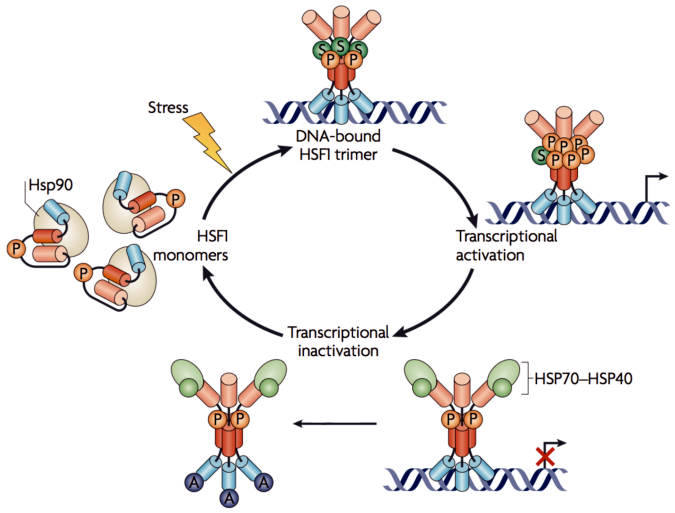

Figure 4: HSF1 activation and attenuation cycle. Under normal conditions, HSF1 is a monomer in both the cytoplasm and nucleus and it interacts with Hsp90 (and Hsp70). Upon stress, Hsp90 dissociates from HSF1, allowing trimerization and binding of HSF1 to HSEs in Hsp genes. Phosphorylation (P) and sumoylation (S) are involved in regulating the transactivation and transcriptional capacity of HSF1. Attenuation involves negative feedback from HSPs, which represses transactivation, and inhibition of DNA binding by acetylation (A) in the DBD of HSF1. Adapted from [35].

ER and Mitochondria Unfolded Protein Responses

Accumulation of unfolded and/or misfolded proteins in the ER lumen causes a homeostatic imbalance and ER stress. A signal transduction pathway transmits information about the folding status in the ER to the nucleus for expression of ER-resident chaperones and other QC genes, in a process referred to as the ER unfolded protein response (UPR^{ER}) (Figure 5) [45-48]. In eukaryotes, the most immediate response to ER stress is the reversible and transient attenuation of mRNA translation to reduce the protein load that enters the ER. Then, as general translation repression is relaxed, signal transduction pathways are set into motion to mediate expression of ER chaperones, by UPR executors IRE1 (inositol-requiring protein-1), PERK (protein kinase RNA-like ER kinase) and ATF6 (activating transcription factor 6) (Figure 5). IRE1 is the most conserved branch of the UPR [47], and encodes a type 1 ER transmembrane protein with a lumenal and a cytoplasmic domains, with a Ser/Thr protein kinase and endoribonuclease C-terminus domains. The most recent studies on IRE1 activity propose that, under physiological conditions, BiP binds to IRE1 in the ER lumen and maintains the protein in an inactive monomeric state. Upon stress, BiP is recruited to misfolded proteins and releases IRE1, leading to its dimerization, cluster formation and activation (Figure 5). Direct interaction of unfolded proteins with the IRE1 stress-sensing domain in the ER lumen may also be involved in IRE1 cluster formation [46,47,49]. IRE1 trans-autophosphorylation triggers IRE1 RNase activity, which undertakes the unconventional splicing of the mRNA encoding the basic leucine-zipper (bZIP) transcription factor XBP1 (X-box binding protein 1 in mammals and metazoans) or Hac1 (homologous to ATF/CREB1 in yeast) (Figure 5) [45]. The spliced form (sXBP1) translocates to the nucleus and activates gene transcription by binding to UPR-specific promoter sequences (UPRE/ERSE) on genes involved in protein folding and ER QC [45,46]. ATF6 is an ER transmembrane bZIP transcription

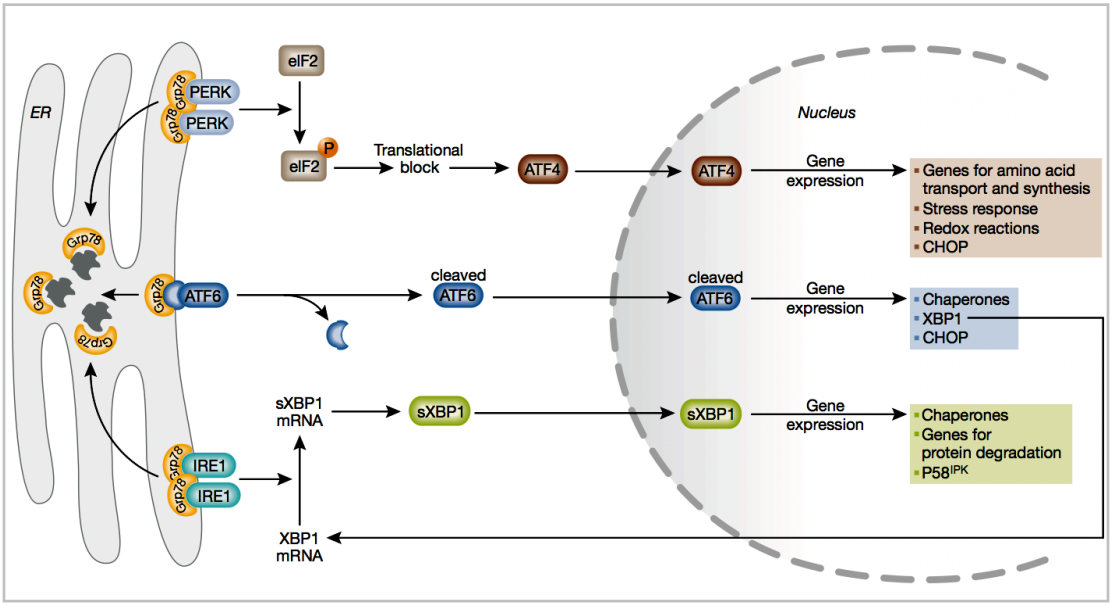

Figure 5: Unfolded protein response. The UPR responds directly to the accumulation of unfolded and misfolded proteins that recruit ER-Hsp70 (Grp78/BiP) in the ER lumen. The UPR consists of three branches, each regulated by distinct transmembrane sensor proteins in the ER: PERK (top), ATF6 (middle), and PERK (bottom). The UPR integrates all three pathways to produce a stress response that results in both translational attenuation of new protein synthesis and transcriptional activation of stress response genes in the nucleus to relieve ER stress. Adapted from [334].

factor, and ER retention and release is also controlled by BiP (Figure 5). Upon stress, ATF6 is released and transported to the Golgi, where it is cleaved by Golgi-resident proteases, first S1P (site 1 protease) and then S2P (site 2 protease), releasing the DNA-binding and transcriptional domains to the nucleus, where it binds to the ATF/cAMP response element (CRE) and to the ERSE to activate gene expression [46,50]. Other related bZIP-containing transcription factors localized at the ER membrane have been identified, such as Luman/LZIP/CREB3 and CREB4 (cyclic AMP-responsive element binding protein 3/4); OASIS (or CREB3-like-1); and the liver-specific CREBH [50]. Finally, PERK is also an ER-localized type I transmembrane protein with a cytoplasmic kinase domain that undergoes activating *trans*-autophosphorylation upon dimerization in ER stressed cells. PERK is responsible for phosphorylation of the α-subunit of the eukaryote translation initiation factor-2 (eIF2α), which inhibits translation activity (Figure 5) [50]. A global reduction in protein translation reduces the load of newly synthesized proteins, many of which are destined to the ER, alleviating ER stress and contributing to a re-establishing of homeostasis. Paradoxically, in addition to translation attenuation, PERK-mediated eIF2α phosphorylation contributes to translation of the fundamental transcription factor ATF4 (activating transcription factor 4, Figure 5), which in turn upregulates amino acid transporters, redox enzymes such as ERO1 (ER oxidoreductin 1), and UPR genes that contribute to amplification of the UPR [46,48]. The ultimate response to stress is cell death by apoptosis, and is triggered if UPR fails to re-establish homeostasis, to protect the tissue or organism from accumulation of misfolded proteins [45,46,50].

Studies performed in *C. elegans* have given evidence for mitochondrial UPR (UPR^{MT}) that relies on the communication between the organelle and the nucleus [28,29]. Mitochondrial Hsp70 (HSP-6) and

Hsp60 are induced by conditions that perturb mitochondrial protein folding and processing, and by accumulation of reactive oxygen species, but not by impaired pathways involved in metabolism or ATP synthesis, suggesting that it is not a general response to mitochondrial dysfunction. However, it is not yet understood if UPR signaling in the mitochondria is activated by direct recognition of misfolded proteins by folding sensors.

Oxidative Stress Response

The redox state of the cell is also a fundamental aspect for homeostasis. The exposure of cells to conditions of oxidative stress leads to accumulation of oxidized-modified molecules, such as carbonylated proteins, lipids and DNA; and predisposes the organism to age-related disorders. Reactive oxygen species (ROS) can be generated exogenously or produced within cellular compartments. Under a set threshold, intracellular generation of ROS has important physiological roles in defense against infection, regulation of cell proliferation, and signaling mechanisms in situations of metabolic stress [51]. Multiple metabolic pathways and cytosolic enzymes contribute to ROS production but the primary source is the mitochondrial electron transport chain, in particular complex I (NADH dehydrogenase) and complex III (ubiquinone-cytochrome c reductase) [51]. Separately, the lumen of the ER is also an oxidizing environment for protein folding and disulfide bond formation, which uses molecular oxygen as the terminal electron acceptor, posing potential for ROS production [52,53]. ROS can also result from exposure to UV radiation, chemotherapeutic agents, hyperthermia and growth factors among others, that perturb the cellular redox state. Oxidative stress increases leakage of Ca^{2+} from the ER lumen, which in turn stimulates mitochondrial permeability, cytochrome C release, disruption of the respiratory chain at the complex III, and even apoptosis. It is the balance between ROS production and the anti-oxidant defenses that determines the degree of oxidative stress [51]. The central mediators of anti-oxidant defense response, include ERK (extracellular signal-regulated kinase), JNK, MAPK (p38 mitogen-activated protein kinase), (NF)-κB nuclear factor and p53 signaling cascades, in addition to the HSR. Altogether, these pathways contribute to the expression of the anti-oxidant enzymes superoxide dismutase (SOD), catalase, thioredoxin reductase glutathione peroxidase (GPX) and peroxiredoxins [51,52]. In *C. elegans*, the transcriptional regulator SKN-1 is important for oxidative stress resistance and regulates the expression of a particular group of anti-oxidant response genes: SOD, GSTs (glutathione S-transferases), cytochrome P450 family proteins, catalase, and also Hsp genes [51,54-57].

1.3. The Protein Homeostasis (Proteostasis) Network

Protein homeostasis, or proteostasis, is by definition, “the state of dynamic equilibrium between protein synthesis, folding and degradation, that allows for the conformational flexibility necessary for function and stability of the proteome” [58,59]. The network of cellular processes that regulate and maintain normal protein folding and function is referred to as the proteostasis network (PN). As a biological network, the PN is defined by nodes (or proteins) and edges (or protein interactions) that broadly cover the processes of protein synthesis, folding, trafficking and degradation. Although largely centered on QC and

the core Hsp70 and Hsp90 chaperone systems in the cytosol and their homologs in the ER, additional network components include metabolic enzymes that influence folding efficiency by regulating availability of organic/inorganic solutes and ligands that promote and stabilize specific conformations [5]. The PN relies on stress sensors and the stress inducible pathways to maintain homeostasis upon different stimuli (system perturbations), and is adjusted through the signaling pathways UPS, UPR, HSR, oxidative stress response, diet restriction, and inflammatory signaling. The PN functions to promote successful development and aging of an organism, by preventing disease amidst constant intrinsic and environmental challenges, by maintaining system homeostasis. Proteome stability is constantly challenged by stimuli (perturbations) like exposure to exogenous insults as well as intrinsic propensity for misfolding that rises with aging [60]. Proteostasis regulation also has a temporal component, as the network adapts to an ever-changing proteome during development and aging [58]. In addition to age-associated decline in PN function (see below), proteostasis maintenance does not seem to be equal in all cells and tissues, as some cell types such as the neurons seem be particularly sensitive to the toxicity of misfolded and aggregation-prone proteins. This seems to be consistent with the late onset of many neurodegenerative disorders. Emerging strategies are focusing on restoring and increasing the network efficiency to prevent or delay the onset, and alter the clinical course, of conformational diseases [58,61].

2. Protein Misfolding Disorders

There is still limited understanding of how protein misfolding and aggregation cause cellular toxicity. Mutations that lead to conformational changes and ultimately to disease do so by either destabilizing the normal protein conformation and function (loss-of-function), favoring premature degradation; or instead by promoting aggregation. In the later case, misfolded proteins may become toxins to cells as a result of their ability to perturb the proteostasis machinery (gain-of-function) [62]. An increasing number of diseases are now recognized to be associated with protein misfolding and aggregation, and the pathological mechanisms start to converge on the inability of the PN to prevent toxicity.

2.1. Protein Loss-of-Function

Protein loss-of-function is typically caused by inherited mutations leading to inefficient folding and premature degradation by the cellular clearance machinery. Mutant proteins destined to the secretory pathway, which fold slowly, have trafficking defects, and are degraded prematurely, are over-represented in loss-of-function genetic diseases [63-65]. Two examples are described. The Cystic Fibrosis transmembrane conductance regulator (CFTR) functions as a cAMP-regulated chloride (Cl^-) channel in the apical membrane of epithelial tissues. Cystic Fibrosis (CF) is an inherited disease of epithelial tissues dominated by chronic lung disease, caused primarily by point mutations that disrupt CFTR folding and

export from the ER to the cellular membrane [66,67]. Over 90% of CF patients carry at least in one allele the Phe508 deletion (F508del) in CFTR that leads to a severe form of the disease. F508del-CFTR folding is kinetically impaired as the mutant fails to acquire the proper conformation at the ER and is maintained bound to chaperones until it is targeted for ERAD. CFTR is a primary example in which point mutations disrupt the folding process, leading to retention and degradation of a still partially functional mutant form of the protein [68]. This is a case where the inability vs. ability of the mutant protein to achieve its functional conformation or destination is dependent on the cohort of chaperones involved in the process. Another example of loss-of-function disorders are the lysosomal storage diseases caused by the inability of mutant lysosomal enzymes to fold in the ER, rendering them susceptible to ERAD and leading to the accumulation of the enzyme substrates in the lysosomes [69]. The most prevalent lysosomal storage disease is Gaucher's disease, caused by the inefficient folding of variants of β-glucocerebrosidase (β-Glu). This results in the accumulation of glucosylceramide, the β-Glu substrate, in the lysosomes of several cell types, leading to disease. As for CFTR, many Gaucher's disease-associated mutant enzymes show sufficient stability and activity in the lysosome, provided they can fold in the ER and be transported to the lysosome [69]. Studies of these diseases reveal that "adjustment" of the chaperone machinery and PN can distinguish between a deleterious mutation and a "tolerable polymorphism", to the point of rescuing normal function and prevent disease phenotypes. Current therapeutic interventions focus on developing compounds that pharmacologically target the QC machinery to increase folding capacity, or substrate-specific compounds that promote folding or stabilize the protein in order to prevent premature degradation [63,65,69].

2.2. Protein Toxic Gain-of-Function and Aggregation

Partially folded or misfolded species that are not readily degraded often tend to self-associate. Hydrophobic forces lead to the formation of amorphous structures in a concentration-dependent manner, a process known as protein aggregation, leading to cellular dysfunction and degeneration. Alternatively, aggregation may consist of the formation of ordered, fibrillar assemblies called amyloid, with a characteristic thermodynamically stable cross-β-structure [4,6]. Neurodegenerative diseases, also called amyloidoses, are some of the most debilitating disorders and include a large number of 20 diseases affecting thinking, movement, cognition and memory [70]. These disorders share common pathological mechanisms and features like inherited origin, late appearance in life and neuronal loss by programmed cell death or apoptosis. These are common and prominent features in Alzheimer's disease (AD), Parkinson's disease (PD), and Amyotrophic Lateral Sclerosis (ALS) (Figure 6). Another group of diseases, known as polyglutamine (polyQ) diseases, are characterized by the expansion of polyglutamine repeats in otherwise unrelated proteins, and include Huntington's disease (HD), spinocerebellar ataxias 1, 2, 3, 6, 7, 17, spinal and bulbar muscular atrophy, and dentatorubral and pallidoluysian atrophy. In addition, muscular dystrophies, metabolic disorders (type II diabetes), and certain cancers are also associated with protein misfolding/aggregation [15,71,72]. Although the initiating aggregation-prone protein for each disease differs in sequence, function and expression patterns, the appearance of aggregates represents an early event

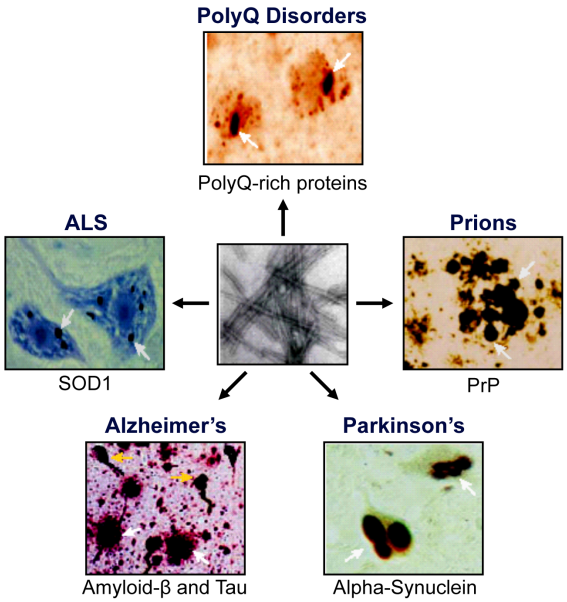

Figure 6: Protein aggregation in neurodegenerative diseases. Amyloid deposits, neurofibrillar tangles and amorphous protein aggregates are forms of protein aggregation, a common characteristic of a group of human neurodegenerative diseases, including polyglutamine disorders, Parkinson's disease, Alzheimer's disease, Prion (PrP) diseases and ALS. These proteins misfold and accumulate in the form of fibrillar polymers, as depicted in the center image. Adapted from [73].

associated with cellular toxicity and symptoms' onset (Figure 6) [62,70,73]. In AD, beta-amyloid peptide (Aβ) plaques are deposited extracellularly in the brain and neurofibrillar tangles composed of hyperphosphorylated Tau protein accumulate in the cytoplasm of degenerating neurons. In PD, aggregates of alpha-synuclein protein (Lewy bodies) are observed in the cytoplasm of brain neuronal cells. Alpha-synuclein toxicity is thought to derive from ER stress, vesicle trafficking defects, impairment of the UPS and mitochondrial dysfunction [74]. In HD patients, the prominent feature is intra-nuclear deposits of polyQ-expanded huntingtin protein (Htt). The molecular pathogenic mechanisms of HD remain poorly understood, but transcriptional, ER and autophagy disruption as well as dysregulation of synaptic function have been described [75,76]. There is an inverse exponential correlation between glutamine (CAG) repeat length in the Htt gene and age of disease onset and severity, with a threshold set at around 39 CAG repeats for disease-causing variants (Figure 7) [77]. There is also considerable individual variation in age of onset within a given repeat-length range, which points to the role of other genetic and environmental factors (Figure 7) [78]. Amongst polyQ diseases, even for the same polyQ length, there are differences in severity and age of disease onset, implicating the polyQ flanking sequences and genetic and environmental factors as modulators of disease [79]. In the inherited/autosomal dominant form of ALS (FALS, 2% of ALS cases), aggregates mainly composed of mutant superoxide dismutase (SOD1) are found in cell bodies and axons of motor neurons, leading to disruption of the neuronal cytoskeleton and muscle atrophy. There is also considerable evidence for microglial role in pathogenesis, excitotoxicity and axonal transport defects, disrupted mitochondrial function and oxidative injury in disease progression [80,81]. In a somewhat different subclass of neurodegenerative disorders, are the diverse forms of transmissible spongiform encephalopaties characterized by the accumulation of protease-resistant aggregates of the prion protein (PrP) [70,73].

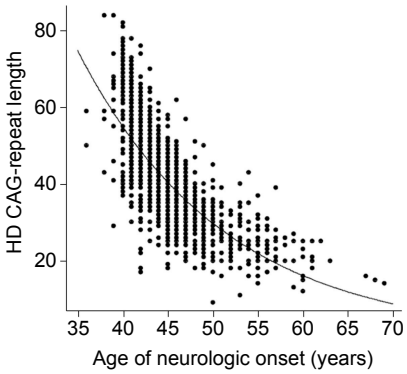

Figure 7: Inverse correlation between CAG-repeats and age of HD onset. The length of polyQ expansion in the Htt-encoding gene, correlates inversely with the age of disease onset. For a given CAG-length, the variability in neurological onset is attributed to other genetic and environmental factors. Adapted from [78].

Aggregation and Toxicity

The events that induce cell degeneration may be related to loss-of-function (lack of activity of the native protein), to gain-of-toxic-activity (neurotoxicity of the misfolded and aggregated protein), both, or due to inflammatory responses. In some diseases, a combination of these mechanisms may occur [73]. Although aggregates have been recognized as a typical feature of degenerative diseases and are usually present in the most damaged areas of the brain, it is not clear whether they are the direct cause of pathogenesis [73,82]. In fact, whether protein aggregates are a cause, a consequence or a by-product of toxicity is still unclear [20,83,84]. Aggregates are responsible for removing an otherwise recyclable pool of amino acids, may form structures that disrupt cellular functions, and can tie up cellular chaperones and proteases, saturating and impairing the QC system [85]. Recent work with artificially synthesized amyloid-like fibrils demonstrated that toxicity in human cells correlates with the propensity for interaction with other cytosolic proteins and to deregulate stress responses, chromatin organization, transcription, translation, and the QC components [86]. Extensive work with cells and animal models expressing the N-terminal mutant Htt fragment or polyQ alone, have also shown that essential cellular components are trapped by aggregates, including the transcription factor TATA binding protein (TBP) and CREB-binding protein (CBP), cytoskeletal proteins, molecular chaperones Hsc70, Hsp70, Hdj1 and Hdj2, as well as ubiquitin and proteasome components [84,87-89]. When the folding machinery is burdened with aggregation-prone proteins it can no longer properly assist other metastable proteins that require vigilant folding assistance for proper conformation [90]. These proteins, although innocuous under normal physiological conditions, can enhance aggregation of disease-related proteins, and contribute to the propagation of misfolding, toxicity and disease progression [75,86,90-95]. It is a “fatal chain of events” that is further enhanced by aging-dependent decline of proteostasis maintenance and reduced stress protection capacity [86].

The cytotoxicity of the oligomeric soluble states formed during aggregation has also been more carefully considered, as the question of the identity of the toxic species remains unanswered. Current evidence suggests that there are probably multiple toxic conformations (Figure 8). It was initially thought that large amyloid-like protein deposits were the species responsible for brain damage, but this was challenged by histopathological, biochemical and cell biological studies that show that large inclusions correlate poorly with onset and severity of neurodegeneration [62,73,96-98]. For example, cerebral damage in the YAC128 mouse HD model was detected in the absence of inclusions [99]. Others have

shown that the presence of soluble Htt oligomers in cultured striatal neurons was a better predictor of cell death: appearance of nuclear Htt inclusions was insufficient to cause neurodegeneration, and accelerated cell death was associated with a reduction in inclusions [100,101]. Likewise, in cell models of PD, expression of α-synuclein showed enhanced toxicity when the formation of inclusion bodies was reduced [98]. In human brains, soluble Aβ showed a higher correlation with the severity of AD than the accumulated insoluble plaques [102-104]. Taken together, these examples support a role for the soluble oligomeric species in toxicity [93,100,105,106]. Biophysical studies have demonstrated that diverse species with progressive degrees of aggregation are present simultaneously and in dynamic equilibrium with each other (Figure 8), making it difficult to evaluate the relative contribution of different species to disease progression [70,107-110]. Recently, synthesis of antibodies that recognize specific types of oligomeric conformations has shed some light on the role of these species on degeneration. The intermediate species formed by different proteins can be recognized by the same antibodies, suggesting a common intermediate motif that is independent of amino acid sequence but shared by the distinct protein oligomeric states [111,112]. Others have also shown that the soluble intermediates have a toxic 'gain-of-function' and that amyloid aggregates may recruit these toxic species, to prevent interaction with other cellular entities [62,72]. Therefore, the formation of protein inclusions may actually serve a cytoprotective function, as part of a cellular organized response when the QC has been overrun [15]. The most accepted hypothesis is that both soluble misfolded intermediates and amyloid-like deposits are toxic, perhaps by different mechanisms.

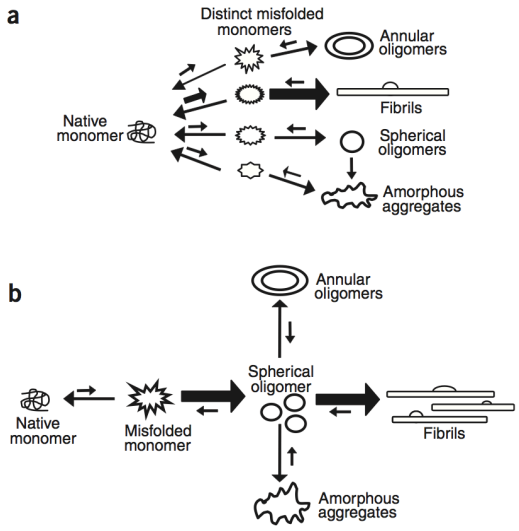

Figure 8: Two models of assembly of misfolded proteins into amyloid-like fibrils or amorphous aggregates. These are predictions for assembly of expanded polyQ proteins. (a) Monomers may co-exist in multiple misfolded conformations, each one originating a specific type of 'aggregate'. However, only one conformer is the precursor of fibrils (most stable), whereas other types of aggregates are metastable by comparison. (b) Oligomeric species are obligatory intermediate precursors of higher order aggregates, including fibrils. Thicker arrows denote, in the polyQ model, the propensity for fibril formation. Figure from **[193]**.

2.3. The Aging Component

The aging process is regulated by transcription factors and signaling pathways that include insulin-like peptides, the insulin-like growth factor (IGF), lipophilic signaling molecules, and sterols [113]. Among the best-characterized genetic regulatory pathways is the insulin-like signaling (ILS) pathway in the worm

C. elegans, the fly *D. melanogaster* and the mouse *M. musculus* [113,114]. The insulin-like growth factor 1 (IGF-1) is a hormone similar to insulin that binds to the insulin-like growth factor 1 receptor (IGF1R, receptor tyrosine kinase). Binding to IGF1R initiates an intracellular signaling cascade, with activation of the AKT signaling pathway and inhibition of the FOXO (forkhead box O) transcription factor by phosphorylation. This pathway has been extensively studied in *C. elegans*, where the *daf-2* gene encodes the only IGF1R and where IGF-1-mediated signaling regulates cell growth and development, DNA synthesis, resistance to oxidative stress, thermo tolerance, resistance to hypoxia, resistance to bacterial pathogens, and neuroendocrine signaling. Activation of the DAF-2 initiates a kinase cascade that includes AGE-1 (phosphatidylinositol 3-kinase/PI(3)K homolog), AKT-1 and AKT-2, PDK-1 and SGK-1 (homologous to serum and corticoid-responsive kinase); and results in phosphorylation and repression of the forkhead transcription factor DAF-16 (FOXO-like) activity [115]. DAF-16 positively regulates longevity determinants and is also a key regulator of heat and oxidative stress resistance, fat storage, fertility and metabolism. Mutations in *daf-2* or *age-1* de-repress DAF-16, and non-phosphorylated DAF-16 is translocated to the nucleus to promote longevity and stress resistance [113,116].

Aging is associated with progressive decay in physiological function and homeostasis. At the molecular level, aging is characterized by a gradual accumulation of deleterious modifications in nucleic acids, proteins, lipids and carbohydrates, together with a decline in the capacity to maintain proteostasis [28,58,60,92]. Alterations in the cellular environment (oxidation, glycation, nitration) also contribute to altered physical and functional protein properties, and accumulation of damaged and disease-associated proteins [28]. Eventually, the chaperone system becomes saturated, leading to the failure of multiple cellular processes, revealing disease symptoms. This offers a plausible explanation for symptoms of many conformational diseases beginning late in life [28,117,118]. Therefore, there is an urgent need to identify the changes that occur in proteostasis regulation during aging, and to define a right homeostatic balance for maintaining or prolonging health span.

QC, Stress Responses and Aging

Aging is associated with a progressive failure in maintaining protein quality control, and reduction in capacity for HSR and UPR, leading to increase in the frequency of misfolding events and accumulation of misfolded proteins [28,60]. Both cytosolic HSR and the UPR^{ER} and UPR^{MT} responses depend on the detection of protein damage, transmission of 'stress signal' to the nucleus, upregulation of stress protective proteins and their translocation to the site of damage. Aging affects all these steps to compromise the overall response. Whereas the levels of HSF1 itself appear to not be affected, the HSR becomes impaired as an apparent result of deregulation of the signal transduction pathways involved [28,92]. Aging is also associated with an elevated expression of Hsp genes in the absence of other external stressors, consistent with the concept of aging as a form of chronic stress. Metastable proteins are a fraction of the proteome that is very sensitive to the gradual deterioration of the cellular QC, and by misfolding exacerbate disruption of protein homeostasis during aging [28]. Recent results obtained in the *C. elegans* model using folding sensor proteins harboring destabilizing temperature sensitive (TS) mutations [90] demonstrated that folding capacity decreases from early adulthood on, coincident with a sharp decline in stress

responses activation, which could be restored by upregulation of HSF-1 and DAF-16 [22,60,119]. Oxidative stress, mitochondrial dysfunction and compromised UPR^{MT} are also associated with aging and neurodegenerative disorders incidence [28,120]. In addition, saturation and inhibition of the proteolytic machinery and decreased autophagy are consequences of age-related increase in protein misfolding, and contribute to the decline in cellular homeostasis [24,28].

3. Genetic Modifiers of Protein Misfolding and Toxicity

The cause for toxicity, cell dysfunction and often cell death in diseases of protein conformation and neurodegeneration has been the focus of intense research. A complementary approach focuses on the incapacity of the PN to deal with the misfolded proteins and maintain homeostasis, to identify pathways that respond more or less efficiently to the stress posed by misfolding and aggregation. It is crucial to identify nodes and processes within the PN that can be modified genetically or chemically (pharmacologically) to enhance proteostasis function and prevent/delay disease onset. Human genetic studies have been able to provide limited mechanistic insight into the molecular processes that determine disease susceptibility, onset or progression. Studies that have identified gene alterations underlying disease pathology, as well as pathways that modify disease progression, have benefitted from the development of model systems (Figure 9).

3.1. *C. elegans* and Other Model Organisms

Much of our understanding of aging related events, stress responses, proteostasis function, and the link to disease, is offered by studies in cultured cells and the model organisms yeast (*S. cerevisiae*), worm (*C. elegans*), fly (*D. melanogaster*) and mouse (*Mus muluscus)* (Figure 9). Animal models provide critical testing platforms for both disease pathogenesis and for potential therapeutics. Mouse and cell culture models continue to complement clinical studies for their complexity and simplicity, respectively. In studying human diseases, one typically employs cell-based models to generate stably expressing lines that phenocopy cellular aspects of disease. However, in many cases, the response of the intact organism is not fully recapitulated in cultured cells because, intercellular physiological pathways and responses (e.g., neurotransmitter circuitry) are eliminated, and new parameters such as those used to immortalize cells are introduced, reducing the ability of cultured cells to mirror *in vivo* pathology. On the other hand, systematic and relatively high-throughput biological analysis approaches are poorly suited to rodent models of disease, and so researchers have turned to less complex model organisms such as nematode worms, fruit flies and yeast. The advantages of using these organisms are multiple but arise mainly from their well defined genetic characteristics, abundance, short life spans and tractability to genetic manipulation. Flies and nematodes combine sufficient complexity that allows investigation of both cellular and behavioral

Figure 9: Model systems for the study of human diseases of protein misfolding.

phenotypes, with simplicity that facilitates rapid, high-throughput testing of hypotheses [121]. Fortunately, despite marked anatomic divergence, basic cell biological processes are highly conserved between nematodes, flies and mammalians. Most importantly, genotype-phenotype correlations of misfolding diseases are recapitulated in the simple model organisms and, in a number of cases, disease gene orthologs have been identified and studied [122,123]. These systems have provided genetic instruments to model aggregation and toxicity of misfolding disease-related proteins, and to identify modifiers of both cellular and behavioral phenotypes, with a relative ease of technical manipulation [119,124-131]. Since a major feature of all of the protein-misfolding diseases is that they manifest late in life, an important practical advantage of using these models is that, while they do show a well-defined biology of aging, they have a short lifespan that enables the progressive stages of age-related disease pathology to be monitored (Figure 10) [132]. The low cost, rapid generation time, and large repertoire of genetic tools available with these models allow speeding the progress of study of genes and pathways involved in complex physiological processes and pathology, and identifying promising therapeutic candidates for testing in mammals [28,133].

To fully understand the causes and consequences of protein misfolding, it is also relevant to find ways of bridging the conclusions drawn from model organisms and powerful *in vitro* biophysical and computational techniques. The molecular elucidation of protein aggregation has received great input from a large number of biophysical *in vitro* studies. These studies are carried out in the simplified environment of the test tube, but have yielded a great amount of information on protein sequence, intrinsic physical-chemical properties and perturbations that affect aggregation propensity [109]. The relevance of this data is then answered in the model organisms. Research has taken advantage of both classical techniques in biophysics and newly developed biological tools, to provide exciting new insights into the molecular determinants of the pathogenesis of protein-misfolding diseases [132].

Caenorhabditis elegans

C. elegans are approximately 1 mm transparent self-fertilizing roundworms of the phylum *Nematoda*, with a 3-day life cycle and a mean lifespan of approximately 18-20 days, when cultured at 20°C (Figure 10) [121,134,135]. In the laboratory, *C. elegans* can be readily cultured in large numbers on agar plates seeded with a lawn of *E. coli*. The adult stage is preceded by progression through embryonic development and four larval stages (Figure 10). Adult *C. elegans* have 959 somatic cells and the complete cell lineage, connectivity of the nervous system and nerve-muscle synaptic connections have been

determined [134]. The body wall consists of tough collagenous cuticle underlain by hypodermis, muscles, and neurons. Striated body wall muscles (BWM, 95 cells) are responsible for locomotion and non-striated muscles have an important role in the function of organs such as the pharynx, intestine, anus, uterus, gonad and vulva [135,136]. The nervous system of adult hermaphrodites is divided into pharyngeal and central nervous systems (longitudinal), and contains 302 neurons, 56 glial and support cells. In the adult worm, embryogenesis occurs in the uterus (Figure 10).

The establishment of C. elegans as a model system for fundamental biological research began in 1963 with the molecular biologist Sydney Brenner. C. elegans is now the best investigated multicellular organism and the standard laboratory strain is Bristol N2 [137,138]. This organism has been particularly advantageous in the functional analysis of human ortholog genes, in the study of aggregation-prone proteins associated with neurodegenerative diseases, in the characterization of physiological changes occurring during aging, in the characterization of stress response pathways in cell and tissue-specific manners, and in the study of the integration of signaling and stress pathways at the organismal level [60,90,119,131,134,135,139-148]. C. elegans is a highly tractable genetic model system that offers ease for genome-wide RNA interference (RNAi) analysis to identify comprehensive set of genes and processes that modulate the protein folding environment.

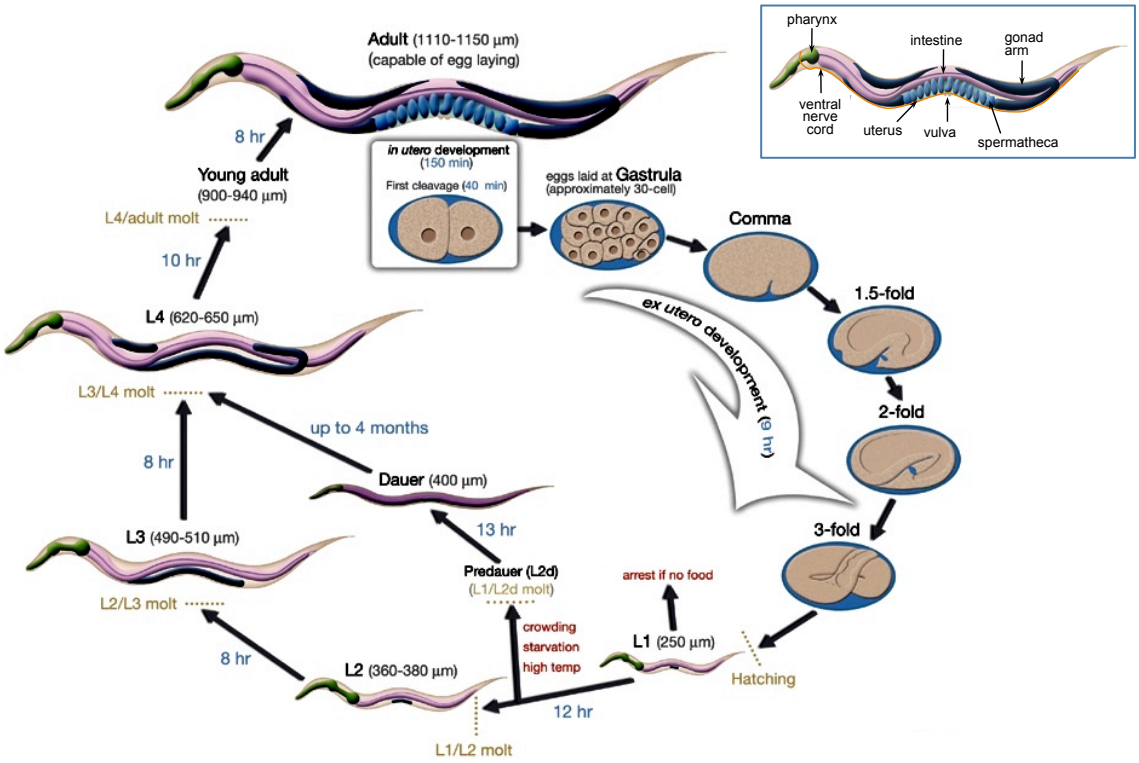

Figure 10: *C. elegans* anatomy (top right corner) and life cycle. *C. elegans* reproductive life cycle, from egg to egg-laying adult hermaphrodite animal. The complete life cycle takes approximately 3 days at 20°C. The insert is a schematic representation of some of the anatomical features of the adult *C. elegans*. Image from the WormAtlas.

3.2. Genetic Screens for Modifiers of Proteostasis Regulation

Model transgenic organisms, expressing human disease-related proteins, together with large-scale genetic screens, ranging from deletion libraries to genome-wide RNAi screens, have been exploited to elucidate the mechanisms of protein-misfolding diseases. The ease of culturing and screening in yeast, worm and fly models renders these organisms uniquely suited for unbiased high-throughput screens to identify novel modifier genes of disease phenotypes and uncovered the basal cellular processes that play a role in pathology [124-128,130,131,144,149-153]. Screens in *C. elegans* have used genome-wide RNAi libraries composed of about 17,000 bacterial strains expressing double-stranded RNA against almost every gene (reverse genetic screens) [154,155]. Screens for modifiers of aggregation initially took advantage of the transparency of *C. elegans* and the amenability of the body wall muscle cells for RNAi. Unfortunately, *C. elegans* neuronal cells are particularly refractory to the effect of gene knockdown by RNAi, and this poses a serious concern about the results from genetic screens, which may have missed genes with a specific role in neurons, the actual site where many misfolded proteins cause disease. In an attempt to identify these factors, mutant *C. elegans* strains hypersensitive to RNAi have also been used [156]. Alternatively, forward genetic screens in *C. elegans* are also a powerful tool to identify mutant gene alleles that modify disease phenotypes. EMS (ethane methyl sulfonate) is a chemical mutagen used to generate random genomic mutations that produce the phenotype of interest, followed by mapping and identification of the mutated gene [157].

An integrative comparison between genetic screens highlights alterations of a wide variety of basic cellular processes associated with protein aggregation-toxicity. The modifiers primarily cover QC proteins that maintain homeostasis and components of the stress response pathways, including the HSF-1 and DAF-16 transcriptomes. The largest common class of genes that act on the pathology of all disease proteins is that involved in protein degradation, followed by molecular chaperones. This is consistent with components of the ubiquitin proteasome system found to co-localize with aggregated proteins in the brain of patients, together with molecular chaperones [158,159]. Furthermore, a link between the molecular mechanisms of aging and protein misfolding is highlighted by screens that point to molecular pathways that regulate lifespan as modifiers of progression of misfolding phenotypes [22,119,130]. Moreover, processes involved in RNA processing, protein synthesis and cellular metabolism have been identified as modifiers of polyQ and SOD1 aggregation (Chapter II) [144], osmotic stress-induced protein damage [160], and heat-induced stress (unpublished), suggesting a core set of processes respond to general protein damage [161]. Notably, results from genetic screens have been successfully extrapolated to human neuronal cells as disease modifier genes. One example is offered by the *C. elegans* genome-wide RNAi screen for modifiers of polyQ aggregation, where TCP-1 chaperonin orthologs were identified [144]. Several studies later confirmed the role of this chaperonin in aggregation of mutant Htt in mammalian cells [93-95]. In a similar way, the ER-Golgi transport regulator, Rab1, identified in a yeast screen as a suppressor of α-synuclein toxicity, rescued different α-synuclein toxicity phenotypes in mammalian neurons [153]. These examples highlight the potential of genome-wide screens in simple organisms to provide

insight into the molecular mechanisms of neurodegeneration in humans. Despite the unifying theme of protein aggregation, the pathology of each disorder seems to be influenced by a disease-protein-specific subset of genes, in addition to an overall overlap in molecular pathways and functional classes to which individual modifiers belong [161]. The processes and genes identified represent potential targets for therapeutics of proteostasis enhancement.

mRNA profiling experiments have also identified genes that are differentially expressed following expression of disease proteins, but produce large sets of data that are not straightforward for extraction of relevant biological information. To bridge the gap between these two forms of high-throughput studies, an algorithm that integrates complementary genetic, physical and transcriptional data has been developed, connecting screen hits to differentially expressed genes and molecular interactions data, to reveal the functional context of genetic hits and additional proteins that participate in the response to misfolding and toxicity [162]. This algorithm (ResponseNet) has successfully provided functional context to many of the genetic hits identified in a screen for α-synuclein toxicity modifiers in yeast and complementary transcriptional data, and pointed to the involvement of several new cellular pathways in disease progression [162].

Cell Autonomous Regulation of Proteostasis

Molecular chaperones and the components of the degradation machinery are among the strongest and most consistent modifiers of protein aggregation and disease-related phenotypes, demonstrating that assistance in folding and the disposal of the misfolded species are crucial. Some features of the response to protein misfolding and aggregation are certainly cell autonomous, and this is the case for the activation of stress pathways that up-regulate folding and QC components [58,92,143]. Accordingly, biochemical data demonstrated that tissue- or cell-specific increase in the levels of chaperones, in particular members of the Hsp70 and TRiC/CCT families, enhances the solubility of polyQ proteins, inhibits the formation of toxic species and protect against cytotoxicity [15,89,94,163]. Overexpression of chaperones may also suppress toxicity by maintaining proper folding of silent mutations within the genome encoding metastable proteins, preventing propagation of proteome instability in the presence of aggregating proteins.

Cell Non-Autonomous Regulation of Proteostasis

The stress response was initially thought to be only a cell-autonomous response, initiated by the presence of misfolded proteins. However, multicellular organisms seem to sense stress differently than isolated cells, as exposure of an organism to stress conditions can result in a selective and asynchronous activation of the stress response in different tissues [143]. A growing body of work shows additional levels of regulation of stress responses at the organismal level, in a cell-non-autonomous manner. Results showing that perturbations of the insulin/IGF-1 pathway in one tissue cause alterations in other tissues to establish homeostasis, argue in favor of an organism-wide regulatory network. Studies in the model organism *C. elegans* have revealed that increase in the levels of the transcription factor DAF-16 in one tissue can increase DAF-16 activity in other tissues and extent organism life span [114]. Similar results have been obtained for HSF-1 and SKN-1. Furthermore, it is now known that cell-autonomous stress

responses are regulated by neuronal and endocrine signaling, yielding an integrated systemic response. The neuroendocrine signaling pathways include the ILS, the transforming growth factor-β (TGF-β) pathway and the nuclear hormone receptor (NR) [164]. Both neuronal and endocrine signaling are transduced to muscle and intestinal cells to improve stress resistance, folding and even lifespan [143,164,165]. Protein misfolding and aggregation within *C. elegans* muscle cells is also influenced cell non-autonomously by neuronal signaling pathways [166,167]. Recently, it has been put forward that perturbation of mitochondrial function in one tissue, specifically at the respiratory chain level, can be detected and have consequences in another tissue and organism life span through activation of the UPR^{MT}, revealing a cell-non-autonomous mitochondrial-mediated effect on longevity [120].

Genetic studies in multicellular model organisms have provided crucial information on the composition, function and hierarchical control of the proteostasis network, starting to unravel the organization of stress regulation at the organismal level, and new target genes and pathways to increase proteostasis maintenance. This aspect is of extreme relevance for the understanding of conformational disorders with tissue-specific pathogenesis and for the development of custom therapeutics.

4. Aims and Perspectives: From Model Organisms to Therapeutics

The cellular processes that ensure proteome quality and function, in normal and stress conditions, as well as during aging, are of great medical relevance since a growing number of conformational and late-age-onset diseases are linked to proteins that misfold and aggregate. Genetic screens and expression data from model organisms for human diseases have provided a wealth of information regarding genes and pathways associated with disease, as well as a cohort of PN protective components that function to prevent toxicity. Compilation and integration of this information still poses a challenge for understanding the processes compromised in disease and aging. One clear conclusion that can be drawn so far, however, is that overexpression of proteostasis core or accessory chaperone components increases folding capacity, and that the “new PN” is likely to have an enhanced protective capability [5]. Meanwhile, increasing information from the genetic screens offers new target genes that can reshape the PN to increase homeostasis maintenance capacity. A positive aspect of a highly integrative network such as the PN is that small readjustments of a single process seem to have global beneficial effects. Thus, pharmacologic up- or down-regulation of the capacity of the PN, by targeting key components such as molecular chaperones and/or protein clearance, provides an avenue for intervention in disease [168].

The complementarity between genetic and chemical modulation of proteostasis reveals great value for models organisms in the search for therapeutic options. Loss-of-function diseases are currently treated by intravenous administration of a wild-type (WT) version of the deficient protein to restore function. Protein replacement therapy is very limited because the injected protein must find its way to the appropriate cell type and to the relevant subcellular compartment through an endocytic trafficking pathway. For instance, in Gaucher’s disease, less than 5% of the injected β-Glu enzyme makes it to the lysosomes. Alternative strategies are clearly necessary when it comes to brain disorders, because recombinant

proteins do not cross the blood-brain-barrier [58]. Another challenge with loss-of-function misfolding diseases is to identify small-molecule pharmacologic agents that selectively or specifically enhance protein stability and function. Currently, pharmacological correctors cover chemical chaperones that mimic the effect of molecular chaperones and stabilize the folded state but in a rather unspecific manner (such as DMSO and glycerol); pharmacological chaperones that are substrate-specific and stabilize the protein of interest in a conformation that prevents premature degradation; and proteostasis regulator compounds (PRs) that modulate the levels and activity of specific chaperones to enhance folding efficiency [5,63,65,69]. PRs offer the advantage of expanding proteostasis capacity for numerous misfolding-prone proteins simultaneously. As an example, small molecule proteostasis regulators that increase the ER Ca^{2+} concentration were shown to enhance the capacity of calnexin to fold mutant β-Glu, increasing the probability of mutant β-Glu to engage the trafficking machinery and escape ERAD in Gaucher's disease. Similarly, proteostasis 'correctors' for CFTR that promote folding and export, and/or enhance activity of the partially destabilized channel are also under clinical trial [5].

Other emerging therapeutic strategies focus on developing pharmacologic chaperones that bind to and increase kinetic stability of proteins, to shift the equilibrium from aggregation to folding in diseases of toxic-gain-of-function [58,168]. Chemical inducers of the HSR and Hsp levels can have a significant effect in cellular and animal models of neurodegeneration [169] (Appendix III). PRs that activate the HSR through HSF1 include triptolide, quercetin, and celastrol [170,171]. Another emerging category of PRs are HDAC inhibitors (HDACi) that presumably function through regulation of gene transcription, by preventing histone deacetylation. Pharmacological activation of SIRT1 by resveratrol prolongs HSF1 binding to target promoters and enhances the HSR [172]. Nonetheless, caution is imposed by observations that HSR induction can have adverse effects in cells and tissues, as seen in rapid proliferating tumor cells. HSF1 is a potent modifier of tumorigenesis and, therefore, a potential target for cancer therapeutics. In fact, chaperone inhibitors, especially Hsp90 inhibitors, decrease cell proliferation in animal models, possibly by counteracting the high demand for folding in tumor cells, preventing growth of specific classes of cancer [5,58].

Here, we describe the work performed with *C. elegans* models of protein misfolding and aggregation to identify and characterize new genetic and small molecule modifiers of the PN function. The aim was to identify novel components of the PN that, when genetically down-regulated or targeted by small molecules, activate protective cell autonomous and non-autonomous pathways that enhance folding capacity, restoring homeostasis and cellular function.

Chapter II

A Genetic Screening Strategy Identifies Novel Regulators of the Proteostasis Network

A GENETIC SCREENING STRATEGY IDENTIFIES NOVEL REGULATORS OF THE PROTEOSTASIS NETWORK

M. Catarina Silva[1,2], Susan Fox[1], Monica Beam[1,3], Happy Thakkar[1], Margarida D. Amaral[2,4], and Richard I. Morimoto[1]

[1]Department of Molecular Biosciences, Rice Institute for Biomedical Research, Northwestern University, Evanston IL, USA
[2]Faculty of Sciences, Centre for Biodiversity, Functional and Integrative Genomics (BioFIG), University of Lisboa, Lisboa, Portugal
[3]Department of Biomedical Engineering, Northwestern University; Evanston, IL 60208-3500, USA
[4]Centre of Human Genetics, National Institute of Health, 1649-016 Lisboa, Portugal

PLoS Genetics, *In Press*

ABSTRACT

A hallmark of diseases of protein conformation and aging is the appearance of protein aggregates associated with cellular toxicity. We posit that the functional properties of the proteostasis network (PN) protect the proteome from misfolding and combat the proteotoxic events leading to cellular pathology. In this study, we have identified new components of the proteostasis network that can suppress aggregation and proteotoxicity, by performing RNA interference (RNAi) genetic screens for multiple unrelated conformationally challenged cytoplasmic proteins expressed in *Caenorhabditis elegans*. We identified 88 suppressors of polyglutamine (polyQ) aggregation, of which 63 modifiers also suppressed aggregation of mutant $SOD1^{G93A}$. Of these, only 23 gene-modifiers suppressed aggregation and restored animal motility, revealing that aggregation and toxicity can be genetically uncoupled. Nine of these modifiers were shown to be effective in restoring the folding and function of multiple endogenous temperature-sensitive (TS) mutant proteins, of which five improved folding in a HSF-1-dependent manner, by inducing cytoplasmic chaperones. This triage screening strategy also identified a novel set of PN regulatory components that, by altering metabolic and RNA processing functions, establish alternate cellular environments not generally dependent on stress response activation, that are broadly protective against misfolded and aggregation-prone proteins.

AUTHOR SUMMARY

A common characteristic of protein conformational diseases is the appearance of protein aggregates associated with late onset symptoms. Here, we have taken an unbiased genetic approach to test the hypothesis of whether protein aggregation and toxicity are co-linked genetic traits that are regulated by a common proteostasis network. To address this, we took advantage of the tractable genetic model *Caenorhabditis elegans* expressing expanded polyglutamines (polyQ), and performed a genome-wide RNA interference (RNAi) screen to identify genes that altered the proteostasis environment and suppressed aggregation and toxicity. These modifiers were subsequently tested on animals expressing mutant SOD1, and on animals expressing endogenous proteins with temperature-sensitive mutations. This screening triage resulted in the identification of nine genes with effects on protein folding, corresponding to new proteostasis pathways involved in metabolism and RNA processing functions.

INTRODUCTION

Protein misfolding is an intrinsic aspect of protein biogenesis that, under optimal conditions, is kept in check by the properties of the proteostasis network (PN), and upon stress, aging, and expression of aggregation-prone proteins causes cellular dysfunction that places the organism at risk for diseases of protein conformation. These are common and prominent features in Alzheimer's disease (AD), Parkinson's disease (PD), Amyotrophic Lateral Sclerosis (ALS), polyglutamine disorders such as Huntington's disease (HD), muscular dystrophies, metabolic disorders, and certain cancers [62,70-73]. Each disease is associated with its own characteristic set of aggregation-prone proteins that differ in sequence, function and expression patterns. Nevertheless, protein misfolding and aggregation have similar consequences to the cell with deleterious consequences on gene expression, protein synthesis, folding, trafficking, clearance, and cell signaling.

The PN of molecular pathways coordinates protein synthesis, folding, trafficking and clearance [58,61,92] and determines the fate of proteins that do not acquire a native conformation. The chronic expression of aggregation-prone proteins, as occurs in conformational disorders, not only affects the function of proteins harboring mutations, but also challenges the stability of the PN, leading to the amplification of protein damage and persistent proteotoxicity [59,70,86,90,91]. While protein aggregates and inclusions represent a prominent feature of many human diseases, it remains unanswered whether a cell responds identically to different protein aggregates. Elucidating the mechanism(s) by which misfolded proteins, oligomeric species, and/or aggregates interfere with cellular function represents a prominent challenge, given the complexity of the aggregation process, and the large number of cellular processes affected as proteostasis decline is propagated across tissues [58,86,98,173]. Many studies have indicated that large inclusions correlate poorly with onset and severity of neurodegeneration and support a role for the soluble oligomeric species in toxicity [96-100,103,173]. Although intermediate species formed by distinct proteins have been suggested to display common structural motifs, it has been difficult to evaluate the contribution of different types of oligomers to toxicity [112]. Furthermore, despite the common theme of protein aggregation, growing evidence suggests that the cause of toxicity for each disease may, in part, be specific to the subset of molecular processes affected by the aggregated protein [174].

An alternative approach to understanding the origin of toxicity in each disease is to identify genetic modifiers that suppress aggregation and prevent the accumulation of metastable and misfolded proteins by enhancing global folding capacity [5]. Multiple *in vitro*, cell-based, and animal model systems have been developed to investigate the molecular events underlying aggregation-driven toxicity and identify modifiers of disease phenotypes [119,140,141,175-180]. While mammalian model systems are notoriously challenging to perform genome-wide screens due to the differences in genetic background and environment, screens performed in *S. cerevisiae*, *C. elegans* and *D. melanogaster* have identified processes that maintain proteome stability, promote folding and clearance. These include among others, molecular chaperones, proteasome subunits, components of the autophagy machinery, and the stress-induced transcriptional regulators DAF-16/FOXO and HSF-1 [127,128,130,144,149,151,181,182].

Here, we established a screening strategy in *C. elegans* to identify novel genetic modifiers of proteostasis that reshape the network to increase the cellular capacity for folding, prevent protein aggregation and suppress toxicity. Our approach was to identify components of the PN, that when down-regulated, enhance the functional properties of the PN to restore folding stability of the various folding sensors employed in the screen. This approach was designed to complement our previous efforts to identify enhancers of misfolding by screening for genes that when down-regulated caused the premature appearance of protein aggregates [144]. We identified 63 genetic modifiers that suppressed both polyQ and mutant SOD1 aggregation in muscle cells, of which 23 also suppressed associated toxicity. Of these, 9 modifiers systematically reduced the misfolding phenotypes of endogenous temperature-sensitive proteins. These modifiers were then characterized for dependence on HSF-1 activation and expression of cytosolic chaperones to enhance folding. This study introduces new proteostasis modifiers with a global effect on the stability of the muscle cell proteome, with likely broader relevance for conformational disorders.

RESULTS

Screening Strategy for Genetic Modifiers of Protein Aggregation

We sought to determine whether modifier genes identified in a genome-wide RNAi screen for suppression of polyQ aggregation and toxicity in *C. elegans* would be efficacious on other disease-associated aggregation-prone proteins and endogenous metastable proteins. With this strategy, we tested the hypothesis of conserved modifier genes and pathways within the PN for protein misfolding and aggregation.

We initiated the screening strategy with a genome-wide RNAi screen to identify genes in *C. elegans* that when knocked down suppress aggregation of expanded polyQ::YFP fusion proteins expressed in body wall muscle (BWM) cells [119]. For this screen, animals expressing Q35 were used, as this is a threshold length for polyQ that exhibits adult onset protein aggregation and toxicity [119]. This screen was accomplished using a semi-robotic assay developed for feeding RNAi bacteria [155] to larval 1 (L1, day 1) stage Q35 animals [144]. During early development, Q35 protein is soluble in muscle cells until animals reach day 3 of age, when aggregation is first detected, and thereafter aggregation and toxicity increase with aging (Figure S1B, D) [119]. Therefore, we selected day 6, corresponding to three days after the onset of Q35 aggregation (Figure S1B), to perform the RNAi screen to identify gene knockdowns that led to suppression of polyQ foci, relative to the empty vector (EV) control. RNAi against *yfp* was used as a control for the efficiency of RNAi gene-knockdown (Figure 1A: VIII, XVI, XXIV; Figure 1C). The screen was highly robust and identified 151 genetic modifiers that suppressed Q35 aggregation (Figure 1A, Table S1). Of these modifier genes, 91 exhibited a strong suppressor effect on aggregation by reducing the number of Q35 foci by 60 to 80% in ≥75% of the RNAi-treated animals (Table S1, Figure 1C). The remaining 60

modifiers gave more variable results and were less effective as suppressors (*i.e.* observed in ~50% of the RNAi-treated animals with ~50% reduction in foci; Table S1).

We next used a counter-screen with animals expressing soluble Q24, as these animals do not exhibit aggregation or toxicity [119], to control for phenotypic changes caused by RNAi that are not related to aggregation, such as changes in YFP fluorescence, body morphology and size, egg-laying and sterility (Table S1). We observed that none of the Q35 aggregation modifiers had any effect on Q24 protein (Figure 1B), suggesting that the RNAi suppressor effect was not due to transgene silencing. The modifiers that did not meet these criteria or had deleterious consequences on animal development and viability were not studied further. Moreover, to assess whether suppression of aggregation was due to changes in polyQ expression, we examined mRNA and steady-state protein levels for a representative group of modifiers. We quantified the levels of *q35::yfp* mRNA by rt-PCR (Figure S2) and the levels of Q35::YFP protein by

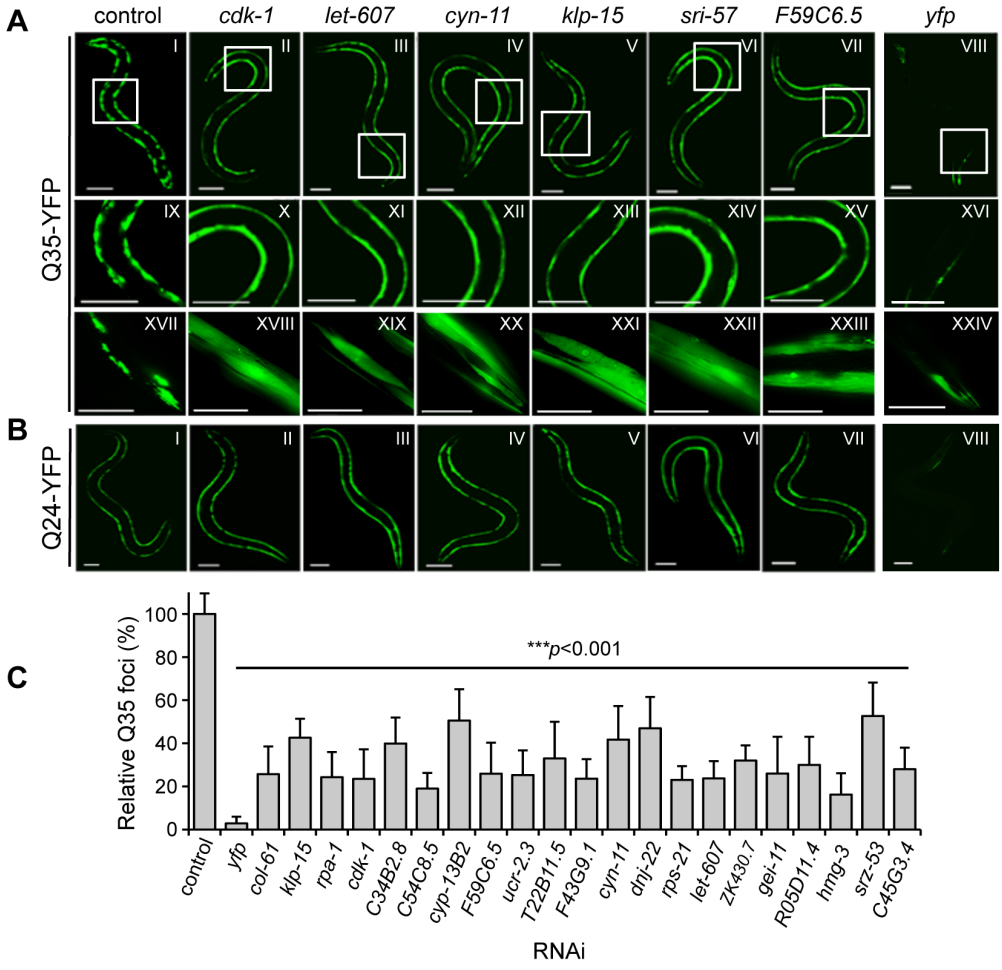

Figure 1. Genome-wide RNAi screen for suppression of Q35 aggregation. (A) Q35 animals (6 days old) show suppression of aggregation relative to EV control. Representative modifier genes: *cdk-1* (cyclin-dependent kinase); *let-607* (CREB/ATF transcription factor); *cyn-11* (cyclophilin); *klp-15* (kinesin-like protein); *sri-57* (serpentine receptor) and *F59C6.5* (NADH-ubiquinone oxidoreductase). *yfp*-RNAi is the control for RNAi efficiency. Panels IX-XXIV are higher magnification images of the boxed areas in I-VIII. Scale bars: 0.1 mm (I-XVI), 0.05 mm (XVII-XXIV)]. **(B)** Animals expressing soluble Q24 were used as a control for RNAi phenotypes dissociated from aggregation (scale bar 0.1 mm). **(C)** Q35 aggregate count (% foci relative to EV control) for a representative group of modifiers (±SD, *n*>3). Student t-test ***p<0.001 relative to control.

SDS-PAGE and western blot analysis (Figure 2A). The results show that, for the RNAi modifiers tested, suppression of aggregation occurred without affecting the polyQ mRNA or protein levels.

To obtain evidence that the suppression of visible Q35 aggregates corresponds to the appearance of soluble Q35 protein (Figure 1A), we used the dynamic imaging method of Fluorescence Recovery After Photobleaching (FRAP). Inclusion-localized Q35 corresponds to an immobile state with very limited fluorescence recovery following photobleaching (Figure 2B and C: Q35 control) [122,144], whereas the fluorescence of diffuse-looking Q35 in animals fed with modifier RNAi recovered immediately, consistent with a diffuse and soluble state analogous to soluble Q24 (Figure 2B *hmg-3* and C). These results provide biophysical evidence for Q35 solubility identified by the visual screening. We further examined the biochemical properties of Q35, for a representative group of modifiers, in total protein extracts. We found that the amount of aggregated polyQ protein detected using native PAGE analysis was reduced, and that the levels of soluble and diffuse species were increased(Figure 2D). Taken together, these results reveal that RNAi knockdown of specific modifier genes suppressed polyQ aggregation by maintaining the protein in a mobile soluble state.

The identity of the RNAi-targeted genes was verified by sequencing of the dsRNA plasmids, followed by Blast analysis in NCBI and Wormbase databases. The Q35 aggregation modifier genes are 88% conserved with predicted human orthologs, and can be grouped into seven functional categories of cell cycle, DNA synthesis and repair; RNA synthesis and processing; protein synthesis; protein folding and turnover; cell structure and protein trafficking; signaling; and energy and metabolism (Table S1, Figure S3A, B). The fraction of modifiers represented in each functional class is significantly distinct from their representation in the *C. elegans* RNAi library (Figure S3A, B) [155], indicating enrichment for cellular processes important for proteostasis.

We next asked whether the Q35 modifiers were effective on another polyQ model as a way to distinguish the most robust polyQ aggregation suppressors. This was done by screening a transgenic line expressing Q37::YFP. These animals exhibit a more rapid onset of aggregation relative to Q35 animals, between day 2 and 3 of age, together with a more rapid decline in motility (Figure S1A, B, D). These phenotypes are dependent solely upon the CAG-repeat length as the levels of Q35 and Q37 are identical (Figure S1C). Q37 animals were fed RNAi from L1 stage (day 1) and aggregation was examined on day 5, corresponding to two days post-aggregation onset (Figure 3A, B). Of the initial 151 modifiers of Q35 aggregation, only 88 of these also suppressed Q37 aggregation, of which 81 corresponded to the strongest Q35 suppressors (Table S1). We designated the set of common modifiers of Q35 and Q37 aggregation as Class A strong modifiers (Table 1); and the remaining 63 genes as Class B weak modifiers (Figure 3C).

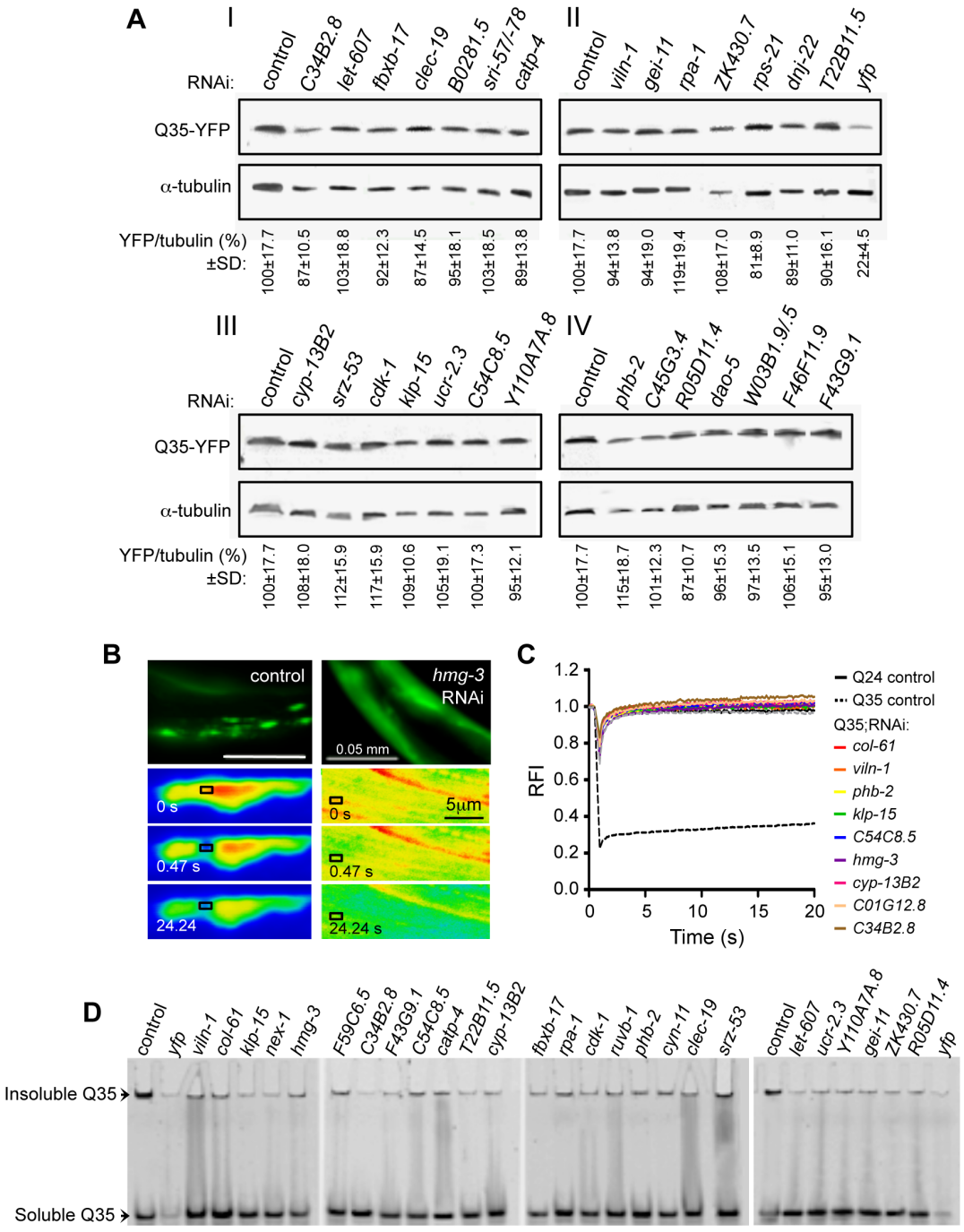

Figure 2. Suppressors of aggregation maintain polyQ in a diffuse state without affecting expression levels. (A) SDS-PAGE and western blotting analysis of protein samples from Q35 RNAi-treated animals (6 days old), immunoblotted with anti-YFP (32 KDa) and anti-α-tubulin (55 KDa) antibodies. Control refers to EV RNAi (I-IV). YFP/tubulin ratios were calculated from protein band intensities and are shown as an average % of the control (±SD, from ≥3 biological replicates, Student t-test $p>0.05$). *yfp*-RNAi in panel II is the positive control for reduced protein levels. **(B, C)** FRAP analysis confirms suppression of polyQ aggregation to a diffuse state. **(B)** Q35 protein was subjected to photobleaching in animals treated with control RNAi (left) or *hmg-3* RNAi (right) and fluorescence recovery was measured at the indicated time points. **(C)** Quantitative FRAP analysis indicates the relative fluorescence intensity (RFI) at each time point, and it represents an average of ≥12 independent measurements for each RNAi (5 for the controls). The soluble Q24 control is shown in black solid line, and the Q35 foci control in black dashed line. **(D)** Native PAGE analysis of whole protein extracts from 6 day old Q35 animals treated with RNAi. Q35 aggregated protein retained at the top of the gel was reduced by each of the modifiers tested.

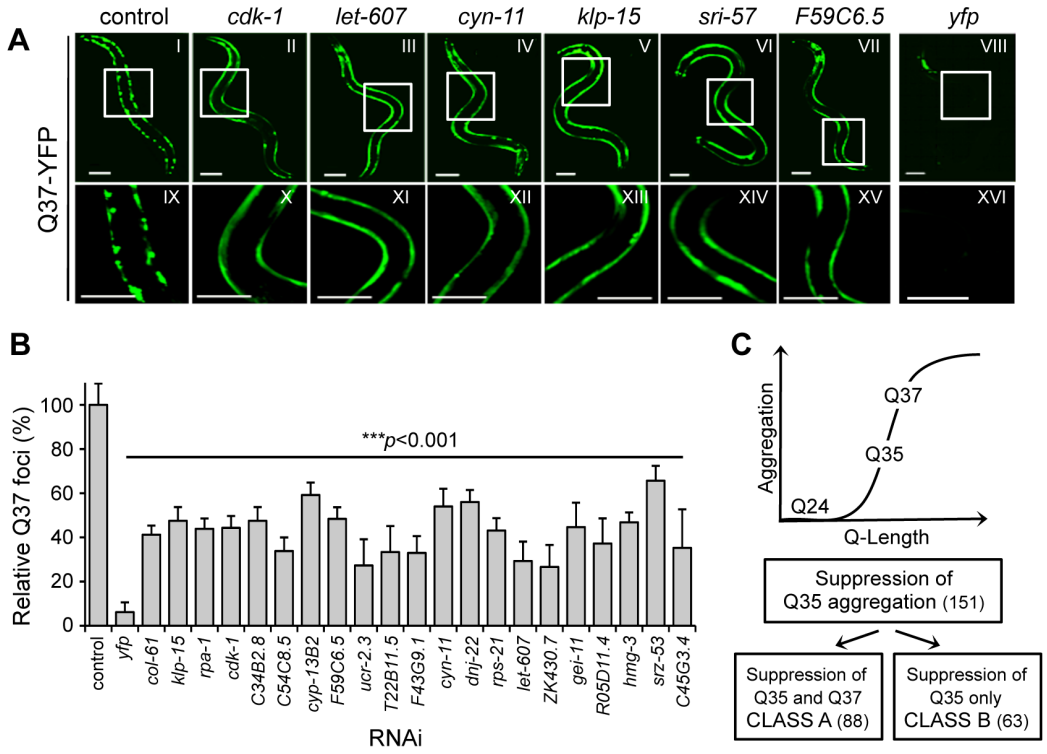

Figure 3. Common RNAi suppressors of Q35 and Q37 aggregation. (A) Counter-screen in 5 day old Q37 animals to identify the strongest suppressors of polyQ aggregation. Panels IX-XVI show a higher magnification image of the boxed areas on I-VIII. Scale bar is 0.1 mm. **(B)** Q37 aggregate count (% foci relative to EV control) for a representative group of modifiers (±SD, *n*>3). Student t-test ***p<0.001 relative to control. **(C)** Screen strategy: genome-wide screen with the threshold Q-length for aggregation Q35, and counter-screens with the soluble Q24 and the higher Q-length Q37 strains. Class A refers to Q35 and Q37 common strong modifiers, and Class B to modifiers only affecting Q35.

Identification of Common Modifiers of PolyQ and Mutant SOD1 Aggregation

We next tested whether the genetic modifiers of polyQ aggregation would be effective on yet another model that expresses the mutant human SOD1^{G93A}. This model shows aggregation onset during embryonic development and a distinctive pattern of foci that persists throughout adulthood (Figure S1E, F) [91]. Of the 88 polyQ aggregation modifiers, 63 also suppressed mutant SOD1^{G93A} aggregation in 5 day old animals (Figure 4A, Table S1), without causing phenotypic changes in SOD1^{wt} animals (not shown). A subset of these common aggregation suppressors were also examined by SDS-PAGE and western blot analysis, and shown not to reduce steady-state protein levels of SOD1^{G93A} (Figure 4B). 95% of the mutant SOD^{G93A} suppressors belong to the polyQ Class A modifiers (Table S1). Unlike Q35 aggregation that is only detected in young adult animals, mutant SOD^{G93A} aggregation occurs in embryos [91], and yet many Class A modifiers were effective suppressors of SOD1 aggregation providing additional support that Class A modifiers are robust modifiers of protein folding. Moreover, these modifiers, that are common to polyQ and SOD1, exhibit a similar overall distribution into functional classes (Figure S3C) as was described for modifiers of polyQ aggregation (Figure S3B), thus identifying new modifier pathways that are common to protein aggregation.

We propose that these new modifiers can either suppress aggregation directly by affecting cellular processes that mediate aggregate formation, or indirectly by altering some aspect of the PN that confers a protective action that increases folding. To distinguish between these two possibilities, we employed genetic tests to determine which modifiers reflect an improvement of the folding environment, by reducing misfolding and associated toxicity.

Table 1: Overview of the modifiers that suppress Q35 and Q37 (Class A) aggregation in *C. elegans* BWM cells.

Process (# Genes)	Molecular Function (# Genes)	Gene
Cell Cycle DNA Synthesis and Replication (8)	Cell Cycle (1)	*cdk-1*
	DNA recombination (2)	*fbxb-11; fbxb-17*
	Meiosis (1)	*F46F11.9*
	Replication (4)	*mcm-2; rnr-2; rpa-1; ruvb-1*
Cell structure and Protein transport (6)	Cellular matrix, cuticle (4)	*ppn-1; col-61; col-69; viln-1*
	Vesicle trafficking (2)	*klp-15; nex-1*
Energy and Metabolism (17)	Metabolism (9)	*C50D2.2; R03D7.1; C47F8.4; C54C8.5; D2030.1; elo-2; W06H3.3; F43G9.1; T22B11.5*
	Electron transport chain (5)	*C34B2.8; F59C6.5; ucr-2.3; cyp-13B2; cyp-33D1*
	Ion transport (2)	*B0281.5; catp-4*
	Mitochondrial function (1)	*F43E2.7*
Protein Folding and transport (7)	Chaperone (6)	*F08H9.3; cyn-11; cyn-12; C30C11.4; dnj-22; phb-2*
	Protein glycosylation (1)	*tag-335*
Protein Synthesis (10)	Mitochondrial ribosome (3)	*C26E6.6; F33D4.5; mrpl-41*
	Ribosomal protein (3)	*rpl-2; rpl-35; rps-21*
	Translation (4)	*krs-1; F17C11.9; H19N07.1; R05D11.4*
RNA Synthesis and Processing (13)	Nucleosome binding (2)	*hmg-3; hmg-4*
	Ribosome biogenesis (1)	*C15H11.9*
	RNA processing, splicing (5)	*F13H8.2; fib-1; let-716; ZK430.7; Y110A7A.8*
	Transcription (5)	*C55A6.9; K03F8.1; fkh-6; gei-11; let-607*
Signaling (10)	Receptor protein (6)	*dao-5; xpo-1; sri-57; sri-78; srz-53; T11F1.6*
	Transduction (4)	*clec-19; pdl-1; rgl-1; W03B1.9*
Unknown (17)	Unknown (17)	*C23G10.10; C45G3.4; F14B8.2; F26E4.2; F47F2.3; K02E7.11; ptr-19; R05D7.2; ril-1; smu-1; T04D3.5; vab-19; F53F10.1; W03B1.5; Y51H7BR.3; fbxa-76; F54C4.3*

Suppression of Aggregation Can Be Uncoupled From Toxicity

Protein aggregation is a common feature of many diseases; however, the relationship between aggregation and cellular toxicity remains controversial. The appearance of aggregates and inclusions has been linked both to cellular dysgenesis and toxicity, as well as protection from toxicity [96-100,103,173]. Therefore, we took advantage of an unbiased genetic approach to test the relationship between suppression of aggregation and toxicity. Because the initial genetic screens were based solely on aggregation phenotypes, we were able to subsequently perform cellular toxicity assays to assess this relationship.

Relative to wt animals or animals expressing soluble polyQ (Q24), Q35 animals exhibit muscle dysfunction resulting in a 40% loss of motility at 6 days of age (Figure S1D) [119]. Therefore, we quantified

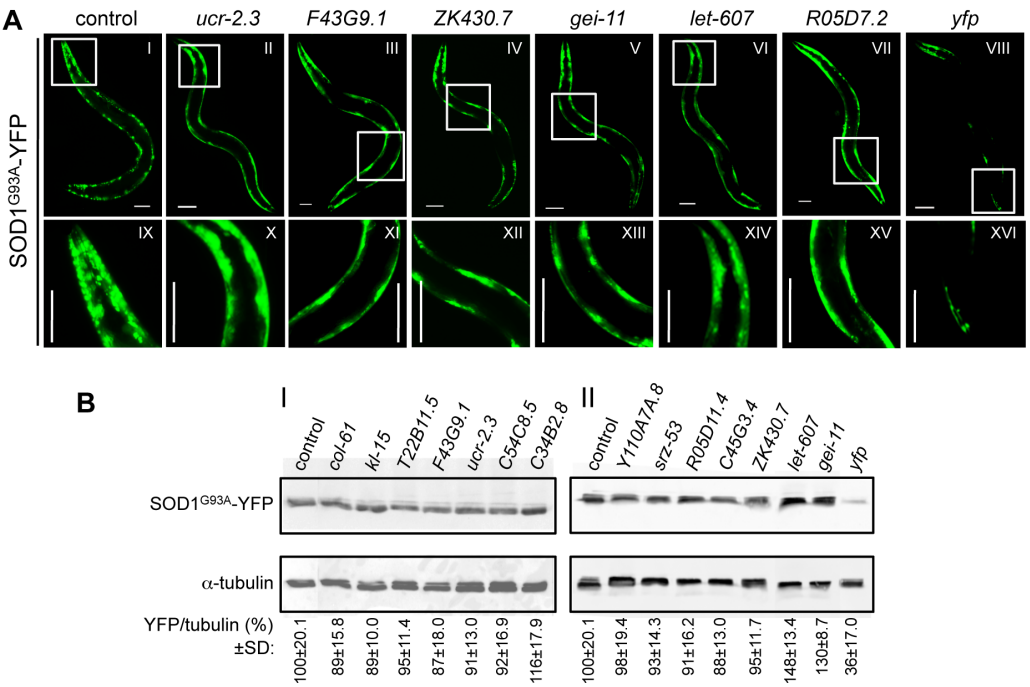

Figure 4. PolyQ aggregation modifiers tested in the mutant SOD1^{G93A} model. **(A)** Representative RNAi suppressors of SOD1^{G93A} aggregation: *ucr-2.3* (ubiquinol cytochrome c reductase); *F43G9.1* (isocitrate dehydrogenase); *ZK430.7* (sof1-like rRNA processing protein); *gei-11* (GEX-3-interacting protein, Myb transcription factor); *let-607* (CREB/ATF transcription factor); *R05D7.2* (unknown) and *yfp* RNAi control. Higher magnification images (IX-XVI) of the boxed areas (I-VIII) show reduced number of SOD1^{G93A} foci in animals treated with RNAi, relative to the EV control. Scale bar is 0.1 mm. **(B)** SDS-PAGE and western blotting analysis of protein samples from SOD1^{G93A} RNAi-treated animals (5 days old), immunoblotted with anti-YFP (32 KDa) and anti-α-tubulin (55 KDa) antibodies. Control refers to EV RNAi. YFP/tubulin ratios (bottom) were calculated from protein band intensities and are shown as an average % of the control (I, II) ±SD, from ≥3 biological replicates (Student t-test p>0.05). *yfp*-RNAi (II) is the positive control for reduced protein levels.

the motility of RNAi-treated Q35 animals as a measure of polyQ-associated cellular toxicity, using an automated worm tracker system analysis, validated by manual methods. As a reference positive control for toxicity suppression, we showed that motility was restored to near wt levels by knockdown of the Q35 transgene expression with *yfp*-RNAi (Figure 5A). All 88 Class A modifiers were tested for effects on the motility of Q35 animals and wt control animals (Table S2). Because we sought to identify improvement of motility directly associated to suppression of Q35 aggregation, we excluded any modifier that, alone, had effects on the motility of wt animals. Of the 88 modifiers tested in wt animals, 33 gene knockdowns (37%) affected the motility of wt animals (Figure 5B), and were excluded from further analysis. For the remaining 55 modifiers, 42% improved the motility of Q35 animals to wt levels, 36% had no effect, and 22% enhanced the toxicity of Q35 (Figure 5A). These results revealed that suppression of aggregation, as detected by visual, biophysical, and biochemical measures, does not necessarily predict that the physiological health of the cell will be restored. The genetic uncoupling between aggregation and toxicity further reinforces previous similar observations [96,98,173]. Taken together, the toxicity in diseases of protein conformation is the outcome of a complex series of misfolding events, involving multiple species and aberrant interactions within the cell.

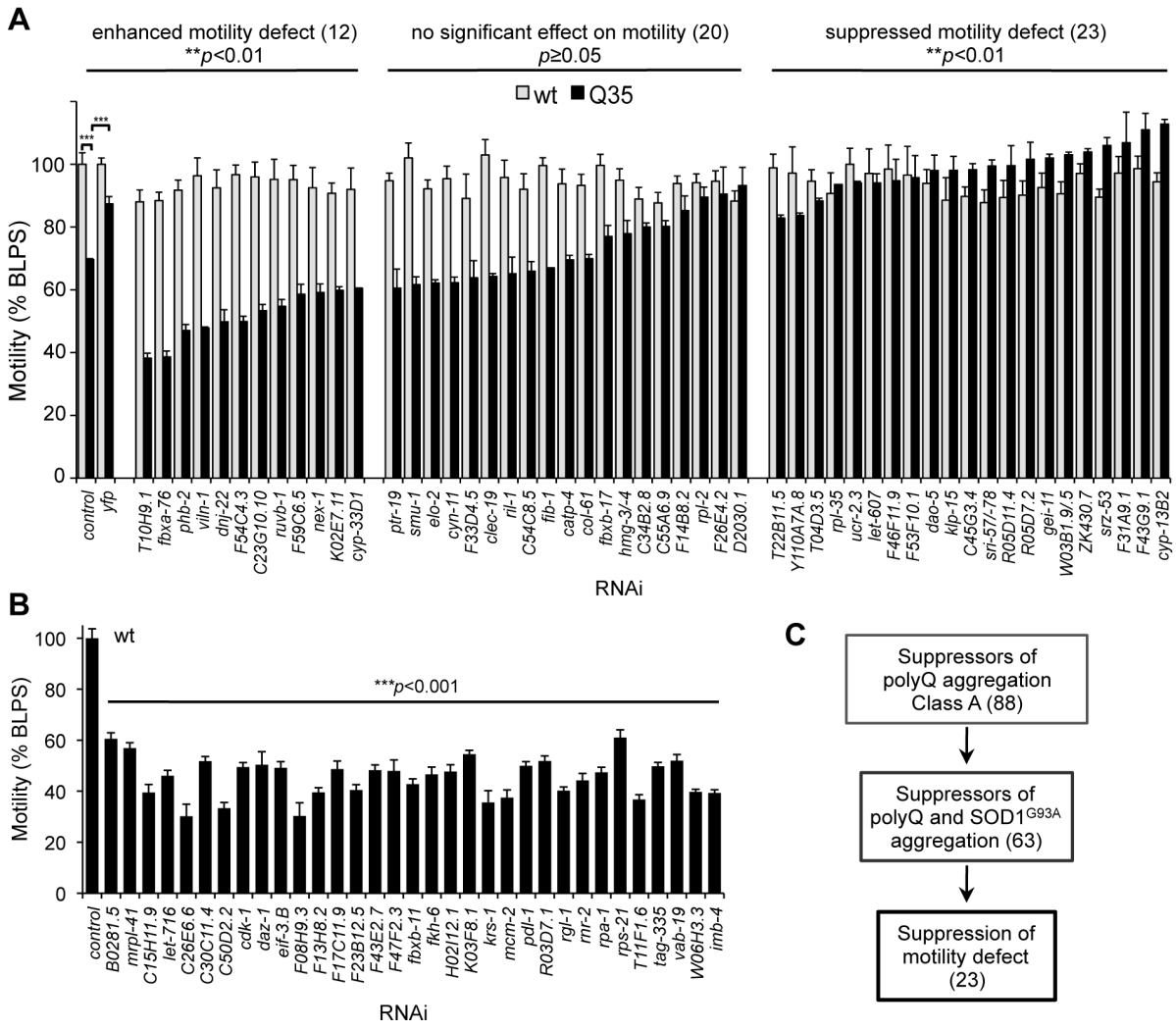

Figure 5. Suppression of polyQ aggregation and toxicity are genetically uncoupled. (A) Motility measurements of Q35 (black) and wt (grey) animals treated with aggregation suppressor RNAi. Motility is measured in body-length per second relative to wt motility in EV control (% BLPS±SEM). Shown here are the modifiers that did not affect wt motility, grouped in three classes that: enhance Q35 motility defect (Student t-test **p<0.001); cause no change (Student t-test p≥0.05); or suppress Q35 motility defect (Student t-test **p<0.01) relative to Q35;EV (red line). T-test ***p<0.001 for Q35 relative to wt in control RNAi. Statistical significance between classes calculated by 1-way ANOVA ***p<0.0001. **(B)** Aggregation modifiers that alone caused a deleterious effect on wt motility (% BLPS±SEM, relative to EV control). Student t-test ***p<0.0001 relative to control. **(C)** Screening triage for modifier suppressors of protein aggregation and toxicity.

Identification of a Core PN by Screening With Endogenous Metastable Proteins

Among the challenges with studies of protein misfolding and aggregation have been the concerns with the physiological imbalance associated with overexpression of heterologous proteins in the respective model systems. To circumvent this concern, we asked whether the PN modifiers that suppressed polyQ and mutant SOD1 aggregation (Figure 5C) would also restore the folding of endogenous metastable proteins harboring temperature sensitive (TS) mutations. TS-mutations represent an important class of highly sensitive folding sensors that are expressed at normal endogenous levels and have quantifiable phenotypes when properly folded at the permissive condition or misfolded at the restrictive temperature

[90,131,167]. This strategy was also used to distinguish between modifiers that directly perturb and suppress the formation of protein aggregates, from the modifiers that reshape the PN to improve the protein-folding environment.

We examined the properties of four TS mutant proteins corresponding to the paramyosin ortholog UNC-15, the basement-membrane protein perlecan UNC-52, the myosin-assembly protein UNC-45, and the myosin heavy chain UNC-54 [90]. At the permissive temperature (15°C), each of these TS-proteins is known to be fully functional and animals harboring these mutants exhibit a wt phenotype, whereas at the restrictive temperature (23° or 25°C) these TS-proteins misfold and cause muscle dysfunction that can be measured as slow movement and paralysis (UNC-15, UNC-54, Figure 6A, C), egg-laying defects leading to swelling and paralysis (UNC-45, Figure 6B), and stiff-paralysis (UNC-52, Figure 6D) (see Materials and Methods) [90,167,183]. These phenotypes are specific to animals expressing the TS mutations, and are not observed in wt animals. We tested all 23 RNAi modifiers that suppressed both Q35 aggregation and toxicity (Figure 5C), on each of the TS strains, and found that a total of nine modifiers reduced the number of animals displaying TS phenotypes by 40% to 90% at 23°C, a slightly lower restrictive temperature at

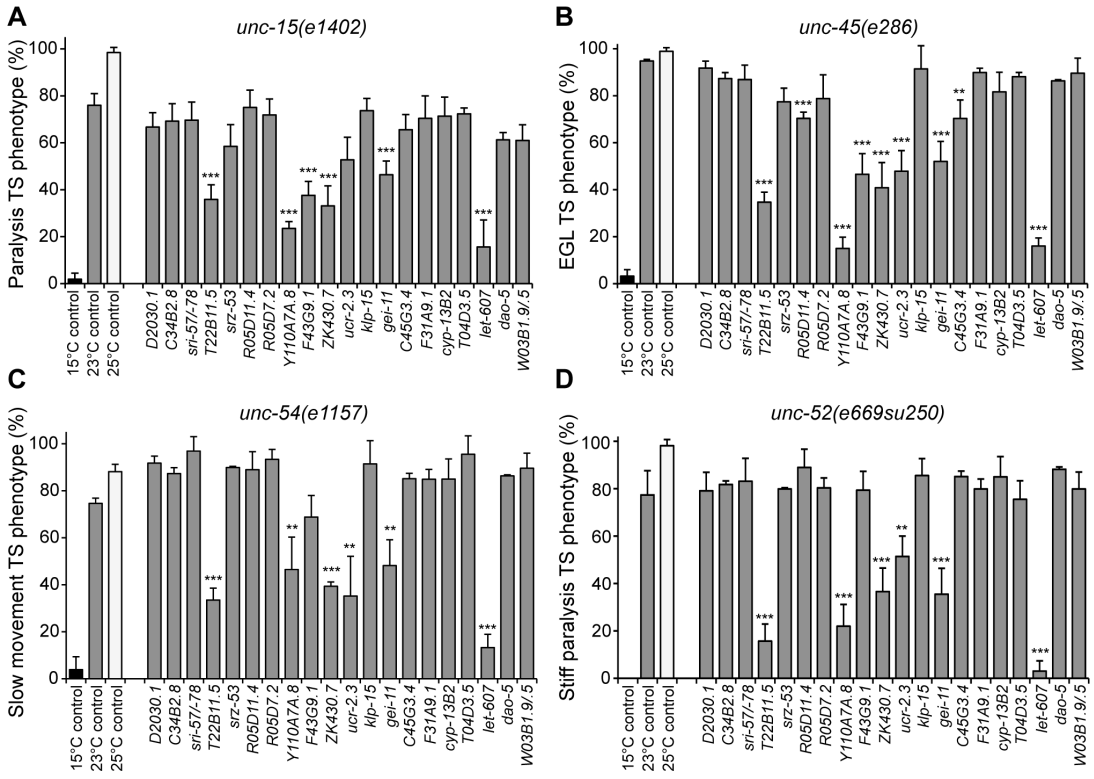

Figure 6: Aggregation modifiers that rescue the folding of endogenous TS mutant proteins. Modifiers of aggregation and toxicity were tested on endogenous muscle TS mutant proteins. 15°C is the permissive temperature, 25°C is the restrictive temperature and 23°C is the temperature used for RNAi. Misfolding of TS mutant proteins was assessed by measuring the % of animals displaying the associated muscle dysfunction phenotype. **(A)** *unc-15(e1402)* (paramyosin), uncoordinated/slow movement; **(B)** *unc-45(e286)* (myosin assembly protein), egg laying and paralysis defect; **(C)** *unc-54(e1157)* (myosin), slow movement/paralysis; **(D)** *unc-52(e669su250)* (perlecan), stiff paralysis (±SD, n>3, Student t-test relative to 23°C control ***p*<0.01, ****p*<0.001). Statistical comparison using 1-way ANOVA ****p*<0.001.

which the efficiency of the RNAi protocol was maintained (Figure 6A-D, Table 2). These results suggest that while protein misfolding is common to all three classes of folding sensors (polyQ, mutant SOD1, and TS-mutant proteins), the cellular environment and the PN are influenced differentially by the modifiers, as reflected by the effects on these sensors. We propose that these final nine modifiers (Figure 7A) are core PN modulators that confer improvement of cellular folding capacity in *C. elegans* muscle cells.

Folding Enhancement by Activation of the Heat Shock Response

Upstream of the core components of the PN is the master cytosolic stress-responsive pathway that leads to HSF-1 activation and expression of molecular chaperones for stability of the proteome. To examine whether the nine PN modifiers (Figure 7A) lead to HSF-1 activation as a general mechanism for proteostasis improvement, we introduced a hypomorphic mutation of *hsf-1(sy441)* into the background of the polyQ strain Q37 and knocked-down each modifier gene (Figure 7B).

Our results show that: suppression of aggregation by *ucr-2.3, gei-11* and *C45G3.4* was completely dependent on HSF-1; whereas *T22D11.5, ZK430.7, Y110A7A.8* and *R05D11.4* exhibited a weaker dependence on HSF-1; and *F43G9.1* and *let-607* were independent of HSF-1. We next examined whether chaperone gene expression was affected downstream of the nine PN modifiers, by monitoring the expression of Hsp70 (*C12C8.1, F44E5.4*) and small Hsp (*hsp-16.1*), upon knockdown of each genetic modifier (Figure 7C). We show that five of nine PN modifiers induced expression of cytoplasmic chaperones. Knockdown of *let-607* (ER-UPR, Table 2) had the strongest effect, suggesting an important regulatory crosstalk between cytoplasmic and ER stress response pathways. Knockdown of the TCA cycle component *T22B11.5* led to upregulation of chaperones and establishes a link between folding and metabolic state, whereas knockdown of *gei-11* (putative negative regulator of cholinergic signal, Table 2) induction of *hsp* suggests an effect of cholinergic signaling on muscle homeostasis (Figure 7C). Reduction of *R05D11.4* (translation) leading to induction of *hsp-70* was consistent with an effect of protein synthesis on folding machinery. For the remaining four PN modifiers, knockdown of *ZK430.7* (RNA processing) had a modest effect on *hsp* expression, while knockdown of *Y110A7A.8* (splicing), *ucr-2.3* (component of the ETC) and *F43G9.1* (TCA cycle) had no effects on *hsp* levels (Figure 7C). This suggests that proteostasis was restored through other pathways involving reduced metabolism and energy production. Taken together, these results demonstrate that improvement of the cellular folding environment by these novel proteostasis modulators is not simply a consequence of a generalized induction of the heat shock response and molecular chaperones but also involve other PN pathways (Table 2), not previously linked to proteome surveillance.

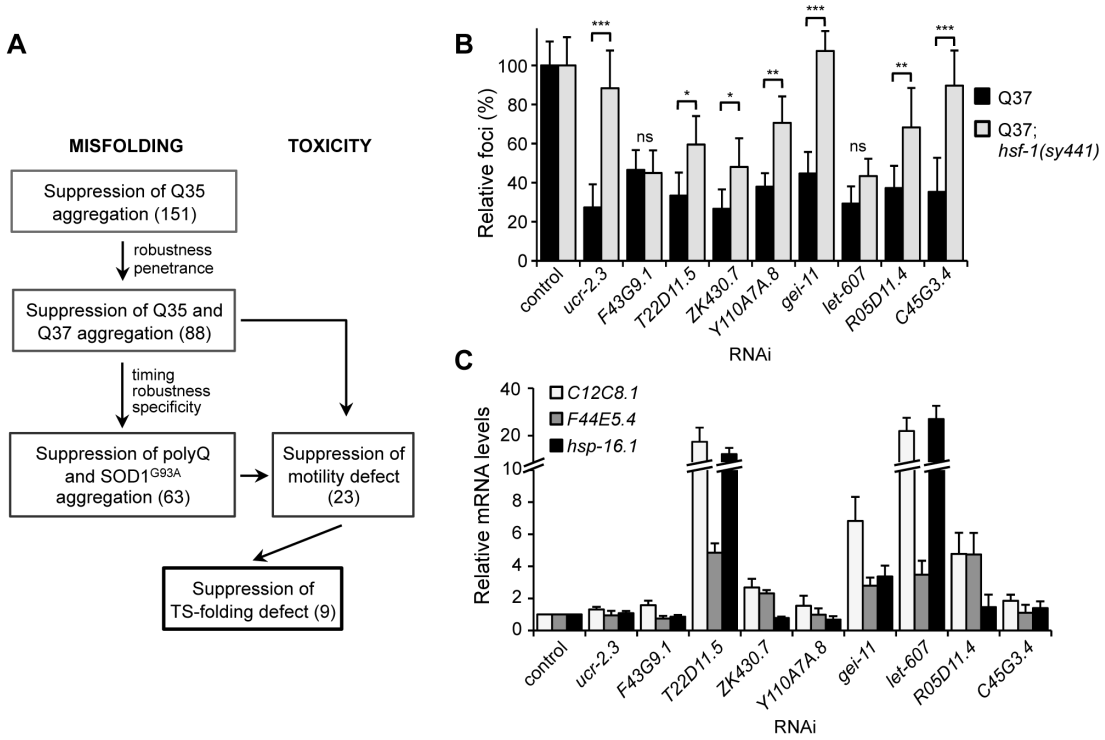

Figure 7: Core PN modifiers and activation of the heat shock response. (A) Screening strategy to identify genetic modifiers that enhance the folding environment and are effective in multiple misfolding models. **(B)** Suppression of polyQ aggregation by the final nine modifiers dependence on HSF-1. Aggregate quantification on RNAi-treated Q37;*hsf-1(sy441)* hypomorphic mutant animals relative to control (±SD). Student t-test *p<0.05; **p<0.01; ***p<0.001 (ns, non-significant). **(C)** Real-time qPCR analysis of the levels of *hsp* (*C12C8.1, F44E5.4, hsp-16.1*) genes in RNAi-treated wt animals. Data are relative to the levels of each gene in wt;EV control (±SD), from 3 biological replicates.

DISCUSSION

Genetic screens have provided invaluable insights into biological processes, and have the advantage of being unbiased and entirely based on endpoint phenotypes. We have employed a genetic strategy to explore how the proteostasis network can be genetically modulated to increase cellular protection against the toxicity of protein aggregation (Figure 7A). This strategy benefitted from certain advantages of *C. elegans* as a metazoan model for the expression of conformationally challenged proteins and the ability to screen the genome for modifiers that suppress both aggregation and toxicity by gene knockdown. This complements the candidate gene approaches that led to the identification of molecular chaperones, ubiquitin proteasome, autophagy, and the upstream stress response signaling pathways. The use of a screening triage approach (Figure 7A) revealed that genetic modifiers that suppress aggregation of polyQ are also effective with mutant SOD1, and revealed the identity of candidates of a core PN. However, only a subset of these suppressors of aggregation also suppressed cellular toxicity, a result that is consistent with the genetic uncoupling between aggregation and toxicity observed in various disease models [96-100,103,173]. This screen ultimately provided a filter that led to identification of a final set of

nine core muscle PN modifier genes (Table 2), not previously shown to be directly involved in protein homeostasis and the restoration of folding in both animal models of protein aggregation and of endogenous metastable proteins.

Table 2: Core modulators of protein homeostasis in *C. elegans* BWM cells.

Gene/ Cosmid	Class	Molecular function	Human ortholog	Expression	TS	Direct Interactors (STRING 9.0)
ucr-2.3	EM	Ubiquinol cytochrome c reductase,	UQCRC2, Cytochrome b-c1 complex III	Ubiquitous, Mitochondrial	3/4	ETC complex III subunits: *cyc-1, isp-1, ucr-2.2, T27E9.2, F45H10.2, T02H6.11, R07E4.3*.
		complex III ETC				*F57B10.14* (unknown).
F43G9.1	EM	Isocitrate dehydrogenase α-subunit, TCA cycle	IDH3A, Isocitrate dehydrogenase, α-subunit	Ubiquitous, Mitochondrial	2/4	Aconitase (*ac-1, aco-2*), ATP synthase (*atp-2*), Isocitrate dehydrogenase subunits (*C37E2.1, idh-1, idh-2, C30F12.7,F35G12.2)* OGDH subunits (*T22B11.5, ZK836.2*)
T22B11.5	EM	2-oxoglutarate dehydrogenase, E1 subunit, TCA cycle	OGDHL, 2-oxoglutarate dehydrogenase E1	Ubiquitous, Mitochondrial	4/4	OGDH subunit (*W02F12.5, ZK836.2*), Isocitrate dehydrogenase subunits (*idh-1, idh-2, C37E2.1,C30F12.7, F43G9.1*), LLC1.3, glutaryl-CoA-
						dehydrogenase (*F54D5.7),* Malonyl-CoA decarboxylase (*F35G12.1)*
ZK430.7	RSP	Sof1-like rRNA processing protein	WDSOF1, WD repeat and SOF domain- containing protein 1	Muscle enriched, Nucleus	4/4	rRNA processing (*fib-1, C05C8.2*), ribosome (*C48B6.2, nep-1, F13H8.2*), acyltransferase (*F55A12.8*), tryptophan protein 2(*F55F8.3*), Bystin(*byn-1*), nucleolar protein (*nol-10*)
Y110A7A.8	RSP	Putative mRNA splicing factor PRP31	PRPF31, U4/U6-SNRP	Oogenesis enriched	4/4	RNA processing and splicing: *prp-8, M28.5, Y59A8B.6, prp-4, rpl-3, ism-6. M03C11.4* (unknown)
gei-11	RSP	GEX-interacting protein 11 MYB-family	SNAPC4, MYBL2, MYB, MYBL1	Nucleus	4/4	Acetylcholine receptor subunit (*unc-29*), tissue morphogenesis (*gex-3*)
let-607	RSP	CREB-ATF transcription factor	CREB3L3/L4, CREBH transcription factor	BWM, neurons, vulva, pharynx, spermatheca ER, nucleus	4/4	-
R05D11.4	PS	ATP-dependent RNA helicase, translation	DDX52, ATP-dependent RNA helicase	Intestine, muscle, cytoplasm	1/4	-
C45G3.4	U	Unknown	Unknown	-	1/4	-

Key: EM (energy and metabolism); RSP (RNA synthesis and processing); PS (protein synthesis); U (unknown); TS (temperature sensitive mutant proteins showing suppression of phenotype/total tested).

New Genetic Modulators of Protein Aggregation

The genome-wide screen for suppression of polyQ aggregation identified a collection of modifier genes from distinct cellular functional classes (Table S1, Figure S3B). Modifiers in the category *cell structure and protein transport*, include cytoskeleton components (filamin) and matrix proteins (*ppn-1, mua-3, gon-1*), supporting observations that aggregation can be affected by disturbing the integrity of cell structure [90]. Other genes in this group encode motor proteins involved in vesicular trafficking (*klp-15, nex-1*), consistent with a role for protein movement and transport in aggregation. *Cell growth and replication* modifiers are involved in progression through the cell cycle (cyclin-dependent kinases), and DNA replication and recombination (transposases), with a likely general effect on growth and development. *Energy and metabolism* modifier genes are involved in energy production and mitochondrial electron transport chain (ETC) function. Restriction in energy levels not only affects overall protein biogenesis, as it

is a highly ATP-dependent process, but also, metabolic enzymes can influence protein folding in the cell by altering the levels of organic/inorganic solutes with effects in polypeptide chain solvation [58]. Notably, reduced ATP synthesis, ETC activity or mitochondrial function have been shown to enhance lifespan, possibly by delaying age-dependent decline in protein folding capacity and by upregulation of stress-response pathways that promote proteostasis and survival [143,147,184,185]. *Gene expression and protein synthesis* related modifiers function in RNA metabolism, ribosome biogenesis, and protein synthesis. This is consistent with reduced translation increasing *C. elegans* lifespan, perhaps by activating a physiological state with increased stress resistance and folding capacities [186-188]. *Post-translational control* modifier genes are involved in chaperone-assisted folding, such as HSP70 superfamily members, DNAJ co-chaperones and cyclophilins, and post-translation modifying enzymes such as SUMO and E3-ubiquitin ligases. The role of chaperones on protein solubility, misfolding and aggregation has been well established [163,189], and an imbalance in certain co-chaperones has been suggested to alter chaperone activity in the cell and folding [67]. *Signaling* RNAi-targeted genes included nuclear hormone receptors, G-protein-coupled receptors, C-type lectins (endocytic receptors), or calcium export and channel-transport activity. These regulators affect reproduction, growth, morphogenesis (development), and locomotion by altering signaling pathways involved in neuronal and muscle function.

Genetic Screens for Enhancer and Suppressor Modifiers of PolyQ Aggregation

Information retrieved from comparative analysis of genetic screens of different misfolded proteins can provide important insights to identify both common and protein-specific pathways for conformational disorders (Table S3). Highly relevant to this point is our ability to compare the modifier genes identified in this study with a previous complementary screen using the same threshold Q-length properties of the Q35 model to identify genes that when knocked-down by RNAi led to enhanced onset of polyQ aggregation [144]. Together, these genome-wide screens identified 341 genetic modifiers that cluster into the same functional classes and pathways, but correspond to distinct genes within these pathways. Specific modifier genes may interfere with the misfolded species at different stages of the aggregation process with opposite outcomes, consistent with the functional properties of a network, where different components within a process can shift the equilibrium in opposing directions to alter the stability of the proteome, to intensify or suppress the polyQ phenotype.

While it might seem counter-intuitive that molecular chaperones could suppress polyQ aggregation when knocked-down, this is consistent with observations that proteome stability can be enhanced or suppressed by changing the composition of the cellular chaperome [67,163,189,190]. For example, reducing the expression of *cyn-11* and *cyn-12* (cyclophilin D isoforms) and *dnj-5*, that function primarily as co-chaperones to regulate Hsp70 and Hsp90 activities [191], promotes a polyQ soluble state. These co-chaperones could function as negative regulators of chaperone function, and their down-regulation results in enhanced chaperone activities leading to suppression of misfolding [163,192,193]. This would be consistent with evidence that Hsp70 folding activity is negatively regulated by co-chaperones and co-factors such as CHIP [194] and BAG-1 [195]. Therefore, enhancement of folding can be achieved by both

positive and negative regulation of chaperones or by a compensatory response that up-regulates other chaperones.

Another functional class common to both Q35 screens is the protein trafficking and cell matrix. Suppression of aggregation by knockdown of cell cytoskeleton proteins, such as intermediate filaments (MUA-3 and MUA-6) and filamin, is supported by experimental evidence that the dynamics of aggregation rely in part on translocation of proteins into inclusions. For example, the active transport of Htt-exon1 along microtubules has been shown to be required for inclusion body formation [196]. In contrast, premature aggregation was observed when the expression of vesicle proteins involved in protein trafficking was knocked-down [144], including TFG-1 COP-II complex, APT-3 and APT-1, and cell membrane assembly proteins (SNAP-25). Interference with these processes can disturb essential steps of the folding and secretory pathways, increase the load of misfolded proteins in the cell and lead to premature polyQ aggregation.

Suppression of PolyQ Aggregation and Toxicity Can Be Uncoupled

An important observation from these studies is that the Class A PN modifiers (Figure 3C, Table 1) were highly effective to suppress polyQ aggregation, and yet only 42% of these modifiers also reduced toxicity, with approximately equal numbers of modifier genes with either no effect on toxicity or even enhancing toxicity (Figure 5A). These results provide independent evidence that suppression of aggregation alone does not predict that the physiological health of the cell will be restored. From a mechanistic perspective, it is increasingly clear that a series of events are associated with the conversion of the nascent polyQ protein into different oligomeric states, immobile aggregate species and inclusion bodies [110,197-199]. We conclude that the genetic suppression of aggregation can occur via a wide range of mechanisms that are dissociated from the effect on toxicity, consistent with previous observations that interference with the aggregation process could in some cases enhance the formation of “toxic oligomeric species” [22,96-101,103,173]. Moreover, each modifier gene is certain to function within its own network of interacting partners, revealing an expanding network through which each modifier can suppress aggregation, but with differential effects on toxicity depending on the affected cellular function. The demonstration that protein aggregates are uncoupled from cellular toxicity has implications for the understanding of the PN and for development of therapeutics.

A Triage Screening Method for Identification of Core Modulators of BWM Proteostasis

We took advantage of *C. elegans* models of protein aggregation-toxicity in addition to folding sensor strains harboring TS mutations in endogenous proteins to identify a core group of modulators that improve folding in muscle cells (Figure 7A). Our results highlight important aspects of the PN, relevant for both ‘gain-of-toxic function’ by aggregation-prone proteins, and ‘loss-of-function’ derived toxicity due to misfolding. The nine PN modifiers that remained at the end of the screening tree function in the mitochondrial respiratory chain and TCA cycle, that regulate metabolism, energy balance and prevention of oxidative stress, in addition to rRNA processing and transcription, that determine gene expression and proteome load (Table 2). While these modifier genes, upon initial inspection, seem not to be directly

involved in folding, perturbation of their specific functions and networks of interactions re-adjusts the PN to enhance its capacity, as suggested by activation of the heat shock response and chaperone expression (Figure 7B, C). Moreover, comparison to other genetic screens performed in *Drosophila* [127,149,182], *C. elegans* [115,128,130,144,148,160,200] and yeast [150,151] (Table S3) provides additional insights into the regulation of the PN by these modifiers. *ucr-2.3* encodes an ubiquinol-cytochrome c reductase subunit of the mitochondrial respiratory chain, and *F43G9.1* and *T22B11.5* encode TCA-cycle enzymes (isocitrate dehydrogenase and 2-oxoglutarate dehydrogenase, respectively) (Table 2). Disruption of the respiratory chain and energy production has been suggested to have consequences on cellular homeostasis [143,185]. Intriguingly, knockdown of *ucr-2.3* was shown to enhance the toxicity of human Tau expressed in *C. elegans* neuronal cells (Table S3) [128]. This discrepancy may be related to Tau-specific proteotoxicity, not derived from aggregation or misfolding, but associated with microtubule binding and disruption. *F43G9.1* was also identified as a enhancer of lifespan [148], which is consistent with a role in proteostasis. *ZK430.7* encodes an rRNA processing factor, *Y110A7A.8* is a putative mRNA splicing factor, and *R05D11.4* encodes an RNA helicase required for translation (Table 2). Thus, perturbing components of the gene expression machinery can enhance proteostasis, likely by altering the expression load of unstable proteins and activating stress responses to restore proteostasis. In particular, knockdown of *Y110A7A.8* activates the osmotic stress response [160] and causes premature onset of polyQ aggregation on 3 day old animals [144], consistent with an increase in misfolding (Table S3). However, on 6 day old animals we show that the number of aggregates is suppressed, which suggests a time-dependent response by the PN to enhance the folding machinery and restore folding. *gei-11* encodes a Myb-family transcription factor proposed to regulate cholinergic receptor function at the BWM cells [201], which affects muscle function and homeostasis [166,167]; and *let-607* encodes a CREBH ortholog transcription factor predicted to be a component of the *C. elegans* ER stress response. The role of *let-607* is particularly intriguing as it reveals a genetic crosstalk between the cytoplasmic and ER lumen stress pathways. Knockdown of *let-607* induces chaperone expression that is not dependent upon HSF-1 (Figure 7B, C), suggesting that other stress responses such as the ER unfolded protein response may be involved in the suppression of cytosolic protein aggregation. Taken together, these results emphasize that diverse genetic and cellular mechanisms can restore cellular proteostasis beyond the traditional heat shock response. These nine gene modifiers of BWM protein homeostasis represent core components of the PN that evoke a robust and effective improvement of disease-related and endogenous metastable protein folding. Identification of these processes is a fundamental step towards identifying new components that constitute the network, and the cellular and organismal mechanisms by which they contribute to protein homeostasis and protect against chronic expression of misfolded toxic proteins.

MATERIALS AND METHODS

C. elegans Strains and Maintenance

Animals were maintained according to standard methods, at 20°C on nematode growth media (NGM) with OP50 *E. coli* [138]. The strains utilized in this work, and previously described, are the following: wild-type (wt) Bristol strain N2; polyQ strains Q0 AM134 (rmIs126[P_{unc-54}::*yfp*]), Q24 AM138 (rmIs130[P_{unc-54}::*q24*::*yfp*]II), Q35 AM140 (rmIs132[P_{unc-54}::*q35::yfp*]I), Q37 AM470 (rmIs225[P_{unc-54}::*q37::yfp*]II) (Supporting Information) [119]; human SOD1 strains $SOD1^{G93A}$ AM265 (rmIs177[P_{unc-54}::$sod1^{G93A}$::*yfp*]) and $SOD1^{WT}$ AM263 (rmIs175[P_{unc-54}::$sod1^{wt}$::*yfp*]) [91]; temperature sensitive (TS) mutant strains CB1402 [*unc-15(e1402)*], CB1157 [*unc-54(e1157)*], HE250 [*unc-52 (e669su250)*] and CB286 [*unc-45(e286)*] [90]. The transgenic polyQ and SOD1 strains had been integrated by gamma-irradiation, 5 times backcrossed, and were previously described [91,119]. The strain Q37;*hsf-1(sy441)* was generated by genetic cross of the original strains AM470 and PS3551[*hsf-1(sy441)*]I.

RNA Interference Screen

The genome-wide RNAi screen for suppression of aggregation in *C. elegans* muscle cells was performed using the commercial RNAi library, with bacteria expressing dsRNA for 87% of the predicted *C. elegans* genes (GeneServiceTM, USA) [144,155]. A semi-automated high throughput setup system was used, consisting of a robotic device (Biomek FX Liquid Handler, Beckman Coulter, Inc., USA) programmed to add bacteria and age-synchronized animals in liquid culture to 96-well plates. RNAi bacterial cultures were grown for approximately 8 h in LB-ampicillin 50 μg/ml (65 μl), at 37°C with continuous shaking at 315 rpm (Orbital shaker, GeneMachines HiGro®, Genomic Solutions, USA), and induced with 0.5 mM isopropyl β-D-thiogalatoside (IPTG, Sigma) for 3 h at 37°C. To obtain an age synchronized population of L1 larvae (first larval state post egg hatching), Q35 gravid adults were bleached with a NaOCl solution [250mM NaOH and 1:4 (v/v) dilution of commercial bleach] and the eggs hatched in M9 buffer overnight at 20°C. Day 1 is defined as 18h following NaOCl age-synchronization and animals are said to be 1 day old (L1 stage). 10 to 15 animals were added to each well in the 96-well plate in a volume of 50 μl of M9 plus [M9, 1 μg/ml cholesterol, 50 μg/ml ampicillin, 10 μg/ml tetracycline, 0.1 μg/ml fungizone and 170 μg/ml IPTG] and incubated at 20°C with continuous shaking at 200 rpm (Innova™ 4430 Incubator Shaker, New Brunswick, USA). Animals were scored 5 days later (6 days old) for reduction in the number of fluorescent foci using the stereomicroscope Leica MZ16FA equipped for epifluorescence (Leica Microsystems, Switzerland). As a negative control, animals were fed bacteria carrying the L4440 empty vector (EV). Suppression of aggregation was scored positive when more than 50% of the animals had a 50% or higher reduction in foci number relative to the EV control, without loss of YFP fluorescence, changes in growth rate or development of the animals. The candidate positive hits were re-screened (n≥3), then tested in the Q24 soluble control strain, and counter screened in Q37 animals (5 day old) and $SOD1^{G93A}$ animals (5 day old). In Q37 and $SOD1^{G93A}$ animals, suppression of aggregation was scored positive when more than 50% of the animals showed a reduction in foci number (>25%). RNAi was always added on day 1. The identity of the RNAi-targeted genes was verified by sequencing of the dsRNA plasmids, followed by Blast analysis in the NCBI and Wormbase databases revealing high specificity of genomic sequence targeting. Gene-knockdown by the respective RNAi was also confirmed for a representative group of hits by rtPCR (data not shown). For RNAi assays on plates (for foci scoring, FRAP and motility analysis, to collect animals for western blot and real-time qPCR; and for TS assays), NGM media was supplemented with 100 μg/ml ampicillin, 1 mM isopropyl β-D-thiogalatoside (IPTG, Sigma) and 12 μg/ml tetracycline (Sigma), and seeded with overnight (16h) RNAi bacteria cultures, pre-induced with IPTG (1 mM, 3 h). One day old (L1) animals (15 to 20 animals) were transferred onto NGM-RNAi bacteria seeded plates and grown at 20°C, and at the time indicated aggregation was scored in at least 50 animals, for each condition (n=3). Aggregates were defined as discrete, bright foci that can be distinguished from their surrounding fluorescence by increased brightness intensity. The detection limit for these foci, measured with the higher resolution Zeiss Axiovert 200 microscope, is in the order of 3 μm in length (for elongated foci in Q35) and ~7 μm^2 in area (for round foci), with the microscopy tools and fluorescence exposure utilized in the genetic screen (Leica MZ16FA). Data collected from different experiments was

compiled to calculate aggregate number averages relative to the control in EV RNAi. Fluorescent microscopy images were taken using an Axiovert 200 microscope with a Hamamatsu digital camera C4742-98 (Carl Zeiss, Germany). All assays were performed blind as to the identity of the RNAi by attributing to each modifier a number corresponding to a well with the dsRNA bacterial stock, in a 96-well plate.

Fluorescence Recovery After Photobleaching Analysis

To examine the biophysical properties of polyQ protein, animals were subjected to FRAP analysis. Animals were mounted on a 3% (w/v) agar pad on a glass slide and immobilized in 2mM levamisole. FRAP was measured using the Zeiss LSM510 confocal microscope (Carl Zeiss, Germany), and the 63X objective lens at 5X zoom power, with the 514nm line for excitation. An area of 0.623μm^2 was bleached for 35 iterations at 100% transmission, after which time an image was collected every 123.35ms. Relative fluorescence intensity (RFI) was determined as previously described [167,202].

SDS-PAGE, Native-PAGE and Western Blotting Analysis

For SDS-PAGE analysis, 6 day old animals grown on RNAi-seeded NGM plates were collected and resuspended in PELE buffer [20 mM Tris pH7.4, 10% glycerol, 2% Triton X-100, 0.5 mM PMSF, 1 μg/ml leupeptin, 1 μg/ml pepstatin, 1 mM EDTA, 1 mM DTT, protease inhibitor cocktail tablet (Roche Diagnostics #11836170001)]. Lysis of ~100 animals was accomplished by a combination of 4 cycles of freeze-thaw, grinding with a motorized pestle (Kontes #749541-000 and #749520-0000), followed by 8 min sonication (Sonicator Bath Branson 1510, Branson). To dissolve the polyQ aggregates, SDS was added to a final concentration of 5.5% (v/v) and samples were boiled for a total of 10min. Total protein concentration was determined using the Bradford assay (Bio-Rad #500-0006). 15μg (for Q35) or 20μg (for SOD1) of total protein, in the linear range for YFP detection [203], were analyzed on a 10% SDS-PAGE followed by Western blotting. For YFP (polyQ and SOD1) detection, blots were probed with the anti-GFP IR800 conjugated antibody (1:5,000 dilution; Rockland Immunochemicals #600-132-215). For α-tubulin detection, blots were probed with the anti-α-tubulin primary antibody (1;4,000 dilution; Sigma #T-5168) followed by the secondary antibody Alexa Fluor®680 goat anti-mouse IgG (1:10,000 dilution; Molecular probes #A-21057). Antibody binding was detected with the Odyssey Infrared Imaging System (LI-COR Biosciences, USA). The ratio between band intensities YFP/α-tubulin was calculated for each sample (Adobe Photoshop 7.0, arbitrary units) and compared to the EV control (relative %). A representative group of modifiers was tested (3 biological replicates). Statistically significant changes in protein amounts were considered if $p<0.05$ (Student's T-test).

For native PAGE analysis, animals (~100) were collected with M9 buffer and resuspended in native-lysis buffer [50 mM Tris pH7.4, 5 mM $MgCl_2$, 0.5% Triton X-100, 0.2 mM PMSF, 1 μg/ml leupeptin, protease inhibitor cocktail tablet (Roche Diagnostics #11836170001)]. Lysis was achieved with 4 cycles of freeze-thaw, and homogenization by grinding with the motorized pestle, always maintaining the tubes on ice. Total protein concentration was determined as before and 40 μg were analyzed on a 5% native PAGE (at 4°C), followed by gel scan (STORM 860, #91393, GE Healthcare, UK). This experiment was done in triplicate.

Motility Assays

Animals (6 days old) grown on RNAi NGM plates at 20°C were picked (20-25 animals) onto the center of a NGM OP50-seeded plate (full surface area covered with OP50), equilibrated at 20°C. Animals' movements were digitally recorded using a Leica M205 FA microscope with a Hamamatsu digital camera C10600-10B (Orca-R2, Leica Microsystems, Switzerland), and the Hamamatsu Simple PCI Imaging software. Videos of 45 s were recorded at 2x2 binning and 5 frames per second, and captured frames were merged into **.avi* format and imported directly into ImageJ. Using the LOCI bio-formats plugin and a custom stack de-flicker plugin (http://www.loci.wisc.edu/bio-formats/imagej), light average intensity was normalized for each frame. To enhance the definition of the animals in the movies, the difference between each frame and the constant background was calculated, using the Maximum Z-stack projection. The resulting movie was converted to binary format using Otsu Thresholding 2. Binary objects representing the animals were tracked using custom ImageJ plugin, wrMTrck (based on "MTrack2" by Nico Stuurman [174]. The average speed of each animal was calculated by dividing the length of each track (corrected for animal body length) by the duration of the track (body length per second, or BLPS). The wrMTrck plugin and scripts for automated analysis

are open-source and publicly available at http://www.phage.dk/plugins. Videos were recorded for a minimum of 75 animals per experiment ($n \geq 3$) and motility measurements are given as a percentage of wt motility (% wt in EV RNAi). RNAi modifiers that affected the motility of wt animals were removed from further analysis. All motility assays were also performed blind as to the identity of the RNAi gene target. Measurements of motility were validated by other read-outs that included manual-based motility assays [90,204]. The first manual assay measured how fast it took animals placed in the center of a ring (circumference only) of OP50 bacteria to reach the food, and the second manual assay monitored the number of worms that traveled 1 cm in 1 minute on OP50 bacteria-seeded NGM plates. All results shown were obtained with the automated worm tracker, which provides reproducible and unbiased results.

Assay for TS Phenotypes

Temperature sensitive (TS) mutant animals were age-synchronized to L1 stage by NaOCl bleaching, grown on RNAi-seeded NGM plates (15-20 animals per plate) from day 1 at a sensitized temperature of 23°C (to maintain the RNAi suppressor effect on aggregation, which was used as a control) and scored for phenotypes on day 5. For the 25°C restrictive temperature control experiment, L1 nematodes were grown on EV RNAi at 15°C until L4 stage to avoid embryonic and developmental phenotypes, then transferred to 25°C and scored 2 days later for the same phenotypes. For the 15°C permissive temperature control experiment, animals were synchronized to L1, added to EV RNAi plates, grown at 15°C and scored for phenotypes on day 6 (to account for slower but normal development at this temperature). At least 50 animals were scored for each specific phenotype, per experiment ($n=3$), as described previously [90,167], and all assays were performed blind. For the slow movement/paralysis assay [*unc-15(e1402)* and *unc-54(e1157)*], 15-20 animals were placed on a OP50-NGM plate at room temperature in the center of a 1 cm circle (drawn on the bottom of the plate). Animals remaining in the 1 cm circle after 5 min were considered to possess a slow movement or paralyzed phenotype. To score for stiff paralysis [*unc-52(e669su250)*], partially paralyzed animals with moving heads and stick-like bodies were scored. For the egg-laying phenotype [*unc-45(e286)*] partially paralyzed animals with a large belly of accumulated eggs were scored.

Real-Time qPCR

Wt animals (5 days old, and ~50) were collected from RNAi-NGM plates and RNA was extracted with the Trizol reagent (Invitrogen), followed by DNase treatment (Applied Biosystems #AM1906). mRNA was then reverse transcribed using the iScriptTM cDNA Synthesis Kit (Bio-Rad #170-8891). 10 ng of cDNA were used for real-time PCR amplification using the iQ™ SYBR® Green Supermix (Bio-Rad #170-8880) and the iCycler system (Bio-Rad) (see Supporting Information). The relative expression levels of each gene were determined using the Comparative C_T Method (Real-Time PCR Applications Guide, Bio-Rad). Gene expression levels were normalized relative to those of actin (*act-1*) in the same sample (internal control), and then relative to the levels of the same gene in EV control sample. Measurements were performed for ≥3 biological samples for each condition.

Acknowledgements: We thank members of the Morimoto lab for discussions and comments, the High Throughput Laboratory and the Biological Imaging Facility at Northwestern University. We thank Dr Anat Ben-Zvi for generating the Q37::YFP(AM470) *C. elegans* strain, and Dr Jesper S. Pederson for helping develop the worm tracker software.

SUPPORTING MATERIALS AND METHODS

Q37::YFP Expression in *C. elegans* Muscle Cells

The *unc-54*p::*q37*::*yfp C. elegans* strain, was generated as described before [119]. The 37 CAG-repeats fused to YFP show a fluorescent diffuse pattern from hatching until day $2^1/_2$ of age, after which small round foci start to appear (onset of aggregation) (Figure S1A, B). The foci correspond to aggregated SDS-insoluble protein retained at the top of the gel as shown by SDS-PAGE western blot analysis, when protein is extracted in native-like conditions (Figure S1C). Expression of Q37 in muscle cells disrupts animal motility by more than 40% relative to the wt or soluble control Q0 and Q24, indicating cellular dysfunction and toxicity (Figure S1D).

Semi-Quantitative RT-PCR

Six day old animals were collected for RNA extraction with the Trizol reagent (Invitrogen #15596-026). Lysis was accomplished by vortexing. Chloroform was added to each sample followed by vortexing and centrifugation (4°C). 2-Propanol was added to each aqueous layer and total RNA was spun down, washed with 75% (v/v) ethanol, air-dried and resuspended in nuclease free water. RNA aliquots of 10 µg were used for DNase treatment (Applied Biosystems #AM1906), and 1 µg purified RNA was used for cDNA synthesis (Bio-Rad #170-8891). cDNA samples were diluted to a final volume of 500µl in water and 1µl was used for PCR amplification with specific primers for the *q35-yfp* sequence (forward primer: CCTGGAGCATTTCCCCAC; reverse primer: GAACTTCAGGGTCAGCTTGCC) and actin (*act-1* forward primer: ATCACCGCTCTTGCCCCATC; reverse primer: GGCCGGACTCGTCGTATTCTTG). A representative group of 22 modifiers were tested. Band intensity ratios *q35-yfp/actin* were calculated with Adobe Photoshop 7.0 (arbitrary units) and are shown as relative % to the EV control.

SUPPORTING FIGURES AND TABLES

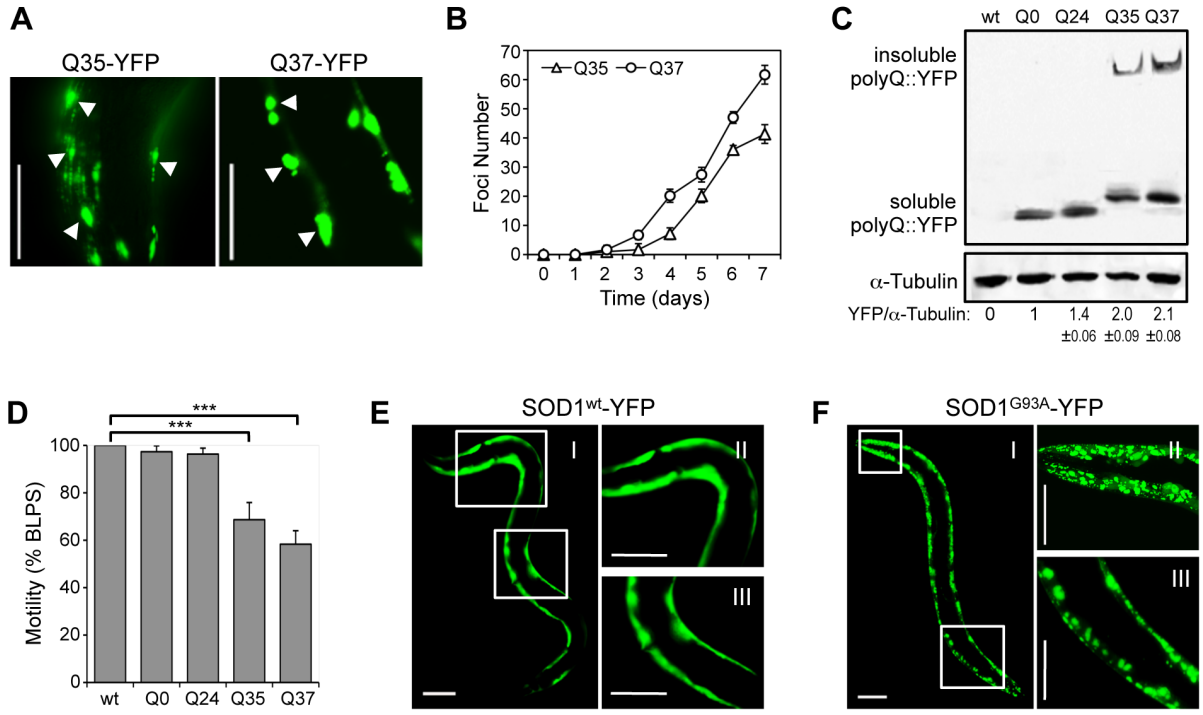

Figure S1. ***C. elegans*** **models of polyQ and human SOD1 aggregation. (A)** Q35 and Q37 body sections show distinct morphology of aggregates (white arrows) in 6- and 5 day old animals, respectively. Scale bar is 0.1 mm. **(B)** Time dependent aggregate count for Q35 and Q37 animals (±SD, n>3). **(C)** SDS-PAGE and western blotting analysis of protein samples from animals (6 days old) expressing polyQ-YFP protein, immunoblotted with anti-YFP (top) and anti-α-tubulin (bottom) antibodies. By standard protein extraction, Q35 and Q37 aggregates are SDS-insoluble and are trapped in the loading well. YFP/tubulin ratios were calculated from protein band intensities (total YFP) and are shown relative to Q0 ±SD. **(D)** Motility measurements (in body length per second/BLPS) of 6 day old wt and polyQ animals show that Q35 and Q37 aggregation in BWM cells causes a motility defect (±SEM, n=3, Student t-test ***p<0.001). **(E,F)** Expression of human SOD1-YFP in muscle cells: while SOD1^{wt} adopts a diffuse soluble fluorescent pattern (E: II and III are zoom in of the boxed areas on I), mutant SOD1^{G93A} displays a pattern of small foci (F: II and III are zoom in of the boxed areas on I). Scale bar is 0.1 mm.

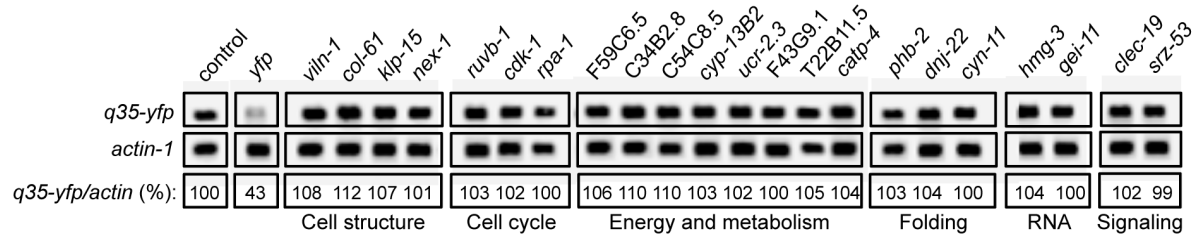

Figure S2. PolyQ mRNA levels in RNAi treated animals. *q35-yfp* mRNA levels from RNAi-treated animals (6 days old) analyzed by reverse transcriptase PCR amplification (top). Control corresponds to EV and *yfp*-RNAi is the positive control for reduced *q35-yfp* mRNA levels. Actin mRNA (bottom) is the control for total mRNA levels. Ratio *q35-yfp/actin* are calculated from band intensities, and averaged from 3 biological replicates. Student t-test p>0.05 for all but *yfp* (***p<0.001).

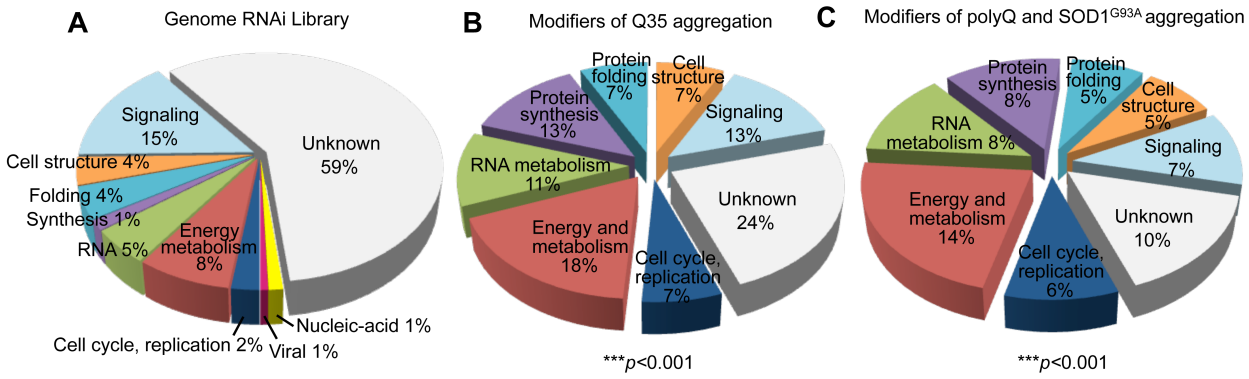

Figure S3. Gene modifiers of aggregation distribution into functional classes. (A) *C. elegans* genes represented in the RNAi library (16,757). **(B)** RNAi suppressors of Q35 aggregation (151). **(C)** Common aggregation suppressors for polyQ and SOD1^{G93A} (63). Statistical significance calculated by the Chi-square test ****p<0.001.*

Table S1: Genetic modifiers identified in the genome-wide RNAi screen for suppression of Q35 aggregation. Listed are all the genes and strains tested, and follow-up secondary screens.

Gene	Functional Class	Molecular function	Description [1]	Human ortholog	Mount [2]	Efficacy [3]	Phenotype [4]	Toxicity [5]	Delayed onset [6]	RNAi @ L4 [7]	Q35	SOD1^{G93A}	*unc-15(e1402)*	*unc-54(e1157)*	*unc-52 (e669su250)*	*unc-45(e286)*
cdk-4	CC/DSR	Cell Cycle	Cyclin-dependent serine/threonine protein kinase. Progression through G1 phase.	CDK4, CDK6	12	+										
cdk-1	CC/DSR	Cell Cycle	Cyclin-dependent kinase 1. Required for cell-cycle progression through M phase.	CDC2	11	++	STE		1 day	✓	✓	✓				
fbxb-11	CC/DSR	DNA recombination	Membrane transposase with a cyclin-like F-box. Protein-protein interactions.	DYNC2H1	12	++			1 day		✓					
fbxb-17	CC/DSR	DNA recombination	Transposase with a cyclin-like F-box.	SIPA1L1	12	++		0			✓	✓				
fbxb-55	CC/DSR	DNA recombination	Transposase with a cyclin-like F-box.	None	0	++										
rnr-2	CC/DSR	DNA replication	Mitochondrial ribonucleoside-diphosphate reductase beta chain (oxidoreductase).	RRM2B	7	++	STE		1 day		✓	✓				
F46F11.9	CC/DSR	Meiosis	Predicted to have a role in meiosis and intracellular transport.	KIAA1012	2	++		-	1 day	✓	✓	✓				
mcm-2	CC/DSR	Replication	Minichromosome maintenance protein 2, DNA replication licensing factor.	None	11	++	STE		1 day	✓	✓					
rpa-1	CC/DSR	Replication	Single-stranded DNA-binding replication protein A (RPA) large subunit.	RPA1	11	++	GRO			✓	✓	✓				
ruvb-1	CC/DSR	Replication	RuvB-like protein 1 DNA helicase.	RUVBL1	5	++		+	1 day		✓	✓				
ppn-1	CS, PT	Cellular matrix	Multidomain glycoprotein orthologous to PaPiliN from *D. melanogaster*.	ADAMTS6	6	++	GRO			✓	✓	✓				
mua-3	CS, PT	Cellular processes	Transmembrane cell adhesion receptor precursor. Muscle Attachment Abnormal fibrillin.	None	0, 14	+										
mua-6	CS, PT	Cellular processes	Muscle Attachment Abnormal protein 6. Intermediate filament protein (MUA-6/IFA-2).	LMNB2	14	+										
unc-84	CS, PT	Cellular processes	Spindle pole body protein.	UNC84A	5	++										
col-61	CS, PT	Cuticle	Collagen protein 61, structural constituent of the cuticle.	COL4A5	16	++	GRO	0			✓	✓				
col-69	CS, PT	Cuticle	Collagen protein 69, structural constituent of the cuticle.	COL4A5	1	++				✓	✓	✓				
viln-1	CS, PT	Cytoskeleton	Actin regulatory protein supervillin.	SVIL	11	++	GRO	+			✓					
Y66H1B.2	CS, PT	Cytoskeleton	Filamin, actin-binding cytoskeleton protein.	None	1	++	GRO									
gon-1	CS, PT	Morphogenesis	Metalloprotease, sub-family of secreted proteases, developmental glycoprotein.	ADAMTS9	1	+	STE									
klp-15	CS, PT	Vesicle trafficking	Kinesin-like protein 15 (KAR3 subfamily). Motor protein, interacts with tubulin, collagen.	KIFC3	7	++	EGL	-			✓	✓				
nex-1	CS, PT	Vesicle trafficking	Annexin family protein 1, calcium-dependent phospholipid binding protein.	ANXA13, ANX13	8	+		+		✓	✓	✓				
C50D2.2	EM	Amino acids	Amino acid transporter, amino acid permease.	SLC7A4	14	++			1 day		✓	✓				
R03D7.1	EM	Amino acids	5-methyltetrahydrofolate-homocysteine methyltransferase. Amino acids biosynthesis.	MTR	20	++					✓	✓				
C34B2.8	EM	Electron transport chain	NADH:ubiquinone oxidoreductase, Complex I B16.6 subunit.	NDUFA13	23	+		0			✓	✓				
F37C12.3	EM	Electron transport chain	NADH-ubiquinone dehydrogenase, complex I. Acyl-carrier protein.	NDUFAB1	2	+										
F55H2.5	EM	Electron transport chain	Cytochrome b, complex III (Cytochrome b-561).	CYB561	2	++										

Table S1: (Continued)

Gene	Functional Class	Molecular function	Description [1]	Human ortholog	Mount [2]	Efficacy [3]	Phenotype [4]	Toxicity [5]	Delayed onset [6]	RNAi @ L4 [7]	Q37	SOD1^{G93A}	*unc-15(e1402)*	*unc-54(e1157)*	*unc-52 (e669su250)*	*unc-45(e286)*
F59C6.5	EM	Electron transport chain	NADH ubiquinone oxidoreductase, Complex I.	NDUFB10	2	++	GRO	+	1 day		✓	✓				
ucr-2.3	EM	Electron transport chain	Ubiquinol-cytochrome C reductase core subunit 2.	UQCRC2	7	++	STE	-	1 day	✓	✓	✓		✓	✓	✓
ZK809.3	EM	Electron transport chain	NADH dehydrogenase (ubiquinone) 1 beta subcomplex 6.	NDUFB6	23	+										
C47F8.4	EM	Glycan metabolism	Beta-1,3-glucuronyltransferase B3GAT1/SQV-8.	B3GAT1	0	++	GRO		1 day		✓	✓				
C54C8.5	EM	Glycan metabolism	Beta-1,3-glucuronyltransferase B3GAT1/SQV-9.	B3GAT2	0	++	GRO	0	1 day		✓	✓				
D2030.1	EM	Glycan metabolism	Mannosyl-oligosaccharide alpha-1,2-mannosidase/ glycosyl hydrolase.	MAN1A1	11	++	STE	0	1 day		✓					
F23B12.5	EM	Glycan metabolism	Pyruvate dehydrogenase E2 component (Dihydrolipoamide acetyltransferase).	DLAT	20	+			1 day			✓				
catp-4	EM	Ion transport	Na+/K+-exchanging ATPase, alpha subunit.	ATP1A2, MHP2	4	++		0			✓					
B0281.5	EM	Ion transport	Polymerase delta-interacting protein PDIP1. Voltage-gated potassium channel complex.	KCTD10	12	++				✓	✓	✓				
elo-2	EM	Lipid metabolism	Palmitic acid elongase, long-chain fatty acids elongase.	ELOVL3	19	++		0			✓					
C34C12.6	EM	Lipid metabolism	Phosphatidylinositol transfer protein SEC14.	SEC14L4	14	+										
F43E2.7	EM	Mitochondrial	Mitochondrial carrier protein.	MTCH2	4	++			1 day	✓	✓	✓				
W06H3.3	EM	Pyrimidines metabolism	CTP synthase, EC 6.3.4.2 (UTP-ammonia lyase).	CTPS2	1	++			1 day	✓	✓	✓				
cyp-13B2	EM	Redox	Cytochrome P450 family.	CYP3A4	12	+		-	1 day		✓	✓				
cyp-33D1	EM	Redox	Cytochrome P450 family.	CYP2J2	13	++		+		✓	✓					
gst-13	EM	Redox	Glutathione S-transferase.	PGDS	19	+										
Y46E12A.3	EM	Redox	Glutaredoxin-related protein.	LOC389207	0	+										
pgp-9	EM	Secondary metabolism	P-Glycoprotein related 9, multidrug resistance protein, ABC transporter family.	ABCB1,PGY1 MDR1, CLCS	27	+										
misc-1	EM	TCA cycle	Mitochondrial 2-oxoglutarate/malate carrier protein.	SLC25A11, SLC20A4	30	+										
F43G9.1	EM	TCA cycle	Mitochondrial Isocitrate dehydrogenase, alpha subunit.	IDH3A	1	++	GRO	-	1 day		✓	✓	✓			✓
fum-1	EM	TCA cycle	Fumarase protein 1. Carbohydrate metabolism; tricarboxylic acid cycle.	FH	2, 7	+										
T22B11.5	EM	TCA cycle	2-oxoglutarate dehydrogenase, E1 subunit.	OGDHL	27	++	GRO			✓	✓	✓	✓	✓	✓	✓
F08H9.3	PFT	Chaperone	Heat shock protein, alpha crystallins of the HSP16 class.	CRYAB	15	++					✓					
tps-2	PFT	Chaperone activity	Trehalose-6-phosphate synthase. Glycosyltransferase.	None	1, 14	+										
cyn-11	PFT	Cyclophilin	Cyclophilin D isoform, peptidyl-prolyl cis-trans isomerase/PPIase.	PPIH	18	++		0			✓	✓				
cyn-12	PFT	Cyclophilin	Cyclophilin protein, peptidylprolyl isomerase.	PPIL1	2	++	GRO		1 day		✓	✓				
dnj-5	PFT	HSP70 co-chaperone	Dnaj domain protein 5 (contains one J domain).	DNAJC14	11	+										
C30C11.4	PFT	HSP70 superfamily	Member of the Hsp70 family of heat shock proteins.	HSPA4L	5	+			1 day		✓					

Table S1: (Continued)

Gene	Functional Class	Molecular function	Description [1]	Human ortholog	Mount [2]	Efficacy [3]	Phenotype [4]	Toxicity [5]	Delayed onset [6]	RNAi @ L4 [7]	Q37	$SOD1^{G93A}$	*unc-15(e1402)*	*unc-54(e1157)*	*unc-52 (e669su250)*	*unc-45(e286)*
dnj-22	PFT	Mitochondrial chaperone	Dnaj domain protein 22. Predicted to be mitochondrial.	DNAJC17	7	+		+			✓	✓				
phb-2	PFT	Mitochondrial chaperone	Mitochondrial prohibitin complex protein 2.	PHB2	20	++		+			✓	✓				
F07E5.5	PFT	Post-translation modification	E3 ubiquitin ligase interacting with arginine methyltransferase. Zinc finger protein.	ZCCHC9		+										
smo-1	PFT	Post-translation modification	SUMO (ubiquitin-related) homolog. Ubiquitin-like protein.	SUMO1, UBL1	2	+										
tag-335	PFT	Protein glycosylation	Mannose-1-phosphate guanylyltransferase.	GMPPB	5	++	STE		1 day	✓	✓	✓				
mrpl-41	PS	Mitochondrial ribosome	39S ribosomal protein L41, mitochondrial.	MRPL41	2	++			1 day	✓	✓	✓				
C26E6.6	PS	Mitochondrial ribosome	Mitochondrial ribosomal protein L3.	MRPL3,RPML3	2	+	STE		1 day		✓	✓				
F33D4.5	PS	Mitochondrial ribosome	Mitochondrial 50S ribosomal protein L1.	MRPL1	2	++		0	1 day		✓					
T23B12.2	PS	Mitochondrial ribosome	Mitochondrial ribosomal protein L4.	MRPL4		+										
tag-264	PS	Mitochondrial ribosome	28S ribosomal protein S30, mitochondrial	MRPS30, PDCD9		+										
rpl-2	PS	Ribosomal protein	60S Ribosomal protein, large subunit L8.	RPL8	23	++	GRO				✓					
rpl-23	PS	Ribosomal protein	60S Ribosomal protein, large subunit L23.	RPL23	23	+	GRO									
rpl-35	PS	Ribosomal protein	60S ribosomal protein L35.	RPL35	23	++	GRO	-		✓	✓		✓		✓	
rpl-7A	PS	Ribosomal protein	60S ribosomal protein, large subunit 7A, isoform c.	RPL7A	23	+										
rps-21	PS	Ribosomal protein	40S ribosomal protein, small subunit S21.	RPS21	23	++				✓	✓	✓				
rps-9	PS	Ribosomal protein	40S ribosomal protein, small subunit S9e.	RPS9	23	+	GRO									
Y73B3A.18	PS	Ribosomal protein	putative 60S ribosomal protein L7A.	RPL7A		+										
daz-1	PS	Translation	Daz protein 1. Translation regulation of specific mRNAs.	DAZ3	7	++			1 day	✓		✓				
krs-1	PS	Translation	Lysyl (K) tRNA Synthetase, class II - protein biosynthesis.	KARS	20	++			1 day		✓	✓				
F17C11.9	PS	Translation elongation	Translation elongation factor, EF-1 gamma subunit.	EEF1G	23	++	GRO		1 day		✓	✓				
H19N07.1	PS	Translation factor	Peptide chain release factor eRF subunit 2.	GSPT2	20	++				✓	✓					
R05D11.4	PS	Translation initiation	ATP-dependent RNA helicase.	DDX52	2	++	STE	-	1 day		✓	✓				✓
eif-3.B	PS	Translation initiation	Eukaryotic initiation factor 3, subunit b (eIF-3b).	None	30	+	GRO		1 day	✓		✓				
fbf-1	PS	Translation repressor	Fem-3 mRNA-binding factor.	Pum1	7	++										
F13H8.2	RSP	RNA processing	WD40-repeat-containing subunit of the 18S rRNA processing complex, mitochondria.	WDR3	5	++	STE		1 day		✓	✓				
hmg-3	RSP	Nucleososme binding protein	Hmg protein 3 - Nucleosome-binding factor SPN, POB3 subunit.	SSRP1	7	++	GRO	0			✓	✓				
hmg-4	RSP	Nucleososme binding protein	Hmg protein 4 - nucleosome-binding factor SPN, POB3 subunit.	SSRP1	11	++	GRO	0			✓	✓				
C15H11.9	RSP	Ribosome biogenesis	Ribosome biogenesis regulatory protein homolog	RRS1		++			1 day		✓	✓				
ZK1127.5	RSP	Ribosome biogenesis	RNA 3'-terminal phosphate cyclase-like protein. 40S-ribosomal-subunit biogenesis.	RCL1	20	++										
fib-1	RSP	RNA processing	rRNA 2'-O-methyltransferase fibrillarin. Pre-rRNA processing.	FBL	20	++		0	1 day	✓	✓	✓				

Table S1: (Continued)

Gene	Functional Class	Molecular function	Description [1]	Human ortholog	Mount [2]	Efficacy [3]	Phenotype [4]	Toxicity [5]	Delayed onset [6]	RNAi @ L4 [7]	Q37	SOD1^{G93A}	*unc-15(e1402)*	*unc-54(e1157)*	*unc-52 (e669su250)*	*unc-45(e286)*
let-716	RSP	RNA processing	rRNA processing protein Rrp5.	PDCD11	20	++	GRO		1 day	✓	✓					
ZK430.7	RSP	RNA processing	Sof1-like rRNA ribosomal processing protein.	DCAF13	30	++		-	1 day	✓	✓	✓	✓	✓	✓	✓
D1054.14	RSP	Splicing	Predicted PRP38-like splicing factor.	PRPF38B	2	++										
Y110A7A.8	RSP	Splicing	Putative mRNA splicing factor PRP31.	PRPF31,RP11	2	++	EGL	-			✓	✓	✓		✓	✓
C55A6.9	RSP	Transcription	RNA polymerase II-associated factor 1 homolog.	PAF1	11	++	EGL	0	1 day		✓					
K03F8.1	RSP	Transcription	Putative Reverse Transcriptase.	ZNF521	0	++			1 day		✓					
dro-1	RSP	Transcription factor	DR1 (One) transcription factor family. Class 2 transcription repressor NC2, beta subunit.	DR1	2	+										
let-607	RSP	Transcription factor	CREB - ATF (Activating Transcription Factor) transcription factor family.	CREB3		++		0		✓	✓	✓	✓	✓	✓	✓
fkh-6	RSP	Transcription factor	Forkhead transcription factor family protein 6.	FOXI1, FKHL10	8	++	GRO	-	1 day		✓					
gei-11	RSP	Transcription factor	gei-11 encodes a protein with Myb DNA-binding domains. GEX Interacting protein 11.	SNAPC4, MYB	11	++		-		✓	✓	✓	✓	✓	✓	✓
dpr-1	RSP	Transcription regulator	Dauer Pheromone Responsive protein 1. Nuclear hormone receptor family.	ESRRB	3	+										
dao-5	S	Insulin signaling	Nucleolar GTPase/ATPase p130.	None	5	++		-	1 day		✓	✓				
xpo-1	S	Nuclear export receptor	Exportin-1, an importin-beta-like protein (Importin beta family protein 4, isoform a).	XPO1	5	++	GRO			✓	✓	✓				
imb-3	S	Nuclear transport	Karyopherin (importin) beta 3.Nuclear transport factor.	RANBP5	5	+										
C01B12.4	S	Receptor protein	Organic solute transporter alpha-like protein, glycoprotein receptor, rhodopsin family.	TMEM34	4	+										
glp-1	S	Receptor protein	Germ Line Proliferation protein 1, fibrillin from the LIN-12/Notch family.	NOTCH2		+										
T10H9.1	S	Receptor protein	Putative serpentine receptor-like protein.	AGTRL1	9	+		+	1 day			✓				
T11F1.6	S	Receptor protein	Predicted receptor, with receptor-L domain.	INSR	0	++			1 day		✓					
sri-57	S	Receptor protein	Serpentine Receptor Class I. Predicted olfactory G-protein coupled receptor.	TAAR6	3	++		-		✓	✓					
sri-78	S	Receptor protein	Serpentine Receptor Class I. 7TM chemoreceptor.	OR10P1	0	++		-		✓	✓					
srz-53	S	Receptor protein	Serpentine Receptor, class Z.	FZD4, EVR1	10	+		-			✓	✓				
grl-7	S	Secreted molecule	Ground-like protein 7. Intercellular signalling.	None	14	+										
C53A5.11	S	Transduction	Protein containing BTB/POZ and Kelch domains.	IPP	10	+										
clec-19	S	Transduction	C-type lectin protein 19.	MRC1	17	++		0			✓	✓				
K07F5.8	S	Transduction	Protein tyrosine phosphatase (PTPs Family), hydrolase.	PTPN12	4	+										
ncx-4	S	Transduction	Na/Ca exchanger; K^+-dependent Ca^{2+}/Na^+ exchanger/solute carrier.	SLC24A2	6	+										
pdl-1	S	Transduction	cGMP-phosphodiesterase, delta subunit. Unc-119 family.	PDE6D	6	+				✓	✓	✓				
R01H10.7	S	Transduction	Inositol-polyphosphate 4-phosphatase (DAF-2 signaling).	INPP4B		+										
rgl-1	S	Transduction	Ral GDS-Like protein 1. Positive regulation of growth rate.	RGL1	1	++			1 day		✓					

Table S1: (Continued)

Gene	Functional Class	Molecular function	Description [1]	Human ortholog	Mount [2]	Efficacy [3]	Phenotype [4]	Toxicity [5]	Delayed onset [6]	RNAi @ L4 [7]	Q37	SOD1^{G93A}	*unc-15(e1402)*	*unc-54(e1157)*	*unc-52 (e669su250)*	*unc-45(e286)*
scd-2	S	Transduction	Protein kinase. Receptor protein tyrosine kinase/ATP binding.	ALK	1	+										
W03B1.9	S	Transduction	Sre G protein-coupled chemoreceptor.	SRRM1	4	++		-			✓	✓				
B0207.6	U	Unknown	Predicted GTPase	ATPBD1B		+										
C14A4.6	U	Unknown	Uncharacterized protein	None		+										
C23G10.10	U	Unknown	Uncharacterized protein	None	10	++		+	1 day		✓					
C45G3.4	U	Unknown	Uncharacterized protein	DUSP10,MKP-5	0	++		-	1 day		✓	✓				✓
C54E10.1	U	Unknown	Uncharacterized protein	PFKFB1		+										
F14B8.2	U	Unknown	Uncharacterized protein	None	8	++	GRO	0			✓	✓				
F26E4.2	U	Unknown	Uncharacterized protein	None	6	++	GRO	0	1 day		✓	✓				
F31A9.1	U	Unknown	Uncharacterized protein	None		+		-	1 day							
F47F2.3	U	Unknown	Uncharacterized protein	KRTAP10-1	10	++			1 day		✓					
F48A11.2	U	Unknown	Uncharacterized protein	None		++										
F49F1.3	U	Unknown	Uncharacterized protein	KIAA1856		+										
F53A2.1	U	Unknown	Uncharacterized protein	SORL1		+										
F53F10.1	U	Unknown	Uncharacterized protein	CCDC102A	6	++	GRO	-	1 day		✓	✓				
F54C4.3	U	Unknown	Ortholog to human histidine rich calcium binding protein	HRC	0	++		+	1 day		✓					
F57A8.2	U	Unknown	Predicted membrane protein	YIF1A		++										
fbxa-76	U	Unknown	F-box A protein	None	8	++		+			✓					
H02I12.1	U	Unknown	Uncharacterized protein	FBN1		+		0	1 day	✓		✓				
K02E7.11	U	Unknown	Uncharacterized protein	LAG1	0	++		+	1 day		✓					
pes-8	U	Unknown	Patterned expression site protein 8	TCERG1		+										
ptr-19	U	Unknown	PaTched Related family, membrane protein	PTCHD1	10	++		0			✓					
R05D7.2	U	Unknown	Uncharacterized protein	VPS39	4	++	EGL	-	1 day		✓	✓				
ril-1	U	Unknown	RNAi-Induced Longevity	None	23	++	GRO	0			✓	✓				
smu-1	U	Unknown	Suppressor of Mec and Unc defects	SMU1	3	++	GRO	0	1 day		✓	✓				
T04D3.5	U	Unknown	Uncharacterized protein	FGD4	12	++		-			✓	✓				
T05A10.3	U	Unknown	Uncharacterized protein	TCHH, THH		++										
T07A9.9	U	Unknown	GTP-binding protein CRFG/NOG1	GTPBP4		+	GRO									
T28A8.4	U	Unknown	Uncharacterized protein	SLK		+										
vab-19	U	Unknown	Ankyrin repeat protein	ANKRD15	1	++			1 day		✓					
W03B1.5	U	Unknown	Uncharacterized protein	B3GAT1	3	++		-			✓	✓				
Y37D8A.16	U	Unknown	Uncharacterized protein	GPR111		+										
Y43C5A.3	U	Unknown	Uncharacterized protein	HNRPA2B1		+										
Y48G8AL.13	U	Unknown	Uncharacterized protein	None		+										

Table S1: (Continued)

Gene	Functional Class	Molecular function	Description [1]	Human ortholog	Mount [2]	Efficacy [3]	Phenotype [4]	Toxicity [5]	Delayed onset [6]	RNAi @ L4 [7]	Q37	$SOD1^{G93A}$	*unc-15(e1402)*	*unc-54(e1157)*	*unc-52 (e669su250)*	*unc-45(e286)*
Y51H7BR.3	U	Unknown	Uncharacterized protein	None	0	++		+	1 day		✓					
Y71F9B.15	U	Unknown	Uncharacterized protein	RNF123		+										
Y87G2A.1	U	Unknown	Uncharacterized protein	RBM28		+										
ZK430.1	U	Unknown	Uncharacterized protein	HEATR1		+										

Functional Classes: (CC/DSR) Cell cycle, DNA synthesis and repair; (CS,PT) Cell structure and protein trafficking; (EM) Energy and metabolism; (PFT) Protein folding and turnover; (PS) Protein synthesis; (RSP) RNA synthesis and processing; (S) Signaling; (U) Unassigned.

[1] Information provided by Wormbase, UniProt and Ensemble databases

[2] Stuart Kim *et al* (2001) Science 293: 2087

[3] Efficacy of aggregation suppression: [+] Suppression in 50% of animals, with ~50% reduction in foci number; [++] Stronger: >75% animals have a >60-80% reduction in foci number

[4] Secondary phenotype observed for all strains fed with RNAi from L1: N2, Q0, Q24, Q35, Q37 and $SOD1^{G93A}$. STE, sterility; GRO, growth delay; EGL, egg-laying defective.

[5] (+) for increase in toxicity (motility defective compared to N2); (-) for less toxicity (motility similar to N2); (0) motility is similar to Q35/no change; (blank) RNAi affects N2 motility.

[6] Refers to the onset of aggregation relative to Q35 control.

[7] RNAi tested at L4 stage. ✓ refers to suppressor effect.

Table S2: Motility assays results for each modifier tested, per assay executed, for wt and Q35 animals.

	wt Assays (normalized to L4440 control)									Q35 Assays (normalized to wt;L4440)								
RNAi	**Trial 1**	**Trial 2**	**Trial 3**	**Trial 4**	**Trial 5**	**n**	**Mean**	**SD**	**SEM**	**Trail 1**	**Trial 2**	**Trial 3**	**Trial 4**	**Trial 5**	**n**	**Mean**	**SD**	**SEM**
L4440 (EV)	1.00	1.00	1.00	1.00	1.00	**107**	1.00	0.00	0.00	0.69	0.71	0.64	0.72	0.72	**210**	0.70	0.04	0.02
yfp	0.98	1.12	0.76			**112**	0.96	0.18	0.10	1.34	0.89	0.68	0.60		**200**	0.87	0.33	0.17
B0281.5	0.71	0.72	0.40			**86**	0.61	0.19	0.11	1.15	0.78	1.62	1.03		**90**	1.15	0.36	0.18
B0432.3	0.62	0.59	0.53			**80**	0.58	0.04	0.03	0.98	0.41	0.71			**96**	0.70	0.28	0.16
C01G12.8	0.91	0.95				**75**	0.93	0.03	0.02	0.58	0.85	0.66			**85**	0.70	0.14	0.08
C15H11.9	0.59	0.28				**82**	0.44	0.22	0.16	0.93	1.23	0.99			**135**	1.05	0.16	0.09
let-716	0.38	0.66				**82**	0.52	0.20	0.14	0.89	0.79	0.91			**68**	0.87	0.06	0.04
C23G10.10	0.89	1.10				**82**	0.99	0.15	0.10	0.41	0.65	0.53			**75**	0.53	0.12	0.07
C26E6.6	0.11	0.59				**89**	0.35	0.34	0.24	1.03	1.49	1.10			**168**	1.21	0.25	0.14
C30C11.4	0.49	0.68				**78**	0.58	0.14	0.10	0.33	0.87	0.59			**58**	0.60	0.27	0.16
C34B2.8	0.84	1.17				**78**	1.00	0.23	0.17	0.63	0.86	0.83	0.93		**100**	0.81	0.13	0.06
C45G3.4	0.74	0.90				**70**	0.82	0.12	0.08	0.84	1.12	0.98			**104**	0.98	0.14	0.08
C50D2.2	0.47	0.26	0.38			**93**	0.37	0.11	0.06	0.87	0.64	0.78			**92**	0.76	0.11	0.07
C54C8.5	0.91	1.17				**80**	1.04	0.19	0.13	0.94	0.94	0.37	0.45	0.53	**114**	0.65	0.27	0.12
C55A6.9	1.07	0.92	0.64			**86**	0.88	0.22	0.13	0.67	1.02	0.72			**109**	0.80	0.19	0.11
cdk-1	0.44	0.59	0.47			**72**	0.50	0.08	0.05	1.34	1.12	0.54			**66**	1.00	0.42	0.24
clec-19	0.91	1.42	0.69			**60**	1.00	0.38	0.22	0.69	0.60	0.65			**98**	0.65	0.04	0.03
col-61	1.19	0.89	0.66			**79**	0.92	0.27	0.15	0.62	0.70	0.79			**75**	0.70	0.09	0.05
cyn-11	0.84	1.32	0.66			**80**	0.94	0.34	0.20	0.76	0.37	0.75	0.61		**102**	0.62	0.18	0.09
cyp-13B2	0.82	0.95	0.76			**69**	0.85	0.10	0.06	1.29	1.19	1.15	0.88		**140**	1.13	0.17	0.09
cyp-33D1	0.87	0.84	0.98			**91**	0.90	0.07	0.04	0.61	0.60		0.59		**101**	0.60	0.01	0.01
D2030.1	0.66	1.44				**67**	1.05	0.55	0.39	0.66	1.20	0.99			**102**	0.95	0.27	0.16
dao-5	0.72	1.18				**76**	0.95	0.33	0.23	0.67	1.29		1.00		**79**	0.99	0.31	0.18
daz-1	0.36	0.71	0.42			**92**	0.50	0.19	0.11	0.66	0.66	0.90			**98**	0.74	0.14	0.08
dnj-22	0.91	1.17				**82**	1.04	0.18	0.13	0.49	0.22	0.79			**95**	0.50	0.28	0.16
eif-3.B	0.49	0.61				**77**	0.55	0.09	0.06	0.94	0.96		0.90		**90**	0.93	0.03	0.02
elo-2	0.60	1.03	1.00			**109**	0.88	0.24	0.14	0.52	0.73	0.63			**196**	0.62	0.10	0.06
F08H9.3	0.14	0.51	0.26			**62**	0.30	0.19	0.11	1.40	0.72	1.00			**150**	1.04	0.34	0.20
F13H8.2	0.36	0.53	0.37			**65**	0.42	0.10	0.06	1.16	0.83	0.99			**100**	0.99	0.16	0.09
F14B8.2	0.87	0.87	0.89			**68**	0.88	0.01	0.01	0.55	1.16	0.85	0.79		**104**	0.84	0.25	0.13
F17C11.9	0.41	0.69	0.29			**70**	0.46	0.21	0.12	0.95	1.12		0.99		**163**	1.02	0.09	0.05
F23B12.5	0.34	0.58	0.40			**60**	0.44	0.12	0.07	1.11	1.54		1.21		**135**	1.29	0.22	0.13
F26E4.2	0.79	0.84	0.95			**86**	0.86	0.08	0.05	0.49	1.22		0.98		**76**	0.90	0.37	0.21
F31A9.1	0.52	1.15	1.19			**58**	0.95	0.38	0.22	0.50	1.64	1.11	0.90		**79**	1.04	0.48	0.24
F33D4.5	0.76	1.35				**75**	1.06	0.42	0.30	0.67	0.91	0.40	0.63		**80**	0.65	0.21	0.10
F43E2.7	0.50	0.59				**70**	0.54	0.06	0.05	1.29	1.25	1.30	1.03		**228**	1.22	0.13	0.06
F43G9.1	0.73	1.11	0.97			**60**	0.94	0.19	0.11	1.86	0.81	0.70	1.09		**156**	1.11	0.52	0.26
F46F11.9	0.98	1.32	0.63			**67**	0.98	0.34	0.20	0.59	0.97	0.89	1.30		**74**	0.94	0.29	0.15
F47F2.3	0.27	0.83	0.35			**63**	0.48	0.30	0.17	0.67	0.67		0.70		**76**	0.68	0.02	0.01
F53F10.1	0.47	1.52				**81**	0.99	0.74	0.53	0.50	1.42	0.89	0.97		**85**	0.94	0.38	0.19
F54C4.3	0.96	0.87	0.90			**80**	0.91	0.05	0.03	0.38	0.62	0.60			**109**	0.53	0.14	0.08
F57B10.1	0.73	1.19				**58**	0.96	0.33	0.23	0.69	1.21	0.92			**80**	0.94	0.26	0.15
F59C6.5	0.95	1.17	0.84			**60**	0.99	0.17	0.10	0.80	0.37		0.65		**90**	0.61	0.22	0.12
fbxa-76	1.07	0.90				**117**	0.99	0.12	0.09	0.28	0.49		0.33		**59**	0.37	0.11	0.06
fbxb-11	0.37	0.42	0.54			**70**	0.44	0.09	0.05	1.34	1.31		1.20		**96**	1.28	0.07	0.04
fbxb-17	1.07	1.17	0.89			**78**	1.04	0.14	0.08	0.85	0.49	0.97			**82**	0.77	0.25	0.15
fib-1	0.87	0.79	0.89	1.20		**89**	0.94	0.18	0.09	0.67	0.67	0.60			**134**	0.65	0.04	0.02
fkh-6	0.22	0.71	0.43			**79**	0.45	0.24	0.14	0.73	0.88	0.58			**92**	0.73	0.15	0.09
gei-11	0.80	1.07				**80**	0.93	0.19	0.13	0.87	1.15	1.14	0.94	1.03	**175**	1.02	0.12	0.05
H02I12.1	0.31	0.78	0.47			**124**	0.52	0.24	0.14	0.71	0.96	0.85			**77**	0.84	0.13	0.07
hmg-3/-4	0.92	0.75	1.00	0.91		**80**	0.90	0.10	0.05	1.34	0.28	0.72			**159**	0.78	0.53	0.31
K02E7.11/Y51H7BR.3	0.96	0.71	0.94	0.83		**100**	0.86	0.12	0.06	0.52	0.67	0.59			**88**	0.60	0.07	0.04
K03F8.1	0.62	0.60	0.54			**104**	0.59	0.04	0.02	0.48	0.99	0.88			**61**	0.78	0.27	0.16
klp-15	0.61	1.17				**56**	0.89	0.39	0.28	1.35	0.74	1.34	0.50		**95**	0.98	0.43	0.22
krs-1	0.20	0.62	0.35			**82**	0.39	0.21	0.12	1.28	0.99	1.30			**90**	1.19	0.17	0.10
mcm-2	0.19	0.67	0.37			**95**	0.41	0.25	0.14	0.57	0.99	0.81			**74**	0.79	0.21	0.12
nex-1	0.70	1.17				**76**	0.93	0.33	0.23	1.02	0.31	0.63	0.40		**134**	0.59	0.32	0.16
pdl-1	0.58	0.53	0.47			**85**	0.53	0.06	0.03	0.87	1.00	0.94			**86**	0.94	0.07	0.04
phb-2	0.86	1.20	0.69			**71**	0.92	0.26	0.15	0.73	0.34	0.45	0.36		**87**	0.47	0.18	0.09
ptr-19	0.88	0.97	0.94			**87**	0.93	0.04	0.02	0.27	0.94		0.54		**62**	0.58	0.34	0.20
R03D7.1	0.49	0.63	0.51			**68**	0.54	0.08	0.04	0.55	0.98		0.69		**80**	0.74	0.22	0.13
R05D11.4	0.57	1.24				**61**	0.90	0.47	0.33	0.68	1.32	0.99			**50**	0.99	0.32	0.18

Table S2: (continued)

	wt Assays (normalized to L4440 control)									Q35 Assays (normalized to wt;L4440)								
RNAi	**Trial 1**	**Trial 2**	**Trial 3**	**Trial 4**	**Trial 5**	**n**	**Mean**	**SD**	**SEM**	**Trail 1**	**Trial 2**	**Trial 3**	**Trial 4**	**Trial 5**	**n**	**Mean**	**SD**	**SEM**
R05D7.2	0.60	1.22				**79**	0.91	0.44	0.31	0.65	1.38	0.94			**93**	0.99	0.37	0.21
rgl-1	0.43	0.48	0.40			**54**	0.44	0.04	0.02	0.58	1.36	0.79			**96**	0.91	0.40	0.23
ril-1	0.81	1.36				**64**	1.09	0.39	0.28	0.93	0.32	0.70			**74**	0.65	0.31	0.18
rnr-2	0.35	0.66	0.44			**55**	0.48	0.16	0.09	0.46	0.96		0.74		**76**	0.72	0.25	0.15
rpa-1	0.53	0.53	0.35			**80**	0.47	0.10	0.06	1.20	0.47	0.83	0.80		**94**	0.82	0.30	0.15
rpl-2	0.75	0.84	0.98	0.93		**75**	0.88	0.10	0.05	0.68	1.11	1.00			**89**	0.93	0.22	0.13
rpl-35	0.70	1.17				**67**	0.94	0.33	0.23	0.94	0.95				**75**	0.94	0.01	0.01
rps-21	0.55	0.83	0.61			**97**	0.66	0.15	0.08	1.93	0.83				**63**	1.38	0.78	0.55
ruvb-1	0.82	1.33				**66**	1.08	0.36	0.26	0.67	0.29	0.40	0.82		**128**	0.55	0.24	0.12
smu-1	0.83	1.62				**120**	1.23	0.56	0.40	0.47	0.85	0.53			**69**	0.62	0.21	0.12
sri-57/-78	0.88	0.87				**76**	0.87	0.01	0.01	1.01	1.17	0.80			**95**	0.99	0.19	0.11
srz-53	0.98	0.88				**96**	0.93	0.07	0.05	1.39	0.71	1.01	1.11		**126**	1.06	0.28	0.14
T04D3.5	0.65	0.92	0.95	1.15		**50**	0.92	0.21	0.10	0.82	0.95	0.90			**108**	0.89	0.07	0.04
T10H9.1	0.82	1.17				**58**	0.99	0.25	0.18	0.23	0.54	0.48			**185**	0.41	0.16	0.10
T11F1.6	0.32	0.51	0.34			**60**	0.39	0.10	0.06	1.30	2.05	1.36			**85**	1.57	0.41	0.24
T22B11.5	0.62	1.17	0.99	1.01		**70**	0.95	0.23	0.12	0.87	0.79				**88**	0.83	0.06	0.04
T24C4.1	1.06	0.92	0.92	1.00		**62**	0.97	0.07	0.03	0.92	0.96		0.94		**73**	0.94	0.02	0.01
tag-335	0.47	0.65	0.48			**100**	0.53	0.10	0.06	0.86	1.20	1.12			**74**	1.06	0.18	0.10
vab-19	0.46	0.71	0.49			**60**	0.56	0.14	0.08	0.72	1.10	0.59			**128**	0.81	0.26	0.15
viln-1	0.87	1.30				**70**	1.09	0.31	0.22	0.46	0.44	0.53	0.48		**170**	0.48	0.04	0.02
W03B1.9/.5	0.86	0.93				**63**	0.89	0.05	0.03	0.99	1.07	1.04			**90**	1.03	0.04	0.02
W06H3.3	0.42	0.47	0.39			**103**	0.43	0.04	0.02	0.81	0.79				**168**	0.80	0.02	0.01
xpo-1/imb-4	0.31	0.71	0.23	0.26	0.56	**266**	0.41	0.21	0.09	1.09	1.03	2.31	1.25	1.23	**131**	1.38	0.53	0.24
Y110A7A.8	0.50	1.50				**55**	1.00	0.71	0.50	0.75	0.95	0.81			**174**	0.84	0.10	0.06
ZK430.7	0.88	0.93	0.94			**67**	0.92	0.03	0.02	0.97	1.11			1.01	**97**	1.03	0.07	0.04

Table S3: Comparative analysis between genetic screens and overlapping gene modifiers.

Genetic Screen (Author, year, screen, organism)	**Overlap with the final group of nine modifiers**	**Other genes in common with Q35 aggregation suppressor modifiers**
Hamilton B *et al.* 2005 (Longevity; *C. elegans)*	*F43G9.1*	-
Hansen M *et al.* 2005 (Longevity; *C. elegans*)	-	*ril-1; C53A5.1*
Murphy C *et al.* 2003 (DAF-16 downstream targets; *C. elegans*)	-	*tps-2; mua-6; Y43C5A.3*
Wang J *et al.* 2009 (neuronal SOD1^{G85R} aggregation; *C. elegans)*	-	*catp-4; C30C11.4*
van Ham T *et al.* 2008 (α-Synuclein Aggregation; *C. elegans*)	-	-
Kraemer B *et al.* 2006 (Tau toxicity; *C. elegans*)	*ucr-2.3*	-
Lamitina T *et al.* 2006 (Osmotic stress; *C. elegans*)	*Y110A7A.8*	*ruvb-1; krs-1; eif-3.B; C55A6.9*
Nollen E *et al.* 2004 (polyQ aggregation; *C. elegans*)	*Y110A7A.8*	*H19N07.1; rps-21; ril-1; rpl-2; rpl-23; rpl-35; rpl-7A; imb-3; T07A9.9*
Zhang S *et al.* 2010 (Htt46Q aggregation; *Drosophila*)	-	*rpl-2; rpl-23; rpl-35; rpl-7A; imb-3; T07A9.9; C30C11.4*
Bilen J *et al.* 2007 (Ataxin toxicity/aggregation; *Drosophila*)	-	*ZK742.1*
Kazemi-Esfarjani P *et al.* 2000 (polyQ toxicity; *Drosophila*)	-	-
Willingham S *et al.* 2006 (Htt53Q toxicity; Yeast)	-	-
Giorgini F *et al.* 2005 (Htt103Q toxicity; Yeast)	-	-
Hodges A *et al.* 2006 (gene expression changes in human HD brain)	-	-

Chapter III

Modulation of Synaptic Activity Restores Proteostasis in Muscle Cells Through HSF-1 Activation

MODULATION OF SYNAPTIC ACTIVITY RESTORES PROTEOSTASIS IN MUSCLE CELLS THROUGH HSF-1 ACTIVATION

M. Catarina Silva[1,2], Margarida D. Amaral[2,3], and Richard I. Morimoto[1]

[1]Department of Molecular Biosciences, Rice Institute for Biomedical Research, Northwestern University, Evanston, IL 60208, USA
[2]Faculty of Sciences, Centre for Biodiversity, Functional and Integrative Genomics (BioFIG), University of Lisboa, 1749-016 Lisboa, Portugal
[3]Centre of Human Genetics, National Institute of Health, 1649-016 Lisboa, Portugal

Manuscript Submitted *(and Reviewed)*

SUMMARY

Regulation of proteostasis and protein conformation represent a prominent challenge to cellular integrity, aging and disease. Much of our understanding on the consequences of protein misfolding and the activation of stress responses has come from studies at the cellular level and exposure to acute environmental and physiological stress conditions. Here, we show in *Caenorhabditis elegans* that a physiologically relevant stimulation of cholinergic signaling at the neuromuscular junction, initiated by increase in expression of the L-type acetylcholine receptor, rescues post-synaptic protein folding. Cholinergic signaling causes calcium release via activation of the voltage-gated calcium channel, EGL-19, and the sarcoplasmic reticulum ryanodine receptor, leading to activation of HSF-1 and expression of cytoplasmic chaperones. The change in muscle proteostasis results in suppression of polyglutamine aggregation and toxicity, and stabilization of metastable proteins. This demonstrated the critical importance of cell non-autonomous control of stress signaling pathways and revealed a novel neuronal regulatory mechanism of proteostasis.

INTRODUCTION

A network of molecular interactions that coordinates synthesis, folding, trafficking and clearance of proteins in the cell is responsible for maintaining proteostasis [58]. When proteostasis is challenged by an acute environmental, chemical, or physiological stress, the cell responds with a precise and rapid activation of stress responses, such as the heat shock response (HSR) or the unfolded protein response (UPR), to restore homeostasis [92]. In contrast, the chronic expression of misfolded and aggregation-prone proteins, as occurs in conformational diseases such as Amyotrophic Lateral Sclerosis (ALS), Alzheimer's disease, polyglutamine (polyQ) disorders, metabolic diseases, cancer, and muscular dystrophy represents a different challenge to the cellular quality control machinery in that proteotoxicity does not abate compared to the response to transient stress [58,70,71,143].

Much of the understanding of the biology of protein conformational diseases has benefitted from genetic model systems to identify components of the proteostasis network that respond to protein aggregation and toxicity. In particular, the invertebrate model organisms *C. elegans* and *D. melanogaster* expressing aggregation-prone proteins that recapitulate important features of conformational disorders, have been used to identify genetic modifiers of protein aggregation, cellular toxicity and behavioral phenotypes [119,122,133,144,161,205]. Among these are genetic pathways that promote protein solubility and clearance within the cell, including molecular chaperones, proteasome subunits, components of the autophagy machinery, and the FOXO and heat shock factor 1 (HSF-1) stress-induced transcriptomes [143]. Moreover, metazoans are representative of the orchestration of cellular functions and processes that

respond in an organized manner to diverse stress challenges in an organism. In contrast to cell-autonomous regulators, tissue-specific genetic modifiers affecting other tissues and organismal processes have highlighted cell non-autonomous regulatory mechanisms of folding and homeostasis, and reveal the presence of a system network of stress responses. In particular, the integration of neuronal and endocrine signaling cascades, transduced to muscle and intestinal cells, were shown to improve stress resistance, folding and even lifespan [143,164,165]. Also, tissue-specific mitochondrial function, including the electron transport chain and the mitochondrial UPR were shown to affect the rate of aging [120]. Understanding how these cellular non-autonomous processes are integrated and regulated offers new genetic and pharmacological strategies to enhance protein homeostasis and health span.

The *C. elegans* model for polyQ aggregation in body-wall muscle (BWM) cells exhibits a Q-length and age-dependent onset of aggregation and toxicity [119], that has been highly useful as a folding sensor to monitor cellular homeostasis and to identify components of the proteostasis network [90,130,144,167]. In this study, we have used the *C. elegans* polyQ model, to characterize a new proteostasis genetic pathway, involving GEI-11, a negative regulator of cholinergic receptor activity at the neuromuscular junction (NMJ) [201]. Whereas cholinergic and GABAergic signaling at the NMJ control muscle contraction [206], a dysregulation of signaling leading to overstimulation of the muscle by total absence of GABA, increases protein misfolding in the post-synaptic cells [167]. Here, we show that the genetic downregulation of *gei-11* results in a distinct moderate increase in cholinergic signaling and enhancement of protein folding capacity in post-synaptic muscle cells. This revealed the existence of a critical range for modulation of cholinergic and GABAergic signaling at the NMJ that leads to activation of HSF-1 and expression of chaperones to restore post-synaptic proteostasis.

RESULTS

Identification of GEI-11, a New Genetic Modifier of PolyQ Aggregation and Toxicity

We performed a genome-wide RNA interference (RNAi) screen for suppression of polyQ aggregation in body wall muscle (BWM) cells, to identify new proteostasis modifiers. *E. coli*-expressing dsRNA corresponding to the genome of *C. elegans* [155], were fed to L1 (first larval stage, day 1) animals expressing Q35-YFP, the highly folding-sensitive polyglutamine aggregation reporter [119]. Animals were scored for reduction in the number of Q35 foci on day 6, corresponding to 3 days after onset of aggregation, relative to the empty vector RNAi control (Figure 1A). As a control for RNAi efficiency, animals were treated with RNAi to *yfp* that reduced the fluorescence signal, as expected (Figure S1A). Here, we report on the modifier gene *gei-11* that suppressed aggregation in Q35 animals (Figure 1A: II, IV, VI) and in two additional muscle protein aggregation models expressing Q37 (Figure S1E: I-IV) and mutant $SOD1^{G93A}$ (Figure S1E: V-VIII) [91]. Suppression of Q35 aggregation by *gei-11* knockdown was not due to reduction in expression of Q35 mRNA or protein steady-state levels (Figure S1B-D).

Next, we examined whether the diffuse pattern of Q35 fluorescence observed in *gei-11*-treated animals (Figure 1A: VI vs. V) corresponded to soluble Q35 protein, using the dynamic imaging method of

fluorescence recovery after photobleaching (FRAP) (Figure 1B). Whereas inclusion-localized Q35 is immobile and exhibits no fluorescence recovery (Figure 1B: Q35;vector) [144], Q35 fluorescence in *gei-11* RNAi-treated animals recovered completely upon photobleaching, indicative of a diffuse state indistinguishable from the soluble Q24 control (Figure 1B). To address whether suppression of Q35 aggregation affected toxicity, we examined muscle function, as aggregation reduces motility of 6 day old animals by 40% relative to wt animals (Figure 1C vector RNAi). *gei-11* RNAi rescued the motility of Q35 animals to 100%, without affecting the motility of wt animals (Figure 1C). As expected, motility was also fully restored by knocking down the polyQ transgene itself with *yfp*-RNAi (Figure 1C). These results show that downregulation of *gei-11* suppressed both aggregation and toxicity of the polyQ protein.

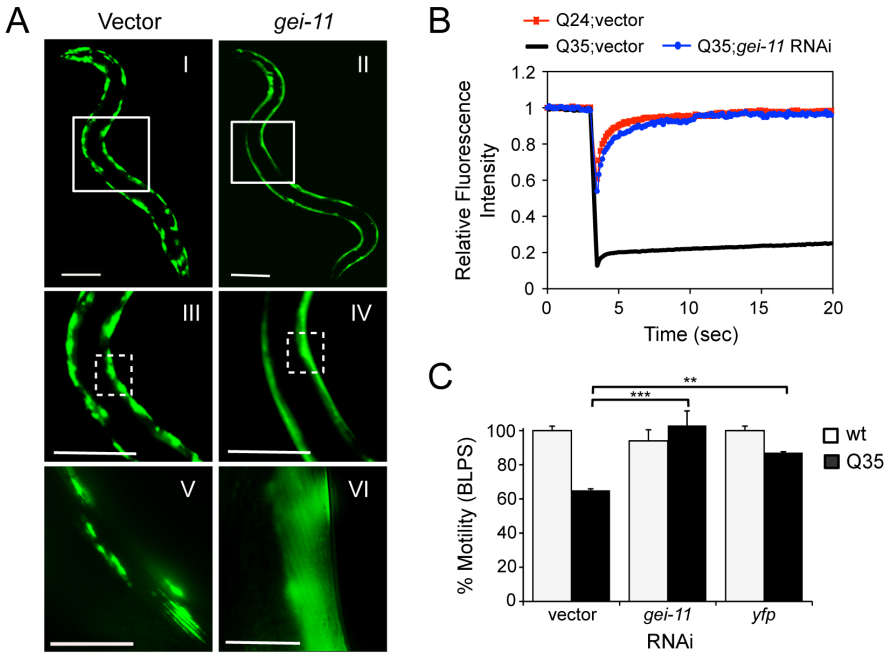

Figure 1: Knockdown of *gei-11* Suppresses PolyQ Aggregation and Toxicity. (A) *gei-11* RNAi suppressed Q35 aggregation in BWM cells of 6 day old animals, shown by the diffuse fluorescent pattern in II, IV and VI, in contrast to a foci-like pattern in the vector control I, III, V. Scale bar: 0.1 mm for I-IV, 0.025 mm for V-VI (boxed areas correspond to magnified images below). **(B)** FRAP analysis shows relative fluorescence intensity recovery at each time point post-photobleaching. Control Q35 foci (black; vector) revealed no fluorescence recovery, while *gei-11*-treated animals showed complete recovery of fluorescence (blue), analogous to the soluble Q24 control (red). Each curve represents an average of >12 independent measurements for *gei-11* RNAi, and >5 for the controls. **(C)** Motility assay for 6 day old Q35 and wt animals fed with *gei-11* or vector RNAi. *yfp*-RNAi is a positive control for suppression of motility defect (±SEM, Student t-test $^{**}p<0.01$, $^{***}p<0.001$). See also Figure S1.

Knockdown of *gei-11* Increases Cholinergic Signaling at the NMJ Through the L-AChR

gei-11 encodes the GEX-3-interacting protein 11 (GEI-11), a member of the Myb superfamily of transcription factors, homologous to mammalian SNAPC4 (snRNA-activating protein complex subunit 4) [207]. *gei-11* was suggested to be a negative regulator of the AChR in *C. elegans* BWM cells, being also expressed in head neurons, germ cells, somatic gonad and intestine [201,208]. At the NMJ of *C. elegans*, two types of ACh receptors are expressed, each with distinct subunit composition and pharmacology [181,209,210]. To test the specificity of GEI-11 regulation of AChR type, we monitored expression of AChR subunits of the L-type (levamisole-sensitive) AChR (*unc-29, unc-38, unc-63* and *lev-8*) and of the N-type (nicotine-sensitive) homomeric AChR (*acr-16*). Knockdown of *gei-11* selectively increased the mRNA levels

of all three essential subunits of the L-AChR (*unc-29, unc-38, unc-63*) by approximately 3-fold, while the levels of N-AChR *acr-16* were unaffected (Figure 2A). We also determined that *gei-11* RNAi did not affect expression of the NMJ GABA receptor ($GABA_R$ *unc-49*, Figure 2A). These results suggest that GEI-11 is a specific modifier of L-type cholinergic receptor expression.

The functional consequence of elevated expression of the three essential AChR subunits on receptor activity was addressed by measuring *C. elegans* sensitivity to the cholinergic agonist levamisole, that selectively activates L-AChR and causes dose-dependent hyper-contraction, paralysis and death [211]. Adult wild-type (wt) animals treated with *gei-11* RNAi showed increased sensitivity and rapid paralysis on 1 mM levamisole plates, relative to vector RNAi-treated wt animals (Figure 2B), consistent with increased number of functional L-AChR. We confirmed that the increased sensitivity to levamisole was due to L-AChR activity, by performing the same paralysis assay with loss-of-function receptor mutant animals (*unc-38(e264), unc-63(x26), unc-29(e1072)*) [181,206]. These L-AChR-deficient animals remained resistant to levamisole upon *gei-11* RNAi treatment (Figure 2B), which supports the role of GEI-11 in the regulation of receptor activity. To further verify receptor specificity, we examined the sensitivity of *gei-11*-treated animals to the agonist nicotine that targets N-AChR, and did not observe a change in sensitivity of wt or N-AChR mutant animals (*acr-16(ok789)*) (Figure S2A) [181,209,210], consistent with the expression data in Figure 2A. Taken together, these results demonstrate the specificity of GEI-11 as a selective negative regulator of the L-AChR. To establish the link between *gei-11*-mediated suppression of polyQ aggregation and increased cholinergic signaling, we employed (+)-Tubocurarine chloride (dTBC), a potent inhibitor of AChR activity [206]. dTBC prevented the suppression of Q35 aggregation by *gei-11* RNAi in a dose dependent manner (Figures 2C, S2B), demonstrating that aggregation suppression in the muscle is a consequence of L-AChR activity.

To determine if aggregation suppression by *gei-11* RNAi was a muscle-specific event, we asked if *gei-11* knockdown could suppress aggregation in another tissue, and found that it had no effect on aggregation of polyQ (Q44) expressed in the intestine (Figure S1F). To further examine if suppression of protein aggregation was a direct consequence of muscle-specific expression of AChRs, we employed a mutant strain that only allows RNAi in muscle cells: Q35;WM118 [212,213]. As a negative control we employed the strain Q35;WM27 that is completely impaired for RNAi (Figure 2D). Having confirmed muscle *gei-11* knockdown (Figure 2D), we show that Q35 aggregation was suppressed by 50% relative to vector control in WM118 animals, but not in WM27 (Figure 2E). Moreover, knockdown of *gei-11* in WM118 animals increased expression (>3-fold) and activity of the L-AChR, as seen by sensitivity to levamisole, comparable to whole-body *gei-11* RNAi (compare Figure 2A, B with F, G). Taken together, these results suggest that suppression of protein aggregation is a consequence of *gei-11* knockdown in muscle cells, through upregulation of AChR expression at the NMJ and increased cholinergic stimulation.

Modulation of Cholinergic Signaling Effect on Metastable Proteins and Health Span

To address whether suppression of protein aggregation by cholinergic signaling reflects a more global effect on post-synaptic proteostasis, we examined the stability of four endogenous muscle-

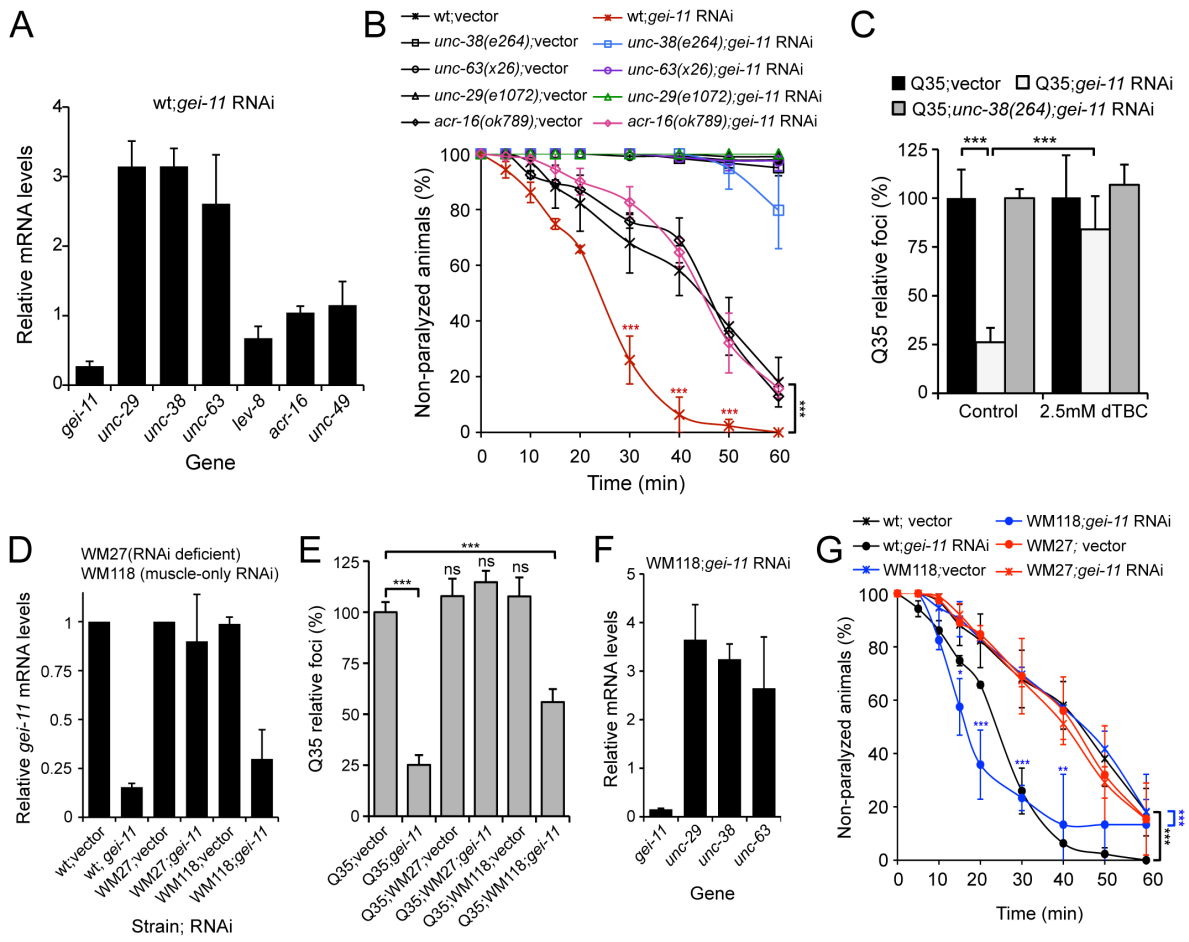

Figure 2: GEI-11 Negatively Regulates Cholinergic Signaling at the NMJ. (A) Real-time qPCR analysis of expression levels of AChR subunits *unc-29*, *unc-38*, *unc-63, lev-8* and *acr-16*, and $GABA_R$ *unc-49,* in 6 day old wt animals fed with *gei-11* RNAi. Data are normalized to the levels of each gene on vector-treated wt animals (±SD). **(B)** Cholinergic sensitivity assay: 5 day old animals treated with *gei-11* or vector RNAi were scored for paralysis on plates containing 1 mM levamisole (±SD). L-AChR mutant animals *unc-38(e264), unc-63(x26)* and *unc-29(e1072),* and N-AChR mutant *acr-16(ok789),* were employed as controls. Two-way ANOVA and Bonferroni Test ***p<0.001 relative to vector control. **(C)** AChR antagonist dTBC (2.5mM at L4 stage) prevented *gei-11* RNAi suppression of Q35 aggregation (±SD). Q35;*unc-38(e264)* is a control for AChR-dependent effect. Student t-test ***p<0.001. **(D)** Real-time qPCR analysis of *gei-11* mRNA levels in wt, WM27 (impaired RNAi) and WM118 (muscle-only RNAi) animals, treated with *gei-11* or vector RNAi. Data are normalized to wt animals (±SD). **(E)** Knockdown of *gei-11* suppressed aggregation by 75% in Q35 animals, and by 50% in Q35;WM118 animals (muscle-specific RNAi). Q35;WM27 animals are the control for impaired RNAi. Foci count is relative to Q35;vector (±SD). Student t-test ***p<0.001, ns/not significant. **(F)** Real-time qPCR analysis shows AChR subunits *unc-29, unc-38* and *unc-63* upregulation by muscle-specific *gei-11* RNAi in WM118 animals (6 day old), relative to vector control (±SD). **(G)** Cholinergic sensitivity assay: 5 day old wt, WM118 and WM27 animals treated with *gei-11* or vector RNAi were scored for paralysis on plates containing 1mM levamisole (±SD). Two-way ANOVA and Bonferroni Test ***p<0.001, **p<0.01, *p<0.05 relative to vector control. See also Figure S2.

expressed metastable proteins [90]. These well-established endogenous sensors of the folding capacity in muscle cells are represented by temperature-sensitive (TS) mutations in the paramyosin ortholog UNC-15, the basement-membrane protein perlecan UNC-52, a myosin-assembly assisting protein UNC-45, and the myosin heavy chain UNC-54 [60,90,91,167]. At the permissive temperature (15°C), all four TS-proteins fold properly and are functional, whereas at the restrictive temperature (25°C) each protein misfolds and results in characteristic muscle dysfunction phenotypes (Figure 3A control). For the purpose of the RNAi

experiments, we employed an intermediate temperature (23°C) at which the TS mutant phenotypes remained highly penetrant (Figure 3A, 23°C vector control). Upon treatment with *gei-11* RNAi, the stability of each protein was increased by 50% to 60% (Figure 3A). These results show that downregulation of *gei-11* enhanced folding of multiple endogenous metastable proteins in muscle cells, suggesting an improvement in cellular folding capacity rather than a protein aggregation-specific effect.

Since protein misfolding and decline in the capacity to maintain proteostasis are associated with aging [28,58,60,92], we examined if improvement in folding capacity by knockdown of *gei-11* would affect lifespan. We found that the mean lifespan of wt animals was increased by 13% upon treatment with *gei-11* RNAi (Figure 3B, Table S1), consistent with a modest improvement in organismal proteostasis and extended health span. In this assay, RNAi for *hsf-1* and *daf-2* were employed as positive controls for decrease and increase in lifespan, respectively [116,214,215], and the effect of *gei-11* on mean lifespan was *hsf-1*-dependent (Figure 3B). Together, these results suggest that the increase in cholinergic signaling has beneficial consequences on muscle protein folding, and a modest overall improvement on organismal proteostasis, as seen by the effect on lifespan.

Restoration of Post-Synaptic Proteostasis by Induction of Cytoplasmic Chaperones and Activation of HSF-1

The proteostasis network is comprised of many pathways that affect the stability of the proteome, therefore, we sought to identify which components were responsible for the enhanced folding in the muscle. We examined if this effect was a consequence of HSR induction, by testing dependence on HSF-1 and HSP-70. Double knockdown of *gei-11* with *hsf-1* or *C12C8.1* (*hsp-70*) did not suppress Q35 aggregation (Figure 3C), suggesting a role for the HSR. Next, we examined the expression of cytoplasmic chaperones regulated by the HSR. Upon *gei-11* knockdown in wt animals, the expression of multiple heat shock genes of the HSP-70 family (*C12C8.1, F44E5.4* and *C30C11.4*) and small heat shock protein family (sHSPs *hsp-16.1, hsp-12.6* and *hsp-16.49*) was upregulated (Figure 3D). The expression of these chaperones was not induced by *gei-11* knockdown in the AChR mutant *unc-29(e1072)*, or in the background of the hypomorphic mutant *hsf-1(sy441)* (Figure 3D), revealing that folding improvement by cholinergic signaling is a consequence of HSR activation. In addition, *hsp* levels were also upregulated in WM118 animals (muscle RNAi) treated with *gei-11* RNAi (Figure 3E), underscoring that the effect on muscle proteostasis is a consequence of events occurring at the NMJ.

To examine directly whether induction of chaperone expression by *gei-11* knockdown is due to activation of HSF-1, we employed an electrophoresis mobility shift assay (EMSA) to directly monitor HSF-1 DNA binding activity [216]. Knockdown of *gei-11* induced HSF-1 DNA-binding activity (Figure 3F: lane 6), to a level equivalent to that of heat shock (lane 3). A similar level of HSF-1 DNA binding activity was also observed in animals treated with *hsp-1* (Hsc70) RNAi, a negative regulator of HSF-1 (lane 9) [40]. The specificity of HSF-1 binding was demonstrated by competition with excess unlabeled HSE (lanes 4, 7 and 10) and by using a mutated HSE radiolabeled oligonucleotide (lanes 5 and 8), for which HSF-1 binding was not observed. These results establish that HSF-1 was activated by *gei-11*-mediated increase in cholinergic signaling, consistent with the up-regulation of cytosolic chaperones.

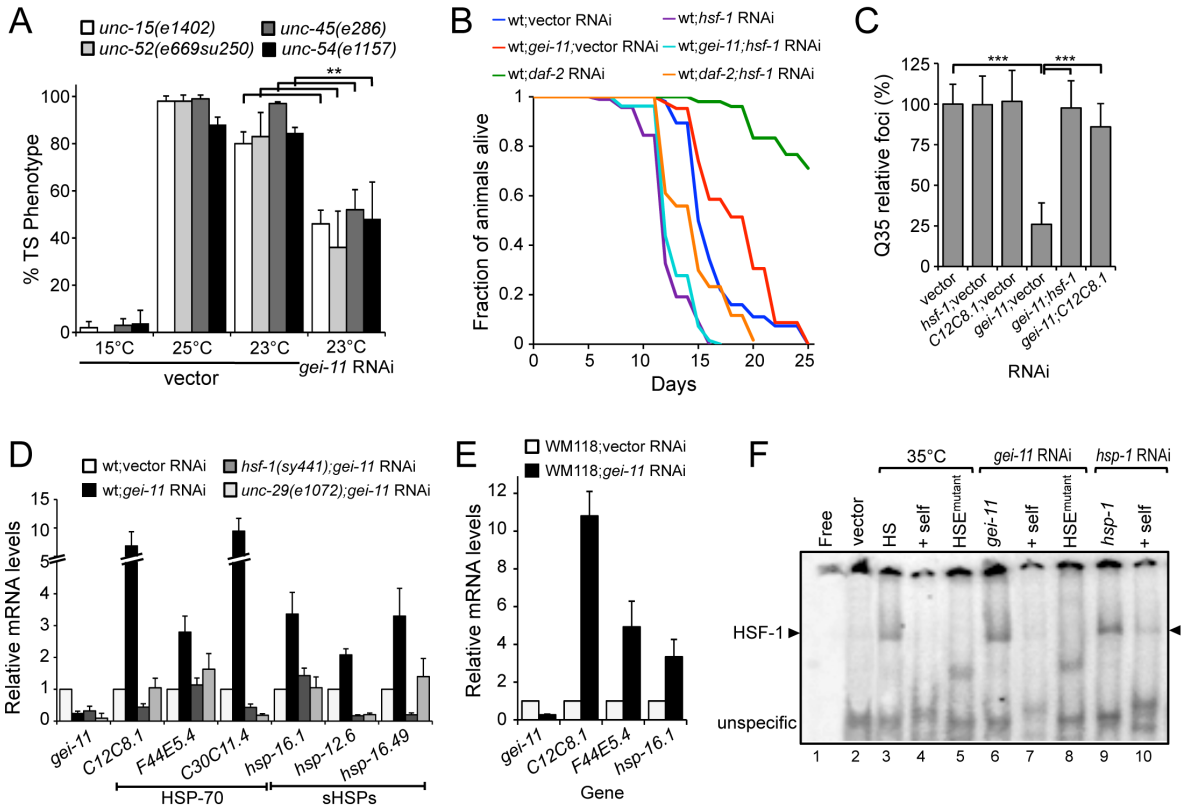

Figure 3: Cholinergic Signaling Rescue of Proteostasis through HSF-1 Activation and Upregulation of Chaperones. (A) *gei-11* RNAi rescued folding of muscle TS mutant proteins as measured by the decrease in the TS phenotypes: UNC-15 (paramyosin; unc/slow movement), UNC-52 (perlecan, stiff paralysis), UNC-45 (myosin assembly, egg laying defect) and UNC-54 (myosin, paralysis). 15°C is the permissive temperature, 25°C is the restrictive temperature and 23°C is the temperature for RNAi (±SD, Student t-test $^{**}p<0.01$). **(B)** Survival curves for wt animals on RNAi bacteria from L2 stage throughout adulthood, at 20°C. Animals treated with *gei-11* RNAi show 13% increase in mean lifespan relative to vector control RNAi. ($p<0.001$ Log-rank/Mantel Cox test). *daf-2* RNAi is the control for extended lifespan, and *hsf-1* RNAi is the control for shorter lifespan. See also Table S1. **(C)** *gei-11* double knockdown with *hsf-1* or *C12C8.1* (*hsp-70*) abolished the suppressor effect on Q35 aggregation (±SD, Student t-test $^{***}p<0.001$). **(D)** Real-time qPCR analysis of chaperone levels in wt or mutant *unc-29(e1072)* and *hsf-1(sy441)* animals, treated with *gei-11* RNAi. Up-regulation of chaperones from the Hsp-70 family (*C12C8.1, F44E5.4, C30C11.4*) and small Hsps (*hsp-16.1, hsp-12.6, hsp-16.49*) by *gei-11* is dependent on AChR (*unc-29*) and HSF-1. Data are relative to wt;vector (±SD). **(E)** Upregulation of *hsp* levels upon muscle specific *gei-11* knockdown in WM118 animals. Real-time qPCR data relative to WM118;vector (±SD). **(F)** Gel mobility shift analysis shows that *gei-11* RNAi induced HSF-1 DNA binding (lanes 6) in a similar way to heat shock at 35°C (lanes 3). *hsp-1* RNAi (*hsc-70*) is a positive control for RNAi-induced HSF-1 activation (lane 9). Assay performed with a [^{32}P]HSE oligonucleotide, HSE^{mutant} refers to a mutated oligonucleotide in the HSE (lanes 5,8) and *+self* refers to competition with 100-fold molar excess of unlabeled oligonucleotide (lanes 4,7,10). Control (lane 2) refers to vector RNAi. See also Figure S3.

Finally, to distinguish between a generalized cell stress response and a selective induction of the HSR, we examined the expression of the UPR-regulated ER chaperones (*hsp-3, hsp-4, dnj-7* and *ero-1*), metabolic stress FOXO/DAF-16 regulated genes (*sod-3* and *mtl-1*) and oxidative stress regulated genes (*hsp-6, gst-4* and *gcs-1*). As shown in Figure S3, the expression of these stress responsive genes was not induced by *gei-11* knockdown. Altogether, these results demonstrate that modulation of synaptic cholinergic signaling leads to the selective activation of HSF-1, expression of cytoplasmic chaperones, and restoration of the folding environment in post-synaptic muscle cells.

Regulation of Cholinergic and GABAergic Signaling Modulates Post-Synaptic Proteostasis

The NMJ integrates multiple pathways that regulate muscle contraction, including neuronal synthesis and release of ACh and GABA neurotransmitters, and receptor synthesis and function at the BWM cell membrane (Figure 4A) [217,218]. We systematically examined the role of each component in the suppression of protein aggregation by *gei-11* (Figure 4B, C, G). Double knockdown of *gei-11* with an essential subunit of the L-AChR (*unc-38, unc-63* or *unc-29*), that inhibits receptor activity, no longer suppressed polyQ aggregation (Figure 4B). By comparison, knockdown with a non-essential subunit (*lev-1*) that only reduces receptor function [181], only weakened the *gei-11* effect on polyQ aggregation (Figure 4B). As expected from the genetics data (Figure 2A), double knockdown with *acr-16* did not affect *gei-11* suppression of aggregation (Figure 4B). We then examined whether increased AChR expression in post-synaptic cells was balanced by neuronal signaling, so as to affect post-synaptic protein aggregation. To address this, neuronal ACh synthesis and release into the synaptic cleft was disrupted by co-knockdown of either the choline acetyltransferase *cha-1* (choline acetyltransferase, together with *unc-17*/ synaptic vesicle ACh transporter), required for neuronal ACh synthesis, or the kinesin-like protein *unc-104*, required for ACh synaptic vesicles transport (Figure 4A) [218], with *gei-11*. In both cases, the level of aggregation suppression was significantly less efficient than by *gei-11* alone (Figure 4C). We also tested the role of neuronal cholinergic activity through the acetylcholine receptor ACR-2R (Figure 4A) [219]. Knockdown of ACR-2R subunits *acr-3* and *acr-12* almost completely abolished suppression of aggregation by *gei-11* (Figure 4C). Collectively, these results indicate that suppression of polyQ aggregation in post-synaptic cells requires neuronal cholinergic signaling, revealing a cell non-autonomous control of muscle proteostasis.

To address the physiological relevance of cholinergic regulation of muscle proteostasis, we asked whether upstream modulation of neuronal cholinergic activity could also correct folding in post-synaptic muscle cells. This would be consistent with observations that post-synaptic transcriptional regulation of AChR expression is controlled cell non-autonomously by nerve-supplied signaling factors [220,221]. To selectively activate neuronal cholinergic signaling, we treated Q35 animals with muscarinic cholinergic agonists Oxotremorine M and Arecolin [203,218,222,223], and found that muscle Q35 aggregation was suppressed by >50% (Figure 4D). This result corroborated that muscle homeostasis can be rescued by chemical modulation of neuronal activity, in addition to genetic regulation of muscle receptor expression.

While upregulation of cholinergic signaling at the NMJ suppressed misfolding and toxicity of multiple proteins in post-synaptic muscle cells, in a previous study we have shown that complete inhibition of GABAergic function, with a null mutation in *unc-30* (Figure 4A), causes misfolding and aggregation in BWM cells [167]. This led to the hypothesis that, while overstimulation of the muscle has deleterious consequences on the folding environment [167], there is a range of cholinergic signaling modulation with a beneficial effect on post-synaptic homeostasis. We used the L-AChR agonist ACh and levamisole to determine if there is a range of agonist concentrations that suppresses or enhances aggregation. Increase in cholinergic signaling with the receptor agonist ACh reduced Q35 aggregation by >50% at 1 mM, while levamisole suppressed aggregation by 40% at 5 μM (Figure 4E). The effect of both ACh and levamisole was dose-dependent (Figure S2C, D), and at a higher concentration of ACh (200 mM) or levamisole (50

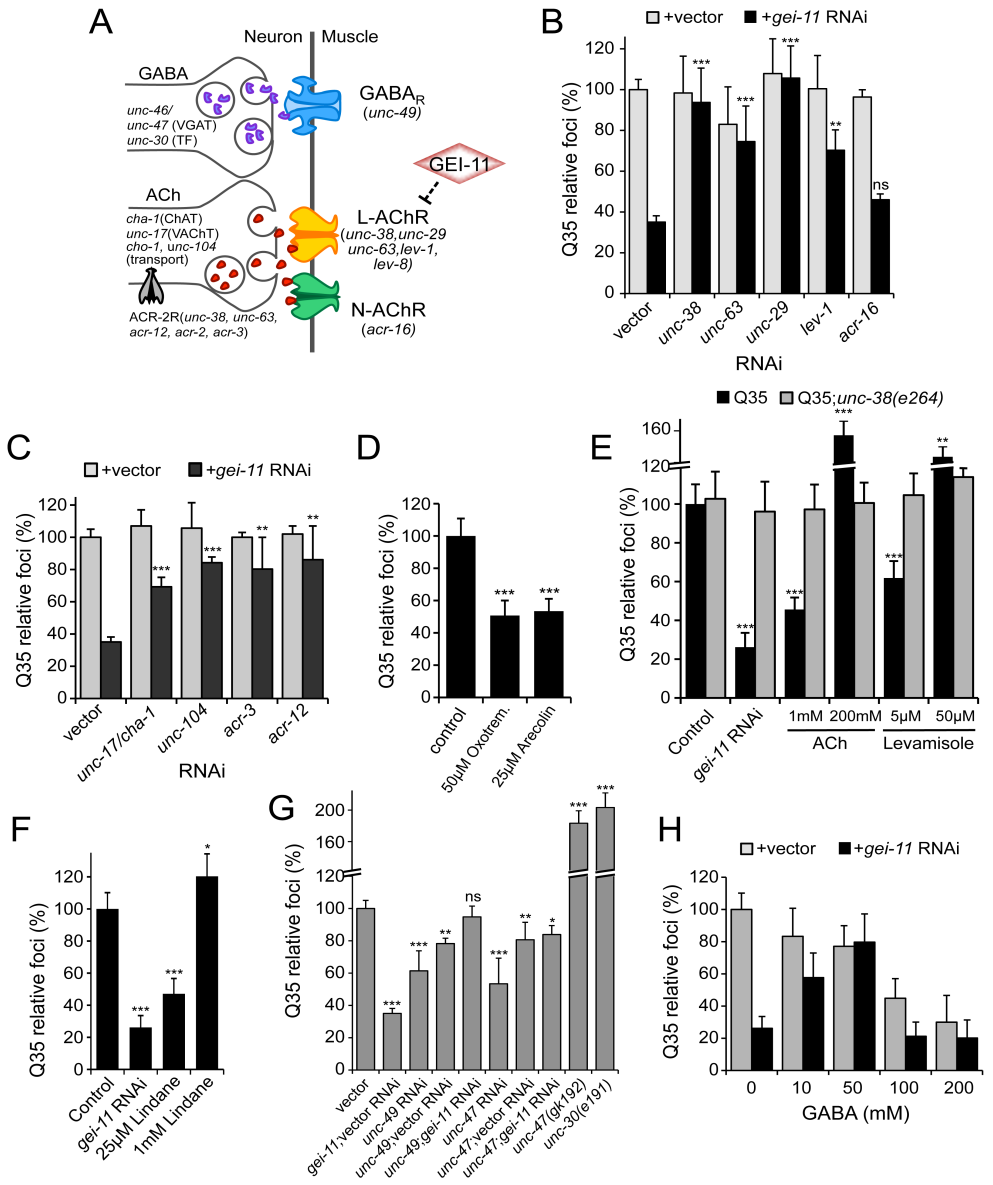

Figure 4: Regulation of Cholinergic and GABAergic Signaling Effect on Post-Synaptic Protein Aggregation. (A) NMJ components required for motor neuronal signal, ACh and GABA synthesis/release: choline acetyltransferase (*cha-1*); ACh vesicle and transport (*unc-17; unc-104, cho-1*); motor neuron AChR (ACR-2R); L-type AChR (*unc-38, unc-29, unc-63, lev-1, lev-8*); N-type AChR (*acr-16*); vesicular GABA transport (*unc-46, unc-47*); GABAergic transcription factor (*unc-30*); $GABA_R$ (*unc-49*). **(B)** Suppression of Q35 aggregation by *gei-11* RNAi was abolished by double-RNAi with L-AChR (*unc-38, unc-63, unc-29, lev-1*) but not with N-AChR (*acr-16)*. Individual RNAi controls included. **(C)** Suppression of Q35 aggregation by *gei-11* RNAi was prevented by disrupting ACh synthesis/transport (*cha-1, unc-17, unc-104*) and neuronal signal (*acr-3, acr-12*) with RNAi. **(D)** Increase in neuronal cholinergic signaling with muscarinic receptor agonists Arecolin (25 μM) and Oxotremorine M (50 μM) led to 50% reduction in Q35 aggregation. **(E)** Increase in cholinergic signaling with L-AChR agonists ACh and levamisole suppressed Q35 aggregation at 1 mM and 5 μM, respectively; but enhanced aggregation at 200 mM and 50 μM, respectively. Mutant AChR *unc-38(e264)* is a control for AChR-mediated effect. **(F)** Reduction in $GABA_R$ function with Lindane suppressed Q35 aggregation at 25 μM, and enhanced aggregation at 1 mM concentration. **(G)** Modulation of GABAergic signaling effect on Q35 aggregation: decrease in GABA by *unc-49* and *unc-47* RNAi, or eliminating GABA with *unc-47* or *unc-30* mutants. **(H)** Incubation with GABA 50-200 mM suppressed Q35 aggregation. GABA at 50 mM abolished the suppressor effect of *gei-11*, possibly by "re-balancing" the GABAergic-cholinergic signaling ratio. Student t-test **p*<0.05, ***p*<0.01 and ****p*<0.001; data and statistics are relative to Q35;vector control (±SD).

μM), Q35 aggregation was enhanced by 50 to 60% (Figure 4E). As expected, these agonists did not affect aggregation of AChR mutant animals (Q35;*unc-38(e264)*) (Figures 4E). These results are consistent with a range for cholinergic stimulation improvement of muscle proteostasis, beyond which overstimulation leads to an opposite deleterious effect.

We characterized further the range of ACh/GABA signaling at the NMJ that restores post-synaptic protein homeostasis. Suppression of Q35 aggregation by moderate increase in AChR activity (*gei-11* RNAi), was mimicked by a moderate decrease in GABAergic activity with the $GABA_R$ antagonist Lindane, at 25 μM (Figure 4F). However, a high concentration of Lindane (1 mM), corresponding to a stronger inhibition of GABAergic signaling and overstimulation of BWM cells, led to enhancement of Q35 aggregation, as reported previously (Figure 4F) [167]. We also tested genetically, if modulating expression of $GABA_R$ or GABA release would have opposite effects on post-synaptic protein aggregation, as seen with the AChR modulators. We "titrated" GABAergic signaling by using *unc-30* (GABA synthesis), *unc-47* (GABA transport) and *unc-49* ($GABA_R$) (Figure 4A) RNAi dilutions and loss-of-function mutations. Knockdown of *unc-47* and *unc-49* suppressed Q35 aggregation, and the effect was less penetrant when RNAi was diluted 1:1 with vector RNAi (Figure 4G). However, *unc-30(e191)* and *unc-47(gk192)* mutants that eliminate GABA signaling had the opposite enhancer effect (Figure 4G), also as previously reported [167]. When combined, knockdown of *unc-47* or *unc-49* with *gei-11*, did not affect Q35 aggregation, as both contribute to increased cholinergic stimulation of the muscle, representing the threshold above which it becomes deleterious (Figure 4G). To further test the effect of cholinergic/GABAergic balance on post-synaptic folding, we exposed *gei-11* RNAi-treated Q35 animals to increasing concentrations of GABA. At low concentrations (≤50 mM) GABA cancelled the *gei-11*-mediated increase in cholinergic signaling and suppression of Q35 aggregation, in a dose-dependent manner (Figure 4H). However, at higher GABA concentrations (50 mM-200 mM), the equilibrium was shifted to the opposite direction leading to aggregation suppression by GABA (Figure 4H) [167].

We then examined HSR activation by modulation of cholinergic/GABAergic signaling. Consistent with the effect on protein aggregation, activation of chaperone expression (*hsp-70: C12C8.1* and *F44E5.4*) was dependent on AChR activity, as shown with the antagonist dTBC (2.5 mM) or AChR mutants *unc-29 (e1072)* and *unc-63(x26)*; and dependent on neuronal cholinergic function, as shown with the double knockdown with *cha-1* or *unc-104*, that abolished HSR induction (Figure 5A). Conversely, increase in cholinergic signaling at the NMJ, by chemical modulation with AChR agonists ACh (1 mM) and levamisole (5 μM), with the $GABA_R$ antagonist Lindane (25 μM), or with the neuronal cholinergic muscarinic agonists Oxotremorine M (50 μM) and Arecolin (25 μM), induced expression of *hsp-70* chaperones (Figure 5B), reflecting rescue of the folding environment (Figure 4E, F). We also show that treatment with muscarinic agonists upregulated expression of the AChR subunits *unc-29* and *unc-38* by >2-fold (Figure 5B), consistent with regulation of AChR transcription by neuronal cholinergic stimulation [220,221], and emphasizing the physiological relevance of cell non-autonomous regulation of muscle proteostasis. Finally, we demonstrate that GABA reduction with *unc-47* or *unc-49* RNAi, equivalent to a moderate increase in AChR function, upregulated *hsp-70* by <9-fold (Figure 5C) and restored folding (Figure 4G),

whereas overstimulation by eliminating GABA with mutants *unc-47(gk192)* or *unc-49(e407)* led to stress and upregulation of *hsp-70* by >50-fold (Figure 5C), consistent with aggregation enhancement (Figure 4G).

Taken together, the results demonstrate that modulation of synaptic activity, by shifting the balance between cholinergic/GABAergic signaling in either direction, can affect post-synaptic proteostasis, within a critical range that leads to activation of chaperone expression and rescue of protein folding. Here, we distinguish between the beneficial consequences of moderate increase in cholinergic stimulation of muscle cells, and the deleterious consequence on the cellular folding environment caused by overstimulation.

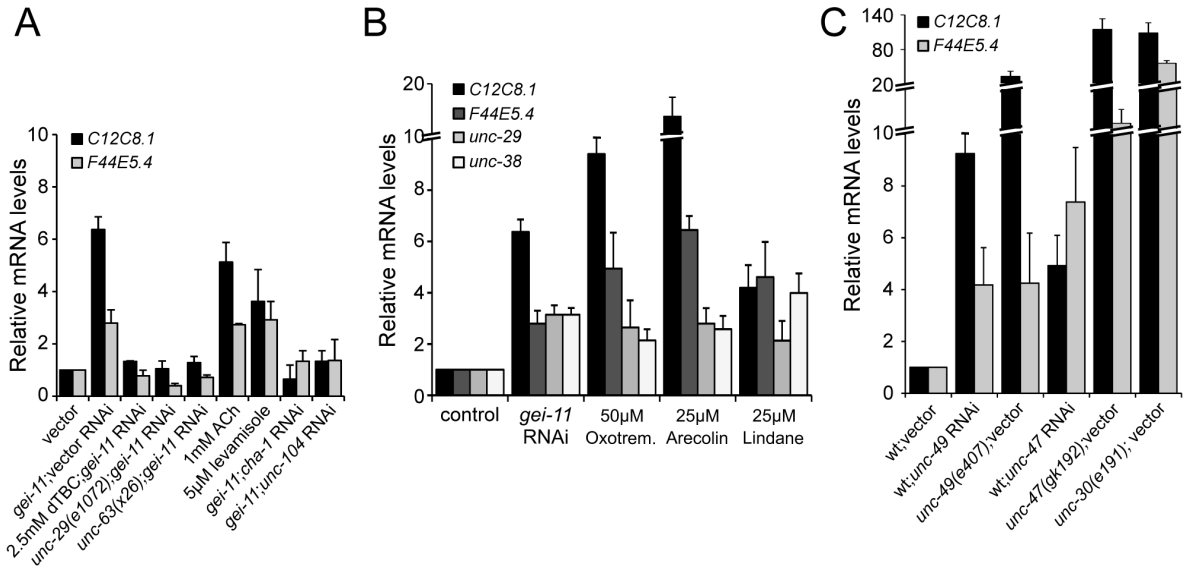

Figure 5: Activation of Chaperone Expression by Regulation of Cholinergic/GABAergic Signaling. Real-time qPCR analysis of *hsp-70* (*C12C8.1, F44E5.4*) levels in 5 day old wt animals **(A)** upon *gei-11* RNAi and AChR antagonist dTBC co-treatment, upon *gei-11* RNAi in the background of AChR mutants *unc-29(e1072)* and *unc-63(x26*), upon treatment with ACh or levamisole, and upon *gei-11* double RNAi with *unc-104* or *cha-1* genes (ACh synthesis and release) (±SD); **(B)** upon treatment with muscarinic agonist (Oxotremorin M or Arecolin) or the $GABA_R$ antagonist Lindane (±SD); **(C)** upon decrease in GABAergic signaling, by either RNAi or mutation of *unc-47*, *unc-49* or *unc-30* (±SD).

Cholinergic Signaling Leads to EGL-19 Activation and Ca^{2+} Influx Upstream of HSF-1 Activation

ACh binding to receptors in BWM cells leads to activation of the voltage-gated calcium channel (VGCC), EGL-19, and the consequent flux of calcium (Ca^{2+}) into the cytoplasm [224] (Figure 6A). We investigated whether Ca^{2+} influx promoted by increased cholinergic activity contributes to HSF-1 activation by using the cell permeant Ca^{2+} chelator BAPTA [224]. BAPTA at 15 μM had no effect on Q35 aggregation, but together with *gei-11* RNAi, prevented suppression of polyQ aggregation and induction of *hsp* chaperones (Figure S4A, B). To further explore the contribution of Ca^{2+} for the folding environment on muscle cells, we examined how genetic modulation of EGL-19 activity affected protein aggregation. We employed a partial loss-of-function mutant, with a 30% decrease in Ca^{2+} flux (*egl-19(n582)*), a weak hypermorphic (*egl-19(n582ad952)*) and a hypermorphic mutant (*egl-19(ad695)*) in the background of Q35 [224,225]. The results show that the magnitude of modulation of Ca^{2+} flux in the muscle had opposing

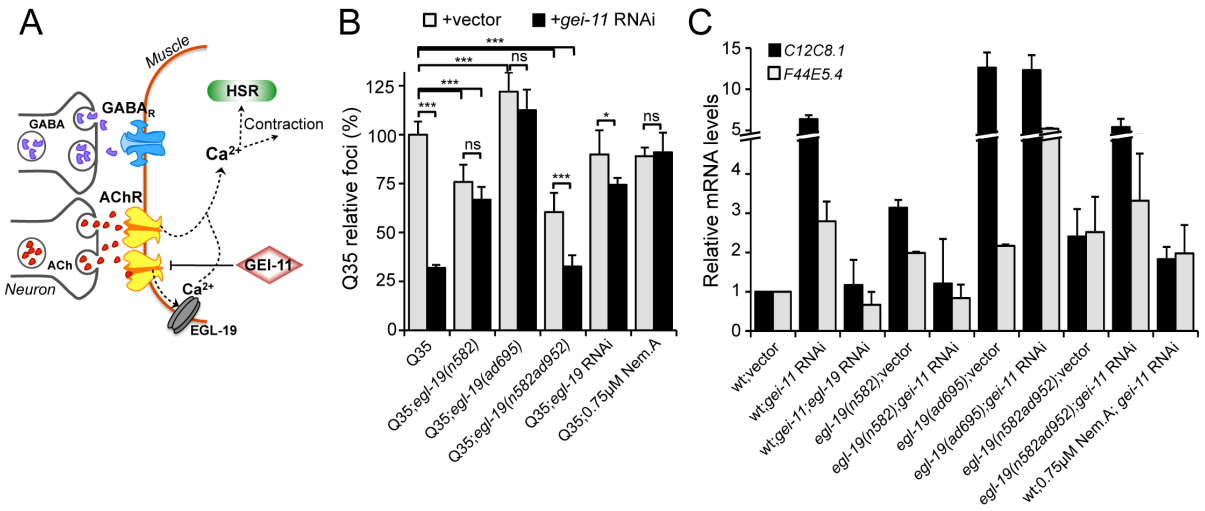

Figure 6: The VGCC EGL-19 is Involved in HSR Activation and Suppression of Aggregation in the Muscle. (A) Cholinergic signaling activates EGL-19 and Ca^{2+} flux into the cytoplasm for muscle contraction. **(B,C)** We tested the effect of Ca^{2+} flux, with and without *gei-11*, on Q35 aggregation (B) and *hsp-70* (*C12C8.1, F44E5.4*) induction in wt animals (C) by employing a hypomorphic mutant *egl-19(n582)*, a weak hypermorph *egl-19(n582ad952)*, a hypermorph *egl-19(ad695), egl-19* RNAi or the specific antagonist Nemadipine A. *gei-11* RNAi did not suppress Q35 aggregation (B) or induce *hsp-70* levels (C) in hypomorphic mutant *egl-19(n582)* animals, in animals co-treated with Nemadipine A (0.75 µM at L2), or with *egl-19* RNAi, showing dependence on EGL-19/Ca^{2+} for folding improvement. Student t-test *p<0.05, ***p<0.001, ns/not significant; data relative to vector control (±SD). See also Figure S4.

effects. Whereas the stronger hypermorphic mutant *ad695* enhanced Q35 aggregation, both the weak hypermorphic *n582ad952* and hypomorphic *n582* mutants suppressed Q35 aggregation (Figure 6B) [167]. Animals where Ca^{2+}-mediated enhanced aggregation was observed (*ad695*), also had a high upregulation of *hsp-70* levels (*C12C8.1, F44E5.4*; 15-fold), consistent with cellular stress, compared to the moderate chaperone induction (3-fold) in animals where Ca^{2+} suppressed aggregation (*n582* and *n582ad952*; Figure 6C). These results reveal that modulation of Ca^{2+} flux and cholinergic signaling had an equivalent effect on muscle proteostasis, with a critical range for rescuing protein folding.

We then treated Q35;*egl-19* mutant animals with *gei-11* RNAi, to determine if suppression of aggregation by *gei-11* was dependent on Ca^{2+} flux through the VGCC (Figure 6B). In the hypomorphic *n582* mutant, *gei-11* knockdown did not suppress Q35 aggregation (Figure 6B) and did not induce *hsp-70* expression (Figure 6C), revealing that Ca^{2+} flux through EGL-19 is required for the *gei-11* effect. This result was supported by using *egl-19* RNAi and the EGL-19 inhibitor Nemadipine A [226], that also abolished the *gei-11* effect on muscle proteostasis (Figures 6B, C and S4C). The effect of the weak hypermorphic mutant *egl-19(n582ad952)* was additive to *gei-11* RNAi in folding rescue (Figure 6B, C), whereas the stronger hypermorphic mutant *ad695* increase in Ca^{2+} seems to be at the threshold for causing deleterious stress, as it did not affect aggregation but induced *hsp-70* expression to higher level (Figure 6C). Taken together, the results show that EGL-19 and Ca^{2+} influx function downstream of cholinergic signaling and contribute to improvement in post-synaptic protein folding. Furthermore, as for cholinergic signaling, we found a critical range for modulation of Ca^{2+} flux that improves proteostasis.

Sarcoplasmic Reticulum Ryanodine Receptor Contributes to Ca^{2+} Effect on Muscle Proteostasis

Activation of the VGCC and Ca^{2+} flux into the cytoplasm triggers the opening of the ryanodine receptor (RYR) at the sarcoplasmic reticulum (SR), that also releases Ca^{2+} into the cytosol (Figure 7C) [227,228]. We hypothesized that Ca^{2+} release by RYR could further amplify the signaling cascade from the AChR, and thus contribute to induction of the HSR. Therefore, we examined whether increased RYR activity could mimic the effect of enhanced cholinergic signaling at the NMJ. Ryanodine (Ryr), a plant alkaloid with high affinity to the RYR, is a pharmacological agent widely used to study intracellular Ca^{2+} signaling in muscle cells [227,228]. At low concentrations (nM range) ryanodine acts as an agonist and sensitizes RYR channels to activation by Ca^{2+} [229,230]. Incubation of Q35 animals with Ryr (50 nM) suppressed aggregation (Figure 7A), and was less effective in the background of the hypomorphic mutant *egl-19(n582)* (60% vs. 40%) (Figure 7A), consistent with our hypothesis that the two Ca^{2+} channels function in the same pathway. These results show that flux of Ca^{2+} from the SR is a component of the mechanism triggered at the NMJ to improve the folding environment.

Recognizing that Ca^{2+} regulates many signaling cascades, we examined the specificity of *gei-11*-dependent Ca^{2+} release by the RYR, on induction of *hsp-70* and suppression of polyQ aggregation by testing RYR agonists and antagonists. As for the natural agonist ryanodine, the clinically used activator 4-Chloro-m-cresol (4-CmC) [231] up-regulated *hsp-70* levels and significantly reduced Q35 aggregation by more than 60% (Figures 7A, B S4D). This emphasizes the contribution of Ca^{2+} release by the RYR to the improvement in folding. At the highest concentrations of 4-CmC (>1mM), we observed toxicity and no effect of aggregation (Figure S4D), consistent with a critical range for Ca^{2+} that restores homeostasis in muscle cells. We next tested dantrolene sodium (DS), a clinically used muscle relaxant that selectively targets RYR and blocks Ca^{2+} release from the SR during muscle contraction [232,233]. This antagonist prevented induction of *hsp-70* and suppression of Q35 aggregation by *gei-11* RNAi (Figures 7A, B, S4E). A similar result was obtained with the RYR mutant *unc-68(kh30)* (Figure 7B) [227], supporting a role for RYR-Ca^{2+} on the mechanism leading to HSR activation. Finally, treatment of EGL-19 hypomorphic mutant animals (Q35;*egl-19(n582)*) with the RYR modulators had no significant effect on aggregation (Figure 7A) supporting the epistatic relationship of the two Ca^{2+} channels. Collectively, these results demonstrate that the downstream events of increased cholinergic signaling, involve Ca^{2+}-dependent activation of the HSR and folding rescue in BWM cells.

The increased flux of cytoplasmic Ca^{2+} promoted the activation of HSF-1, leading us to propose that this could occur through activation of Ca^{2+}-dependent kinases. Previous studies on HSR regulation have shown that HSF-1 activity is regulated by phosphorylation in multiple serine residues, implicating Ca^{2+} and Ca^{2+}-dependent kinase activities [35,234-239]. Here, we have tested a large group of kinases known to be calcium regulated in *C. elegans* (Figure S5A), and we have identified the ortholog kinases to be required for HSR induction by *gei-11* RNAi (Figure S5B, C): calmodulins *cal-2* and *cal-4*; *unc-43*/CaMKII ortholog; *pkc-1, pkc-3*, and *gsk-3*. This overlap places these kinases at a critical step between Ca^{2+} flux and activation of HSF-1, and it will be interesting to further explore if they represent the direct link between increase in Ca^{2+} levels in the cytosol, triggered by increased cholinergic signaling, and activation of HSF-1 in *C. elegans*.

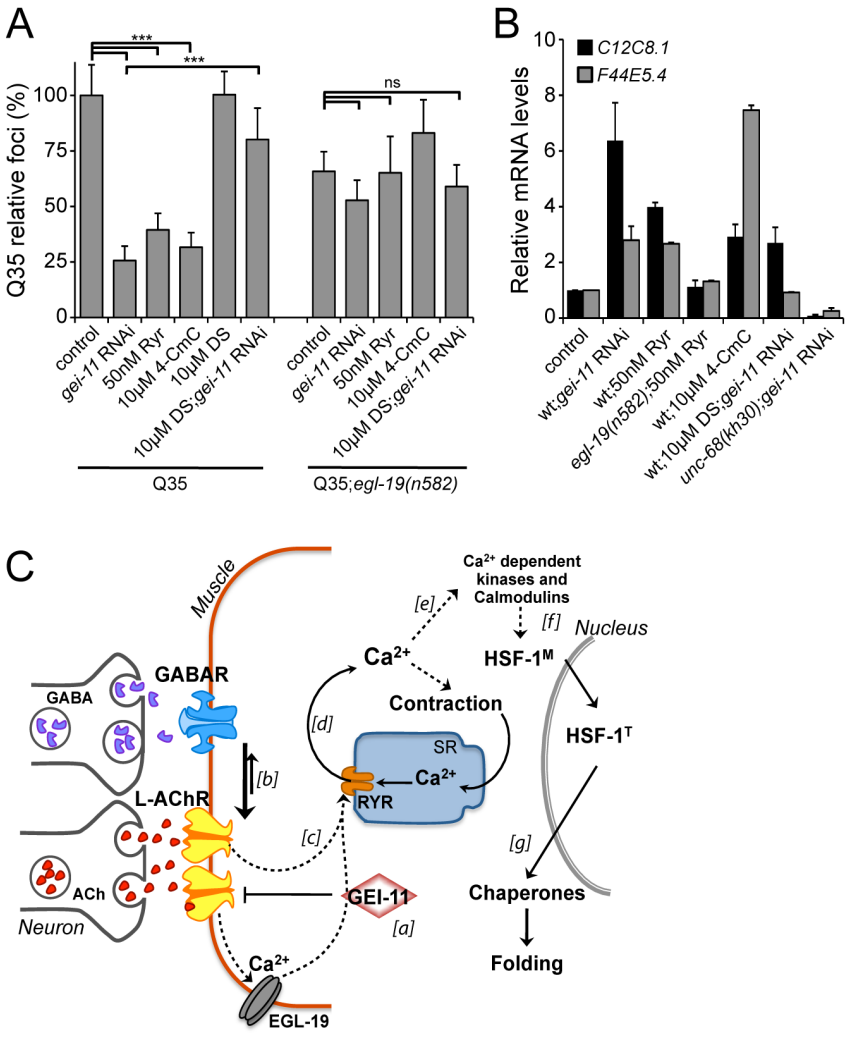

Figure 7: RYR-Mediated Ca^{2+} Contribution to HSR and Folding Improvement. (A) The RYR agonists ryanodine (50 nM) and 4-CmC (10 µM) suppressed Q35 aggregation in a similar way to *gei-11* RNAi (at L2), but were less efficient in Q35;*egl-19(n582)* hypomorphic mutant animals. Treatment with the RYR antagonist DS (at L2) together with *gei-11* RNAi prevented suppression of Q35 aggregation. % Foci are relative to vector (±SD). Student t-test ***p<0.001, n.s./no significance. **(B)** Real-time qPCR analysis of *hsp-70* (*C12C8.1, F44E5.4*) levels: RYR agonists Ryr (50 nM) and 4-CmC (10 µM) up-regulated *hsp-70* in wt animals but not in mutant *egl-19(n582)* animals. Chaperone induction by *gei-11* RNAi was prevented in the RYR mutant (*unc-68(kh30)*) and by co-treatment with DS (±SD). **(C)** Model for GEI-11 modulation of proteostasis in BWM. GEI-11 negatively regulates cholinergic signaling at the NMJ, through L-AChR activity. [a] Knockdown of *gei-11* leads to an increase in L-AChR activity and excitatory signaling into the muscle [b]. ACh binding to AChRs activates the VGCC EGL-19. [c] Depolarization, conformational changes and Ca^{2+} influx through EGL-19 triggers the opening of RYR at the SR and further release of Ca^{2+} into the cytosol [d]. Ca^{2+} activates signaling cascades to promote muscle contraction [e], HSF-1 activation and expression of cytosolic chaperones that rescue protein folding in the cytosol [f-g]. See also Figures S4 and S5.

DISCUSSION

This study provides new insight on the role of synaptic signaling on cell non-autonomous control of proteostasis. A moderate increase in cholinergic signaling at the NMJ, either by genetic upregulation of L-AChR activity (*gei-11*) or downregulation of GABA, led to selective activation of HSF-1, up-regulation of cytosolic chaperones and rescue of the folding environment in muscle cells (Figure 7C). The important distinction in the results presented here and the previous work describing the consequences of blocking GABA with an *unc-30* null mutation [167] is that enhanced protein aggregation occurs when GABAergic signaling is completely inhibited, thus resulting in maximum cholinergic overstimulation of muscle cells. Here, we characterize the biological consequences of increased AChR expression (≤3-fold) and an

intermediate level signaling response. We make the distinction between the beneficial and biologically relevant consequences of moderate increase in cholinergic stimulation, and the deleterious consequence on the cellular folding environment caused by overstimulation of the muscle cells. Therefore, we demonstrate a critical range for modulation of cholinergic/GABAergic signaling at the NMJ that leads to rescue of protein folding. In agreement with our model, high cholinergic stimulation of the muscle with high concentrations of AChR agonists or complete inhibition of GABAergic signaling was deleterious to muscle cells, as shown by enhanced protein aggregation. In contrast, a mild stimulation of muscle cells, either with low concentrations of AChR agonists or by dampening GABA signaling suppressed aggregation. As for cholinergic signaling, modulation of Ca^{2+} flux to improve protein folding in muscle cells also occurs at a critical range. The activation of both EGL-19 and RYR channels, leads to increased cytoplasmic Ca^{2+} to a level that was sufficient to activate HSF-1, but below the threshold that causes ER or mitochondrial stress. These results shift the emphasis from extreme environmental forms of stress to characterization of *in vivo* physiologically relevant stress signaling pathways.

In *C. elegans*, neurotransmitters are released in a graded fashion, such that the intensity of postsynaptic currents correlates with the strength of neuronal stimulation [240]. This trait provides a broad dynamic range for neuronal control of muscle function and protection against protein damage. There is a growing body of evidence for the neuronal regulation of protein homeostasis; in particular that neuronal dysfunction impairs HSR capacity in somatic cells [164], induces post-synaptic muscle protein misfolding and proteolysis [166,167], and affects longevity [120]. Our studies have identified GEI-11 as a new genetic modifier of neuro-muscular regulation of proteostasis. In the proposed model (Figure 7C), downregulation of *gei-11* and subsequent increase in cholinergic stimulation of muscle cells, improved the folding of metastable proteins in muscle cells through the activation of HSF-1 and chaperone expression. The regulation of the HSR in a cell non-autonomous manner by cholinergic signaling at the NMJ represents an organismal strategy that is likely to be of broad relevance for communication of proteostatic imbalance across tissues. Our results with neuronal cholinergic/muscarinic agonists corroborate that muscle function and homeostasis can be rescued by chemical modulation of neuronal activity, in addition to genetic regulation of muscle receptor expression. This is a relevant observation for complex pathologies such as neurodegenerative and neuromuscular disorders, where scenarios of protein misfolding initiated at one tissue have both autonomous and non-autonomous consequences on cellular and tissue function, organismal health and lifespan. For example, selective neuronal degeneration leads to muscle weakness and paralysis in motor neuron disorders such as ALS, hereditary spastic paraplegia, and spinal muscular atrophy [80]. Consequently, an understanding of the regulatory signaling cascades that trigger protective responses across tissues is of fundamental importance to delay or prevent organismal collapse of proteostasis. Modulation of signaling events at the NMJ to rescue muscle function, such as described here for *gei-11*, represent new therapeutic targets for genetic and chemical modulation of proteostasis maintenance.

Our findings strongly suggest that cell non-autonomous control of proteostasis, through neuronal signaling and Ca^{2+}-dependent activation of the HSR in stressed cells, is a critical new mechanism in the cellular challenge to maintain homeostasis and proteome health. During aging and chronic stress, as the

cellular quality control systems are challenged by the persistent expression of misfolded toxic proteins, an imbalance in neuronal signaling may therefore lead to dysregulated proteostasis. Fine-tuning of neuronal cholinergic signaling, within a well-defined physiological range, represents a new target to re-shape the functional properties of the proteostasis network. Our results contribute to the growing understanding of the organizational properties of stress response networks as an integrated organismal response to diverse homeostasis challenges to the health of the cell and lifespan of the organism.

EXPERIMENTAL PROCEDURES

***C. elegans* Strains:** Animals were maintained according to standard methods, at 20°C on nematode growth media (NGM) with OP50 *E. coli* (Brenner, 1974). The strains utilized in this work, and previously described, are the following: wild-type (wt) Bristol strain N2; polyQ strains Q24 AM138 (rmIs130[P_{unc-54}::*q24*::*yfp*]II), Q35 AM140 (rmIs132 [P_{unc-54}::*q35*::*yfp*]I), Q37 AM470 (rmIs225[P_{unc-54}::*q37*::*yfp*]II) (Morley et al., 2002; Nollen et al., 2004); human $SOD1^{G93A}$ AM265 (rmIs177[P_{unc-54}::$sod1^{G93A}$::*yfp*]) (Gidalevitz et al., 2009); temperature sensitive (TS) mutant strains CB1402 [*unc-15(e1402)*], CB1157 [*unc-54(e1157)*], HE250 [*unc-52(e669su250)*] and CB286 [*unc-45(e286)*] (Gidalevitz et al., 2006); WM27 [*rde-1(ne219)*] and WM118 [*rde-1(ne219);neIs9[myo-3::HA::RDE-1+pRF4(rol-6(su1006))]*] (Bolz et al., 2010; Qadota et al., 2007); CB1072 [*unc-29(e1072)*], CB904 [*unc-38(e264)*], ZZ26 [*unc-63(x26)*], RB918 [*acr-16 (ok789)*], VC311 [*unc-47(gk192)*], CB845 [*unc-30(e191)*], CB407 [*unc-49(e407)*] (Garcia et al., 2007), MT1212 [*egl-19 (n582)*], DA952 [*egl-19(n582ad952)*], DA695 [*egl-19(ad695)*] (Jospin et al., 2002; Lee et al., 1997), HK30 [*unc-68 (kh30)*], PS3551 [*hsf-1(sy441)*]. Genetic crosses of mutant animals with Q35 were generated where indicated.

RNAi Assays: RNAi gene knockdown in *C. elegans* was performed as described previously, using the commercial RNAi library (GeneServiceTM, USA) (Kamath and Ahringer, 2003; Nollen et al., 2004). Briefly, animals were added to RNAi bacteria (in liquid or RNAi-seeded NGM plates) at the L1 stage (first larval, day 1), incubated at 20°C for 5 days and scored for reduction in the number of aggregates at 6 days old (which corresponds to 3 days after the onset of Q35 aggregation), using the stereomicroscope Leica MZ16FA (Leica Microsystems, Switzerland). Aggregates were identified as discrete, bright fluorescent foci-like structures distinguishable from the surrounding fluorescence. As a negative control, animals were fed bacteria carrying the L4440 empty vector (vector). Liquid RNAi treatment was performed in 96-well plates, with a total volume of 60 µl per well, consisting of 15-20 worms and RNAi bacteria. Bacteria was grown overnight (~16h), induced with isopropyl β-D-thiogalatoside (IPTG Sigma, 1 mM for 3 h at 37°C), pelleted and resuspended in S-medium complete (S-Basal supplemented with 3 mM $MgSO_4$, 3 mM $CaCl_2$, 10 mM KCitrate, 100 mg/ml Ampicillin and 1 mM IPTG) so that the final OD_{595nm} was 0.9 in the well. For RNAi assays on plates, NGM media was supplemented with 100 µg/ml ampicillin (Sigma), 1 mM IPTG and 12 µg/ml tetracycline (Invitrogen), and seeded with overnight (~16h) RNAi bacteria cultures, pre-induced with IPTG (1 mM for 3 h at 37°C). For double knockdown experiments, equal volumes of each RNAi bacteria were mixed (1:1 ratio) prior to plate seeding. Q35 aggregation was scored in at least 50 animals, for each condition, always at 6 days of age ($n \geq 3$). Fluorescent microscopy images were taken using an Axiovert 200 microscope with a Hamamatsu digital camera C4742-98 (Carl Zeiss, Germany). All RNAi plasmids were sequenced to confirm correct and specific gene-target identity. Gene knockdown by RNAi was confirmed by PCR.

FRAP Analysis: Animals were mounted on a 3% (w/v) agar pad on a glass slide, immobilized with 2 mM levamisole (Sigma), and subjected to FRAP analysis using the Zeiss LSM510 confocal microscope (Carl Zeiss, Germany), and the 63X objective lens at 5X zoom power, with the 514 nm line for excitation. An area of 0.623 μm^2 was bleached for 35 iterations at 100% transmission, after which time an image was collected every 123.35 ms. Relative fluorescence intensity (RFI) was determined as previously described (Garcia et al., 2007; Phair and Misteli, 2000).

Motility Assays: Six day old animals grown on RNAi-seeded NGM plates were picked (~20 per assay) onto plates seeded with OP50 bacteria and equilibrated at 20°C. Their movements were digitally recorded using a Leica M205 FA microscope with a Hamamatsu digital camera C10600-10B (Orca-R2, Leica Microsystems, Switzerland), and the Hamamatsu Simple PCI Imaging software. Videos of 45 s were recorded for a minimum of 75 animals per experiment and the animals were tracked using a custom ImageJ plugin wrMTrck (see Extended Experimental Procedures). The average speed of each animal was calculated by dividing the distance of each track, corrected for body length, by the

duration (in seconds) of the track (body length per second BLPS). Motility measurements are given as a percentage of wt motility in vector RNAi (100%) and *n≥3*.

Real-Time qPCR Analysis: RNA from ~50 animals was extracted with Trizol (Invitrogen), followed by DNase treatment (Applied Biosystems #AM1906). mRNA was reverse transcribed using the iScriptTM cDNA Synthesis Kit (Bio-Rad #170-8891). 10 ng of cDNA were used for real-time PCR amplification using the iQ™ SYBR® Green Supermix (Bio-Rad #170-8880) and the iCycler system (Bio-Rad) (see Extended Experimental Procedures). Expression levels of each gene were determined using the Comparative C_T Method (Real-Time PCR Applications Guide, Bio-Rad), normalized to actin (*act-1*) in the same sample (internal control), and then determined relative to the non-treated or vector control sample. Measurements were performed for ≥3 biological samples.

Paralysis Assays with Cholinergic Agonists: Five day old animals grown on RNAi-seeded NGM plates at 20°C (≤40) were transferred onto fresh NGM plates, equilibrated at 20°C, containing 1 mM Levamisole (Sigma), 30 mM Nicotine (Sigma) or the solvent (water or ethanol, respectively). Sensitivity to the drugs was followed by visual inspection every 2 to 5 min and defined as paralysis, or lack of movement in response to prodding on the nose and tail of the animal (*n=3*). Compound stock solutions: 800 mM levamisole (Sigma) in water, 300 mM nicotine (Sigma) in ethanol.

Compound Assays: Compound assays were performed in liquid culture as described previously (Voisine et al., 2007), with 60 µl of final volume per well, 15-20 animals (added in S-Basal complete), compound at the appropriate concentration and bacteria (OP50 or RNAi) at a final OD_{595nm} of 0.9 (also resuspended in S-Basal complete). We included replicates of each condition per assay plate. Animals were incubated with each drug from L1 stage (ACh, levamisole, GABA, Oxotremorine M, Arecolin), L2 stage (Lindane, Ryanodine, Nemadipine A, Dantrolene Sodium, 4-CmC) or L4 stage (dTBC, BAPTA), until day 6 of age, at 20°C (*n≥3*) (see Extended Experimental Procedures). At this time animals were transferred from liquid culture onto NGM plates for aggregate quantification (Leica MZ16FA), and/or collected for real-time qPCR analysis.

Assay for TS Phenotypes: Temperature sensitive (TS) mutant animals were age-synchronized to L1 stage, grown on RNAi-seeded NGM plates (~20 animals per plate) from day 1 at a sensitized temperature of 23°C (to maintain the RNAi suppressor effect on aggregation, used as control) and scored for phenotypes on day 5. For the 25°C restrictive temperature control experiment, L1 nematodes were grown on EV RNAi at 15°C until L4 stage to avoid embryonic and developmental phenotypes, then transferred to 25°C and scored 2 days later for the same phenotypes. For the 15°C permissive temperature control experiment, L1 animals were added to RNAi plates, grown at 15°C and scored for phenotypes on day 6 (to account for slower but normal development at this temperature). >50 animals were scored for each TS phenotype, per assy, as described previously: slow movement/paralysis assay for *unc-15(e1402)* and *unc-54 (e1157)*, stiff paralysis for *unc-52(e669su250)*, and egg-laying phenotype for *unc-45(e286)* (partially paralyzed animals with a large belly of accumulated eggs) (*n=3*) (Garcia et al., 2007; Gidalevitz et al., 2006).

Gel Mobility Shift Analysis: Native nuclear protein extracts were prepared from >200 µl of pelleted worms (grown on NGM RNAi-seeded plates), with the commercial Thermo Scientific NE-PER Nuclear and Cytoplasmic Extraction Kit (# 78835), as described previously (Mah et al., 2007). Electrophoretic mobility shift analysis (EMSA) was performed as before (Mosser et al., 1988) using a [^{32}P]-labeled probe containing the proximal heat shock element (HSE) from the *C. elegans hsp-70* (*C12C8.1)* gene promoter. Nuclear extracts (40 µg) were incubated with the [^{32}P]-labeled probe (HSE or mutant) for 20 min at room temperature. For heat shock treatment (HS) the samples were pre-incubated at 35°C for 30 min. For competition experiments, a 100-fold molar excess of the same unlabeled oligonucleotide was added to the mixture. The samples were analyzed by electrophoresis on a 4% (w/v) polyacrylamide native gel that was dried and

scanned using a PhosphorImager (Molecular Dynamics, Sunnyvale, CA). Oligonucleotide probes: HSE.F: taaattgtagaaggttctagaagatgccaga; HSE.R: tctggcatcttctagaaccttctacaattta;
HSE^{mut}.F: taaattgtaaaaggaaataaaagatgccaga; HSE^{mut}.R: tctggcatcttttatttccttttacaattta.

ACKNOWLEDGEMENTS: We thank members of the Morimoto lab for discussions and comments, Monica Beam for help with the FRAP experiments and the Biological Imaging Facility at Northwestern University, and Dr. Patricjia Hawle for the Q35;WM118 and Q35;WM27 crossed strains. These studies were supported by grants from the Portuguese *Fundação para a Ciência e Tecnologia* SFRH/BD/28461/2006 (to MCS) and FCT/POCTI/BIA-BCM/56609/2004 (to MDA); and from the National Institutes of Health (NIGMS, NIA, NINDS), the Huntington's Disease Society of America Coalition for the Cure, and the Daniel F. and Ada L. Rice Foundation (to R.I.M).

Extended Experimental Procedures

Motility Assays: Videos of 45 s were recorded at 2x2 binning and 5 frames per second, and captured frames were merged into **.avi* format and imported directly into ImageJ. Using the LOCI bio-formats plugin and a custom stack deflicker plugin (http://www.loci.wisc.edu/bio-formats/imagej), light average intensity was normalized for each frame. To enhance the definition of the animals in the movies, the difference between each frame and the constant background was calculated, using the Maximum Z-stack projection. The resulting movie was converted to binary format using Otsu Thresholding 2. Binary objects representing the animals were tracked using custom ImageJ plugin, wrMTrck (based on "MTrack2" by Nico Stuurman (Klopfenstein and Vale, 2004)). The average speed of each animal was calculated by dividing the length of each track (corrected to animal body length) by its duration (body length per second, or BLPS). The wrMTrck plugin and scripts for automated analysis are open-source and publicly available at http://www.phage.dk/plugins.

PCR Analysis: Animal lysis and RNA extraction were accomplished by vortexing with Trizol (Invitrogen). Chloroform was added to each sample, followed by vortexing and centrifugation at 13,500xg for 15 min (4°C). 2-Propanol was added to the aqueous layer and total RNA was spun down at 18,000xg (4°C) for 10 min. RNA pellets were washed with 75% (v/v) ethanol, air-dried and resuspended in nuclease free water. RNA aliquots of 10 µg were used for DNase treatment (Applied Biosystems #AM1906), and purified RNA was used for cDNA synthesis (Bio-Rad #170-8891). For real time PCR analysis, 10 ng of cDNA were used for PCR amplification with specific primers for each gene (see list below) and the iQ™ SYBR® Green Supermix (Bio-Rad #170-8880), in the iCycler system (Bio-Rad). For standard PCR, cDNA samples were amplified with the following primers:
actin.F 5'-ATCACCGCTCTTGCCCCATC-3'; actin.R 5'-GGCCGGACTCGTCGTATTCTTG-3';
Q35-yfp.F 5'-GCTGCCCGACAACCACTAC-3'; Q35-yfp.R 5'-TGGCGATCTGATGACAGCGG-3'.
Amplified products were ran on a 1% (w/v) agarose-TBE gel with ethidium bromide, and scanned with the UV scanner Alpha Imager EC (Alpha Innotech).
Primers used for real-time qPCR:
gei-11.F ctctcgatgcatcggttaagc; *gei-11*.R gttgttcgtcttcaaccagc;
unc-29.F gaggaccaaccgactatcatgg; *unc-29*.R cacattgatgagcaacaccaac;
unc-38.F catgggatccagtgaattatggg; *unc-38*.R atactcttgaagattgctggtg;
unc-63.F ggaccaaatgaccacggttttgc; *unc-63*.R gaacgtcaccacgagtgtctctc;

acr-16.F ctcatctcgtgcgcaattcttgc; *acr-16*.R cgtcaattatttgttggagggc;
unc-49.F gttgccgcagtttgtacttcagtc; *unc-49*.R cgacaatcaggacagatggtag;
lev-8.F ggagagccacatatcacaatcac; *lev*-8.R gtttctccgtcattcgaccatcc;
C12C8.1.F actcatgtgcggtatttatca; *C12C8.1*.R acgggctttccttgtttt;
C30C11.4.F gcttcgtactattgtggaatctc; *C30C11.4*.R ggagatcttgcttgtagattcc;
F44E5.4.F gtcttgatgcaaagctattggtatc; *F44E5.4*.R cgtcgtccaatcaatccttttgcatc;
hsp-16.1.F actttaccactatttccgtccagc; *hsp-16.1*.R gataatgtatgtccatccaaatta;
hsp-12.6.F atgatgagcgttccagtgatggctgacg; *hsp-12.6*.R ccatgtgaatccaagttgctcttg;
hsp-16.49.F ccatattggagaaatgctgatcac; *hsp-16.49*.R cttctggtagccgcctcattttg;
mtl-1.F ggcttgcaagtgtgactgcaaaaacaagc; *mtl-1*.R ttaatgagccgcagcagttccctggtgttgatgg;
sod-3.F gcttcaaagcttgttcaaccggttgcg; *sod-3*.R cagcgctggttggagagcaattgc;
hsp-6.F caggccgttaccaactctgc; *hsp-6*.R gcagtttccttcatcttcatc;
gcs-1.F gtgcaagtgtcgacgatcgtac; *gcs-1*.R gcgaatatgttttgccagtggctc;
gst-4.F cgactccatttggccagc; *gst-4*.R gatcagcgtcacttctag;
hsp-4.F gcagatgatcaagcccaaaaag; *hsp-4*.R ggagacgattggttgaacaacag;
hsp-3.F cctacggacttgacaagaaggac; *hsp-3*.R gaacggcacgattgtctttgc;
dnj-7.F gagcacggatagtacggac; *dnj-7*.R gaggcaagccatccagtc;
ero-1.F cgacgaaatgcagtgaatatg; *ero-1*.R gtgtagcgttccggattcttcg;

Compound Assays: Assays were performed in 96-well plates with 15-20 animals per well in a total volume of 60 µl, compound at the appropriate concentration and bacteria (OP50, vector RNAi or *gei-11* RNAi bacteria). RNAi bacteria grown overnight (~16h) was induced with IPTG (1 mM for 3.5 h at 37°C), pelleted and resuspended in S-medium complete (S-Basal supplemented with 3 mM $MgSO_4$, 3 mM $CaCl_2$, 10 mM KCitrate, 100 mg/ml Ampicillin and 1 mM IPTG) so that the final OD_{595nm} is 0.9 in the well. Compound stock solutions: 550 mM Acetylcholine (Sigma) in water; 500 mM GABA (Sigma) in water; 1 mM Levamisole (Sigma) in water; 200 mM (+)-Tubocurarine Chloride (D-Tubocurare/dTBC, Sigma) in water; 100 mM Lindane (Sigma) in 10% ethanol; 10 mM Oxotremorine M (Sigma) in water; 10 mM Arecolin (Sigma) in water; 5 mM Ryanodine (Tocris Bioscience) in 100% ethanol; 1 mM Nemadipine A (Nem.A, Sigma) in 100% DMSO (dilutions in water); 5mM BAPTA (Invitrogen) in 100% DMSO; 10mM Dantrolene Sodium (DS, Sigma) in 100% DMSO; 20mM 4-Chloro-m-cresol (4-CmC, Supelco Analytical) in water.

SDS-PAGE and Western Blotting Analysis*:* Six day old animals (50 to 100 animals) grown on RNAi-seeded NGM plates at 20°C, were collected with M9 buffer, pelleted at 3,000xg and resuspended in PELE buffer [20 mM Tris pH7.4, 10% glycerol, 2% Triton X-100, 0.5 mM PMSF, 1 µg/ml leupeptin, 1 µg/ml pepstatin, 1 mM EDTA, 1 mM DTT, protease inhibitor cocktail tablet (Roche Diagnostics #11836170001)]. Lysis was accomplished by a combination of 4 cycles of freeze-thaw, grinding with a motorized pestle (Kontes #749541-000 and #749520-0000), followed by 3 cycles of 2 min sonication (Sonicator Bath Branson 1510, Branson) and mixing. SDS was added to a final concentration of 5% (v/v) and samples were boiled for 5 min. Total protein concentration was determined using the Bradford assay (Bio-Rad #500-0006). 16 µg of total protein were loaded onto a 10% (w/v) SDS-PAGE followed by Western blotting. For Q35-YFP detection, blots were probed with the anti-GFP IR800 conjugated antibody (1:5,000 dilution; Rockland Immunochemicals #600-132-215). For α-tubulin detection (55 KDa), the same blots were probed with the anti-α-tubulin primary antibody (1;4,000 dilution; Sigma #T-5168) followed by the secondary antibody Alexa Fluor®680 goat anti-mouse IgG (1:10,000 dilution; Molecular probes #A-21057). Antibody binding was detected with the Odyssey Infrared Imaging System (LI-COR Biosciences, USA) and intensity of the bands was measured using Adobe Photoshop 7.0. To determine relative Q35 protein levels, the ratio YFP/α-tubulin between band intensities was calculated (arbitrary units) and compared to the EV control sample (*n≥3).*

SUPPLEMENTAL FIGURES

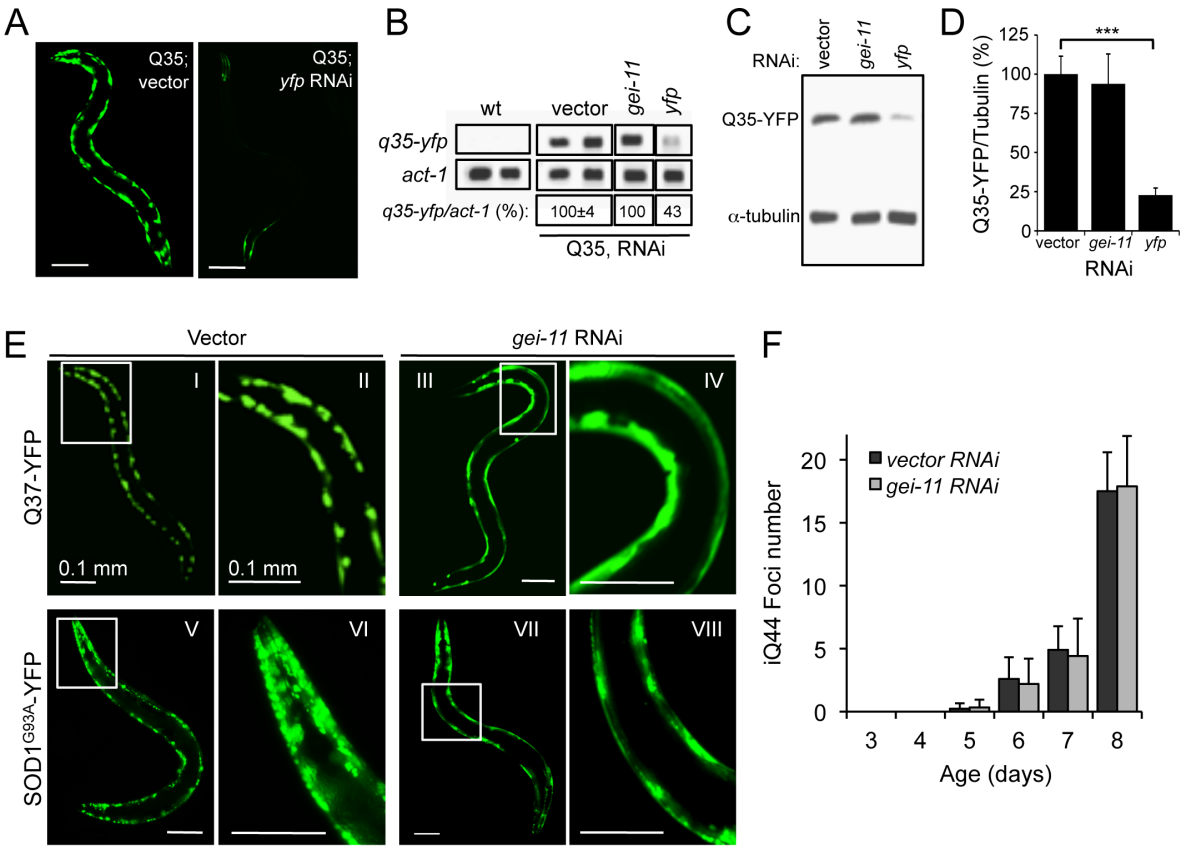

Figure S1: Suppression of Protein Aggregation in BWM cells by *gei-11* RNAi, Related to Figure 1. (A) *yfp*-RNAi was a control for RNAi efficiency, causing a significant decrease in fluorescence. **(B)** RT-PCR amplification of *q35-yfp* (top panel). mRNA from wt animals was a negative control for transgene amplification (left); *yfp*-RNAi was a positive control for reduced *q35* mRNA levels. Actin (bottom panel) was the control for total mRNA. Band intensities were used to calculate relative mRNA levels to control (*n*=3). **(C,D)** SDS-PAGE and western blotting analysis of Q35 protein levels, with anti-YFP (top) and anti-α-tubulin (bottom) antibodies. Q35 protein levels relative to tubulin were calculated from band intensities on (C), and are shown as a relative percentage of the vector control (*n*=3, Student t-test ***p<0.001, ±SD). **(E)** *gei-11* RNAi suppressed Q37 (I-IV) and SOD1^{G93A} (V-VIII) aggregation in BWM cells of 5 day old animals, shown by the diffuse fluorescent pattern in III, IV, VII and VII in contrast to a foci-like pattern in the vector control I, II, V and VI. Panels II, IV, VI and VIII are high magnification images of the boxed areas in I, III, V and VII, respectively (scale bar 0.1 mm). **(F)** *gei-11* knockdown did not affect polyQ aggregation in the intestine (iQ44), relative to control RNAi animals.

RNAi	Mean Lifespan (days) ± SEM	N	% control lifespan	*p-value*
Vector only	16. ± 0.32	109	100	-
gei-11;vector	18.7 ± 0.39	86	113	< 0.001
daf-2	23.9 ± 0.23	102	144	< 0.001
hsf-1	12.4 ± 0.20	93	75	< 0.001
gei-11;hsf-1	12.9 ± 0.20	80	78	< 0.001
daf-2;hsf-1	14.7 ± 0.32	77	89	0.003

Table S1: Effect of *gei-11* RNAi on lifespan of wt animals at 20°C. RNAi for *hsf-1* and *daf-2* are negative and positive controls, respectively, for extension of lifespan. Statistical *p*-value calculated with the Log-rank/ Mantel Cox test.

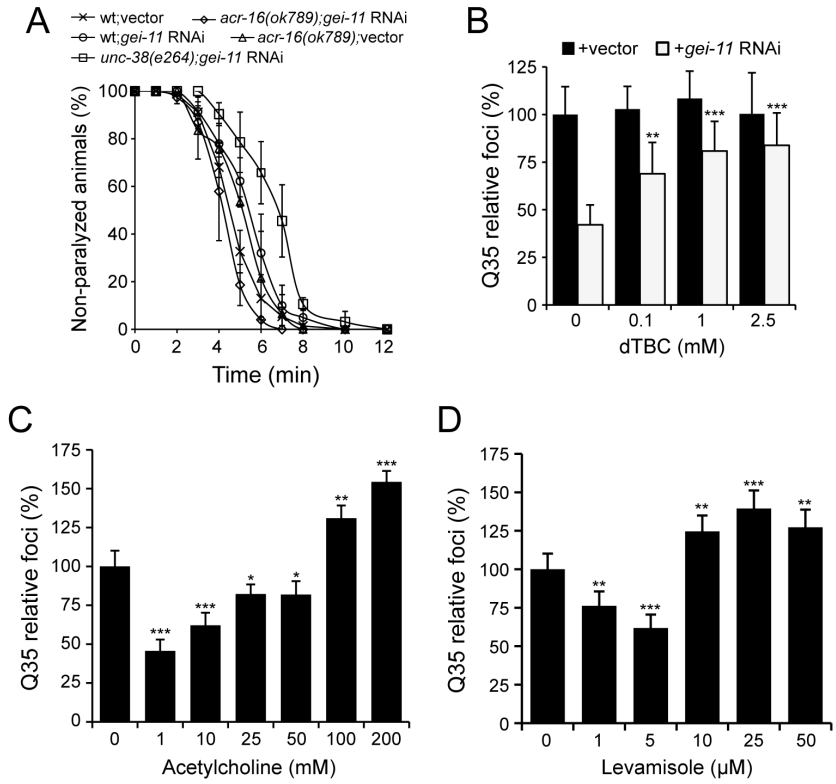

Figure S2: Suppression of Aggregation by Cholinergic Signaling, Related to Figures 2 and 4. (A) Cholinergic sensitivity assay: 5 day old animals treated with *gei-11* or vector RNAi were scored for paralysis on plates containing 30 mM nicotine (±SD). N-AChR mutant *acr-16(ok789)* and L-AChR mutant *unc-38(e264)* were used as controls for receptor specificity. Two-way ANOVA $p>0.05$ relative to vector control. **(B-D)** Dose-dependent effect of cholinergic antagonist dTBC and cholinergic agonists ACh and levamisole on Q35 aggregation (±SD). Student t-test $*p<0.05$, $**p<0.01$ and $***p<0.001$; data and statistics are relative to Q35;vector (±SD).

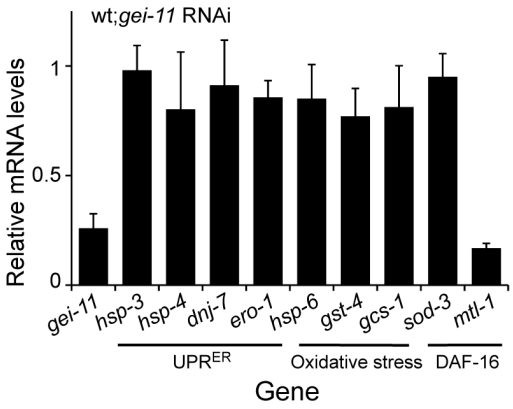

Figure S3: Effect of *gei-11* Knockdown on Stress Responses, Related to Figure 3. Real-time qPCR analysis of wt animals treated with *gei-11* RNAi did not show induction of UPR-regulated ER chaperones, metabolic stress FOXO/DAF-16 regulated or oxidative stress regulated genes (±SD, data normalized to the levels of each gene in vector control).

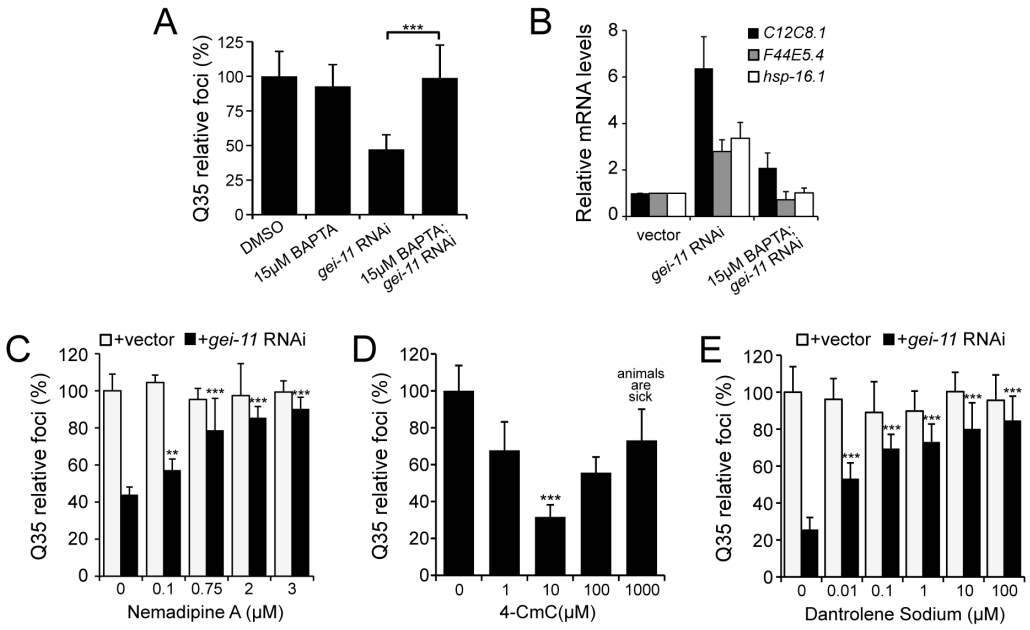

Figure S4: Suppression of Q35 Aggregation by Increase in Ca^{2+} Flux, Related to Figures 6 and 7. (A,B) Suppression of Q35 aggregation and *hsp* induction by *gei-11* RNAi are calcium dependent, and were prevented by co-treatment with the chelator BAPTA (15 μM at L4). Data are relative to Q35;DMSO control (±SD). **(C)** Dose-dependent effect of Nemadipine A on suppression of Q35 aggregation by *gei-11* RNAi. Data are relative to Q35 in vector RNAi (±SD). **(D,E)** Dose-dependent effect of the RYR agonist 4-CmC and the antagonist DS on Q35 aggregation. % of foci are relative to Q35;water control for 4-CmC and Q35;DMSO for DS (±SD). Student t-test ***p<0.001 and **p<0.01.

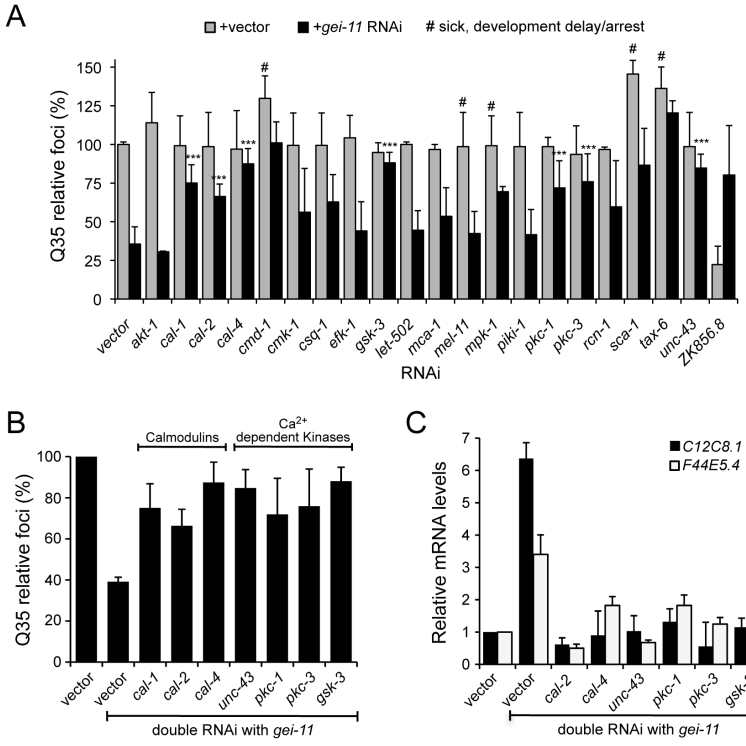

Figure S5: Ca^{2+}-Dependent Kinases and Calmodulins Required for Folding Improvement, Related to Figure 7. **(A)** RNAi of Ca^{2+}-dependent kinases and calmodulins tested for effect on Q35 aggregation, with and without *gei-11*, by double RNAi (±SD). **(B)** Double knockdown of *gei-11* with calmodulin *cal-1, cal-2,* or *cal-4*; or Ca^{2+}-dependent kinase *unc-43, pkc-1, pkc-3,* or *gsk-3*, prevented suppression of Q35 aggregation (±SD). % of foci are relative to Q35 in vector RNAi; Student t-test p<0.001. **(C)** Real-time qPCR analysis of *hsp-70* levels in wt animals upon *gei-11* double RNAi with the indicated genes (±SD). Data are relative vector-treated wt animals.

CHAPTER IV

GENERAL DISCUSSION

GENERAL DISCUSSION

As protein folding and homeostasis are essential for cellular function, they are kept under tight surveillance by a network of pathways that constitute the proteostasis network. Yet, the stability of the proteome is constantly put at risk by both intrinsic factors (*e.g*. genetic mutations, aging) and extrinsic stress agents (*e.g*. drastic temperature change, exposure to toxins and pathogens) that disrupt homeostasis beyond the functional capacity of the PN, and often leading to disease states (Figure 1). These include conditions that derive from the accumulation of misfolded proteins in toxic and aggregated aberrant conformations, such as Alzheimer's, Parkinson's and Huntington's diseases, as well as muscular distrophies, ataxias and some metabolic disorders. Although protein aggregation is a common characteristic among these pathologies, the events leading to cellular toxicity are quite more complex. In fact, great attention has been drawn to the identity of the "toxic species" causing disease, and evidence indicates that multiple misfolded and oligomeric species may contribute to cellular toxicity by disrupting various cellular functions [86]. Although aggregates are found in the areas of the brain most affected by neurodegeneration, the highest content of insoluble aggregates and amyloid plaques does not correlate with disease severity [102-104]. In fact, in model systems for disease, toxicity is often exacerbated when inclusions formation is prevented or reduced and in other cases, the presence of oligomers is a better predictor of disease progression [98-101]. Recent work has demonstrated that oligomeric toxic conformations have similar conformations (or epitopes) that are recognized by a specific set of antibodies designed to bind and reduce the toxicity of these species [111,112,241]. Altogether, it is clear that the cellular events involved in protein aggregation, toxicity and ultimately degeneration are intricate and still rather poorly understood. This is among the

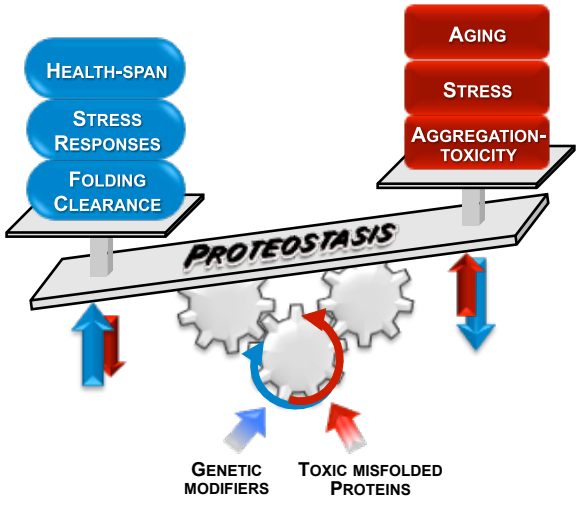

Figure 1: Proteostasis network function ("balance") dictates disease propensity and health span. Proteostasis is composed by a network of cellular processes responsible for maintaining homeostasis, resistance to stress and health-span/longevity. Expression of aggregation-prone proteins poses a chronic insult to PN function (imbalance), leading to aging-related diseases. Genetic screens performed in model organisms have identified gene modifiers of proteostasis that increase folding capacity and protection against stress of protein aggregation, preventing or delaying disease-related events (re-balance).

main reasons hindering the development of efficient therapeutics.

Another way of addressing the problem is by asking why the QC system cannot maintain homeostasis, or why the stress responses are not activated by the noxious proteins. It is currently understood that neurodegenerative and motor-neuron diseases derive from the toxicity of the misfolded species and not from their loss-of-function. Then, the determinant of disease becomes the proteostasis network itself, and its (lack of) ability to deal with these proteins, *e.g.* by to promoting degradation thus avoiding the accumulation of toxic conformations. The absence of this response suggests that the functional capacity of the PN becomes saturated and overwhelmed by the chronic expression of aggregation-prone proteins, in a time-dependent manner. This is in part the reason why most of these diseases have a late onset. Here, we tested the hypothesis that the PN functional capacity can be modified to improve folding function, maintain homeostasis and delay/prevent disease-related cellular/ organismal phenotypes. We have taken advantage of the metazoan *C. elegans* as a tractable genetic model system for expression of conformationally challenged proteins and for the ability to screen the genome for modifiers of protein folding. The power of genetics in model systems is then complemented by small molecules to unravel new regulators of proteostasis and new target pathways for development of therapeutics (Figure 2).

1. Genetic Suppression of Protein Aggregation and Toxicity

We took a genetic approach to examine whether the proteostasis network can be genetically modulated to increase capacity of protection against the toxicity of protein aggregation (Chapter II). This study was complementary to previous work that led to the identification of the QC components: molecular chaperones, ubiquitin-proteasome, autophagy, and the upstream stress response signaling pathways. Here, we employed a screening triage method that initially revealed genetic modifiers that suppress aggregation of polyQ and are also effective with mutant SOD1, defining candidates of a core PN. Only a subset of the suppressors of aggregation (42%) also suppressed cellular toxicity, with approximately equal numbers having either no effect on toxicity or even enhancing toxicity. This demonstrated that aggregation and toxicity can be genetically uncoupled, supporting that aggregation and toxicity are not obligatory co-linked genetic traits. Furthermore, to examine if the monomeric vs. oligomeric vs. aggregated state of the protein (polyQ) was correlated with the outcome in toxicity, we monitored the biophysical properties of the polyQ protein upon suppression of aggregation with the dynamic imaging technique fluorescence correlation spectroscopy (FCS) (Appendix I). At the detection limit, suppression of aggregation led to mixed populations of protein species, including soluble monomers and oligomers. No discrete populations of oligomers were correlated with enhanced or suppressed toxicity, arguing against the concept that a single toxic species causes the disease state. Even when aggregation and toxicity were both suppressed, heterogeneous populations of soluble polyQ proteins were still detected. Similarly, on an age-dependent study, we found that the heterogeneous oligomeric species pattern is also intensified at older age. We

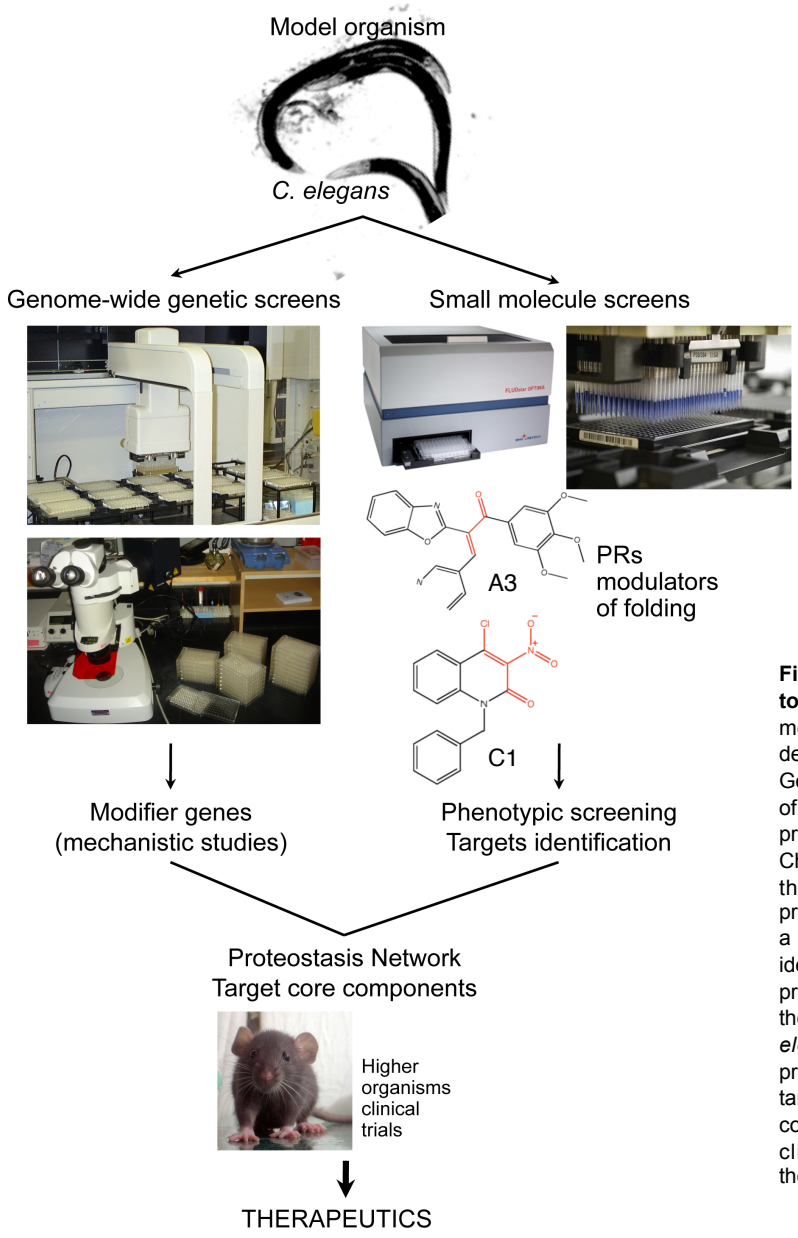

Figure 2: From genetic model organisms to the development of therapeutics. The model organism employed in the work described here was mainly *C. elegans*. Genetic screens using RNAi provided a list of modifier genes of PN function, that affect protein misfolding, aggregation and toxicity. Characterization of these genes allowed for the discovery of new mechanisms of proteostasis maintenance. Simultaneously, a large scale small molecule screen identified new small molecule regulators of proteostasis, followed by characterization of the mode of action in cellular models and *C. elegans*. Together, these two methods provide a platform to uncover important and targetable pathways within the PN, that could be tested in higher organisms and clinical trials for the development of therapeutics of conformational disorders.

concluded that multiple oligomeric states can co-exist in the cell as inert oligomeric and misfolded conformations, with potential to turn into toxic conformers and aggregates if the PN becomes "unbalanced" or saturated, as would be the case during aging or chronic expression of aggregating proteins.

From a mechanistic perspective it is increasingly clear that a series of events are associated with the conversion of the nascent polyQ protein into different oligomeric states and inclusion bodies. Likewise, the genetic suppression of aggregation can occur via a wide range of mechanisms. Each modifier gene functions within its own network of interacting partners, revealing an expanding network through which each modifier can suppress aggregation, with differential effects on toxicity as well, depending on the affected cellular function. We predicted that the modifiers could suppress aggregation in one of two ways: (1) either by directly interfering with the inter-molecular interactions, nucleation dynamics or recruitment of

species into inclusions; or (2) indirectly by activating stress responses and chaperone expression, therefore enhancing proteostasis capacity and preventing formation of toxic species. It was our goal to identify the aggregation modifiers that enhanced proteostasis function. We reasoned that modifiers that suppressed both aggregation and toxicity in the aggregation models would be strong candidates. We then identified 9 modifier genes that also improved the folding of multiple endogenous metastable proteins, revealing a core group of PN genes never before linked to quality control nor to proteostasis. Perturbation of each of these 9 genes re-adjusts the PN to enhance its functional capacity, activating distinct stress responses (not shown) that affect folding and health span. The study of these genes promised to reveal new mechanisms involved in protein homeostasis, both at the cellular and at organismal levels.

2. New Regulators of Homeostasis: Activation of Stress Responses to Rescue Folding

The PN core modifiers that we identified either play a role in the mitochondrial respiratory chain and TCA cycle, thus regulating metabolism, energy balance and prevention of oxidative stress, or are related to rRNA processing and transcription, processes that determine gene expression and the proteome load. Identification of these processes is an important contribution to understanding of the components that constitute the PN, beyond the “typical” QC machinery. In terms of the relevance of these functional classes to protein folding, reduction in ATP or ETC activity have been shown to slow down aging, possibly by delaying the age-dependent collapse in proteostasis [60], and compromised mitochondrial function can lead to the upregulation of multiple stress-response pathways that ultimately promote homeostasis and survival [120,147,184,185]. Restriction in energy levels also hinders overall protein biogenesis, as synthesis, folding and clearance activities are ATP-dependent. Metabolic enzymes influence protein folding in the cell by providing organic/inorganic solutes that affect polypeptide chain solvation and hence, solubility [58]. On the other hand, reduced RNA processing/gene expression (and protein synthesis) have been proposed to extend the organism lifespan by activating a physiological state with increased stress resistance, folding and repair capacities [186-188]. In addition to these predicted consequences on proteostasis, we characterized further the role of two of the modifiers.

We then pursued the characterization of the genetic modifier *gei-11* and found that its downregulation caused an increase in expression of the L-type AChR in muscle cells, leading to muscle cholinergic stimulation. This, in turn, provoked Ca^{2+} influx through the voltage-gated calcium channel (EGL-19) and the ryanodine receptor (UNC-68) in the cytoplasm, as well as activation of HSF-1 and chaperone expression that ameliorate folding (Chapter III). This finding is complementary to an earlier study where a deletion mutant of *unc-30* that regulates GABA expression in *C. elegans* neurons, results in enhanced polyQ aggregation in muscle cells [167]. An important distinction in the genetics that led to these discoveries must, however, be emphasized. Previously, enhanced protein aggregation was observed upon complete inhibition of GABAergic signaling (due to the null mutation in *unc-30*), resulting in maximum

cholinergic overstimulation of muscle cells. Whereas, in the current study, upon *gei-11* knockdown, the effect of increased AChR expression is quite different from the complete inhibition of GABA signaling, in part because the signaling response occurs at an intermediate level. This makes an important distinction between the beneficial consequences of a moderate increase in stimulation of the muscle, and the deleterious consequence to the folding environment of complete overstimulation. This distinction reveals the importance of a threshold for the level of induced stress, in this case by muscle cholinergic stimulation (too much is bad but a little is good). This is not too far from the different consequences observed for other HSR inducers, depending on the "magnitude" of the stress. Mild heat shock treatment of cells and *C. elegans* has been shown to upregulate chaperones, cause thermo-adaptation, improve homeostasis and extend lifespan [38,146,242]. However, an acute heat shock treatment has deleterious consequences, such as cell cycle arrest and apoptosis [243]. This reveals that there is a critical range of signaling that leads to chaperone expression and improvement of the folding environment. Moreover, the relevance of neuronal control of post-synaptic homeostasis is becoming increasingly evident. In particular, it has been shown that neuronal dysfunction impairs HSR capacity in somatic cells [164], induces post-synaptic muscle protein misfolding and proteolysis [166,167], and affects longevity [120]. Therefore, the activation of post-synaptic HSR and homeostasis by moderate increase in cholinergic signaling at the NMJ (and muscle stimulation) is prone to be highly biologically relevant for pathologies such as neurodegenerative and neuromuscular disorders, i.e., scenarios where selective neuronal degeneration leads to muscle weakness and paralysis (ALS, hereditary spastic paraplegia, and spinal muscular atrophy) [80]. Fine-tuning of neuronal cholinergic signaling, within a well-defined physiological range, represents a new target to re-shape the functional properties of the proteostasis network at the organismal level. An understanding of the regulatory signaling cascades that trigger protective responses across tissues is of fundamental importance to delay or prevent organismal collapse of proteostasis during aging and disease. Together, these studies provide compelling evidence for the control of stress responses through tissue-specific signaling events and these findings could have only been discovered using an organismal model system. Moreover, because cholinergic and GABAergic signaling are conserved, these results are of broad relevance to the study of muscle cell function, neuronal stimulation of muscle cells, and muscle wasting diseases. Altogether, this work also shifts the emphasis from extreme environmental forms of stress to *in vivo* physiologically relevant stress signaling and sensing.

We have also initiated the characterization of the gene *let-607*, which we show to affect cellular homeostasis in a cell-autonomous manner (Appendix II). LET-607 is predicted to be the *C. elegans* CREBH ortholog, involved in UPR [244] and activated for transcriptional function similarly to ATF-6 [46]. In mammals, CREBh is involved in immune response and hepatocyte's homeostasis [52]. Knockdown of *let-607* in *C. elegans* activated the UPR, the HSR, and expression of both ER and cytosolic chaperones. Upon *let*-607 RNAi the dependence of HSR activation on UPR, through *xbp-1* levels and splicing, suggested that compartmental stress responses can "crosstalk" to reduce protein misfolding and rescue homeostasis. Very little is known about this type of interaction, although it has been shown that impairment of either UPR or HSR can exacerbate the toxic effects of ER or HS-type stress [245,246]. Characterization of the signaling cascade activated at the ER by *let-607* knockdown, and transduced to the nucleus for

HSF-1 activation, promises to reveal new insights into the co-regulation of the ER and cytosolic stress responses, as a measure to rescue proteostasis.

The discovery of folding improvement by knockdown of *let-607* and *gei-11* are two examples of the valuable information provided by genetic screens. In particular, the triage strategy implemented allowed us to select, from an initial large number of hits, the gene candidates with higher probability of having a relevant role in the proteostasis network, by identifying modifiers of the folding capacity instead of protein aggregation-specific modifiers. These pathways within the network are strong candidates for therapeutics targeting.

3. Genetics and Chemical Biology

Despite the increasing understanding of the regulation of stress responses and the organization of the proteostasis network at the cellular and organismal, the inability of this system to prevent protein misfolding in disease and in late age are still very intriguing. With the identification of core components of the PN from genetic screens and elucidation of the roles of key transcription factors in stress response (HSF-1, SKN-1/Nrf2 and DAF-16/FOXO), chaperone activation and proteome stability, it becomes prominent to identify novel small molecules that modulate their activity, in particular HSF-1, with the goal of developing efficient therapeutics for a large number of diseases that still go untreated (Figure 3). Several small molecule activators of HSF-1 are known, and some of these have shown protective effects in models of Huntington's disease and ALS [35,169,170]. Despite the potential benefits shown, further development of these small molecules will be necessary prior to their use as therapeutic agents, mainly due to the high toxicity of some of these compounds [247,248]. Furthermore, while some small molecules like geldanamycin (GA) and other derivatives that inhibit Hsp90 are currently in pre-clinical and clinical trials for the effective treatment of a number of cancers, their efficacy in diseases associated with protein misfolding seems to have limited therapeutic potential. An effort to find new small molecule regulators of proteostasis (proteostasis regulators, PRs) that represent strong therapeutic candidates led to a new large-scale small molecule screen in human cells for HSF-1-dependent activators of chaperone expression (Appendix III). We discovered and characterized novel small molecule PRs that, by enhancing HSF-1 activity, restore proteostasis in multiple disease models, including cytosolic and compartment-specific conformation disorders. A further understanding of these PRs and their ability to activate the HSR and restore protein folding in multiple disease models through genetic studies, offers new strategies for development of small molecule chaperone therapeutics for protein conformational diseases. These PRs represent novel chemical series and, by comparison to previously identified small molecule activators of the HSR, they do not cause protein misfolding, proteasome inhibition, or Hsp90 inhibition. Interestingly, the novel PRs exhibit complex stress response signatures. In addition to inducing HSF-1 and the expression of multiple cytoplasmic chaperones, we have observed the induction of other major components of the PN, including the UPR and the antioxidant response genes (Figure 3). This activation of stress-signaling pathways, in

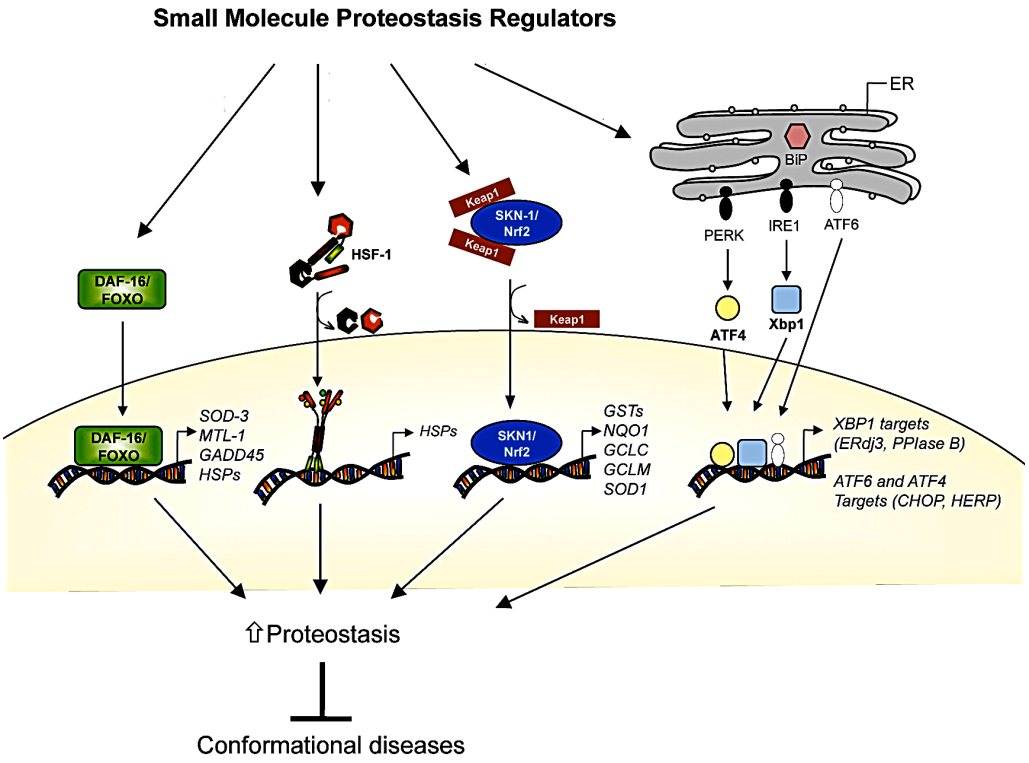

Figure 3: Model depicting the proposed target stress pathways by which small molecules ameliorate conformational diseases. The small molecules PRs work by activating some of the major PN machineries, inducing components of the quality control machinery and other cytoprotective stress response genes. We have found PRs that suppress misfolding and toxicity in disease models that depend on HSF-1 and DAF-16/FOXO or SKN-1/Nrf2 transcription factors. Adapted from Appendix III.

turn restores the stability and functionality of the proteome. The ability of these PRs to activate one or more stress response pathways suggests a mechanism that employs the cell's biological response to damaged proteins to protect cells against chronic disease. In other words, to face the challenges caused by chronic stress and toxicity, the compounds target and enhance the properties of the same biological pathways that are already employed by the cell to manage proteostasis, under physiological conditions.

4. Conclusion and Prospectus

4.1. Concluding Remarks

The main components of the folding machinery have been identified and characterized exhaustively, but when it comes to late-onset diseases of protein aggregation, it has been a difficult task to pin point what goes weary with this machinery. Therefore, we focused on identifying mechanisms causing the enhancement of the proteostasis network function to prevent disease-related events. Altogether, genetic screens for modifiers of disease-related phenotypes in multiple model systems have provided a plethora of genes and pathways that can be modulated to delay and even prevent disease states. How

does research translate from basic genetics to disease therapeutics? The answer is chemical biology. Advances in the small molecule synthesis, testing in cultured cells and model organisms, and elucidation of mechanism of action offer strong therapeutic options.

Here we show that the “fine-tuning” of PN pathways, that are already physiologically employed by the cell for keeping cellular function and homeostasis, enhances the efficacy of stress sensing, reducing misfolding and toxicity of metastable and disease-related proteins. Both GEI-11 and LET-607 modifiers act on specific cellular processes to activate a response that translates into chaperone expression and enhancement of folding. For GEI-11 in particular, we have not only identified a physiological process of neuronal control of muscle function and homeostasis, but also we show for the first time that the neuromuscular junction is under a tight regulatory balance between cholinergic and GABAergic signaling, that can be targeted and modulated to restore folding in disease scenarios. We demonstrate that activation of the HSR and chaperone expression only rescues folding efficiently at a specific magnitude of muscle stimulation but not at more drastic overstimulation conditions. This is a very important aspect when targeting biologically relevant pathways that respond to stress to rescue folding instead of causing even more deleterious stress. We believe that this fits the motto “a little stress could be good”. On the other hand, small molecule PRs of the HSR provide a potentially powerful approach to obtaining proteome balance in both loss- and gain-of-function diseases by providing a superior corrective environment based on properties of the stress pathways. Besides the usefulness for potential therapeutic development, small-molecule inducers of the HSR can be used as research tools for further dissecting the multi-step activation pathway of HSF-1. A better understanding of the regulation of HSF-1 activation pathway and signaling mechanisms could lead to the discovery of compounds that exhibit stress signatures that are HSF-1 selective, rather than activators of multiple stress pathways. Drug target and mechanism of action studies have gained considerable attention, given that many small molecules are initially described to be specific and later found to have multiple additional targets [249,250]. Considerable improvement has been made into drug design to increase specificity, but it is still crucial for pharmacogenetics studies to determine all targets and potential side interactions for each compound.

4.2. Future Work

To complete the characterization of the PN gene modifiers identified and described in this thesis (Chapter II), we have initiated a genetic approach to determined which stress pathways are activated by each modifier. We have asked how downregulation of genes that function primarily in cellular metabolism and RNA processing, alter the PN and through activation of which stress pathways. This approach is consistent with modulation of specific cellular functions causing stress within a particular range, to activate protective mechanisms that ultimately improve folding capacity and restore homeostasis, without causing further cellular/organismal toxicity. This is well illustrated in the characterization of the gene modifier *gei-11.* Through this study we uncovered a novel pathway that can be targeted for modulating neuronal control of muscle function. It will be extremely relevant to identify other components of the neuronal circuitry, either involved in signal magnitude, receptor expression or neurotransmitter synthesis/release, that can be

modulated to alter neuronal function and effect on post-synaptic cells homeostasis. This will be especially relevant for diseases of neuromuscular dysfunction leading to muscle atrophy and early death.

Moreover, we are currently completing the characterization of the modifier gene *let-607*, described in Appendix II, by determining the "type of stress" caused by *let-607* downregulation at the ER, and how that stress is "communicated" to the cytosol for activation of the HSR. We will also validate this mechanism of proteostasis maintenance in mammalian cells, using the ortholog CREBH.

By employing tissue-specific and cellular compartment-specific folding sensors, research is moving towards the characterization of both cell autonomous and cell non-autonomous processes responsible for proteostasis, as an integrated stress response system that is responsible for organismal health- and life-span. Altogether, genetic and chemical modulation of the PN and direct or indirect activation of the HSR, for improvement of protein folding capacity, contribute to the identification of all factors composing the PN, as well as the nodes that can be targeted to promote the most robust improvement in cellular homeostasis/function.

Appendices

Appendix I

Dynamic Imaging of Polyglutamine Aggregation States by Fluorescence Correlation Spectroscopy

Dynamic Imaging of Polyglutamine Aggregation States by Fluorescence Correlation Spectroscopy

Monica Beam[1,3], M. Catarina Silva[1,2], and Richard I. Morimoto[1]

[1]Department of Molecular Biosciences, Northwestern University,
Rice Institute for Biomedical Research, Evanston, IL 60208-3500, USA
[2]Department of Chemistry and Biochemistry, Faculdade de Ciências da Universidade de Lisboa, 1749-016 Lisboa, Portugal
[3]Department of Biomedical Engineering, Northwestern University, Evanston, IL 60208-3500, USA

Submitted

ABSTRACT

Protein misfolding and aggregation are molecular events that become exacerbated with aging and are risk factors for neurodegeneration, metabolic disease, and cancer. Misfolding can lead to the appearance of multiple protein conformational states, including oligomeric and aggregate species. Here, we employ fluorescence correlation spectroscopy (FCS) to analyze the diverse biophysical states of polyglutamine (polyQ) proteins expressed in a *Caenorhabditis elegans* model that exhibits age- and polyQ-length dependent aggregation and toxicity. By employing FCS and fluorescence recovery after photobleaching (FRAP) methods, we detected mixed populations of protein species, including soluble monomers and oligomers, as well as large immobile aggregates, in strains carrying the longer lengths of polyQ and upon aging. Moreover, when RNAi genetic modifiers suppressed aggregation, we detected different heterodisperse populations of soluble polyQ oligomers. These studies reveal that the transition from soluble monomers to immobile aggregates involves intermediate species, but does not support a model in which formation of a discrete population of oligomers is associated with toxicity.

INTRODUCTION

Protein misfolding and aggregation have been implicated in a wide variety of diseases including Amyotrophic Lateral Sclerosis, at least nine CAG-repeat diseases, Alzheimer's disease and Parkinson's disease [73,251]. Many models have been put forth to study the basis of cellular toxicity in these diseases, implicating different conformational and oligomeric states of mutant SOD1, TDP-43, huntingtin, ataxins, Aβ, tau, alpha-synuclein, and parkin, respectively. However, the events leading to aggregation and toxicity remain poorly understood. The majority of studies to elucidate the misfolding pathway have been performed *in vitro* and have proposed four general pathways that lead to aggregates: monomer directed conversion, nucleated polymerization, template assembly, and nucleated conformational conversion (Kelly, 2000). These studies further suggest that more than one of these pathways can contribute to the kinetics of aggregation of specific proteins. For example, studies of Aβ suggest that both template assembly [252-254] and nucleated conformational conversion [255,256] play a role in aggregation. Studies with polyQ suggest that nucleated polymerization [257,258] and template assembly are involved [259,260]. Techniques employing thioflavin T binding and turbidity measurements have indicated the presence of a lag time, growth phase and finally a plateau in formation of fibrils [257,261-263]. More recently, techniques including AFM (atomic force microscopy), EM (electron microscopy), and dynamic light scattering have shown that, during the lag phase, proteins adopt multiple conformational states including oligomers and soluble aggregates [110,193,259,264,265].

While *in vitro* aggregation studies have provided the majority of the kinetics of aggregation data, they also have demonstrated that the kinetics and pathway of aggregation are highly dependent on the environment. Changes in pH, salt concentration, protein concentration and solvent characteristics can have a large effect on lag-time, secondary structures and the type of aggregate species formed [260]. Therefore, *in vivo* conditions may lead to different aggregation events due to the continual generation of monomers and the presence of other proteins such as chaperones that directly interact with misfolded proteins. In fact, dynamic imaging methods including FRAP and FLIP have revealed variability in the [266]

packing structure of *in vivo* aggregates, as well as dynamic interactions with Hsp70 and other molecular chaperones [93,94,163,192,193,266-269].

A technique that offers excellent potential for the study of oligomers both *in vitro* and *in vivo* is fluorescence correlation spectroscopy (FCS), a detection method that can measure changes in diffusion rate at the single molecule level for fluorophore-tagged proteins [270,271]. The FCS analysis autocorrelation function, G(τ), measures the self-similarity of the fluorescent signal after a time (τ) interval [272-274]. Signal fluctuations, arising from changes in molecular physical parameters such as diffusion rate, size, concentration, and brightness intensity, can be determined with precision [95,198,274,275]. Specifically, FCS has been used to detect changes in particle mobility as a result of protein-protein or protein-DNA interactions, or changes in cellular localization [276-280]. FCS has also been used to measure changes in aggregation through detection of appearance of higher order oligomers [281,282], but has not been employed yet to resolve different populations of oligomeric states formed.

The goal of these studies was to monitor the polyQ aggregation pathway in *C. elegans*, and the effect of genetic suppressors of aggregation on the polyQ biophysical properties, using multiple dynamic imaging techniques. Our approach consisted in utilizing FCS based techniques coupled with FRAP and fluorescence imaging to monitor the three main species of the aggregation pathway: monomers, oligomers and aggregates. We show all three states co-exist in the *C. elegans* polyQ model for multiple Q-lengths and ages. We also show that for the aggregation suppressor modifiers tested, oligomers were maintained in a heterogeneous state, although the distribution varied between modifiers, independently of the effect on polyQ toxicity.

MATERIALS AND METHODS

***C. elegans* Strains and Maintenance**: Worms were maintained according to standard methods, at 20°C on nematode growth media (NGM) with OP50 *E. coli* [138]. The polyglutamine strains, expressing different lengths of CAG-repeats fused with YFP, have been described elsewhere (Q0 AM134; Q24 AM138; Q35 AM140; Q37 AM470; and Q40 AM141 in CGC) [119].

Fluorescence Imaging and RNA Interference: To obtain age synchronized populations of L1 larvae (first larval state post egg hatching) for the different polyQ strains, gravid adult animals were bleached with a NaOCl solution [250 mM NaOH and 1:4 (v/v) dilution of commercial bleach] and the eggs were allowed to hatch in M9 buffer overnight at 20°C. Age synchronized L1 animals (day 1) were transferred onto NGM-OP50 bacteria plates and grown at 20°C for different time periods (see Figure 1). Fluorescent microscopy images were taken using the Axiovert 200 microscope with a Hamamatsu digital camera C4742-98 (Carl Zeiss, Germany). RNA interference (RNAi) assays were performed using the commercial *C. elegans* RNAi library, as previously described (GeneService™, USA) [154,283]. NGM plates supplemented with 100 μg/ml ampicillin, 0.5 mM isopropyl β-D-thiogalatoside (IPTG) and 12 μg/ml tetracycline were seeded with overnight RNAi bacteria cultures (~16 h), induced with 1 mM IPTG for 3 hours at 37°C. Age synchronized L1 larvae (day 1) animals were transferred onto NGM-RNAi seeded plates, grown at 20°C for 5 days, and assayed for aggregate count using the stereomicroscope Leica MZ16FA equipped for epifluorescence (Leica Microsystems, Switzerland) (detailed methodology in Chapter II).

Motility Assays: See Chapter II Materials and Methods for detailed description of this assay.

Fluorescence Recovery After Photobleaching (FRAP) Analysis: Animals were mounted on a 3% (w/v) agar pad on a glass slide, immobilized with 2 mM levamisole and subjected to FRAP analysis using the Zeiss LSM510 confocal microscope (Carl Zeiss, Germany), with the 63X objective lens at 5X zoom power, and the 514 nm line for excitation. An area of 0.623 μm^2 was bleached for 35 iterations at 100% transmission, after which time an image was collected every 123.35 ms. Relative fluorescence intensity (RFI) was determined by using $RFI = (T_t/C_t)/(T_0/C_0)$; where T_0 and C_0 represent the intensity of the bleached and control unbleached regions, respectively, prior to bleaching, and T_t and C_t represent the intensity at time t after photobleaching for the bleached and unbleached region, respectively [202].

Fluorescence Correlation Spectroscopy (FCS)

Sample Preparation and Data Collection: Six day old animals (or at the time points indicated in Figure 2D) grown on RNAi or OP50 bacteria were collected and washed with M9 and re-suspended in native-lysis buffer [50 mM Tris pH 7.4, 5 mM $MgCl_2$, 0.5% Triton X-100, 0.2 mM PMSF, 1μg/ml leupeptin, protease inhibitor cocktail tablet]. Lysis was achieved with 4 cycles of freeze-thaw, followed by grinding with a motorized pestle. The lysates were spun at 1,000xg for 3 minutes to remove the larger aggregated species. Centrifugation conditions were determined based on approximation of the sedimentation coefficient for the large visible aggregates at 150,000 S, so that these species were removed from the fraction analyzed by FCS. Total protein concentration was determined using the Bradford assay (Bio-Rad #500-0006). Protein lysates were aliquoted and only thawed once, to ensure minimal effects on oligomers stability. FCS measurements were collected on the Confocor3 system (Carl Zeiss, Germany) using the Apochromat 40x 1.2NA water immersion objective lens. Each sample was loaded into 3 wells of a Nunc #1 coverslip 8-chamber slide (Lab-Tek Chambered Coverglass w/ CVR #155411, Nalge Nunc International, USA) at a total protein concentration of 0.5μg/300μl. YFP was excited with the 514 nm laser line and emission signal was detected by the BP 530-610 IR filter. Each well was sampled for a total of 1500s (either 5x300s, or 50x30s). Each set of measurements was performed twice and each experiment was done in duplicate (at least). This gives a minimum of 5 total hours of FCS data collection per sample, necessary to obtain a large statistical sampling of oligomers present in small relative concentrations.

Autocorrelation curves and fitting: Autocorrelation curves $G(\tau)$ were generated by the Confocor3 software analysis (Carl Zeiss, Germany) [273], and averaged over the different data collections to generate the final plot. Initially attempts were made to fit the data using the autocorrelation function (Equation 1) and fitting software provided by Zeiss.

$$G(\tau) = \frac{1}{N}\sum_{i=1}^{n} b_i \left(\frac{1}{1+\frac{\tau}{\tau_{Di}}}\right)\left(\frac{1}{1+\left(\frac{r}{l}\right)^2\frac{\tau}{\tau_{Di}}}\right)^{\frac{1}{2}} \qquad \text{Equation 1}$$

Brightness Histograms: To generate the brightness histograms we used a program written in Python. Briefly, raw FCS data is examined for local maxima greater than 150 kHz. All peaks are output for further statistical analysis, performed using the Graphpad Prism software. The log of the brightness of the peak was taken, as there are log-fold differences in peak brightness. These values were then placed in bins of width 0.2 on the log scale to generate the final brightness histogram. The *x*-axis represents the bin center which relates to the Log (brightness), where brightness is photon counts per second. The *y*-axis is the fraction of oligomers (out of 1), at a given brightness range. Statistical analysis and significance between values was determined using the Bonferroni t-test (*$p<0.05$*).

Purified Single Molecule FCS: To determine the hydrodynamic size of the oligomers, data was analyzed using the "purified, single-molecule" FCS method, previously described [284]. This technique uses single molecule fluorescence burst analysis. Specifically, bursts of fluorescence (signal greater then 150kHz) are found along the time-scale over which the burst occurs. The region to be analyzed is expanded around the burst by 10-fold the time-width of the burst on either side. By being restrictive in the data set analyzed, the method excludes other bursts within the region that would complicate analysis. Once the specific region has been extracted, the data can be fit with the standard autocorrelation function yielding information on the diffusion rate of the bright species. Results from every burst are plotted in a diffusion rate histogram, allowing the comparison of the distribution of diffusion rates for Qn::YFP in different backgrounds.

RESULTS

Multiple Aggregation States Co-Exist Across Diverse PolyQ Lengths and Ages

In transgenic *C. elegans* expressing different CAG-repeat (polyQ) lengths, Q35 represents the threshold length for time-dependent protein aggregation and toxicity with onset at young adult stage [119]. The age- and Q-length-dependent aggregation pattern was monitored using three methods: fluorescence microscopy, FRAP and FCS.

PolyQ aggregates were observed in Q35, Q37 and Q40 young adult animals but not in Q0 and Q24 animals (Figure 1A). For Q35 animals, the appearance of visible aggregates was age-dependent: Q35 remained soluble until day 4, and the number of aggregates, detected as bright foci by fluorescence

microscopy, increased during adulthood (Figure 1D). The transition from soluble to aggregated state during aging (Figure 1E) is also associated with increased cellular toxicity [119]. A similar profile was observed for Q37 animals (not shown). By FRAP analysis the diffuse state of soluble Q35 and Q37 protein was indistinguishable from Q0 and Q24 (Figure 1B). In contrast, Q40 animals only have immobile aggregates, as measured by FRAP analysis (Figure 1B). The Q-length and age-dependent solubility transitions (Figure 1A-B, D-E) were used to investigate the dynamics of protein aggregation.

Characterization of the Soluble PolyQ Species by FCS

To further characterize the population of soluble polyQ species expressed in the transgenic animals, we employed fluorescence correlation spectroscopy (FCS), to measure diffusion rates, brightness and concentration of the polyQ, and therefore, the distribution of the oligomeric population(s).

Analysis of the soluble fraction of the native protein lysates from different Q-lengths by FCS demonstrated the presence of oligomeric species for Q35, Q37 and Q40, but not for Q24 and Q0 (Figure 1C). This is shown by the diffusion rates (proportional to $1/\tau_{Di}$) of the YFP-tagged molecules in solution. The Q0 (YFP) and Q24 autocorrelation (AC) curves (Figure 1C) overlap, indicating that the mobility of the Q24 species corresponds to a monomeric state, indistinguishable from YFP alone (Figure 1C). For the longer aggregation-prone Q-lengths, Q35, Q37 and Q40, the autocorrelation curves shift towards the right, corresponding to decreased diffusion rates due to the presence of slow moving oligomeric species (Figure 1C). These results reveal the presence of larger oligomers, that were not distinguishable by FRAP measurements, and that co-exist with immobile aggregates.

FCS analysis of protein native extracts from Q35 animals (soluble faction only, see Experimental Procedures), between day 2 and day 6, revealed transition from monomeric soluble species to oligomeric (Figure 1F). The AC curves of Q35 protein at day 2, 3 and 3.5 were indistinguishable from the Q0 curve, and suggest that Q35 is largely monomeric through day 3.5 of age (Figure 1F). AC curves from day 4 adults were shifted to the right, indicative of the formation of oligomeric species (Figure 1F), also consistent with the adulthood onset of visible aggregates. As animals continue to age through day 6, we observed a further increase in the size and concentration of the Q35 oligomeric species, as shown by the further rightward shift of the curves, corresponding to lower diffusion rates (Figure 1F).

Efforts to extract additional information revealed that we could not fit the AC curves to a 1, 2 or 3 component autocorrelation function for a majority of the samples due to large residuals, oscillations in the residual curve, inconsistent fitting results, and diffusion rate and concentration parameters that did not coincide with known values for the monomer fraction. We interpret this to suggest that there is a heterogeneous distribution of both size and brightness in the samples. Therefore, we introduced two complementary analyses to provide more detailed information: *Brightness Histograms* that gives information on the number of Qn-YFP molecules per oligomer; and *"Purified Single Molecule" FCS* that measures the oligomeric hydrodynamic size. For the brightness analysis, a simple and complementary non-correlation-based method measures the brightness of particles in samples where oligomer concentration is low and the species distribution is diverse in size and concentration [285]. The highest signal-to-noise light bursts from each fluorescent species transiting through the focal volume are used to determine the brightness distribution (τ_D) of the oligomeric species . Likewise for "purified" FCS, these bursts were identified, and together with the surrounding data, fitted using the AC function. The fitting results were binned to generate a histogram of the τ_D distribution that relates to the hydrodynamic size of the oligomers.

Through the use of brightness analysis and "purified" FCS, we show that soluble polyQ, of different Q-lengths and from animals of different ages, exhibit a heterodisperse state (Figure 2). It was particularly

noteworthy that the histograms for Q35, Q37 and Q40 showed similar heterodisperse distribution of oligomers, revealing the absence of discrete sub-populations of Q-length-dependent species (Figure 2A, B). In Q35 animals the burst histograms revealed oligomers at day 2, 3 and 3.5, which were not detected by the AC curves (Figure 2C). We observed a higher concentration of dim species at day 2 and 3 that had decreased by day 4 together with a corresponding increase in brighter species (Figure 2C). Taken together, the brightness and τ_D analysis reveal that oligomers increase in both size and brightness as the animals age, but the heterodisperse distribution is maintained without detection of any prominent oligomeric sup-population (Figure 2C, D).

By employing complementary FRAP and FCS imaging methods we have demonstrated that populations of oligomeric species co-exist with both aggregates and monomers. Moreover, age-dependent Q35 aggregation occurs in parallel with an increase in frequency and size of soluble oligomers, as detected by brightness analysis (Figure 2C). For the later age time points and longer Q-lengths, the oligomer brightness distribution was unaltered suggesting that the monomer-oligomer-aggregated species reach a dynamic equilibrium.

Suppression of PolyQ Aggregation Is Genetically Uncoupled From Oligomeric Distribution

Having identified the distribution of polyQ species associated with aggregation, we next asked whether suppression of polyQ aggregation by genetic modifiers of proteostasis would affect the distribution of oligomers, specifically if it would lead to the appearance, increase or decrease in frequency of discrete species associated with toxicity. To accomplish this, we took advantage of a genome-wide screen for suppression of polyQ aggregation using RNA interference (RNAi) (Chapter II). We selected a subset of these modifiers (Figures 3A, S1, S2) to ask whether distinct modifiers alter the cellular environment in the same or distinct manner to prevent aggregation. Both fluorescence microscopy and FRAP analysis demonstrated that these modifiers suppressed the formation of large visible Q35 aggregates (Figure S1B, Chapter II). Knockdown of *phb*-2 (mitochondrial prohibitin complex), *col-61* (collagen-type protein), *viln-1* (actin regulatory villin-related protein), *klp-15* (kinesin-like protein), *C34B2.8* (cell death regulatory protein), *C01G12.8* (CATP-4, Na^+/K^+ ATPase) and *F59C6.5* (NADH-ubiquinone oxidoreductase) was accomplished by feeding RNAi to Q35 animals at the L1 larval stage of development (day 1). As shown in Figures 3A and S1A, RNAi-treated animals showed a significant reduction in Q35 foci number relative to control. The fluorescence recovery curves indicate that the diffusion rate of soluble Q35 was similar to YFP alone, confirming the strong suppression of visible aggregates by these genetic modifiers (Figures 2B and S1A, B).

While all the modifiers had the same suppressor effect on Q35 aggregation, we wanted to examine the effect on the distribution of oligomers. FCS analysis revealed heterodisperse populations of oligomeric states upon genetic suppression of aggregation (Figure 3B and S2A). Relative to the control Q35 curve, the AC curves for the aggregation suppressors did not shift in the same direction (Figures 3B, S2A). Some led to the appearance of increased (*C01G12.8*) or decreased (*phb-2)* diffusion rates, while other modifiers (*klp-15*, *viln-1*, *col-61*, *C34B2.8*) had no apparent effect on the diffusion rate (Figure 3B and S2A). These results further support our earlier conclusion that FRAP analysis cannot distinguish monomers from higher molecular weight soluble species.

The brightness histograms indicated that each aggregation suppressor-modifier generated heterodisperse populations of Q35 oligomers (Figures 3C and D and S2B), rather than leading to the conversion of a discrete oligomeric state. The Q35 oligomer populations, however, were not identical. For example, *phb-2* and *F59C6.5* RNAi decreased the concentration of specific dim species in the bin center 2.2, whereas *C01G12.8* RNAi increased the concentration of these species. Conversely, *C01G12.8* RNAi

decreased the concentration at bin center 3.2, whereas *phb-2* and *F59C6.5* increased this concentration. FCS analysis not only confirms the heterodisperse nature of the Q35 oligomers, but it also provides quantitative information on the subpopulations of oligomers based on brightness intensity, for each aggregation suppressor tested. The largest group of modifiers tested, while suppressing polyQ aggregation, maintained the polyQ in an indistinguishable oligomeric states from the control Q35 (Figure S2A). Furthermore, "purified single-molecule" FCS, shows that Q35 species with similar brightness distributions correspond to different diffusion rates (Figure 3C-E). For example, while both *phb-2* and *F59C6.5* RNAi generated Q35 oligomers with similar brightness distributions, the T_D values for the latter were shifted to the left relative to *phb-2*. This suggests tighter packing for *F59C6.6* RNAi-generated Q35 oligomers, or could reflect difference in the composition of *phb-2*-generated Q35-containing species. This type of comparison not only provides information regarding the molecular packing of oligomers, but also reveals possible existing heterotypic interactions with other proteins.

The relationship between oligomeric states and cellular toxicity has been an area of great interest. Q35 animals exhibit a 40% reduction in motility relative to wt animals, associated to protein aggregation in the muscle cells (Figure S3). Of the aggregation suppressors examined in this study, there were three different toxicity outcomes, with decreased (*klp-15* and *C34B2.8*), unaffected (*col-61* and *C01G12.8*), and enhanced (*phb-2*, *viln-1* and *F59C6.5*) motility defect (Figure S4). The modifiers *phb-2* and *F59C6.5* had similar effects on the oligomer distribution, but did not have the same effect on toxicity. Conversely, *F59C6.5* and *C01G12.8* did not affect toxicity, but had opposite effects on the oligomer distribution. These results begin to suggest that there is no simple relationship between oligomers and toxicity.

Taken together, the use of FCS-based analyses has provided new resolution for the oligomeric states adopted by polyQ during aggregation, aging and in a cellular environment with suppressed tendency for aggregation. While some aggregation modifiers affected the heterodisperse oligomeric distribution, others had no obvious effect, while still suppressing visible aggregates. These results argue against the presence of discrete dominant species of oligomers associated with toxicity.

DISCUSSION

The methodology employed here provides information about the *in vivo* polyQ aggregation pathway, revealing that oligomers appear in a time-dependent manner leading to visible aggregates formation, consistent with a nucleation-dependent reaction similar to the kinetics resolved *in vitro* for many aggregation-prone proteins [109,261,286,287]. Interestingly, for the later time points and higher Q-lengths analyzed, the distribution of oligomers is maintained, suggesting that an equilibrium is reached perhaps through interactions with other cellular factors such as chaperones, or due to the continual regeneration of monomer. The results with the genetic modifiers of polyQ aggregation were consistent with the often contradictory observations regarding the effect of enhancement or suppression of aggregation on oligomers and toxicity (see Discussion in Chapter II). Our results suggest that the aggregation pathway is not solely linear, but that it can be driven in multiple directions depending on the genetic environment. In addition, suppression of aggregation does not appear to be a simple reversal of the oligomerization/ aggregation events, and instead it results in multiple distributions and new oligomeric states suggesting once again a multitude of ways by which aggregation can be suppressed or prevented.

The work described here provides a novel way to assess the aggregation pathway, which can be employed to understand disease related events and aggregation-dependent toxicity. An important aspect of this work is that the tools are not limited to one misfolding disease or one model system but can be used

in any misfolding system that can be fluorescently labeled. The new FCS analyses can provide information about the frequency, size and brightness of the oligomers. Recently others have also focused on developing tools to better study oligomers formed *in vivo* [288-290]. Together, these methodologies can provide valuable information about the misfolding pathway in different model systems and for different aggregating proteins.

Acknowledgements: We thank Morimoto lab members for advice and comments on the manuscript; and Dr. William Russin and the Biological Imaging Facility at Northwestern University. We thank Dr. Ted Laurence (Lawrence Livermore National Laboratory, CA, USA) for developing the “purified, single-molecule” FCS analysis software; and Patrick McMullen (Northwestern University) for assistance in developing the brightness histogram software.

FIGURES

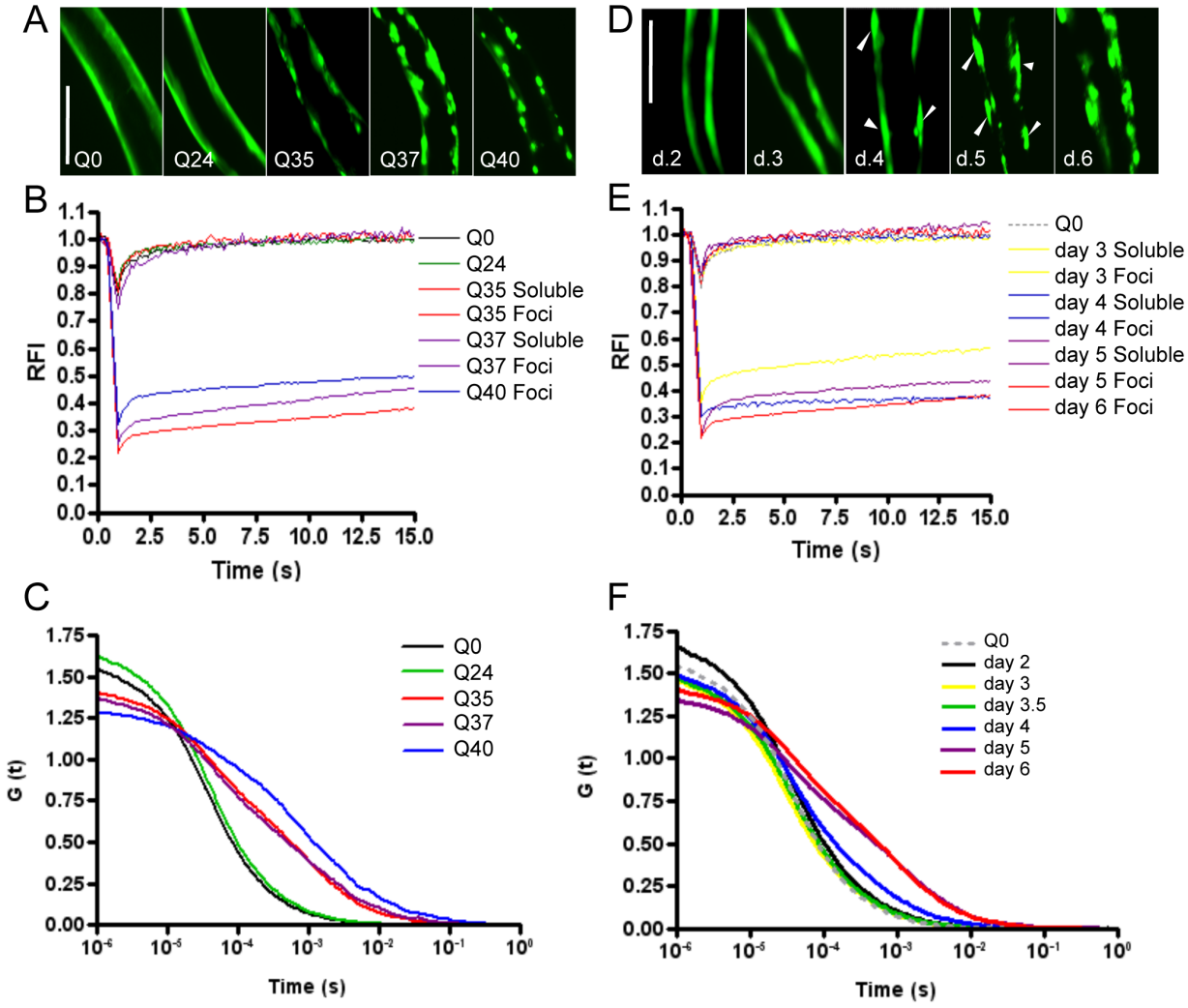

Figure 1: PolyQ aggregation in *C. elegans* analyzed by fluorescence microscopy, FRAP and FCS. (A) Fluorescence microscopy images show Q-length dependent aggregation of polyQ::YFP in *C. elegans* muscle cells (5 day old animals). Scale bar is 0.1 mm. **(B)** FRAP analysis of areas that appear either aggregated (foci) or soluble confirm that Q0 and Q24 are entirely soluble, whereas Q35, Q37 and Q40 contain both soluble and aggregated (foci) forms of the polyQ protein. **(C)** FCS autocorrelation curves from protein samples of 6 day old animals. Q35, Q37 and Q40 curves are shifted to the right as Q-length and aggregation propensity increase. Q0 (YFP) and Q24 maintain monomer-like diffusion rates. **(D)** Fluorescence microscopy images of a Q35 animal head show age-dependent aggregation (white arrows). Scale bar is 0.1 mm. **(E)** FRAP of Q35 animals confirms age dependent appearance of aggregates (foci). Q0 is used as a control for diffuse polyQ. **(F)** FCS autocorrelation curves of Q35 protein samples from different time-points show a gradual shift toward the right, reflecting a decrease in diffusion rate of the species formed. Q0 (grey dashed curve) is the control for monomeric state.

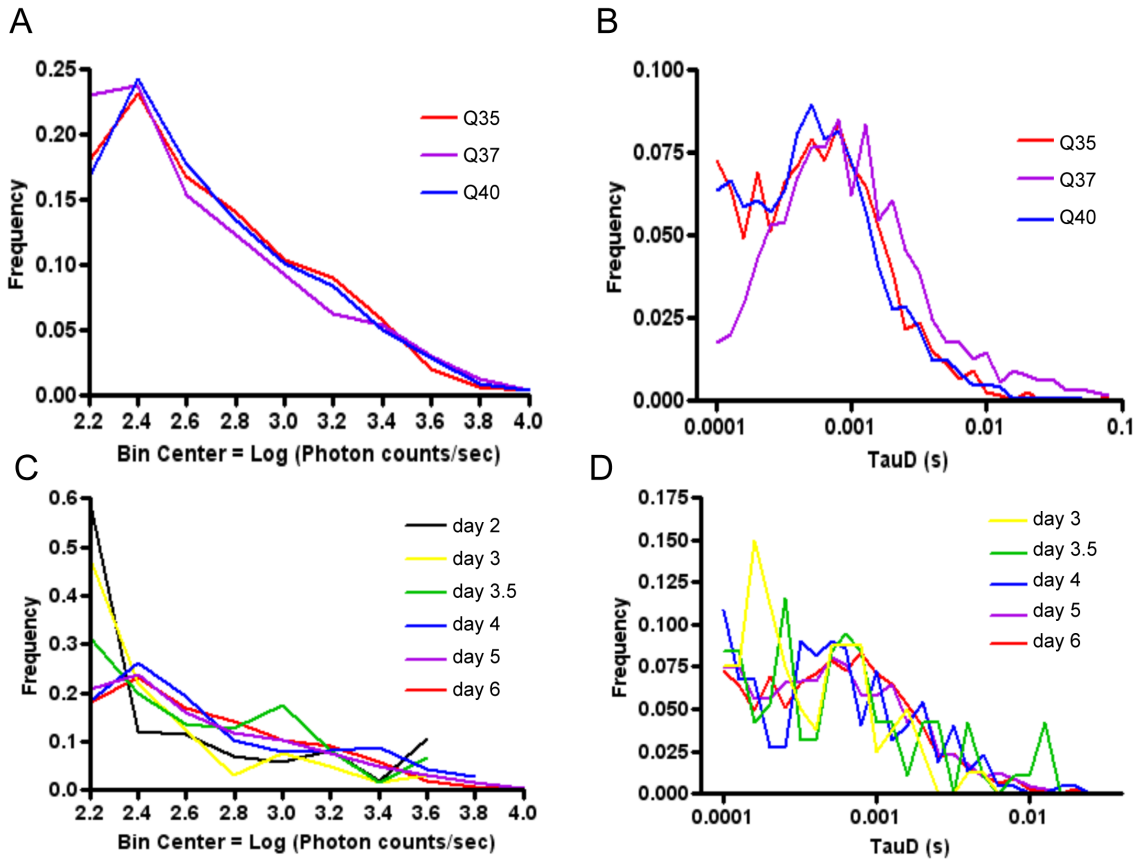

Figure 2: Brightness Histograms and "Purified Single Molecule" FCS analysis of Q-length and age-dependent changes in PolyQ. (A,C) Brightness intensity analysis determines the distribution of Qn::YFP species (fraction) into intensity bins (logarithmic scale), for various Q-lengths/ages. **(B,D)** "Purified single-molecule" FCS analysis determines the distribution and frequency of diffusion times (TauD) for Qn::YFP soluble oligomers (proportional to the hydrodynamic radius).

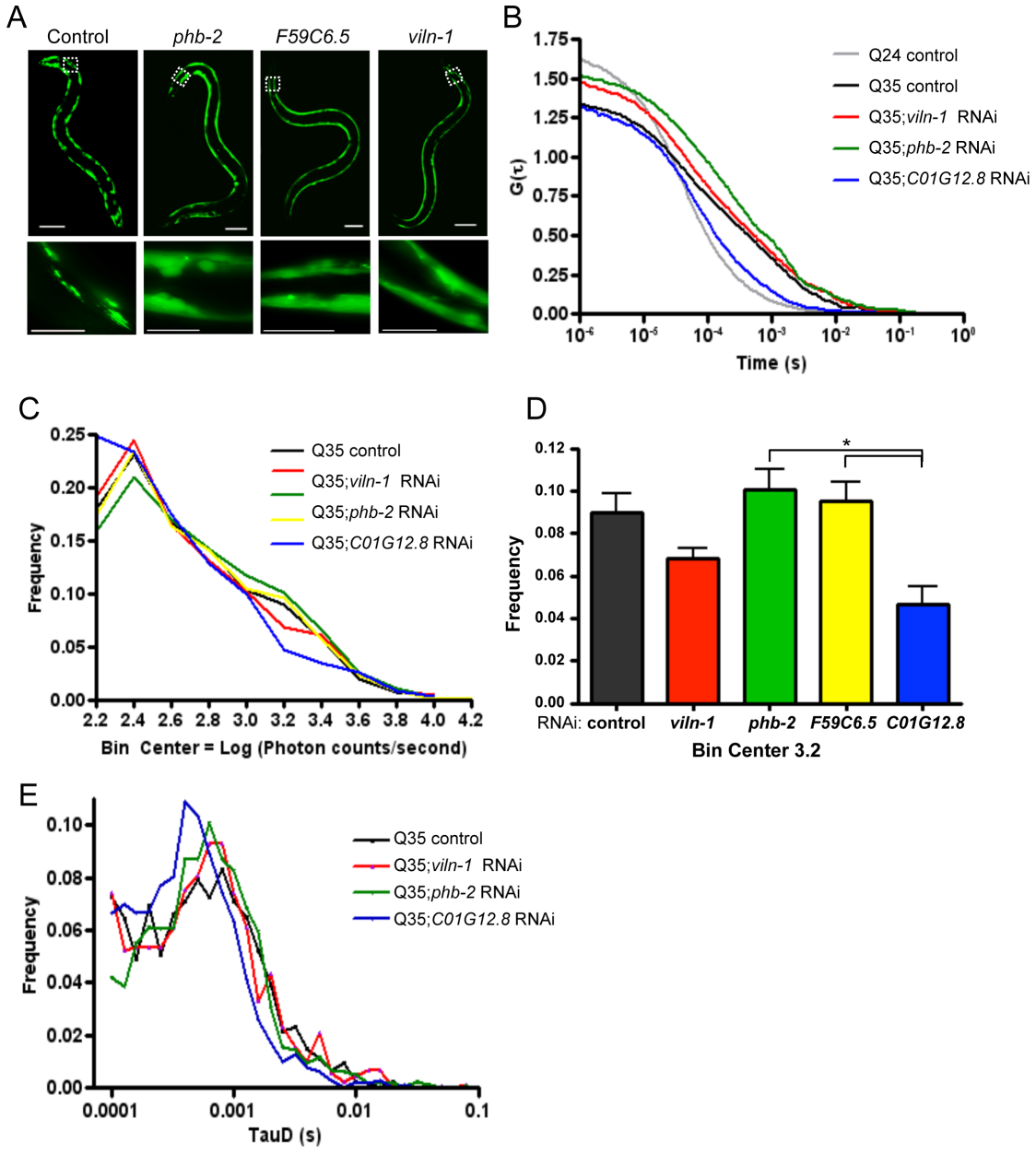

Figure 3: FCS based techniques detect changes in oligomeric state that occur when the aggregation pathway is modified. **(A)** Fluorescence microscopy images show suppression of visible Q35::YFP aggregates upon RNAi knockdown of specific genes in *C. elegans* muscle cells compared to control (5 day old animals). Scale bar is 0.1 mm (top) and 0.05 mm (bottom), and lower panels show a magnified imaged of the boxed area on top. **(B)** FCS analysis of protein samples from 6 day old RNAi-treated Q35 animals. Q24 and Q35 curves represent the monomeric and aggregated controls, respectively. Suppression of aggregation by RNAi leads to a change in amount and size of the soluble oligomeric molecules as shown by curves' shift to the right (slower mobility/larger species for *viln-1, phb-2*) or left (faster mobility/smaller species for *C01G12.8*) of the Q35 control curve (black). **(C, D)** Brightness intensity analysis determines the distribution of Q35::YFP species (fraction) into intensity bins (logarithmic scale). The suppression of aggregation does not lead to the same oligomer distribution for all the modifiers. **(D)** Specifically, for the brightness bin centered at 3.2 [Log(photon counts/Sec)] there is a statistically significant increase in oligomers of this size between *phb-2* and *F59C6.5* compared to *C01G12.8*. **(E)** "Purified single-molecule" FCS analysis determines the distribution and frequency of diffusion times (TauD) for Q35::YFP soluble oligomers when aggregation is suppressed (proportional to the hydrodynamic radius).

SUPPLEMENTARY FIGURES

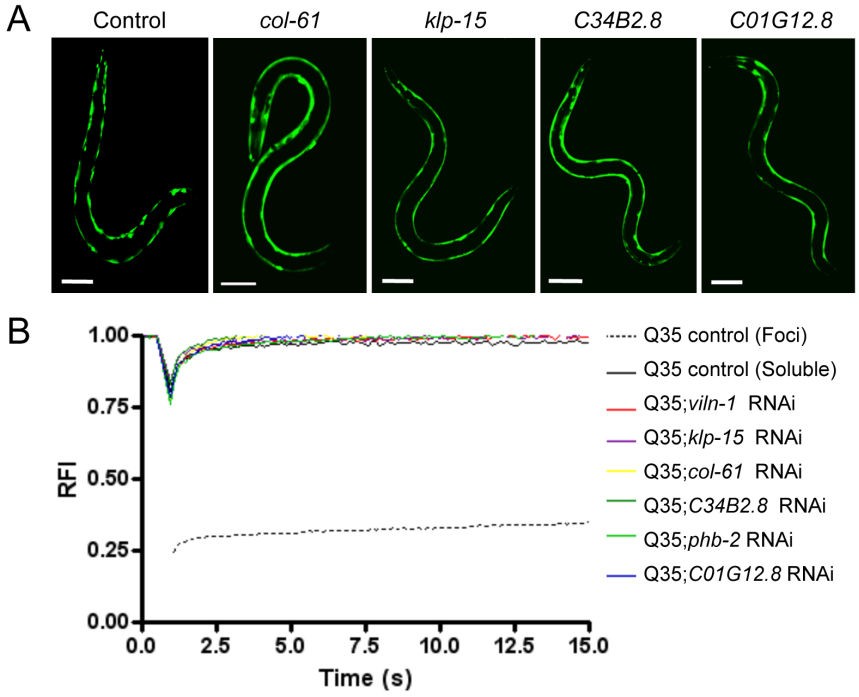

Figure S1: **Suppression of Q35 aggregate formation by RNAi. (A)** Fluorescence microscopy images show suppression of visible Q35::YFP aggregates upon RNAi knockdown of specific genes in *C. elegans* muscle cells compared to control (5 days old animals). Scale bar is 0.1 mm. **(B)** FRAP confirms that areas that appear soluble recover fluorescence.

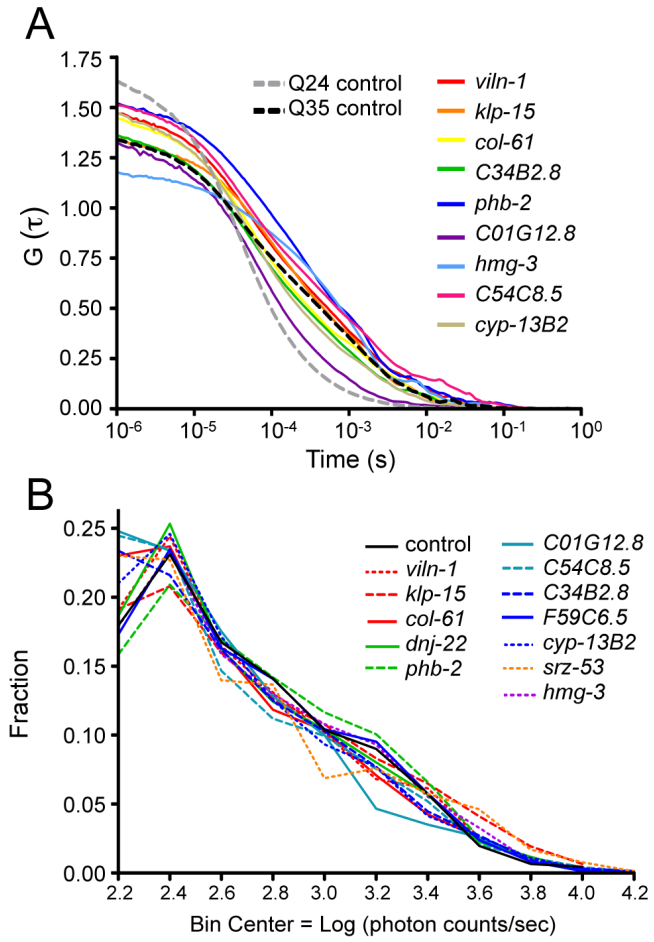

Figure S2: **Oligomer distribution upon suppression of aggregation**. **(A)** FCS analysis of protein samples from 6 day old RNAi-treated Q35 animals. Q24 and Q35 dashed curves represent the monomeric and aggregated controls, respectively. The curves appear to be similar to Q35 control. **(B)** Brightness histograms for many of the modifiers do not significantly differ from each other or Q35 control.

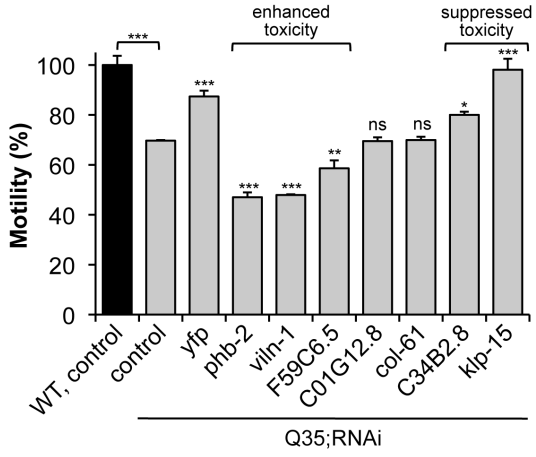

Figure S3: Effect of genetic modifiers on toxicity. RNAi treated animals were assayed for motility, as a read-out for polyQ-induced muscle dysfunction. Control Q35 and WT (N2) animals were treated with the empty vector L4440. Motility is given as a relative percentage of WT motility (black). Error bars represent ±SEM, Student t-test *p<0.05, **p<0.01, ***p<0.001 relative to Q35 control; and n≥3.

Appendix II

Let-607: A New Modulator of Stress Responses in C. *elegans*

LET-607: A NEW MODULATOR OF STRESS RESPONSES IN C. *ELEGANS*

INTRODUCTION

Protein homeostasis, or proteostasis, maintenance relies on a sophisticated network of pathways that ensure folding, quality and stability of the proteome. The folding environment is monitored within each compartment through tight regulation of molecular chaperones levels and function [29]. Perturbation of this environment by stress conditions, such as fluctuations in temperature, chemical insults, and infectious pathogens, or alternatively by chronic expression of mutant, misfolded and/or aggregated proteins, leads to the activation of protective stress response pathways. Whereas perturbation of the cytosolic folding environment selectively activates the heat shock response (HSR) and cytoplasmic chaperone expression [35], interference with endoplasmic reticulum (ER) or mitochondrial folding preferentially activates expression of ER- and mitochondria-localized chaperones, respectively [28,46].

In eukaryotes, the ER is the primary site for synthesis and checkpoint of secretory pathway proteins. The ER is also a major Ca^{2+} storage organelle and the site of lipid and oligosaccharide synthesis [244]. Key chaperones and folding sensors reside in the ER, including the Ig-binding protein (BiP)/glucose-regulated protein 78 (GRP78), GRP94, calnexin, calreticulin and protein disulphide isomerase (PDI) [291]. When accumulation of unfolded proteins in the ER exceeds the folding capacity of these chaperones, an intracellular signal transduction pathway, designated unfolded protein response (UPR), is activated. The UPR is a transcriptional and translational regulatory pathway that alters the expression of numerous genes of the secretory pathway, and affects cell fate and metabolism of proteins, amino acids and lipids [46]. The first level of response to ER stress consists in a transient reduction in protein synthesis, to reduce protein load entering the ER. Sequentially, there is transcriptional activation of UPR target genes, including those that function as part of the ER protein-folding machinery, to increase ER folding capacity. If homeostasis is not re-established then cell death is triggered, which has been proposed to be a mechanism of organismal protection against cells affected by proteotoxicity. The three main ER stress transducers are the transmembrane proteins inositol-requiring protein-1 (IRE1), the activating transcription factor-6 (ATF6), and the protein kinase RNA (PKR)-like ER kinase (PERK). Signaling is initiated by the transmembrane protein that senses folding requirements in the ER lumen, and transmits the information across the ER membrane to the cytosol and nucleus. On the ER lumen side, the chaperone BiP/GRP78 is predicted to retain these transmembrane proteins in an inactive state. When the critical level of unfolded proteins is exceeded, BiP/GRP78 dissociates from IRE-1, PERK and ATF6, releasing them to initiate the ER stress response [46,292]. Activated PERK phosphorylates the translation initiation factor eIF2a, slowing down protein synthesis. Activated ATF6 translocates to the Golgi, where it is cleaved by proteases to form an

active transcription factor that enters the nucleus and upregulates the transcription of genes encoding ER chaperone proteins [293]. IRE-1 activation results in X-box-binding protein 1 (XBP-1) splicing and activation. The activated spliced form of XBP-1 acts as a transcription factor of genes involved in ER homeostasis, export and degradation of misfolded proteins [294,295]. In *C. elegans*, ire-1, pek-1, and atf-6 regulate UPR, and are also required for growth and survival (developmental UPR) [244]. Cell growth and differentiation of specialized cells, and a high demand for protein synthesis during development, causes a constant low-level of ER stress, or basal/constitutive UPR.

Despite the growing knowledge on the effectors of the UPR, there is limited understanding of possible co-regulation of different stress pathways across cellular compartments to promote cellular homeostasis. Nonetheless, recent studies in *C. elegans* have shown that XBP-1 and DAF-16 can function synergistically to activate genes that promote ER stress resistance and longevity in animals with compromised insulin/IGF-1 signaling [28,296]. It remains to be determined whether the IRE-1/XBP-1-UPR arm is modified during aging, which would impede coordination with other stress response factors and consequently impair the ER stress response [60]. Moreover, studies in *S. cerevisiae* have shown that HAC1/*xbp-1* mRNA transcription levels are also regulated [246], in addition to IRE-1-mediated splicing activation, revealing an additional regulatory step. Whereas normal ER stress inducers, such as DTT (dithiothreitol, reducing agent) or tunicamycin (TM, glycosylation inhibitor/blocks the synthesis of all N-linked glycoproteins), activate HAC1 mRNA splicing by IRE1; a concomitant increase in temperature (heat shock) led to an additional up-regulation of HAC1 mRNA levels [246]. Strikingly, the regulation of HAC1 mRNA levels were independent from the IRE-1 pathway, revealing a new transcriptional program triggered to promote cell survival upon acute and intensive stress. The combined upregulation of mRNA levels and splicing of HAC1 was designated “Super-UPR” [246]. Accordingly, it has been shown that IRE-1 and XBP-1 have additional divergent functions and non-overlapping subset of downstream target genes under basal conditions, separate from the “classical UPR” [244]. Another study has also demonstrated that HSR activation can relieve ER stress [245]. That is, HSR by constitutively active HSF-1 can rescue the growth of *ire-1* null cells, by restoring secretory pathway function. This is consistent with the finding that more than 25% of the genes unregulated by HSR are common UPR targets. This work offered a strong evidence that HSR can relieve ER stress in UPR-compromised cells, suggesting a “crosstalk” between the two stress responses or at least a compensatory mechanism employed by the cell to promote survival [245].

Here, we have employed the *C. elegans* polyglutamine (polyQ) model [119] to identify new genetic pathways involved in proteostasis maintenance and describe a new proteostasis modifier, *let-607*, that encodes a bZIP transcription factor homologous to mammalian CREBH [244]. The genetic downregulation of *let-607* by RNAi resulted in activation of the UPR and the HSR, with upregulation of ER and cytosolic molecular chaperones that rescued folding and reduced toxicity of multiple misfolded proteins. This work suggests a new role for *let-607*, as a co-regulator of multiple stress responses to maintain cellular homeostasis.

RESULTS

LET-607 is a New Genetic Modifier of Protein Misfolding and Toxicity

We performed a genome-wide RNA interference (RNAi) screen for suppression of polyglutamine (polyQ) aggregation in *C. elegans* body wall muscle (BWM) cells, to identify new modifiers of protein misfolding. *E. coli* expressing dsRNA corresponding to the genome of *C. elegans* [155], were fed to L1

(first larval stage, day 1) animals expressing Q35-YFP [119]. Animals were scored for reduction in the number of Q35 foci on day 6, that corresponds to 3 days after onset of aggregation, relative to the empty-vector RNAi control (Figure 1A). As a control for RNAi efficiency, animals were treated with RNAi to *yfp* that reduced the fluorescence signal, as expected (see Chapter II). Here, we report on the modifier gene *let-607* that suppressed aggregation in Q35 animals, in animals expressing Q37 and in animals expressing mutant SOD1^{G93A} (Figure 1A). Suppression of Q35 aggregation by *let-607* RNAi was not due to reduction in expression of Q35 mRNA or protein steady-state levels (see Chapter II). We tested if knockdown of *let-607* at a later time point would still be effective in suppressing aggregation and found that upon RNAi at L4 stage (day 3), the aggregation suppressor effect was even stronger and the animals appeared healthier. From here on we present data with RNAi always at L4 stage.

To address whether suppression of polyQ aggregation affected toxicity, we examined the motility defect associated to Q35 aggregation in the muscle of 6 day old animals. Whereas Q35 animals display a 40% reduction in motility relative to wt animals, *let-607* RNAi rescued motility to near 100%, without affecting the motility of WT animals (Figure 1B). As expected, motility was also fully restored by knocking down the polyQ transgene itself with *yfp*-RNAi (Figure 1B). These results show that knockdown of *let-607* suppresses both aggregation and toxicity of the polyQ protein.

To determine if the effect of *let-607* on polyQ aggregation and toxicity reflects a more global effect on folding capacity, we examined the stability of four endogenous muscle-expressed proteins represented by temperature-sensitive (TS) mutations in the paramyosin ortholog UNC-15, in the basement-membrane

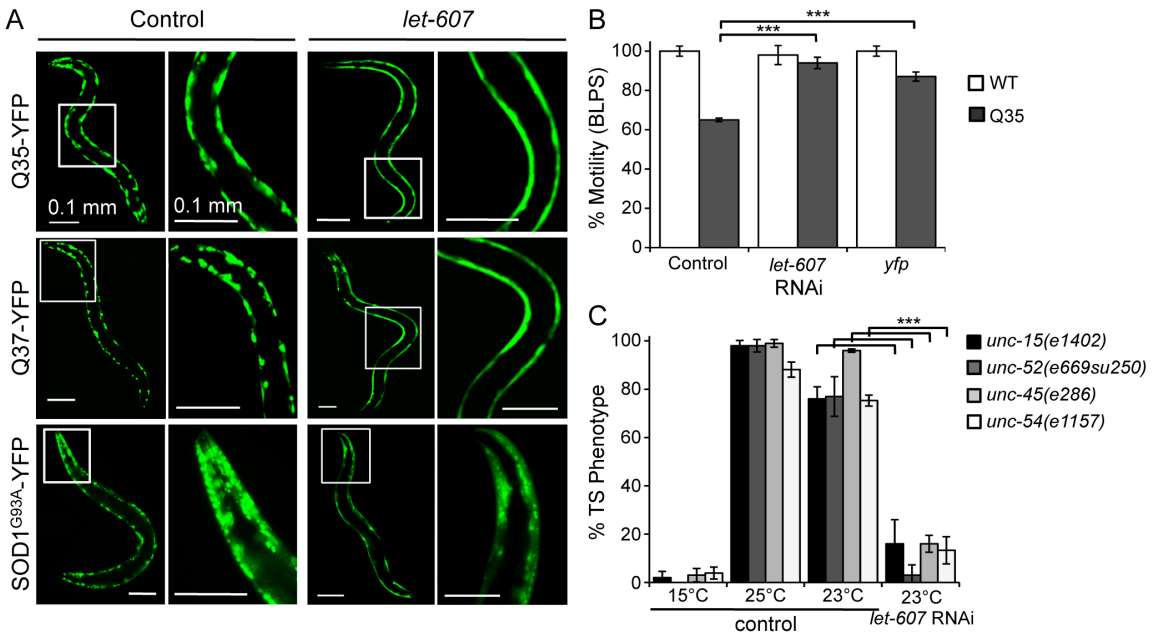

Figure 1: RNA interference screen for suppression of protein misfolding and toxicity. (A) We identified a new genetic modifier, *let-607* that when knocked down suppressed aggregation of polyQ (Q35 and Q37) and mutant SOD1^{G93A} proteins in 6 day old *C. elegans* muscle cells. The control refers to vector RNAi treatment. **(B)** Motility assay for 6 day old Q35 and WT animals fed with *let-607* or vector RNAi. *yfp*-RNAi is a positive control for suppression of muscle dysfunction. (±SEM, Student t-test ***p<0.001). **(C)** *let-607* RNAi rescued the TS phenotype of muscle mutant proteins by >80%: UNC-15 (paramyosin; unc/slow movement), UNC-52 (perlecan, stiff paralysis), UNC-45 (myosin assembly, egg laying defect) and UNC-54 (myosin, paralysis). 15°C is the permissive temperature, 25°C the restrictive temperature and 23°C an intermediate temperature for RNAi efficiency (±SD, Student t-test ***p<0.001).

protein perlecan UNC-52, in the myosin-assembly assisting protein UNC-45, and in the myosin heavy chain UNC-54 [90]. At the permissive temperature (15°C), all four TS-proteins fold properly and are functional, whereas at the restrictive temperature (25°C) each protein misfolds and results in characteristic muscle dysfunction phenotypes (Figure 1C control, see Chapter II). For the purpose of the RNAi experiments, we employed an intermediate temperature (23°C) at which the TS mutant phenotypes remained highly penetrant (Figure 1C, 23°C control), but upon *let-607* RNAi, the stability of each protein was increased by >80% (Figure 1C). These results show that downregulation of *let-607* not only prevented protein aggregation, but also enhanced the folding of multiple endogenous metastable proteins, suggesting an improvement in protein folding capacity in muscle cells.

Induction of the UPR by *let-607* Downregulation

The gene *let-607* was previously described as a new component of the inducible UPR, both in *C. elegans* and mammals [244]. This gene encodes a bZIP transcription factor of the CREB/ATF family, homologous to the mammalian CREBH (Figures S1, S2). Both basal and inducible levels of *let-607* expression have been shown to be *xbp-1/ire-1* and *atf-6* dependent, but not *pek-1*-dependent [244]. LET-607 seems to be also required for developmental UPR, since the null mutant is lethal, and RNAi against *let-607* from L1 stage causes some developmental morphological phenotypes (not shown).

Given the predicted role for LET-607 in the UPR, we tested how *let-607* knockdown affects the ER quality control and stress response machinery. Animals treated with *let-607* RNAi showed activation of a specific arm of the UPR, with upregulation of *ire-1/xbp-1*, *hsp-4* (ER *hsp70*), and *ero-1*, a sensor for ER stress, in an *xbp-1*-dependent manner (Figure 2A). Activation of IRE-1/XBP-1 led to increase in *xbp-1* splicing, as we observed by semi-quantitation of the spliced form on a DNA gel (Figure 2B and C). Concomitant upregulation of *xbp-1* levels and splicing by *let-607,* was consistent with UPR transcriptional activation and *hsp-4* expression. We also found that the levels of *let-607* are dependent on the UPR transducers IRE-1/XBP-1 and ATF-6, but not PEK-1 or calnexin, as predicted (Figure 2D). Knockdown of either isoform of the ER Hsp70, *hsp-4* or *hsp-3*, or treatment with TM, resulted in UPR activation and *let-607* upregulation (Figure 2D), strengthening the predicted role of *let-607* in UPR. Together, the results demonstrate that downregulation *let-607* activated the ER stress response through IRE-1/XBP-1, and enhanced protein folding in the cytosol.

Restoration of Protein Folding by Induction of Cytoplasmic Chaperones and Activation of the HSR

Although *let*-607 is involved in ER stress response, the master regulator of protein folding in the cytosol is the HSR. So, we asked if enhanced folding of metastable proteins and suppression of aggregation by *let-607* downregulation was a consequence of activation of the HSR. Hsp70 (*C12C8.1*p-GFP) reporter animals incubated with *let-607* RNAi, showed increase in GFP fluorescence, consistent with an up-regulation of Hsp70 expression (Figure 3A). Next, we examined the expression of cytosolic chaperones regulated by HSF-1, and found that upon *let-607* RNAi, the expression of multiple heat shock genes of the Hsp70 family (*C12C8.1, F44E5.4* and *C30C11.4*) and small Hsp family (*hsp-16.1, hsp-12.6* and *hsp-16.49*) were upregulated in WT animals (Figure 3C). To examine whether induction of chaperone expression was due to activation of HSF-1, we took a genetic approach. Double knockdown of *let-607* with *hsf-1,* or on *hsf-1(sy441)* hypomorphic mutant animals, only caused a slightly lower upregulation of chaperone expression (Figure 3C), and aggregation was still suppressed (Figure 3B). Nonetheless, upregulation of *hsp70* (*C12C8.1*) was absolutely required for *let-607*-mediated suppression of aggregation (Figure 3B). Together, these results establish that the HSR was activated by *let-607* knockdown, consistent with the up-regulation of chaperones leading to enhanced protein folding. Yet, the effect is not fully HSF-1

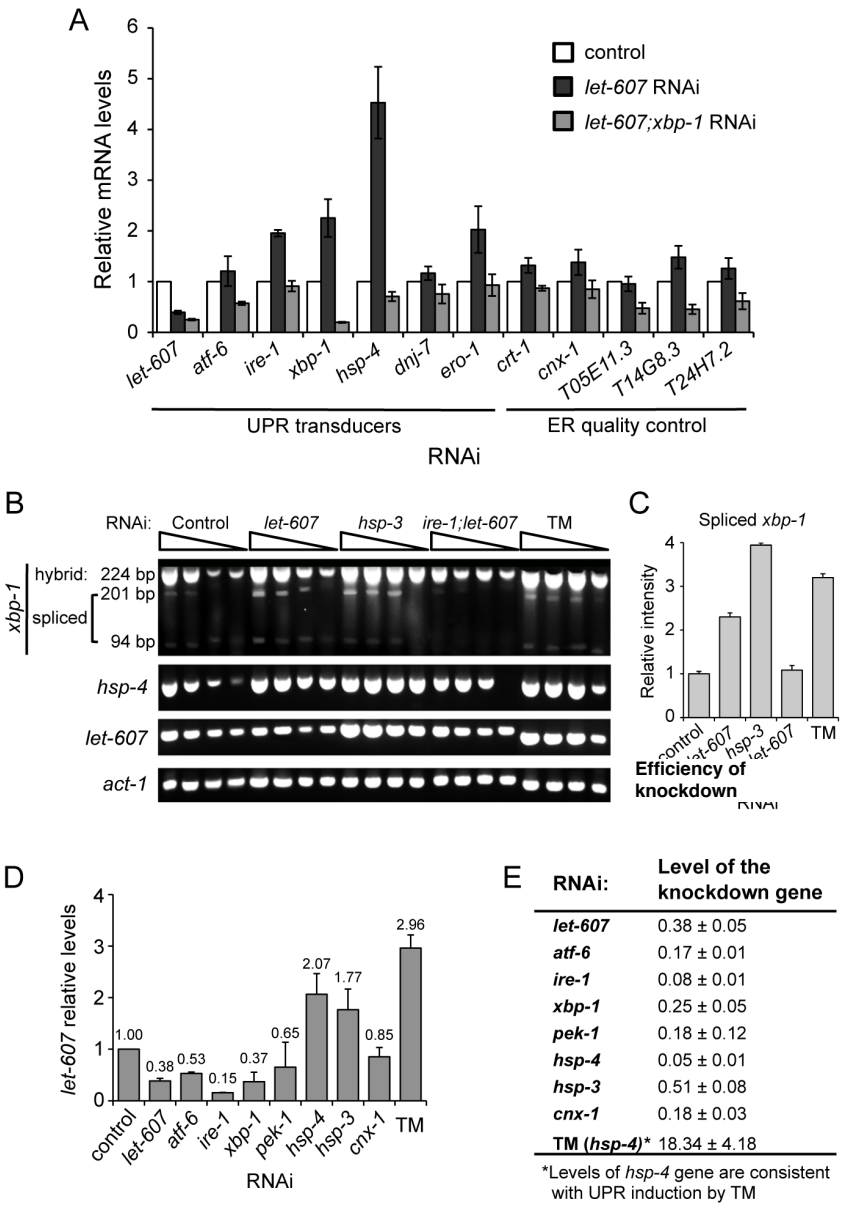

E

RNAi:	Level of the knockdown gene
let-607	0.38 ± 0.05
atf-6	0.17 ± 0.01
ire-1	0.08 ± 0.01
xbp-1	0.25 ± 0.05
pek-1	0.18 ± 0.12
hsp-4	0.05 ± 0.01
hsp-3	0.51 ± 0.08
cnx-1	0.18 ± 0.03
TM (*hsp-4*)*	18.34 ± 4.18

*Levels of *hsp-4* gene are consistent with UPR induction by TM

Figure 2: The effect of *let-607* knockdown on UPR. (A) Real-time qPCR analysis of WT animals treated with *let-607* RNAi or co-treated with *let-607* and *xbp-1* RNAi from L4 stage (RNAi bacteria dilution controls included), showing up-regulation of UPR genes by *let-607* knockdown, in a *xbp-1*-dependent manner (*crt-1*/calreticulin; *cnx-1*/calnexin; *T05E11.3*/Grp94*; T14G8.3*/Hsp70 member*; T24H7.2*/Hsp70 member). Data are relative to EV control RNAi (±SD). **(B,C)** DNA gel analysis of *xbp-1* splicing by *let-607* RNAi. RNAi for *hsp-3* and TM treatment are positive controls for UPR induction and *xbp-1* splicing, and *ire-1* RNAi is the control for specificity. The levels of *hsp-4* were used as control of UPR induction. (C) shows semi-quantitation of the *xbp-1* spliced form (by measuring the intensity of the 201 bp band relative to total *xbp-1* and actin). **(D)** Real-time qPCR analysis of *let-607* mRNA levels upon knockdown of each ER-UPR and quality control components. **(E)** The efficiency of RNAi knockdown was measured by qPCR (±SD).

dependent, indicating other contributing factors. Since LET-607 is predicted to be the *C. elegans* CREBH, an ER protein translocated to the nucleus upon stress (Figure S1) [244], we postulated that the events occurring at the ER by *let-607* knockdown were transmitted to the cytoplasm/nucleus for HSF-1 activation.

Activation of the UPR Occurs Up-Stream of the HSR

Knockdown of *let-607* activated two distinct stress responses, usually thought to be independent and confined to the respective organelles. We asked if *let-607* could function as a negative regulator of the HSR by directly inhibiting *C12C8.1* transcription at the gene-promoter level. This did not seem to be the case as we found that upregulation of *let-607* expression (by TM) did not impair *C12C8.1* expression upon heat shock treatment (not shown). To examine whether activation of each stress response was independent or dependent on the other, we started by asking if other UPR inducers could cause a similar

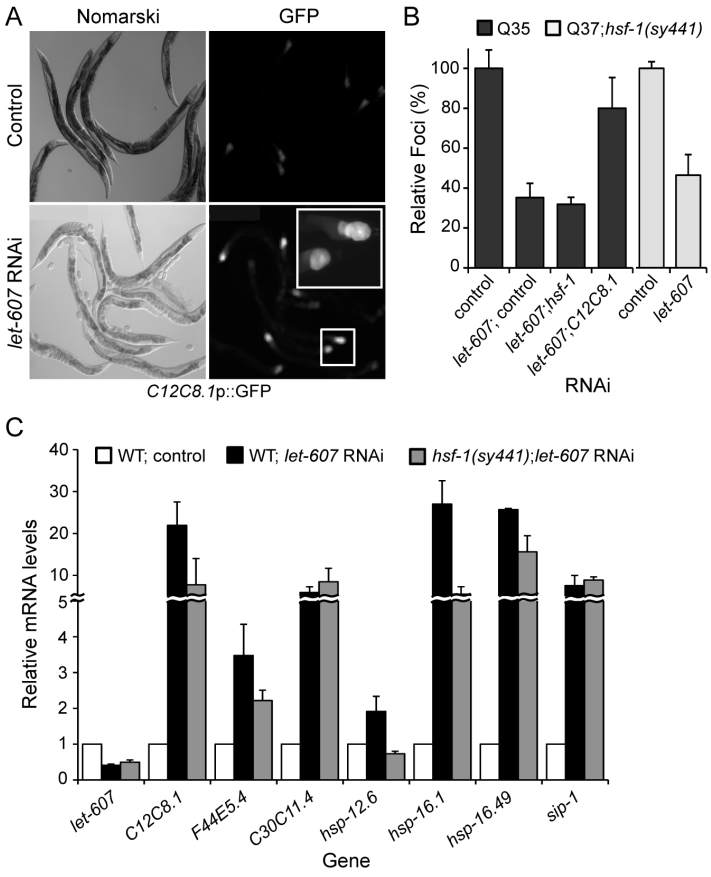

Figure 3: Induction of the heat shock response by *let-607* knockdown. (A) Fluorescence images show activation of the *C12C8.1*p::GFP reporter. **(B)** Suppression of aggregation in Q35 and Q37 animals is dependent on *C12C8.1* chaperone levels, but not dependent on HSF-1. Foci number is shown relative to the total number of foci in each strain in vector conditions (±SD). **(C)** Real-time qPCR analysis of WT and *hsf-1(sy441)* animals treated with *let-607* RNAi showed upregulation of cytosolic chaperones from the HSP-70 family (*C12C8.1, F44E5.4, C30C11.4*), small HSPs (*hsp-16.1, hsp-12.6, hsp-16.49*), and the stress-inducible protein *sip-1*. This up-regulation showed contribution by HSF-1 but not total dependence. Data are relative to WT;vector RNAi (±SEM).

effect on cytosolic chaperones as *let-607*. To induce UPR, we employed *hsp-3* RNAi or the chemical TM. In animals treated with TM, the HSR was not induced and cytosolic chaperones were not upregulated (Figure 4A). However, when animals were treated with *hsp-3* RNAi, both the UPR (seen by the levels of *hsp-4* that compensates for the absence of the isoform *hsp-3*) and the HSR (*C12C8.1, F44E5.4*, *hsp-16.1*) were activated, to a similar magnitude or higher as for *let-607* RNAi (Figure 4A). This suggested that UPR-mediated activation of the HSR is not the simple result of ER stress caused by disruption of the secretory pathway (TM result), but may be specific to the disruption of the ER chaperone machinery. Supporting this hypothesis, we found that *let-607*-mediated upregulation of cytosolic chaperones, was strongly dependent on *xbp-1* (Figure 4B). Co-downregulation of *let-607* and *xbp-1* abolished chaperone induction (Figure 3C, 4B). These results suggest that induction of the UPR through *xbp-1* is epistatic to the activation of the HSR in the cytosol, revealing a new “crosstalk” between stress pathways, mediated by *let-607*. This is consistent with the requirement of *xbp-1* for *hsp-3/hsp-4* expression and subsequent up-regulation of cytosolic chaperones. In turn, *let-607* seems to function like a “switch” that communicates to the cytosol the folding ‘status’ in the ER upon stress.

To determine if the “crosstalk” between ER and cytosolic stress responses is specific to *let-607*, we examined the relationship between the two canonical stress responses in *C. elegans*. Is HSF-1 function required for UPR activation? Is intact UPR required for HSR activation? We tested HSR induction in impaired UPR animals by knocking down the UPR transducers *atf-6* and *xbp-1*. In both cases, heat shock treatment caused *hsp-70* and *shsp* upregulation to the same level as in the control animals (Figure 5A). Then, we tested UPR induction in *hsf-1(sy441)* hypomorphic mutant animals, and found that TM-mediated

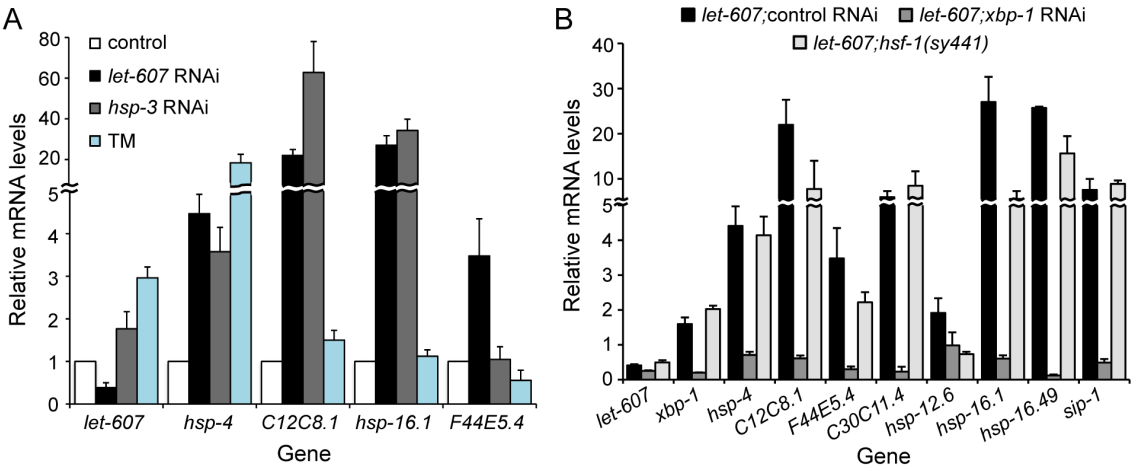

Figure 4: Real-time qPCR analysis of the stress responses induced by *let-607* knockdown in WT animals. (A) Induction of UPR by *hsp-3* RNAi, but not by TM treatment, up-regulated cytosolic chaperones' expression in a similar manner to *let-607* RNAi. **(B)** Upregulation of cytosolic chaperones (Hsp70 and sHsp) and *sip-1*, by *let-607* RNAi is dependent on *xbp-1* but also results from HSF-1 activity as shown by reduced induction in the hypomorph *hsf-1(sy441)* (data are relative to levels in vector control, ±SD).

up-regulation of *hsp-4* levels was reduced by half (from 20-fold to 10-fold) in *hsf-1* mutant animals (Figure 5B). Moreover, whereas HS treatment activated UPR (*hsp-4* levels, Figure 5A), TM did not activate the HSR (Figure 5B). This once again pointed towards a "crosstalk" between pathways for a robust protection against stress, but also corroborated that the UPR requirement for HSR induction is a *let-607* specific observation (Figure 4B, 5A, 6).

Another Layer of Stress: DAF-16 Nuclear Translocation Upon *let-607* Knockdown

To examine exhaustively how *let-607* knockdown affects cellular homeostasis and protein folding, we tested all known stress-inducible pathways, as we hypothesized that enhancement of protein folding was a consequence of stress response activation and consequent upregulation of chaperones. In addition to the UPR and HSR, we found that *let-607* RNAi treatment of a *daf-16*p::DAF-16::GFP reporter strain increased DAF-16 nuclear localization, as shown by GFP fluorescence (Figure 5C). This results showed that *let-607* knockdown at the ER activated DAF-16 (FOXO) nuclear translocation and possibly transcriptional activity, which still needs to be tested. We also examined the effect of *let-607* knockdown in a *daf-16(mu86)* mutant strain and found that cytosolic chaperones were strongly up-regulated (Figure 5D). These results suggest a compensatory effect between pathways that lead to chaperone expression and proteostasis maintenance (Figure 6).

Discussion and Future Directions

In mammals, CREBH (or CREB3L3) is a liver-enriched transcription factor closely related to LZIP. CREBH has a transmembrane (TM) domain and it localizes to the ER. Under ER stress, proteolytic cleavage by site-1 and site-2 proteases (S1P, S2P) removes the TM domain and liberates the CREBH amino-terminal fragment that translocates to the nucleus to activate transcription of hepatic gluconeogenic

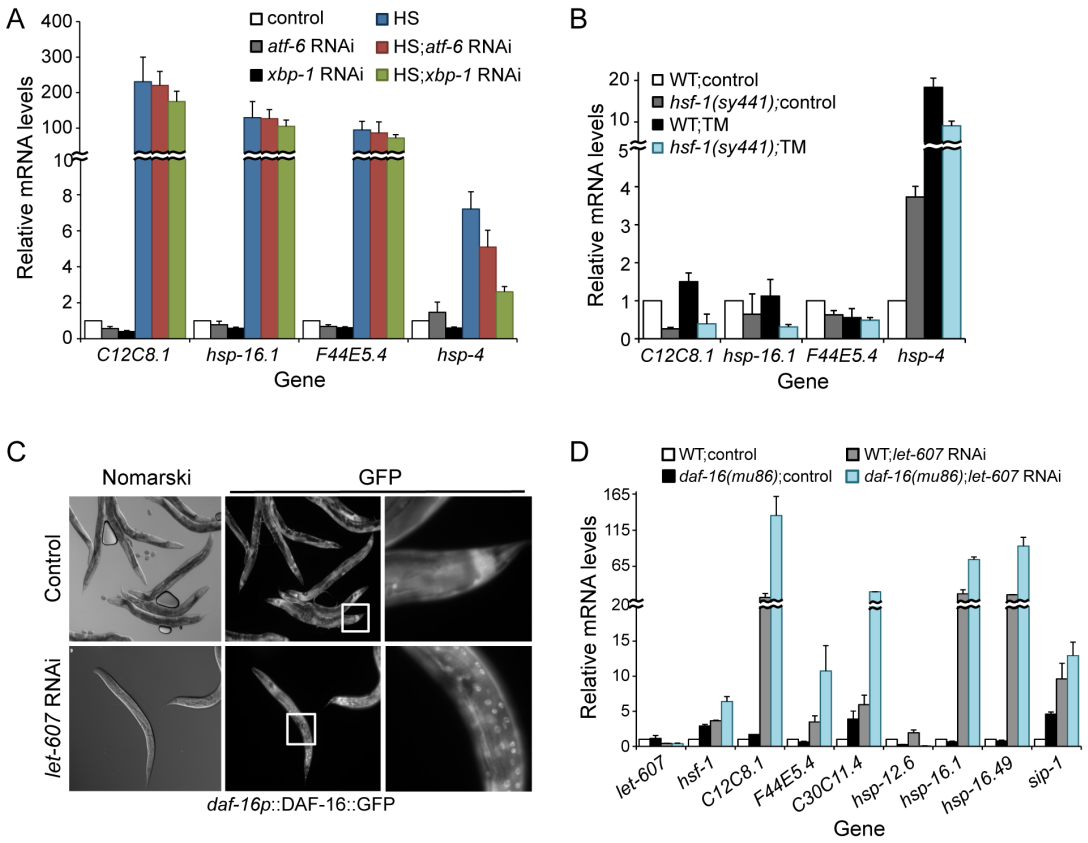

Figure 5: Potential "crosstalk" between cellular stress pathways, mediated by *let-607*. (A,B) Real-time qPCR analysis of cytosolic (*C12C8.1, F44E5.4, hsp-16.1*) and ER (*hsp-4*) chaperones upon (A) heat shock (HS) treatment of WT animals with impaired UPR response (*xbp-1* and *atf-6* RNAi). HS induction of chaperones did not require functional UPR. (B) UPR induction by TM treatment of WT or HSR-deficient (*hsf-1(sy441)*) animals, showed that in the *hsf-1* hypomorphic mutant, UPR was less robust. Data are relative to WT animals in EV control (±SD). **(C)** DAF-16 protein reporter shows nuclear localization upon *let-607* RNAi. **(D)** Real-time qPCR analysis of chaperone expression in the *daf-16(mu86)* mutant background, by *let-607* RNAi (relative to WT;control animals ±SD).

enzymes and acute phase response (APR) genes (Figure S2) [297-299]. CREBH activates transcription by binding to the cAMP-responsive element (CRE), box B and ATF-6-binding element of target genes [298]. CREBH is up-regulated by pro-inflammatory cytokines and fatty acids, that also induce UPR, and is a growth suppressor that becomes aberrantly down-regulated in liver cancers (Figure S2B) [298]. CREBH establishes a link between ER stress and growth, innate immunity and nutritional regulation [300]. In *C. elegans*, ATF-6 and XBP-1 are predicted to be upstream regulators of *let-607* during inducible UPR [244], and LET-607 seems to have a role in development. Otherwise, the physiological role and downstream targets of this predicted transcription factor are largely unknown.

Here, we found that *C. elegans* UPR induction by *let-607* downregulation is *xbp-1* dependent, and occurs upstream of HSR activation (Figure 6). Moreover, the effect of *let-607* RNAi as a UPR and HSR inducer is not common to other UPR inducers, such as TM or DTT (not shown), and is reminiscent of the "Super UPR" previously described [246]. We then asked how the effect of *let-607* on the UPR/HSR "crosstalk" compared to the relationship between these two canonical pathways. HSR induction did not require intact UPR components, but induction of UPR by TM was slightly lower when HSR was impaired

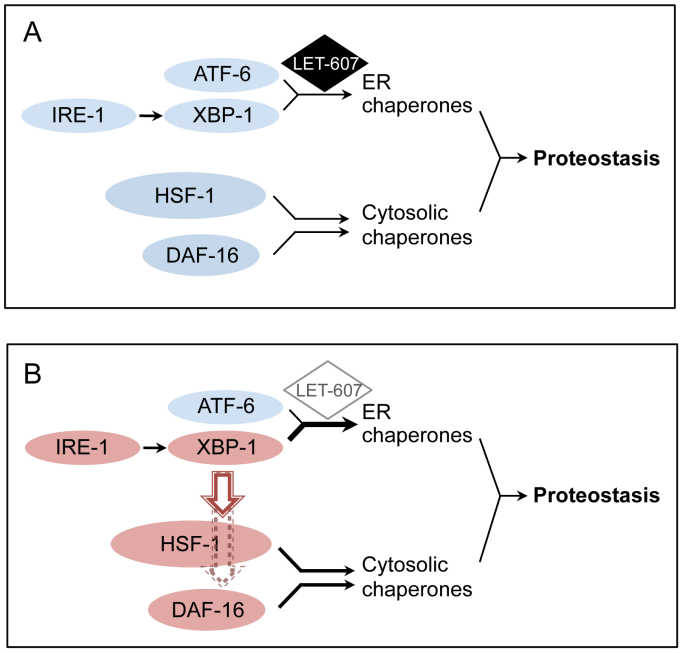

Figure 6: Working model for the "crosstalk" between ER and cytosolic stress responses through LET-607. (A) Under physiological conditions LET-607 is a member of the UPR, with a role in constitutive and developmentally required UPR. **(B)** When *let-607* is down-regulated, it activates the IRE-1/XBP-1 UPR pathway and up-regulates the expression of ER chaperones. Through this pathway, ER stress "signals" are transmitted to the cytosol for HSF-1 activation and HSR. This translates in expression of multiple cytosolic chaperones. Altogether, these stress pathways work to maintain proteome stability and cellular proteostasis.

(mutant *hsf-1*). It remains to be determined whether XBP-1 is a direct transcriptional activator (promoter binding activity) of cytosolic chaperones or even HSF-1. From a preliminary analysis, we found that the *C12C8.1* promoter region contains 3 XBP-1-binding elements (not shown), which would be consistent with the hypothesis of XBP-1-dependent HSR activation. We also found that the *let-607* promoter region contains 1 XBP-1/ATF-6 binding element (TGACGT) and 3 DAF-16 binding sites (TGTTTAC, CTTATCA, TATTTAC) (not shown). Together, gene promoter analysis may strengthen the hypothesis of co-regulation of multiple stress pathways for overall homeostasis (Figure 6).

We list here a number of questions we intend to see answered in order to characterize the role of *let-607* in proteostasis maintenance:

• It will be crucial to demonstrate that LET-607 is an ER resident protein, and for that we are generating a LET-607::GFP reporter strain.

• Under physiological conditions, what is the stimuli that activates LET-607 translocation to the nucleus? Cleavage of LET-607 at the ER/Golgi and translocation to the nucleus can be monitored by western blot with an antibody against human CREB3L3 (host rabbit, polyclonal, Orbigen PAB-10965) that recognizes *C. elegans* LET-607 [297,299].

• Does it have nuclear transcriptional activity? What are the transcriptional downstream targets and what is the promoter binding element (does it bind to CRE)?

• Is LET-607 a new ER-stress transducer in *C. elegans*? According to sequence alignment predictions, LET-607 strongly resembles mammalian CREBH with an ER transmembrane domain (Figure S1, S2). Elucidating whether LET-607 is cleaved and activated similarly to ATF-6 under ER stress, and identifying the downstream transcriptional targets will broaden our understanding of the UPR components and physiological relevance.

• We will also employ electrophoresis mobility shift (EMSA) to look at HSF-1 and XBP-1 transcriptional activation upon *let-607* downregulation.

Finally, CREBH has been described to be involved in nutrient sensing and metabolism [300]. It will be important to determine if the effect of *let-607* on protein homeostasis is a consequence of reduced

synthesis and metabolism, known to affect proteostasis. We will test if the levels of synthesis components are altered by *let-607* RNAi (e.g. Abu genes, fatty acid metabolic enzymes, amino acid transporters and peptide transporters). In fact, a set of genes involved in ER stress from the Abu family (*abu/pqn*) have been proposed to be involved in protein folding and longevity [301], supporting a link between ER homeostasis and overall cellular and organismal health and lifespan.

MATERIALS AND METHODS

***C. elegans* Strains.** Animals were maintained according to standard methods, at 20°C on nematode growth media (NGM) with OP50 E. coli **[138]**. The strains utilized in this work were: wild-type (WT) Bristol strain N2, polyQ strains (Q24 AM138; Q35 AM140) **[119]**; Q37-YFP strain (AM470, see Chapter II); SOD1 strains ($SOD1^{G93A}$ AM265; $SOD1^{wt}$ AM263) **[91]**; reporter strains *C12C8.1*p::*gfp* reporter fusion (AM446) [Morley 2004]; *daf-16p::*DAF-16::GFP (TJ356); temperature sensitive (TS) mutant strains *unc-15(e1402)*, *unc-54(e1157)*, *unc-52(e669su250)* and *unc-45(e286)* (CB1402, CB1157, HE250 and CB286, respectively) **[90]**; and the mutant *hsf-1(sy441)* (PS3551).

RNAi Assays. A genome-wide RNAi screen for suppression of Q35 aggregation in *C. elegans* muscle cells was performed as described in Chapter II, using the commercial RNAi library (GeneServiceTM, USA) **[155]**. Briefly, animals were added to RNAi bacteria at the L1 or L4 stage (day 1 or day 3, respectively), incubated at 20°C for 5 or 2 days, respectively, and scored for reduction in the number of aggregates at 6 days old using the stereomicroscope Leica MZ16FA (Leica Microsystems, Switzerland). As a negative control, animals were fed bacteria carrying the L4440 empty vector. For RNAi assays on plates, NGM media was supplemented with 100 µg/ml ampicillin, 1 mM isopropyl β-D-thiogalatoside (IPTG, Sigma) and 12 µg/ml tetracycline, and seeded with overnight RNAi bacteria cultures, pre-induced with IPTG (1 mM). For double knockdown experiments, equal volumes of each RNAi bacteria were mixed (1:1 ratio) prior to plate seeding. Fluorescent microscopy images were taken using an Axiovert 200 microscope with a Hamamatsu digital camera C4742-98 (Carl Zeiss, Germany). For all experiments, efficient gene knockdown was confirmed by qPCR, and all RNAi plasmids were sequenced to confirm target specificity.

Motility Assays. Animals grown on RNAi-seeded plates (6 days old, ~25) were picked onto OP50-NGM plates equilibrated at 20°C and their movements digitally recorded using a Leica M205 FA microscope with a Hamamatsu digital camera C10600-10B (Orca-R2, Leica Microsystems, Switzerland), and the Hamamatsu Simple PCI Imaging software (see Chapter II for detailed methodology). The average speed of each animal was calculated by dividing the distance of each track, corrected for body length, by the duration of the track (body length per second, BLPS).

Assay for TS Phenotypes. Temperature sensitive (TS) mutant animals were age-synchronized to L1 stage, grown on RNAi-seeded plates at a sensitized temperature of 23°C for RNAi efficiency (the permissive temperature is 15°C, and the restrictive temperature 25°C), and >50 animals scored for each specific phenotype 4 days later as described previously (n=3) **[90,167]** (see Chapter II for detailed methodology).

Reverse Transcriptase PCR Analysis. RNA was extracted with the Trizol reagent (Invitrogen), followed by DNase treatment (Applied Biosystems #AM1906). mRNA was reverse transcribed using the iScriptTM cDNA Synthesis Kit (Bio-Rad #170-8891). cDNA was used for real-time PCR amplification with the iQ™ SYBR® Green Supermix (Bio-Rad #170-8880) and the iCycler system (Bio-Rad) (see Chapter II). The relative expression levels of each gene were determined using the Comparative C_T Method (Real-Time PCR Applications Guide, Bio-Rad). Measurements were performed for ≥3 biological samples of each condition. For standard PCR analysis, cDNA was amplified with Taq Polymerase (NEB) followed by electrophoresis on a 2% (w/v) agarose-TBE gel.

ER and Cytosolic Stress Induction. For DTT (Dithiothreitol 2.5 mM in water, Sigma) and TM (Tunicamycin 28 µg/ml in methanol; Sigma) treatment, drug solutions were poured onto the plates where the animals were growing, covering the entire plate surface, and incubated at 20°C for 4h. Then, animals were washed with M9 buffer, allowed to recover on new OP50 plates for 1h, and finally collected for mRNA extraction. For heat shock (HS) treatment, animals were incubated in M9-OP50 at 33°C for 15 min, allowed to recover for 30 min on OP50 plates at 20°C, and then collected for mRNA extraction.

Acknowledgments: This project was performed in collaboration with Daniel Czyz in the Morimoto lab.

SUPPLEMENTARY FIGURES

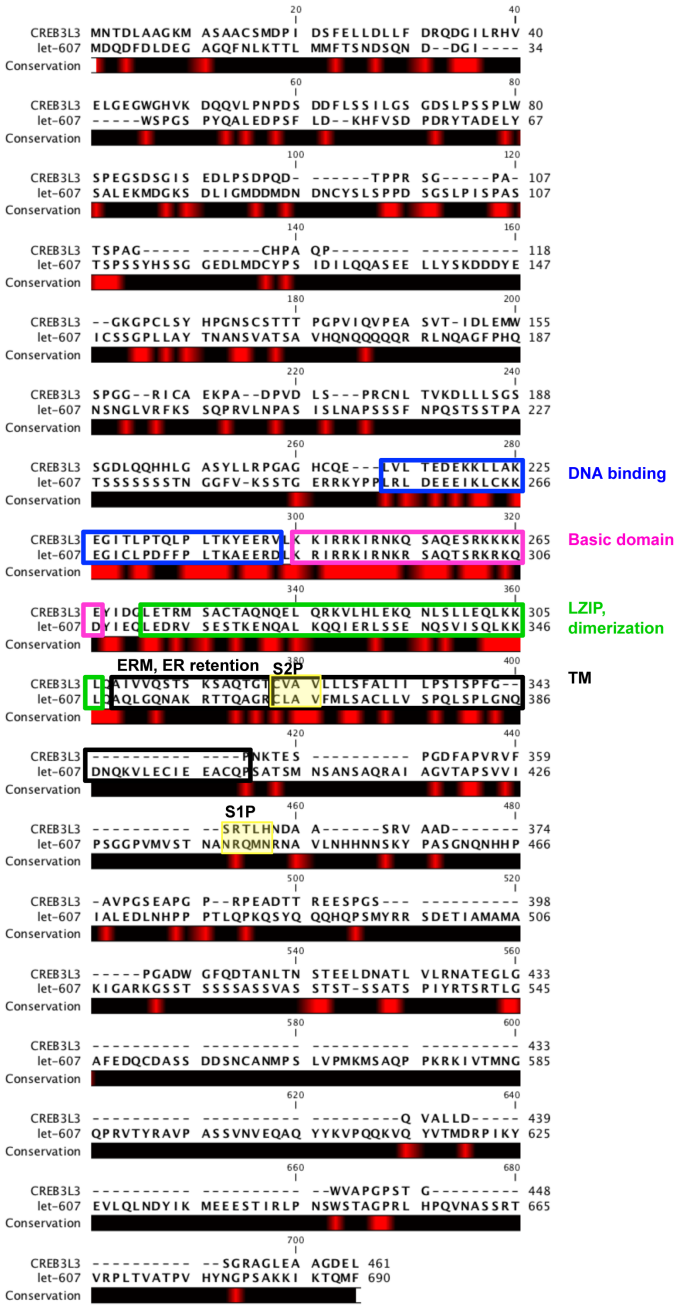

Figure S1: Sequence alignment between *C. elegans* LET-607 and the human ortholog CREB3L3 (CREBH), obtained with the CLC DNA Workbench software. Highlighted are the predicted domains of CREBH.

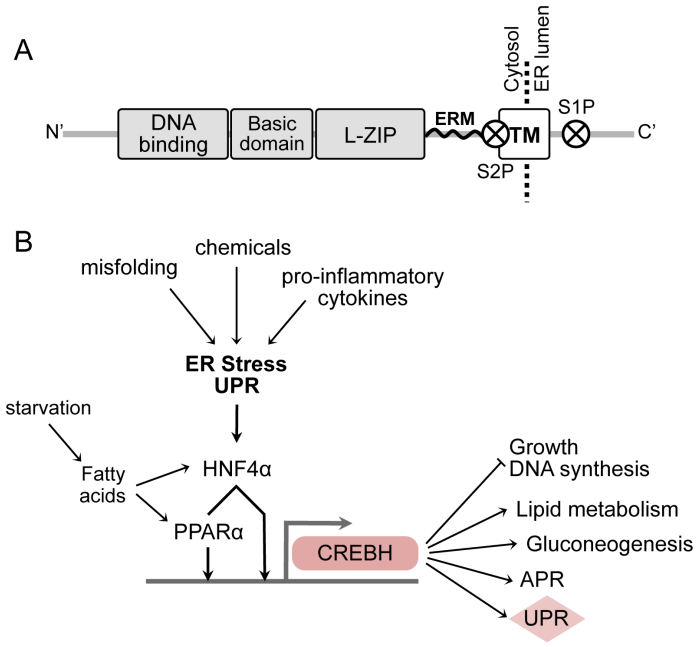

Figure S2: (A) Predicted LET-607/CREBH domains based on sequence similarity and alignment. ERM is the ER retention membrane proximal determinant, and S1P and S2P are the sites for RIP (regulated intramembrane proteolysis) for ER-to-nucleus translocation. **(B)** Overview of CREBH upstream and downstream regulatory pathways, in mammalian cells. HNF4α is the nuclear hormone receptor; PPARα is the peroxisome proliferator-activated receptor alpha; APR stands for acute phase inflammatory response genes. Our results are consistent with CREBH regulation of UPR in *C. elegans* [244,297,299].

Appendix III

Small Molecule Proteostasis Regulators for Protein Conformational Diseases

SMALL MOLECULE PROTEOSTASIS REGULATORS FOR PROTEIN CONFORMATIONAL DISEASES

Barbara Calamini[1], Maria Catarina Silva[1,2], Franck Madoux[3], Darren M. Hutt[4], Shilpi Khanna[5], Monica A. Chalfant[4], Sanjay A. Saldanha[3], Peter Hodder[3], Bradley D. Tait[5], Dan Garza[5], William E. Balch[4], and Richard I. Morimoto[1,*]

[1]Department of Molecular Biosciences, Rice Institute for Biomedical Research, Northwestern University, Evanston, IL, USA
[2]Faculty of Sciences, Centre for Biodiversity, Functional and Integrative Genomics (BioFIG), University of Lisboa, Lisboa, Portugal,
[3]Scripps Research Institute Molecular Screening Center, Lead Identification Division, The Scripps Research Institute, Scripps Florida, Jupiter, Florida, USA
[4]Department of Cell Biology and Chemical Physiology, Institute for Childhood and Neglected Diseases, The Scripps Research Institute, La Jolla, CA, USA
[5]Proteostasis Therapeutics Inc., Cambridge, MA, USA

Nature Chemical Biology, *In Press*

ABSTRACT

Protein homeostasis (proteostasis) is essential for cellular and organismal health. Stress, aging, and the chronic expression of misfolded proteins, however, challenge the proteostasis machinery and the vitality of the cell. Enhanced expression of molecular chaperones, regulated by heat shock transcription factor-1 (HSF-1), has been shown to restore proteostasis in a variety of conformational disease models, suggesting a promising therapeutic approach. We describe the results of a ~900,000 small molecule screen that identified novel classes of small molecule proteostasis regulators (PRs) that induce HSF-1-dependent chaperone expression and restore protein folding in multiple conformational disease models. The beneficial effects to proteome stability are mediated by HSF-1, DAF-16/FOXO, SKN-1/Nrf-2, and the chaperone machinery through mechanisms that are distinct from current known small molecule activators of the HSR. We suggest that modulation of the proteostasis network by PRs represents a promising therapeutic approach for the treatment of a variety of protein conformational diseases.

INTRODUCTION

Proteostasis regulates the functional properties of the proteome to minimize the damage of misfolded and aggregated proteins through a network of pathways for protein synthesis, folding, trafficking and degradation [5,58]. Loss of proteostatic control has been implicated in aging and multiple disorders of protein misfolding including metabolic diseases, cancer, and neurodegenerative diseases [5,58,92]. Eukaryotic cells have developed compartment-specific quality control mechanisms for proteome maintenance, to guide protein folding and transport, and to direct faulty proteins for refolding or clearance. Likewise, each compartment induces a cell stress response to detect and restore balance: the heat shock response (HSR) for cytoplasmic folding and misfolding, and the unfolded protein responses (UPR) in the endoplasmic reticulum (UPR-ER) [46] and mitochondria (UPR-MT) [302]. Across these compartments are other stress responses that detect specific classes of protein damage caused by metal stress and antioxidants (ARE) [92,303,304].

The cytosolic HSR is governed by a family of heat shock factors (HSFs) of which HSF-1 is essential for proteotoxic stress and regulation of heat shock proteins (Hsps) [35]. Many Hsps are molecular chaperones that guide the conformation of proteins during biogenesis and prevent misfolding and aggregation that interfere with cellular function [305]. Induction of the HSR not only prevents protein damage from persisting, but also restores the cell to the pre-stress condition. Despite these essential cellular stress pathways, the chronic expression and accumulation of misfolded, oxidized and aggregated proteins, as occurs in aging and disease, leads to cellular dysfunction when the quality control machineries become compromised [59,90]. There is increasing evidence that misfolded proteins expressed in diseases of protein conformation are not efficiently counterbalanced by a compensatory induction of cellular stress responses such as the HSR [59]. Enhancing the activity of HSF-1 and the levels of molecular chaperones

by genetic techniques or pharmacological manipulation has been shown to restore proteostasis in several models of disease [214,306-313].

Given the prominent roles of HSF-1 to maintain cellular proteostasis by upregulation of chaperone expression, there has been substantial effort to identify novel small molecule PRs that modulate HSF-1 activity. Several small molecule activators of HSF-1 are known [35,169], including proteasome inhibitors and compounds that selectively bind to the chaperone Hsp90, including radicicol, geldanamycin (GA), and 17-AAG. Another plant-derived compound, the triterpenoid celastrol, identified from a consortium screen for molecules with protective effects in models of Huntington's disease and ALS was shown to potently activate the HSR in mammalian cells. Most recently, a yeast-based high-throughput screen for small molecule activators of HSF-1 identified the compound HSF1A that was shown to activate HSF-1 without associated proteotoxicity [309].

Despite the potential benefits, as shown in multiple cellular and animal models of diseases of protein conformation, further development of these small molecules will be necessary prior to their use as a therapeutic agent [247,248]. For example, although GA and other derivatives that inhibit Hsp90 are currently in pre-clinical and clinical development for the effective treatment of a number of different cancers [314], their use for diseases associated with protein misfolding may have limited therapeutic potential. Given the imminent challenges facing the care of individuals afflicted with protein conformational diseases, and the lack of effective therapeutics, we propose that further investigation into small molecule PRs that activate HSF-1 is urgent. Here, we describe the discovery and characterization of novel small molecule PRs that, by enhancing HSF-1 activity, restore proteostasis in multiple diseases of protein conformation. We propose that modulation of the proteostasis network by HSF-1 PRs represents a new therapeutic approach for the treatment of both cytosolic and compartment-specific conformation disorders.

RESULTS

Cell-based HTS for Small Molecule Activators of the HSR

We developed a high-throughput screen (HTS) that measures the activation of the HSR in HeLa cells stably transfected with a heat shock-inducible reporter containing the proximal human Hsp70.1 promoter sequence upstream of a luciferase (luc) reporter gene (Fig. 1a) [170,315]. To assess the sensitivity and robustness of the cell-based assay before undertaking the HTS campaigns, we established dose-response profiles using three positive controls, celastrol, cadmium chloride ($CdCl_2$), and MG132 (Fig. 1b). The derived EC50 values for celastrol and MG132 were ~3 and 5 μM respectively, in agreement with previous reports [169]. Optimization and miniaturization of the HTS formats were carried out independently at the Scripps Research Institute Molecular Screening Center (SRIMSC, Florida) and at the Southern Research Institute (SRI) (Supplementary Table 1). MG132, due to its sigmoidal profile, and $CdCl_2$, because of its ability to strongly induce the reporter (Fig. 1b), were subsequently employed as positive controls at the SRIMSC and Southern Research Institute, respectively (Supplementary Table 2). Assessment of critical variables of the assay was carried out during the miniaturization and optimization steps to achieve 384 and 1,536-well plate formats (Supplementary Table 1). The Z' values for the miniaturized cell-based assays were ≥0.6, indicative of consistency and reproducibility. The HeLa-luc assay was validated by pre-screening two different libraries, the 1,280-molecule Library of Pharmacologically Active Compounds

(LOPAC) from Sigma at the SRIMSC, and a 2,000-compound set of known biologically active compounds from MicroSource Discovery Systems at Southern Research Institute.

Identification of Novel Classes of Small Molecule PRs

Two primary screens of 803,587 and 100,000 compounds were performed independently at the SRIMSC and at SRI, respectively. The small molecule libraries consisted of: (i) 607,408 compounds from the Scripps Drug Discovery library and 196,179 compounds from the Molecular Libraries Probe Production Center Network (MLPCN) library, both run at the SRIMSC; and (ii) 100,000 compounds from the National Institute of Neurological Disorders and Stroke (NINDS) library, run at the Southern Research Institute. Assay performance was consistent across plates, with robust Z' factors and signal-to-background ratio (Supplementary Fig. 1 and Supplementary Table 2). The data obtained from the primary screens was normalized to each positive control set as 100% activation. The screen performed at the SRIMSC identified 759 primary hits, whereas 37 primary hits were identified at SRI (Supplementary Table 2).

False-positive hits were excluded by performing a triplicate run on the primary hits that yielded 263 confirmed compounds (Supplementary Table 2). Although the more stringent conditions elicited by CdCl2 led to a lower number of primary hits, these conditions also identified a smaller fraction of false positives, as demonstrated in the confirmatory secondary assays (Supplementary Table 2). Confirmed hit compounds were reordered as dry powders from commercial vendors (ChemDiv, Enamine, ChemBridge, and Asinex) or re-synthesized for retesting in a full dose response. The active compounds were clustered by structure with a 0.8 Tanimoto (Butina, 1999 cutoff followed by manual inspection to merge clusters sharing a common scaffold. This analysis resulted in 233 hits grouped into seven clusters (A through G, Fig. 1c) that did not show structural similarities with the remaining 30 hits. Many compounds contained reactive moieties known to activate the HSR, such as reactive α,β-unsaturated carbonyls [316,317], but other series had no obvious reactive groups.

The two primary screens performed with different positive controls, chemical libraries and compound concentrations, independently identified three common scaffolds (C, E and F, Fig. 1c and Table 1), providing cross-validation of the cell-based screen. These active compounds were subsequently tested in the HeLa-luc cells to establish dose-response curves and compound toxicity. EC50 and CC50 values were determined: most hits exhibited a sharp activation profile, with only few compounds displaying sigmoidal dose-response curves. Subsequent studies were initially performed with fourteen representative compounds (A1, A2, A3, B1, B2, B3, C1, C2, D1, E1, F1, F2, G1 and G2, Table 1) belonging to the largest clusters A-G (Fig. 1c). The dose-response activity and toxicity profiles for the selected compounds are shown in Supplementary Figure 2. We refer to these compounds as small molecule proteostasis regulators (PRs).

Induction of Hsps and Activation of HSF-1 by the PRs

The results of the HTS screen were further validated by direct demonstration that the expression of endogenous Hsp mRNAs and proteins were induced by representative PRs. Exposure of HeLa cells to the PRs induced Hsp70 mRNA levels from 2 to 5-fold (Fig. 2a and Supplementary Fig. 3a). Likewise, western blot analysis (Fig. 2b) showed that the levels of multiple chaperones (Hsp70, Hsp40 and Hsp27) were induced from 2 to 6-fold, similar to the positive controls, respectively (Fig. 2b and Supplementary Fig. 3b).

The elevated expression of multiple Hsp genes by the PRs can be most directly explained by induction of the HSR and activation of HSF-1. To address this, we employed electrophoretic gel mobility shift assays (EMSA). Of the fourteen PRs previously tested for chaperone induction (Fig. 2a and b), 7

compounds representative of each chemical cluster were selected for this study (A1, A3, B1, C1, D1, E1, F1). Incubation of HeLa cells with the PRs strongly induced HSF-1 DNA-binding activity (Fig. 2c). The specificity of HSF-1 induction (lanes 3-7 and 18-23) was demonstrated by competition with excess unlabeled HSE oligonucleotide (lanes 8-12) and by anti-HSF-1 antibody supershift experiments (lanes 13-15 and 24, 26-29). The results of EMSA analysis were further confirmed by chromatin immunoprecipitation (ChIP) experiments. The PRs that most strongly induced HSF-1 activation in the gel mobility shift assay (A1, A3, C1, D1 and F1, Fig. 2c) were selected for ChIP analysis and the results showed occupancy of HSF-1 to the endogenous Hsp70.1 (Fig. 2d and Supplementary Fig. 3c), Hsp40 and Hsp27 promoters (Supplementary Fig. 4), but not to the negative control promoter.

From a chemical mechanism perspective, many previously identified small molecule inducers of the HSR have been suggested to activate HSF-1 by causing direct protein thiol oxidation. Compounds A1, A3, C1, D1 and F1 contain cysteine reactive moieties such as unsaturated-carbonyls (Supplementary Table 3). No close analogs of these five compounds that lacked these reactive groups were present in the HTS libraries, and therefore they were not tested. To determine whether the PRs A1, A3, C1, D1 and F1 caused protein thiol oxidation, we tested if their activity could be inhibited by treatment with reducing agents such as N-acetyl cysteine (NAC) and dithiothreitol (DTT). Induction of the HSR by celastrol was inhibited by NAC (2 mM) and DTT (250 μM) treatment, as expected (Supplementary Fig. 5f and l). Only the activity of PR F1 was completely inhibited by NAC and DTT treatment, indicating that F1 may cause oxidative damage by modifying protein cysteine residues (Supplementary Fig. 5e and k). In contrast, the activities of C1 and D1 were only slightly less affected (Supplementary Fig. 5c-d and i-j) and activation of the HSR by A1, and A3 was unaffected (Supplementary Fig. 5a-b and g-h), indicating that these PRs do not act through this mechanism.

PR Activity on Hsp Genes Requires HSF-1 and the HSE

Activation of HSF-1 by the PRs correlates with enhanced expression of chaperone genes, but does not formally demonstrate a requirement for a wild type HSE sequence or a dependence upon HSF-1. To directly address this, we tested the five PRs for their ability to induce luciferase expression in HeLa cells transfected with a mutated HSE sequence fused to a luciferase gene. As expected, cells lacking a wild type HSE failed to induce luciferase expression (Supplementary Fig. 6), indicating that an intact HSE is necessary for activation of the HSR by the PRs. We then treated wild type (WT) and hsf-1 null (hsf-1-/-) mouse embryonic fibroblasts (MEFs) with the PRs and showed that PR-induction of Hsp70 mRNA was detected only in WT cells and not in hsf-1-/- cells (Fig. 3a and Supplementary Fig. 7a). These results provide conclusive evidence that PR induction of chaperone expression is dependent upon activation of HSF-1.

PRs Activate Multiple Proteostasis Network Pathways

We next examined the gene signature of the PRs using a multiplex gene expression analysis to identify additional proteostasis mechanisms regulated by the PRs. We asked whether the PRs could activate other stress responsive proteostasis network (PN) pathways such as the unfolded protein response (UPR) and the antioxidant stress response, in addition to the HSR. Therefore, we monitored the expression of the UPR-inducible gene GRP78/BiP, the antioxidant responsive genes heme oxygenase 1 (HO1) and the regulatory subunit of glutamate-cysteine ligase (GCLM), and the proapoptotic growth arrest- and DNA damage-inducible gene 153 (GADD153, also known as CHOP). WT and hsf-1-/- MEF cells were treated with PRs and the positive controls MG132 (MG) and geldanamycin (GA) that induce the HSR, oxidative stress, and the UPR; tunicamycin (Tm) that induces the UPR; and sulphoraphane (Sul) that

activates the antioxidant response (Fig. 3b and g). Untreated (Unt) and DMSO-treated cells served as negative controls (Fig. 3b and g).

The PR stress response signatures were established in WT and hsf-1-/- MEF cells (Fig. 3c-f and h-k). At a range of concentrations of PRs A3, C1, D1, and F1, Hsp70 mRNA levels were induced from 9 to 30-fold in WT MEF cells (Fig. 3c-f). Compound D1 (Fig. 3e) was selective and only induced the expression of Hsp70, whereas A3 and C1 strongly induced Hsp70, in addition to a 3-fold increase in BiP (A3 and C1) and HO1 (A3 only) expression (Fig. 3c and d). Likewise, compound F1 induced multiple responses and strongly induced Hsp70, the oxidative stress response genes (HO1 and GCLM), and a 2.5-fold upregulation of BiP (Fig. 3f).

In performing parallel experiments on hsf-1-/- cells (Fig. 3h-k), we noticed that the level of induction of HO1 was dramatically enhanced from 12 to 130-fold, whereas the expression of GCLM and BiP was comparable to WT MEF cells (Fig. 3h-k). These results suggest that up-regulation of an anti-oxidant stress response compensates for HSF-1 deficiency. At the highest PR concentrations, induction of the cell death pathway (GADD153) was also observed. Our previous experiments employing DTT treatment indicates that PRs A1, A3, C1 and D1 did not activate the HSR by causing oxidative stress, yet we observed potent induction of the antioxidant responsive gene HO1 in absence of HSF-1 (Fig. 3h-k). There may be at least two explanations for this apparent discrepancy. First, if the induction of HO1 by the PRs were due to the generation of oxidative stress, then we would expect a concerted upregulation of the antioxidant GCLM gene, as occurs for compound F1. This, however, is not observed in WT cells. In addition, transcriptional regulation the HO1 gene indicates that expression is regulated by multiple stimuli, and not solely dependent upon oxidative stress [318].

PRs Protect Cells Against Severe Stress and Apoptosis

Activation of the HSR and induction of molecular chaperones has been shown to protect cells from the deleterious consequences of protein damage and apoptosis. Therefore we tested if the PRs A1, A3, C1, D1 and F1 displayed cytoprotective properties. Pretreatment with either 42°C heat shock or the PRs A3, D1 and F1 significantly protected cells from cell death induced by a 35 min severe heat shock (Supplementary Fig. 8a). On the contrary, the PRs A1 and C1 did not display any cytoprotective properties and instead increased the fraction of cell death after the 45°C treatment compared to the DMSO control.

We next determined if the PRs protected against apoptotic cell death induced by oxidative stress. Assessment of cellular apoptosis and necrosis was performed by staining HeLa cells with Annexin V and propidium iodide (PI). In agreement with the cytoprotection data, treatment with the PRs A3, D1 and F1 led to a two-fold protection from H_2O_2–induced apoptosis, as indicated by the reduced number of Annexin V-stained cells compared to the untreated cells (Supplementary Fig. 8b). On the contrary, cells pretreated with PRs A1 and C1 exhibited both an apoptotic (A1 and C1) and necrotic pattern (C1), (Supplementary Fig. 8b).

Proteostasis Restoration in Models of Conformational Disease

In addition to its well-established role in maintaining cytoplasmic proteostasis, HSF-1 has also been recently shown to ameliorate ER stress [245]. We therefore asked whether the PRs, by enhancing chaperone expression, would reduce protein misfolding in diseases in which expression of mutant proteins accumulates in either the cytoplasm or the ER.

As a representative cytosolic model, we examined the effects of the PRs on Huntingtin aggregation in PC12 cells, conditionally expressing human Huntingtin (htt) exon 1 containing an expansion of 74 glutamines, fused to green fluorescent protein (GFP) (httQ74-GFP) [319]. In these cells, httQ74-GFP

aggregates are detected after 48 hours of induction. PC12 cells were treated with the PRs and visually monitored for aggregate formation. Incubation with A1, D1 and F1 caused a reduction (from 2 to 3-fold) of httQ74-GFP protein aggregates without altering the levels of httQ74-GFP protein (Fig. 4a and b and Supplementary Fig. 9a-f), whereas PRs A3 and C1 had no effect, although Hsp70 levels were induced (Fig. 3c and d).

We next investigated the PRs on a cellular model of cystic fibrosis. This model corresponds to a human bronchial epithelial cell line (CFBE41o-) stably co-expressing the ΔF508 mutation of the CFTR and a halide-sensing mutant of YFP (H148Q/I152L-YFP). ΔF508-CFTR is defective both in trafficking from the endoplasmic reticulum to the plasma membrane and in channel gating [320]. Correction of ΔF508-CFTR trafficking by the PRs would lead to increased level of active protein at the cell surface, affording increased flow of extracellular halides into the cell, resulting in reduction of YFP fluorescence intensity.

The same PRs tested in the Huntington's disease cell model were also tested in ΔF508-CFTR expressing cells and positive results were obtained for A3, C1 and F1 (Fig. 4c and Supplementary Fig. 10a). The extent of YFP quenching detected was comparable to that seen with corrector 4a, a commonly used positive control for this assay (Fig. 4c). It is worth noting that compound F1 represents the first characterized small molecule capable of enhancing the correct folding of proteins expressed in two different cellular compartments.

To further confirm that the PRs A3, C1 and F1 rescued ΔF508-CFTR trafficking, we monitored the processing of ΔF508-CFTR. Treatment of CFBE41o- cells expressing ΔF508-CFTR with the PRs generated higher molecular mass forms of ΔF508-CFTR, consistent with full glycosylation (Fig. 4d-f and Supplementary Figs. 10b and 11), indicating that the PRs partially rescued the cell-surface expression and maturation of ΔF508-CFTR. In addition, we show that rescue of ΔF508-CFTR trafficking by the PRs coincides with Hsp70 upregulation, suggesting that the PR action depends on HSF-1 and the induction of molecular chaperones.

Suppression of Aggregation and Toxicity in *C. elegans*

We asked whether the efficacy of the PRs to reduce protein aggregation could be also observed in a *C. elegans* model for expression of expanded polyglutamines (35 glutamines fused to YFP, Q35::YFP) in body wall muscles, that displays age-dependent aggregation and toxicity [119]. This model exhibits many characteristics of polyglutamine diseases, such as Huntington's disease, and has been a valuable tool in the identification of genetic and chemical modifiers of aggregation and toxicity [144,167].

Age-synchronized Q35 animals were treated with the PRs and the effects on aggregation and toxicity scored at 6 days of age. We used 17-AAG as a positive control inducer of the HSR that induces chaperone expression and reduces polyQ aggregation [306,312]. Treatment of *C. elegans* with 17-AAG induced the HSR (Fig. 5d), and showed a marked reduction in protein aggregates and toxicity (Fig. 5a-c). Treatment with PRs A1, D1 and F1 suppressed Q35 aggregation (Fig. 5a and b) without affecting overall levels of Q35 protein (Supplementary Fig. 9g and h). Suppression of polyQ aggregation also ameliorated aggregation-associated toxicity. Expression of Q35 in the body wall muscles reduces motility by 50% relative to WT, and PR treatment of Q35 animals restored (80%-100%) motility to near WT (Fig. 5c). These results reveal that the PR-induced suppression of aggregation also prevented polyQ toxicity.

We then confirmed that the effect of the PRs on polyQ aggregation and toxicity was associated with expression of molecular chaperones and induction of the HSR (Fig. 5d). Chaperone expression was HSF-1-dependent (Fig. 6a-c) and moreover downregulation of HSF-1 by RNAi abrogated the PR-induced protection against Q35 aggregation (Fig. 6d).

PRs Stabilize the Folding of Metastable Proteins

To begin examining the basis for PR induction of the HSR, we asked whether these small molecules caused protein damage and therefore activated a HSR, or alternatively that the PRs activated specific homeostasis regulators to induce chaperone expression. To address this, we used *C. elegans* strains harboring temperature-sensitive (TS) mutations in specific endogenous muscle proteins, including the basement-membrane protein perlecan UNC-52, and a myosin-assembly protein UNC-45. These conditional mutations do not interfere with folding and function at the permissive temperature (15°C), but cause a complete loss of function at the restrictive temperature (25°C), resulting in distinctive muscle dysfunction (Fig.6e, DMSO 15°C and 25°C). These metastable proteins therefore serve as folding sensors that monitor changes in cellular proteostasis [90]. To determine whether the PRs induce protein misfolding, we incubated both *unc-52(e669su250)* and *unc-45(e286)* animals with PRs A1, D1 and F1 (10 μM) at 15°C. We reasoned that enhancing misfolding would unmask the TS phenotypes at the permissive condition, which was not observed. Alternatively, to determine whether the PRs enhanced the folding environment, we incubated animals with PRs, transferred them to 25°C, and scored for TS phenotypes 2 days later (Fig. 6e). While PR A1 caused an intermediate 35% suppression of the *unc-45(e286)* TS phenotype, the most potent effect was observed with F1, that suppressed both *unc-52(e669su250)* and *unc-45(e286)* phenotypes by 80% and 90% respectively (Fig. 6e). These results suggest that the PRs do not activate the HSR by interfering with cellular protein folding in general, but rather promote folding of metastable proteins.

PRs Depends on the Folding and Quality Control Machinery

The striking improvement in protein homeostasis, following treatment with the PRs, prompted us to investigate the requirements for other regulatory components of the PN such as DAF-16 (FOXO ortholog, insulin/IGF-1-mediated signaling transcription factor) and SKN-1 (oxidative stress response transcription factor). We simultaneously treated Q35 animals with the PRs and RNAi to knockdown the stress regulators DAF-16 and SKN-1. We examined the effects on induction of *hsp-70* (*C12C8.1, F44E5.4*) and small HSP *hsp-16.1* and show that A1 and D1-mediated chaperone expression requires both HSF-1 and DAF-16 (Fig. 6a and b), whereas F1 activity is dependent upon HSF-1 and SKN-1 (Fig. 6c).

We explored the role of these stress responses on PR-regulated folding by monitoring the expression of downstream targets of SKN-1 and DAF-16, and other protein folding components including HSP-90 and co-chaperone genes, ubiquitin, and components of the ER HSP-70 (UPR). Compounds D1 and F1 elicited induction of *sod-1* (SKN-1 target), *hsp-4* (UPR-ER) and *hsp-90* and its co-chaperone (*ZC395.1*) (Fig. 6f). Meanwhile, A1 induced ER *hsp-70* levels, and ubiquitin protein *ubq-2* (Fig. 6f and Supplementary Fig. 12). We examined the expression of a number of oxidative stress, UPR, mitochondrial-UPR and lifespan/aging regulators (Supplementary Fig. 12), and observed that only genes encoding folding and chaperone components were affected (Fig. 6f). These results indicate that the pathways that are activated to enhance the folding environment depend on HSF-1, DAF-16 and SKN-1 and the chaperone and quality control machinery.

PRs are not Inhibitors of the Proteasome or Hsp90

Having demonstrated that the PRs themselves do not cause protein misfolding, we examined whether the PRs activated the HSR via inhibition of the proteasome or Hsp90 function. For these experiments, we selected the PRs A1, A3 and F1 because A1 and F1 suppressed aggregation in cellular and *C. elegans* models of conformational diseases and stabilized folding of TS mutant proteins, and A3 and F1 improved the folding stability of mutant CFTR. Exposure of HeLa cells to MG132 and lactacystin for

3 and 6 hours (Fig. 7a and Supplementary Fig. 13a), reduced proteasome activity to 20 percent relative to DMSO-treated cells (Fig. 7a) and increased the levels of polyubiquitinated substrates (Fig. 7b). By comparison, treatment with the PRs A1, A3 and F1 neither inhibited proteasome activity nor increased polyubiquitinated proteins (Fig. 7a and b).

We next monitored the effects of the PRs on Hsp90 by assessing Hsp90 client protein degradation [239]. The levels of three well characterized Hsp90 client proteins, Cdk4, Raf-1, and Akt, were quantified by western blot analysis of PR-treated HeLa cells. Relative to the DMSO-treated control cells, a reduction in the levels of the Hsp90 client kinases was observed with the PR A1 (10 μM) after 6 hours of treatment (Supplementary Fig. 13b), whereas treatment with the other two PRs had no effect. The clearance of these Hsp90 clients was even more dramatic after 16 (Supplementary Fig. 13c) and 24 h (Fig. 7c and Supplementary Fig. 7b) of PR treatment, and was comparable to the inhibitory effects of 17-AAG on Hsp90 function.

Since classical Hsp90 inhibitors such as geldanamycin, 17-AAG and radicicol bind competitively to the ATP site of Hsp90, we investigated whether the PRs A1, A3 and F1 had a similar mode of action. We therefore tested whether the PRs could compete in vitro with geldanamycin for binding to the ATP binding pocket of Hsp90. Whereas the positive control 17-AAG competed effectively with geldanamycin, none of the three PRs disrupted the interaction between geldanamycin and Hsp90 even at concentrations in excess of 100-fold (Supplementary Fig. 13d).

Although the competition assay may suggest that the PRs A1 is not an inhibitor of Hsp90 activity, it is also possible that the compound acts through a different mechanism compared to known Hsp90 inhibitors. To further confirm that the previous results were not due to a direct inhibition of Hsp90, we performed a chaperone-dependent protein refolding assay. Refolding of denatured luciferase was monitored in rabbit reticulocyte lysates (RRL) by measuring luciferase activity. In the presence of DMSO, luciferase recovered 40-45% activity, whereas 17-AAG (2 μM) caused only about a 25% recovery (Fig. 7d). Incubation of RRL with the PR A1 (10 μM) did not inhibit luciferase refolding (Fig. 7d). These results indicate that A1 is not a direct inhibitor of Hsp90 activity. Although PR A1 did not directly inhibit Hsp90 activity, we offer possible explanations for the increase in client protein degradation by PR A1. A1 could disrupt the interaction between Hsp90 and its co-chaperone Cdc37 implicated in shuttling kinase clients to Hsp90, or A1 could inhibit Hsp90 activity by binding to a site different than the ATP binding pocket.

DISCUSSION

In this study we describe the results of a large-scale small molecule screen in human cells for HSF-1-dependent activators of chaperone expression. We identified 263 PRs that chemically induce the HSR and result in the activation of HSF-1 and elevated expression of multiple chaperone gene families. The PRs described here represent novel chemical series and, by comparison to previously identified small molecule activators of the HSR, do not cause protein misfolding, proteasome inhibition, or Hsp90 inhibition. A further understanding of these PRs and their ability to activate the HSR and restore protein folding in multiple disease models offers new opportunities and strategies for small molecule chaperone therapeutics for protein conformational diseases with novel specificities and reduced toxicity.

An intriguing observation is that the PRs exhibit complex stress response signatures. In addition to inducing HSF-1 and the expression of multiple cytoplasmic chaperones, we have observed the induction of

other major components of the PN including the UPR and the antioxidant response genes. Our PR strategy is based on the proposition that small molecules can mimic the molecular signals recognized by the cell associated with a proteostatic imbalance (Supplementary Scheme 1). This activation of stress-signaling pathways, in turn restores the stability and functionality of the proteome. The ability of these PRs to activate one or more stress response pathways suggests a therapeutic approach that employs the cell biological response to damaged proteins to protect cells against chronic disease. By this approach, we are employing our growing understanding of stress biology to promote the health of the cell. In doing so, we are using compounds to enhance the properties of biological pathways that are already employed by the cell to manage proteostasis, even when challenged by stress and disease. We suggest that this systems and network approach represents an alternative for drug discovery as we harness the protective abilities of cellular stress responses to protect the cell against the multitude of deficiencies that occur during chronic proteotoxicity and stress.

The central role for HSF-1 in maintaining and restoring proteostasis makes this transcription factor and the HSR an attractive target for therapeutic intervention in conformational diseases. The observation that diverse chemical types have in common the ability to induce the HSR, despite their broad activities, supports our proposal that HSF-1 is a stress network hub that integrates multiple stress signaling pathways to coordinate regulatory responses to maintain proteostasis in health, aging, and disease. Of the 263 hits identified in this study that activate HSF-1, we have focused our attention on the 7 major clusters represented by the chemical series: β-aryl-α,β-unsaturated-carbonyls (cluster A), β–nitrostyrenes (cluster B), β-Cl-α,β-unsaturated-carbonyls (cluster C), nitrobenzofurazans (cluster D), nitrofuranylamides (cluster E), unsaturated barbituric acids (cluster F), and 2-cyanopentadienamide (cluster G). These chemical series exhibit a broad range of pharmacological indications and diverse mechanisms of action and, to our knowledge, have not been previously linked to proteostasis and the HSR. For example, compounds in cluster A are chalcone and curcumin analogues and have antibacterial, antioxidant and cancer chemopreventive activities [321,322]. These compounds are known to inhibit NF-κb and modulate the Keap1-Nfr2 complex [323,324]. Nitrobenzofurans (cluster E) have antitubercular activity, and nitrofuran antibiotics, i.e. nitrofurantoin, are currently used as second-line agents for urinary tract infections. The nitroimidazole antibiotics are structurally related; for example, metronidazole, is a widely used antibiotic for treatment of anaerobic bacterial and protozoan infections [325]. Compounds belonging to cluster F are barbiturate analogs associated with anti-inflammatory side effects; in particular thiobarbiturates reduce activation of NF-κb. Thiopental, but not the oxy-analogue pentobarbital, is the only barbiturate suggested to activate the HSR and this property has been attributed to thiopental reactivity with protein thiols [326]. Of interest, barbiturate analogues have been previously reported as potentiators of defective ΔF508-CFTR channel gating [327]. Our results reveal unexplored mechanisms by which these chemical classes exert their beneficial effects, and suggest new pathways involved in activation of HSF-1. We propose that the ability of barbiturate analogs to rescue mutant CFTR defective channel gating can now be linked to the activation of the HSR and/or of the UPR. Likewise, the neuroprotective effects attributed to curcumin [328], a chalcone analog, may be due to the induction of chaperone expression [329]. Taken together with the data presented here, we propose that compounds of the same chemical classes identified in our HTS can be reclassified as PRs.

We describe a first generation series of tool compounds that, by activating HSF-1 and other cell-protective stress responses, demonstrate efficacy in cellular and animal models of protein conformational diseases. Although we have shown that the PRs are effective in multiple misfolding disorders, i.e. cystic fibrosis and Huntington's diseases, these molecules may have a broader efficacy. For example, PRs that restore proteostasis by simultaneously inducing the HSR and the UPR should be able to enhance the

folding, trafficking and activity of mutant enzymes in a variety of diseases, including lysosomal storage diseases (i.e. Tay-Sachs, Gaucher and Pombe's diseases) and retinitis pigmentosa, that require both ER and cytoplasmic proteostasis [330-333]. Likewise, PRs selective to the HSR may be beneficial for diseases in which the expression of the affected protein is primarily cytoplasmic and nuclear, as in ALS and in the multiple forms of spinal cerebellar ataxia. Considering that the pathogenesis of many diseases, such as Alzheimer's, Parkinson's, ALS and cystic fibrosis disorders, is also associated with oxidative stress, the activation of the ARE pathway in conjunction with the HSR may be highly beneficial. In support of this, we show that the small molecule PR F1, that simultaneously induced both stress-protective pathways, was the only PR that restored proteostasis in distinct cellular compartments.

In conclusion, we propose that the adjustment of the proteostasis network by small molecule PRs of the HSR provides a previously unexploited and potentially powerful approach to obtaining proteome balance in both loss- and gain-of-function diseases by providing a superior corrective environment based on the principle of proteome balance. Besides the usefulness for potential therapeutic development, small-molecule HSR inducers can be used as pharmacological tools for further dissecting the multi-step activation pathway of HSF-1. We believe that a better understanding of the regulation of HSF-1 activation pathway and of its signaling mechanisms could lead to the discovery of compounds that exhibit stress signatures that are HSF-1 selective or activate multiple stress pathways that can be effective in the control of diseases of protein conformation.

MATERIALS AND METHODS

Cell-based High-throughput Assays. HeLa-luc cells were used to screen three compound libraries consisting of 903,663 structurally diverse small molecules. A library of 100,000 compounds (NINDS library, http://www.ninds.nih.gov/funding/areas/technology_development/HTS_Facility.htm) was screened at the Southern Research Institute and two libraries of 607,408 and 196,179 compounds (Scripps Drug Discovery library and MLPCN library, http://mli.nih.gov/mli/mlpcn/) were screened at the SRIMSC. Detailed protocol and analysis are described in Supplementary Methods.

Reverse Transcription-PCR. RNA was purified using the RNeasy Mini kit (Qiagen, Valencia, CA) according to the manufacturer's instructions. After the reverse transcription reaction, PCR was performed using PCR primers specific for Hsp70 and GAPDH. The human Hsp70 primers were: 5′-AGAGCCGAGCCGACAGAG-3′ (forward) and 5′-CACCTTGCCGTGTTGGAA-3′ (reverse); the mouse Hsp70 primers were: 5'-CACCAGCACGTTCCCCA-3' (forward) and 5'-CGCCCTGCGCCTTTAAG-3' (reverse); the human GAPDH primers were: 5′-GTCGGAGTCAACGGATT-3′ (forward) and 5′-AAGCTTCCCGTTCTCAG-3′ (reverse); the mouse GAPDH primers were: 5'-TGCACCACCAACTGCTTAG-3' (forward) and 5'-GGATGCAGGGATGATGTTC-3 (reverse). PCR products were amplified with Taq polymerase (Promega, Madison, WI) by using standard cycling conditions.

Western Blot Analysis. Analysis of chaperone expression was carried out using HeLa cells that were treated with the indicated compounds for 8 h. Cells were lysed in a buffer containing 20 mM HEPES (N-2-hydroxyethylpiperazine-N'-2-ethanesulfonic acid; pH 7.9), 25% (vol/vol) glycerol, 0.42 M NaCl, 1.5 mM MgCl2, 0.2 mM EDTA, 0.5 mM phenylmethylsulfonyl fluoride, 0.5 mM dithiothreitol and 2 mg/ml of complete protease inhibitor cocktail (Roche, Switzerland) for 30 min on ice. 15 μg of whole cell extracts were run on 7.5% SDS-PAGE gels and transferred to nitrocellulose. Primary antibody incubations were for 12 hours at 4°C in 10% BSA. The following primary antibodies were used: a rabbit polyclonal HSF-1 #47 [170], a mouse monoclonal Hsp70 antibody (4g4, Affinity Bioreagents Inc., Golden, CO), a mouse monoclonal Hsp40 (αHdj-1 clone 25) [170], a mouse monoclonal Hsp27 (MA3-0015, Affinity Bioreagents, Inc., Golden, CO). All primary antibodies were used at a dilution of 1:10,000, except for the Hsp27 antibody, which was diluted 1:500. The anti-β-tubulin antibody (Sigma, St. Louis, MO) was diluted 1:5,000 and used to verify equal protein loading. The secondary antibody was an Alexa Fluor 680 goat anti mouse IgG diluted 1:5,000 (Invitrogen, Carlsbad, CA). Western analysis was performed with the Odyssey system (Li-COR, Lincoln, NE).

Gel Mobility Shift Analysis (EMSA). Detailed protocol is described in Supplementary Methods.

Chromatin Immunoprecipitation Assays (ChIP). ChIP was performed essentially as described previously (Westerheide et al., 2004). Detailed protocol is described in Supplementary Methods.

Effect of NAC and DTT on the PR Activity. HeLa-luc cells were seeded in a white 96-well plate at a density of 10,000 cells/well. Cells were pretreated with either 2 mM NAC or 250 μM DTT for 1 h before addition of the positive control celastrol (Cel; 2.5 and 5 μM) or the selected small molecule PRs (A1, A3, C1, D1 and F1; 2.5, 5 and 10 μM). Cells were incubated with compounds for 24 h before luminescence signal acquisition. DMSO-treated cells were used as negative control.

Multiplex Gene Expression Analysis. WT and hsf-1-/- MEFs were treated with serially diluted compounds in a 7-point dose dependent manner. Cell lysates were pooled with mouse 8-gene multiplex probe sets and with 8 different sets of magnetic capture beads (Luminex Technology, Austin, TX) in a 100 μl/well volume. Fold changes in gene expression were obtained for each gene per well by normalizing the raw data first to the DMSO control and then to the TATA-box binding protein (TBP) housekeeping gene. Detailed protocol is described in Supplementary Methods.

Protein Aggregation Analysis in PC12 Cells. PC12 cells expressing httQ74-GFP were seeded in tissue culture treated 96-well plates as 7,500 cells/well and induced with doxycyclin (1 μg/ml). Compounds A1, A3, C1, D1, and F1 were used at concentrations ranging from 0.75 to 25 μM. GA (200 nM) was used as positive control. Final DMSO concentration was 0.5%. Fluorescence images were taken with a Zeiss Axiovert 200 fluorescence microscope (Carl Zeiss, Germany) at 20x magnification and images deconvoluted with the Axiovision software. For quantification of fluorescence microscopy analysis, approximately 500 cells were counted for each treatment.

ΔF508-CFTR YFP Quenching Assay. Human bronchial epithelial cells (CFBE41o-) stably expressing ΔF508-CFTR as well as H148Q/I152L-YFP (CFBE41o- -YFP) were treated with the indicated concentration of compounds in complete growth media and incubated at 37oC, 5% CO_2 for 24 h. Cells were subsequently stimulated with a final concentration of 10 μM forskolin (fsk) and 50 μM genistein (gen) for 15 min prior to addition of PBS + NaI (replacement of NaCl with 137 mM NaI). Fluorescence was monitored every second for a total of 30 seconds (3 seconds prior to addition of NaI and 27 seconds after addition of NaI). Detailed protocol and analysis are described in Supplementary Methods.

ΔF508-CFTR Transport Assay. CFBE41o-cells stably expressing ΔF508-CFTR were treated with the indicated concentration of compound in complete growth media and maintained at 37oC, 5% CO_2 for 24 hrs. Cells were lysed on ice and the supernatant was collected for analysis. Equal amount of total protein (15 μg) was separated by SDS-PAGE (8% gel) and transferred to nitrocellulose. The blot was probed overnight at 4oC for CFTR (3G11 rat monoclonal antibody at 1:500 dilution) and indicated chaperone proteins. Detailed protocol is described in Supplementary Methods.

***C. elegans* Assays for Aggregation and Motility Defects.** The treatment with chemical compounds was performed in a 96-well plate format, in liquid culture. The animals were scored for changes in aggregation (number of fluorescent foci) using the stereomicroscope Leica MZ16FA equipped for epifluorescence (Leica Microsystems, Switzerland). For the motility assay, animals' movement was digitally recorded using a Leica M205 FA microscope with a Hamamatsu digital camera C10600-10B (Orca-R2, Leica Microsystems, Switzerland), and the Hamamatsu Simple PCI Imaging software. Detailed protocol is described in Supplementary Methods.

ACKNOWLEDGEMENTS

We acknowledge Dr. Joseph Maddry, the SRI and the NINDS for support in performing the primary screen; Peter Chase and Pierre Baillargeon of Scripps Florida for executing the SRIMSC screening activities; Sue Fox, James West, Sandy Westerheide, Jason Moran, Monica Beam and Kai Orton for technical assistance; Dr. Jesper S. Pedersen for help developing the worm tracker system; the Morimoto laboratory, in particular Drs. Tali Gidalevitz, Janine Kirstein, Cindy Voisine and Anan Yu for helpful comments. PC12 httQ74-GFP cells were kindly provided by Dr. David Rubinsztein. Purified Hsp90β was a generous gift of Dr. Ahmed Chadli. We thank Dr. Aaron Ciechanover for the rabbit polyclonal anti-ubiquitin antibody. The CFBE41o- -YFP cells were a generous gift from Dr. Luis Galietta. This work was supported by the National Institutes of Health Training Grant in Signal Transduction and Cancer T32 CA70085 and the National Institutes of Health Training Grant in Drug Discovery in Age Related Diseases T32 AG000260 (to B.C.), Portuguese PhD fellowship from Fundação para a Ciência e Tecnologia (SFRH/BD/28461/2006) (to M.C.S.), National Institutes of Health grants HL 079442, GM42336 and DK785483 (to W.E.B.), a fellowships from the Canadian Institutes for Health Research (CIHR) (to D.M.H.), the National Institutes of Health Molecular Library Screening Center Network MH084512 (to F.M., S.S. and P.H.) and National Institutes of Health grants GM038109, GM081192, AG026647, and NS047331 (to R.I.M.).

FIGURES

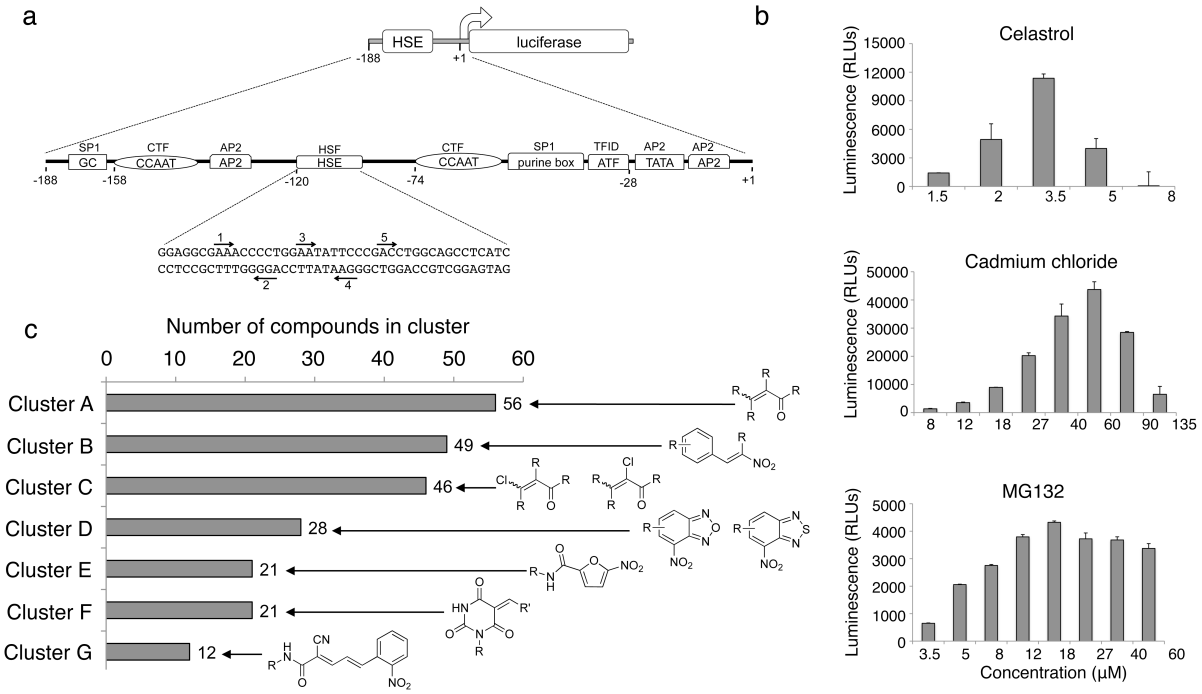

Figure 1. Identification of small molecule proteostasis regulators (PRs) by high-throughput screening. (a) HeLa-luc cells were used to screen compound libraries to identify small molecule PRs. The Hsp70.1pr-luc construct is diagrammed. The sequences of the upstream region of the human Hsp70.1 promoter from +1 to -188 are represented by a line. The locations of transcription factor binding sites are depicted as boxes and their corresponding genetic elements are indicated in the boxes. The transcription factors that bind to these regions are indicated above the boxes. The nucleotide sequence of the HSE is shown and the inverted nGAAn repeats, to which HSF-1 binds, are labeled with arrows and marked 1 through 5. (b) HeLa-luc cells were treated with celastrol, cadmium chloride and MG132 at the indicated concentrations and luciferase activity was measured after 24 h. Each experiment was performed in triplicate. The standard deviation is shown. (c) Confirmed hits (263) were clustered accordingly to their chemical substructure and a total of 7 clusters were identified. The number of hits per cluster is shown.

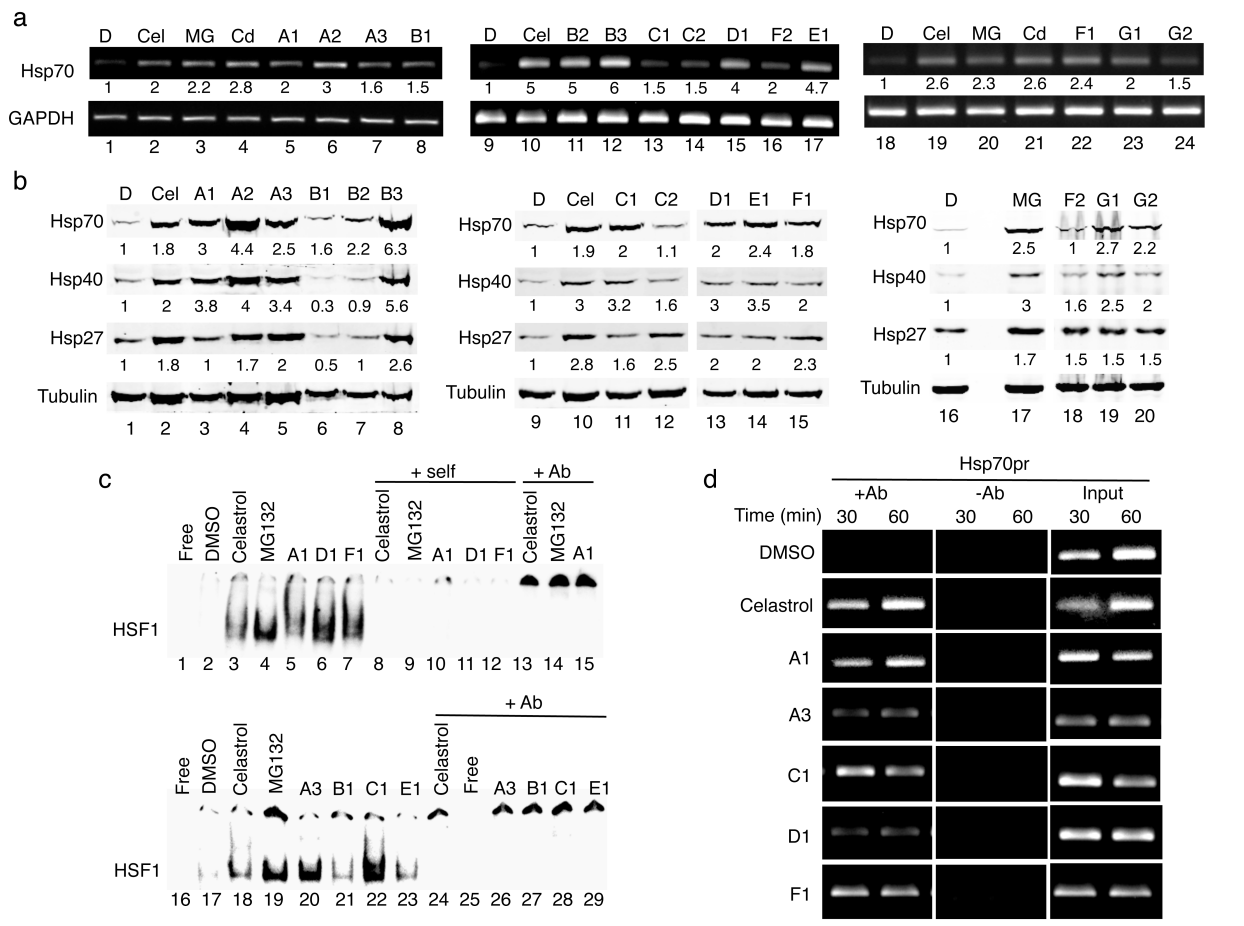

Figure 2. The small molecule PRs induce Hsp expression by activating HSF-1. (a) HeLa cells were treated with DMSO, celastrol (Cel, 3 μM), MG132 (MG, 10 μM), CdCl2 (Cd, 50 μM) and selected PRs for 4 h. Similar results were obtained in two independent experiments. Densitometric measurements of Hsp mRNA levels normalized to GAPDH in relation to control DMSO-treated cells were performed using ImageJ software. (b) Western blot analysis of HeLa cells treated with DMSO, celastrol (Cel, 3 μM), MG132 (MG, 10 μM) and selected PRs. Fold induction was calculated as the ratio of normalized Hsp values between a compound-treated sample and the untreated control. Densitometric measurements of Hsp levels normalized to tubulin were performed as in (a). (c) Gel mobility shift assay was performed with a [32P]HSE oligonucleotide and HeLa cell whole cell extracts. DMSO: lanes 2 and 17; celastrol (3 μM): lanes 3 and 18; MG132 (10 μM): lanes 4 and 19; small molecule PRs (10 μM): lanes 5-7 and 20-23. Lanes marked self (lanes 8-12) contained a 200-fold molar excess of unlabeled complementary oligonucleotide. Lanes marked +Ab (lanes 13-15 and 24-29) contained a HSF-1 antibody. (d) HeLa cells were treated with DMSO, celastrol (3 μM) and selected PRs (10 μM) for 30 and 60 min and then chromatin was cross-linked, harvested, and immunoprecipitated with HSF-1 antibody (+Ab). The samples were then analyzed by PCR with primers specific for the Hsp70.1 and the dihydrofolate reductase (DHFR) promoters. The controls include input DNA and a no antibody control (-Ab).

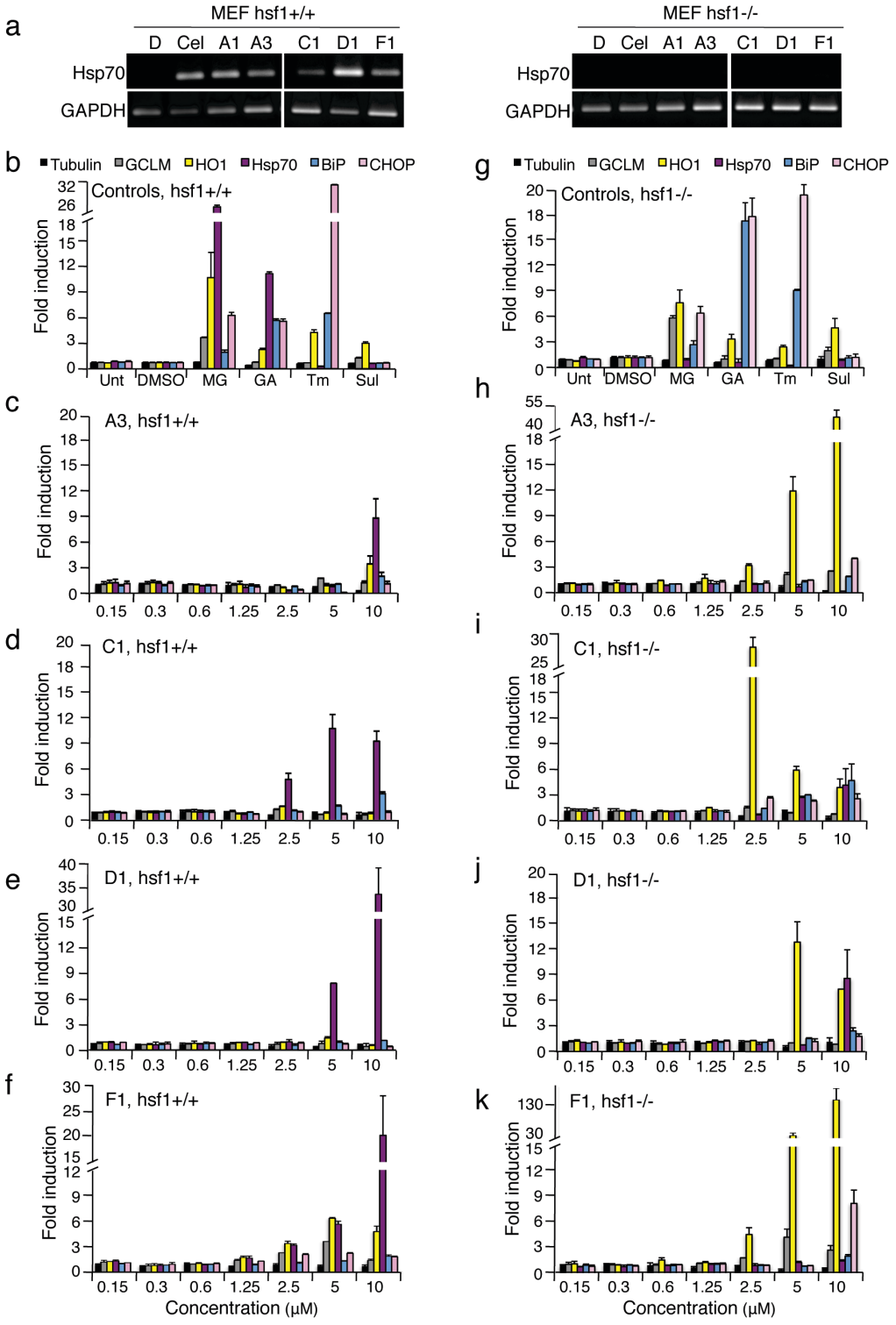

Figure 3. The PRs are HSF-1-dependent. (a) Wild type (hsf-1+/+) and HSF-1 null (hsf-1-/-) mouse embryonic fibroblasts (MEFs) were treated for 4 h with DMSO vehicle, celastrol (3 μM) or indicated PRs (10 μM). RNA was extracted and reverse-transcribed. PCR reactions were performed on cDNA for the indicated transcripts. GAPDH RNA levels were assayed to determine equal loading. (b-f) WT and (g-k) hsf-1-/- MEFs were treated for 4 h with either DMSO, MG132 (MG, 1 μM), geldanamycin (GA, 1 μM), tunicamycin (Tm, 1 μM), sulphorahane (Sul, 1 μM) or selected PRs (A3, C1, D1 and F1) at the indicated concentrations. Relative levels of multiple cytoprotective genes were measured by real-time PCR (qPCR) with tubulin serving as a reference gene.

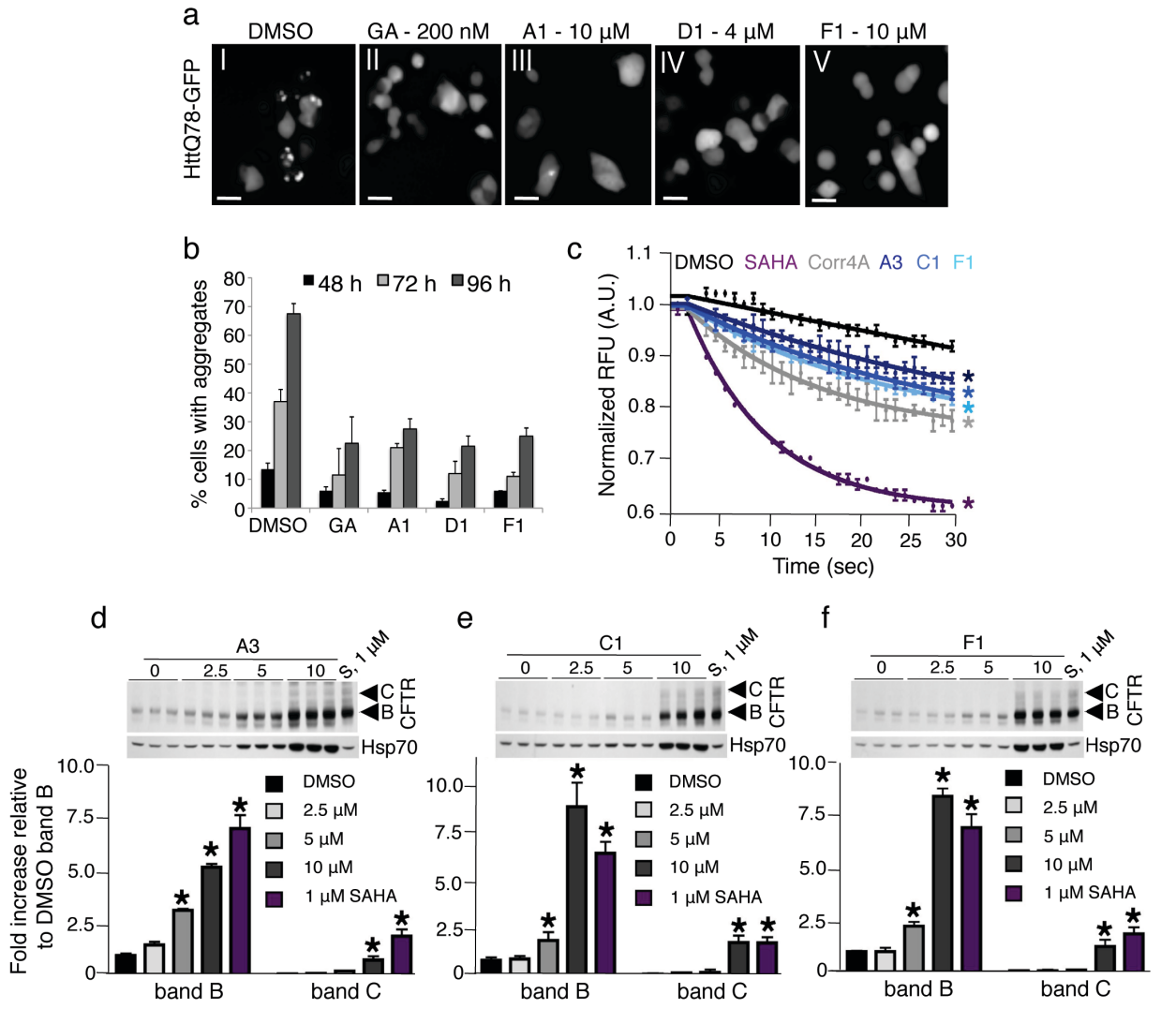

Figure 4. The PRs restore proteostasis in cell-based models of cytoplasmic and compartment-specific conformational diseases. (a) PC12 cells expressing httQ74-GFP were treated either with DMSO (panel I), geldanamycin (GA, 200 nM, panel II) or with selected PRs (panels III-V). The representative fluorescence pattern of httQ74-GFP after 72 h of induction is shown. Scale bar: 10 µm. (b) Quantification of results shown in panel (a). Cells containing aggregates were counted and are shown as a percentage of the total number of cells counted. The data shown are derived from three independent experiments. (c) CFBE41o- YFP cells were treated with 0.1% DMSO (black), the positive controls 5 µM SAHA (purple), 10 µM Corrector 4a (Corr4a) (grey) and the PRs A3 (dark blue), C1 (royal blue) and F1 (cyan) at 10 µM for 24 h. Fluorescence quenching is indicative of restored ΔF508-CFTR trafficking (mean ± s.e.m.; n = 3). Color-coded asterisks indicate statistically significant differences from DMSO control at the 30 s time point. (d) CFBE41o- cells were treated with 0.1% DMSO, SAHA (S, 1µM) and selected PRs at the indicated concentrations for 24 h. ΔF508-CFTR trafficking was analyzed by monitoring the band B and C glycoforms (fold increase relative to DMSO band B ± s.e.m.; n = 3) at the various concentrations of PRs. The level of Hsp70 was also monitored by western blot as an indicator of HSF-1 activation. 15 µg of protein were loaded and equal loading was confirmed by staining the membrane with Ponceau S.

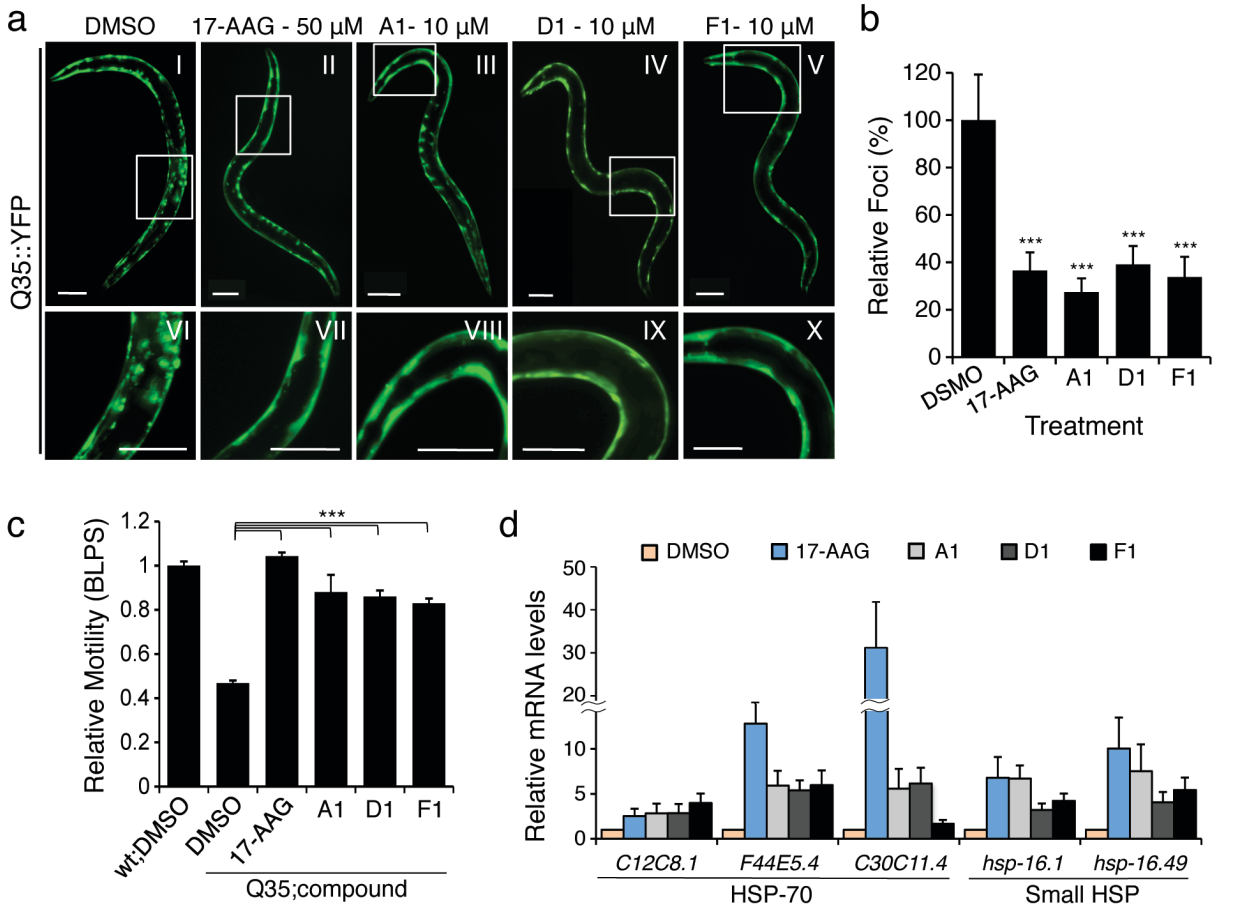

Figure 5. The PRs reduce aggregation/toxicity in *C. elegans* models of diseases associated with polyQ expansions. (a) *C. elegans* expressing YFP-tagged Q35 protein were treated with either DMSO (panel I) or PRs (panels III-V) at different concentrations (1, 5, 10 and 15 µM) for 4 days. 17-AAG was used as positive control (50 µM, panel II). Fluorescence microscopy images show the PRs that reduced Q35 aggregation at a concentration of 10 µM in 6-day old animals. Panels VI-X show higher magnification images of the boxed areas on the top panels. Scale bar: 0.1 mm. (b) PRs suppress Q35 aggregation as shown by the quantification of fluorescent foci in 6-day old animals, relative to DMSO control. (c) Rescue from polyQ-associated toxicity was determined by comparing the motility of Q35 animals treated with either DMSO alone or the candidate PRs compounds (10 µM) to that of WT animals in DMSO. 17-AAG (50 µM) was used as positive control. Standard error of the mean is shown. (t-test ***p-value<0.001). (d) The PRs up-regulate mRNA expression of cytosolic chaperones (HSP-70 family members and small Hsps) at the concentrations needed to suppress aggregation and toxicity. Real-time qPCR was performed on samples extracted from animals treated with either DMSO, 17-AAG (50 µM), or PRs (10 µM). Standard deviation is shown.

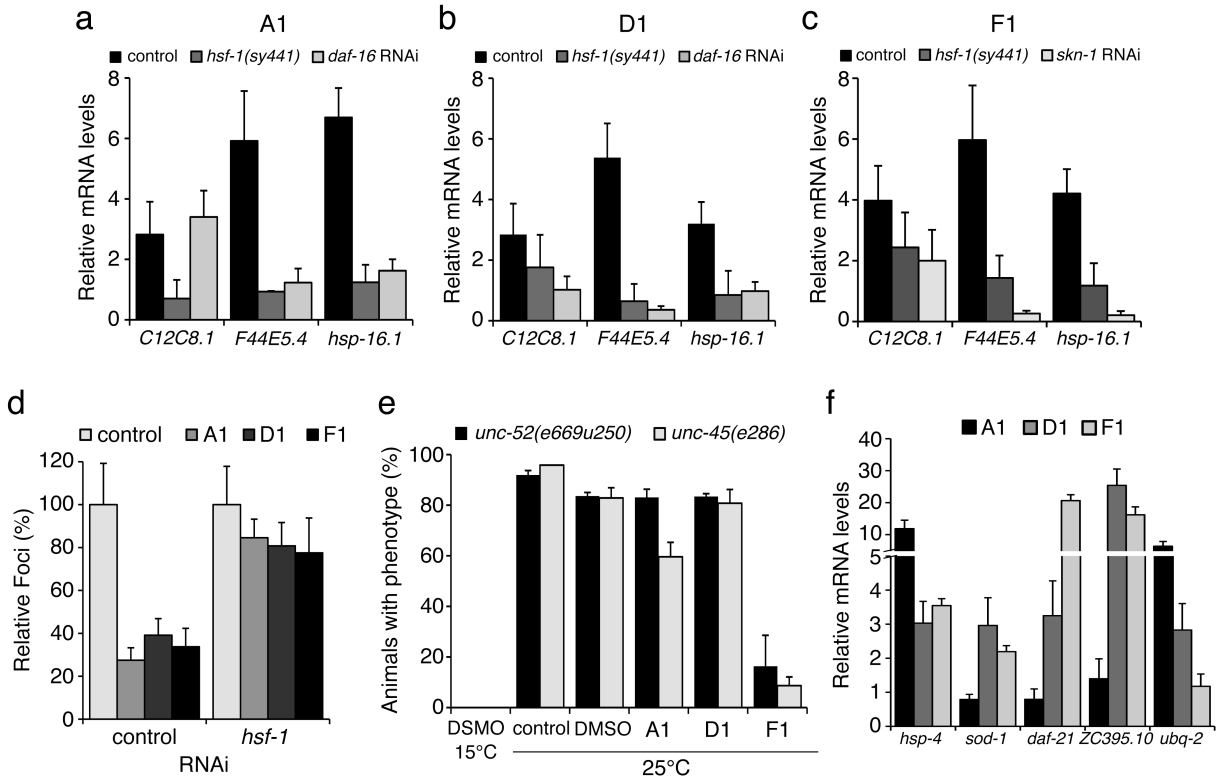

Figure 6. Chaperone expression and reduction in polyQ aggregation in *C. elegans* is HSF-1-dependent. (a-c) For each of the PRs, chaperone up-regulation is HSF-1 dependent. Wild type (control) and HSF-1 mutant (*hsf-1(sy441)*) animals were treated with each of the PRs or the positive control 17-AAG, and real-time qPCR was performed to show that both HSP-70 (*C12C8.1, F44E5.4*) and small Hsps (*hsp-16.1*) induction does not occur in the *hsf-1* mutant background. For compounds A1 and D1, DAF-16 also contributes to chaperone up-regulation, as SKN-1 does for F1. Standard deviation is shown. (d) Suppression of Q35 aggregation by the PRs (shown as % of fluorescent foci) is HSF-1 dependent and is not observed when *hsf-1* is down regulated by RNAi. (e) Animals carrying temperature sensitive mutations in muscle proteins UNC-52 (perlecan, stiff paralysis) and UNC-45 (myosin assembly, egg laying defect) were incubated with the PRs. At the restrictive temperature of 25°C, F1 suppressed the muscle dysfunction phenotypes, indicating improved folding of UNC-52 and UNC-45. (f) Stress related genes up-regulated by each of the PRs relative to control (DMSO): *hsp-4* (ER HSP-70), *sod-1* (oxidative stress), *daf-21* and *ZC395.10* (HSP-90 and co-chaperone) and *ubq-2* (ubiquitin). Standard deviation is shown.

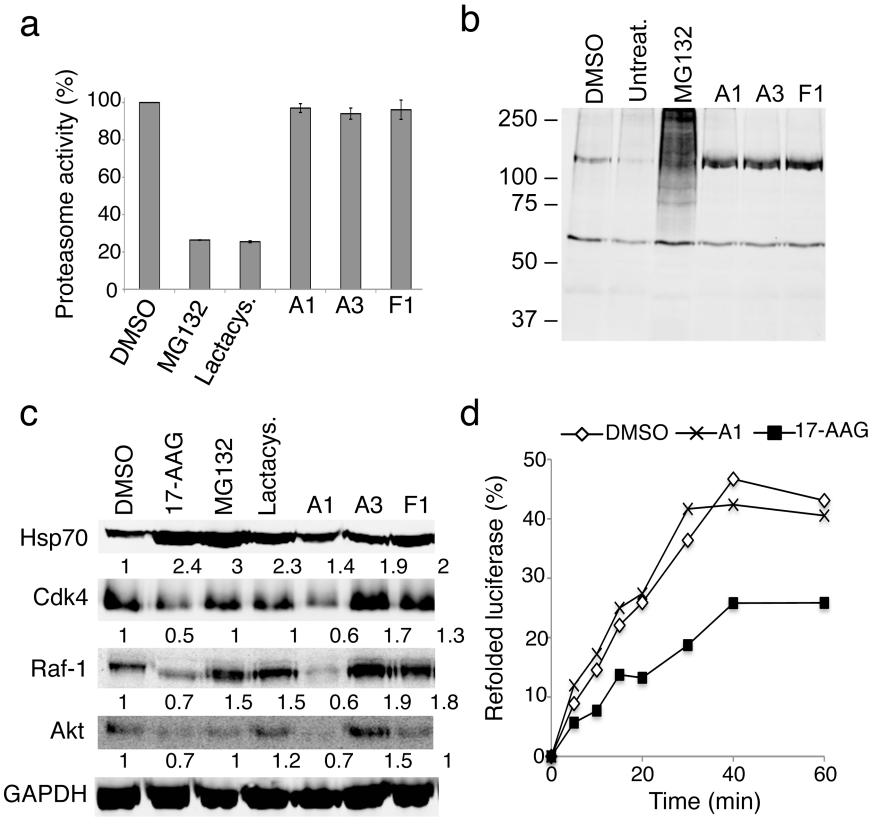

Figure 7. The PRs are not proteasome or Hsp90 inhibitors. (a) HeLa cells were incubated with either DMSO, MG132 (10 μM), lactacystin (lactacys., 6 μM) and the PRs A1, A3 and F1 (10 μM) for 6 h. Proteasome-associated chymotrypsin activity was assessed using the fluorogenic substrate Suc-Leu-Leu-Val-Tyr-7-amido-4-methylcoumarin (suc-LLVY-AMC) as described in Materials and Methods. (b) HeLa cells were either left untreated or treated with DMSO, the proteasome inhibitor MG132 (10 μM), or the PRs A1, A3 and F1 (10 μM) for 16 h. Whole cell extracts of HeLa cells were separated by SDS-PAGE, transferred to membranes, stained with Ponceau S to visualize total protein and probed using a rabbit polyclonal antibody to detect ubiquitin. (c) HeLa cells were treated with either DMSO, 17-AAG (2 μM), MG132 (10 μM), lactacystin (lactacys., 6 μM) or the PRs A1, A3 and F1 (10 μM) for 24 hr. Protein levels of various Hsp90 client proteins (Cdk-4, Raf-1 and Akt) in equal amounts of whole-cell lysates were assessed by western blot analysis. GAPDH was used as loading control. Densitometric measurements of Hsp90 client protein levels normalized to GAPDH in relation to control DMSO-treated cells were performed using ImageJ software. (d) Refolding of chemically-denatured firefly luciferase was assessed in RRL containing 2 mM ATP in the presence of either DMSO (◊), 17-AAG (2 μM, ■) or the PR A1 (10 μM, ×). Luciferase activities are expressed as percent of the native enzyme control. The result shown is representative of three experiments.

Table 1. Chemical structure of the selected small molecules PRs

Cluster A	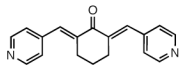 A1	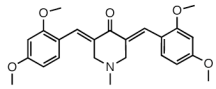 A2	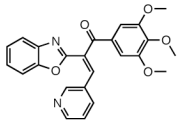 A3
Cluster B	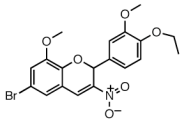 B1	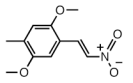 B2	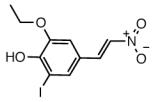 B3
Cluster C	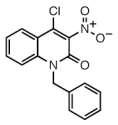 C1	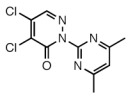 C2	
Cluster D	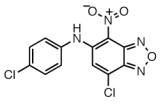 D1		
Cluster E	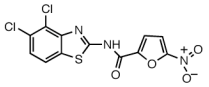 E1		
Cluster F	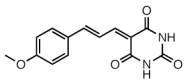 F1	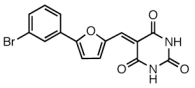 F2	
Cluster G	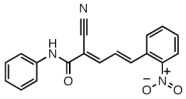 G1	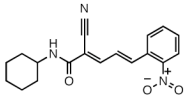 G2	

SUPPLEMENTARY FIGURES

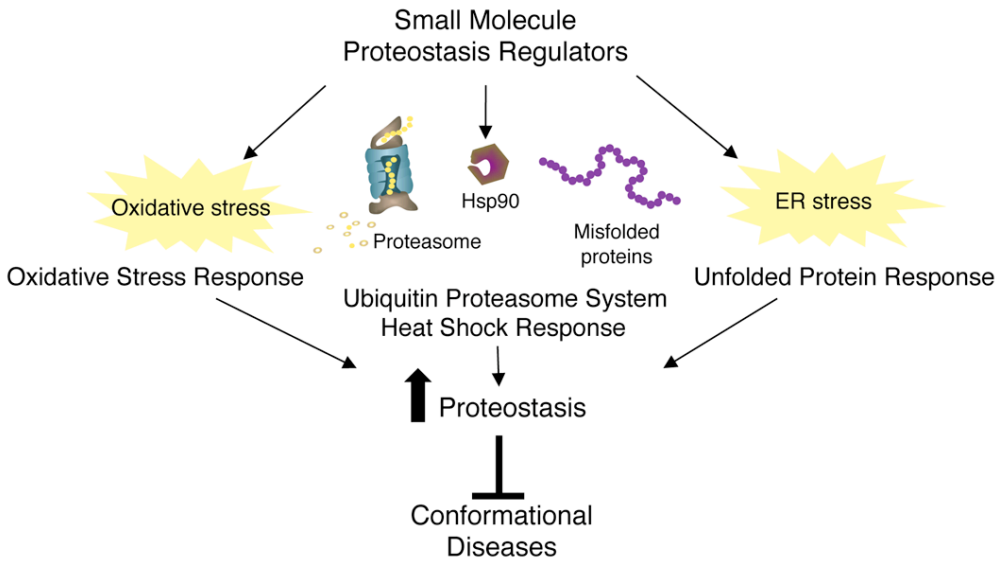

Supplementary Scheme 1. Model Depicting the Proposed Mechanism by which the Small Molecules PRs Ameliorate Conformational Diseases. The small molecules PRs work by activating some of the major PN machineries therefore inducing components of the quality control machinery and other cytoprotective stress response genes.

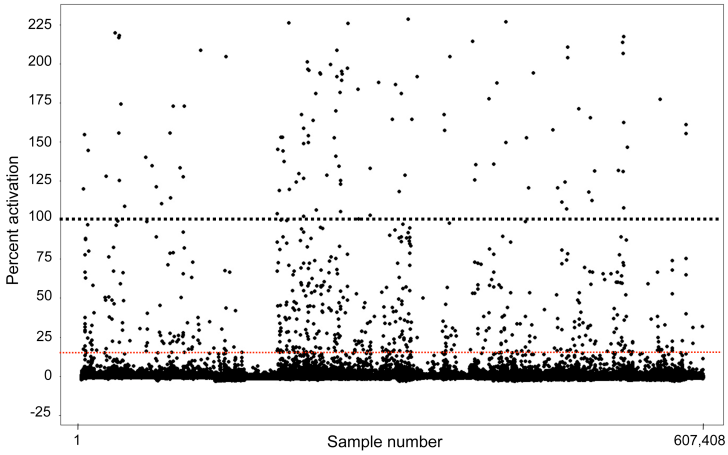

Supplementary Figure 1. Graphical representation of the results of the miniaturized HeLa-luc assay screened against a collection of 607,408 compounds of the Scripps Drug Discovery library. Each of the 476 different 1,536-well plates run for this assay contained both positive (black dotted line) and negative internal controls (not shown). The red dotted line represents the activity cutoff, which was calculated at 15.86% activation. Compounds with percent activation higher than the calculated cutoff were designated as primary hits.

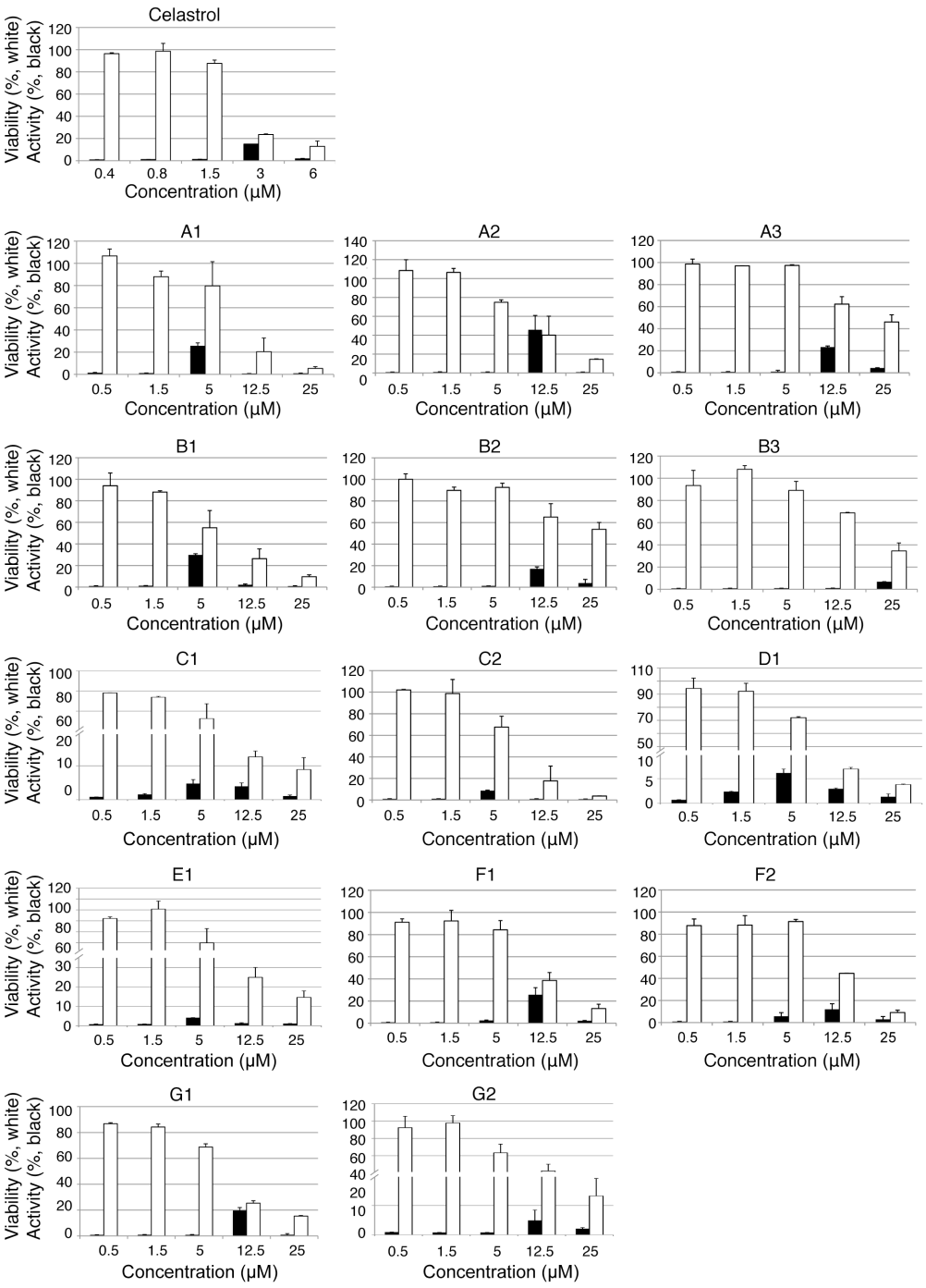

Supplementary Figure 2. Dose-response activity and toxicity profiles for the selected small molecule PRs. HeLa-luc cells were treated with increasing concentrations (0.5, 1.5, 5, 12.5 and 25 μM) of the selected PRs (A1, A2, A3, B1, B2, B3, C1, C2, D1, E1, F1, F2, G1 and G2) for 24 h. Celastrol was used as positive control. Compound activity (black columns) and toxicity (white columns) were measured as described in Supplemental Materials and Methods.

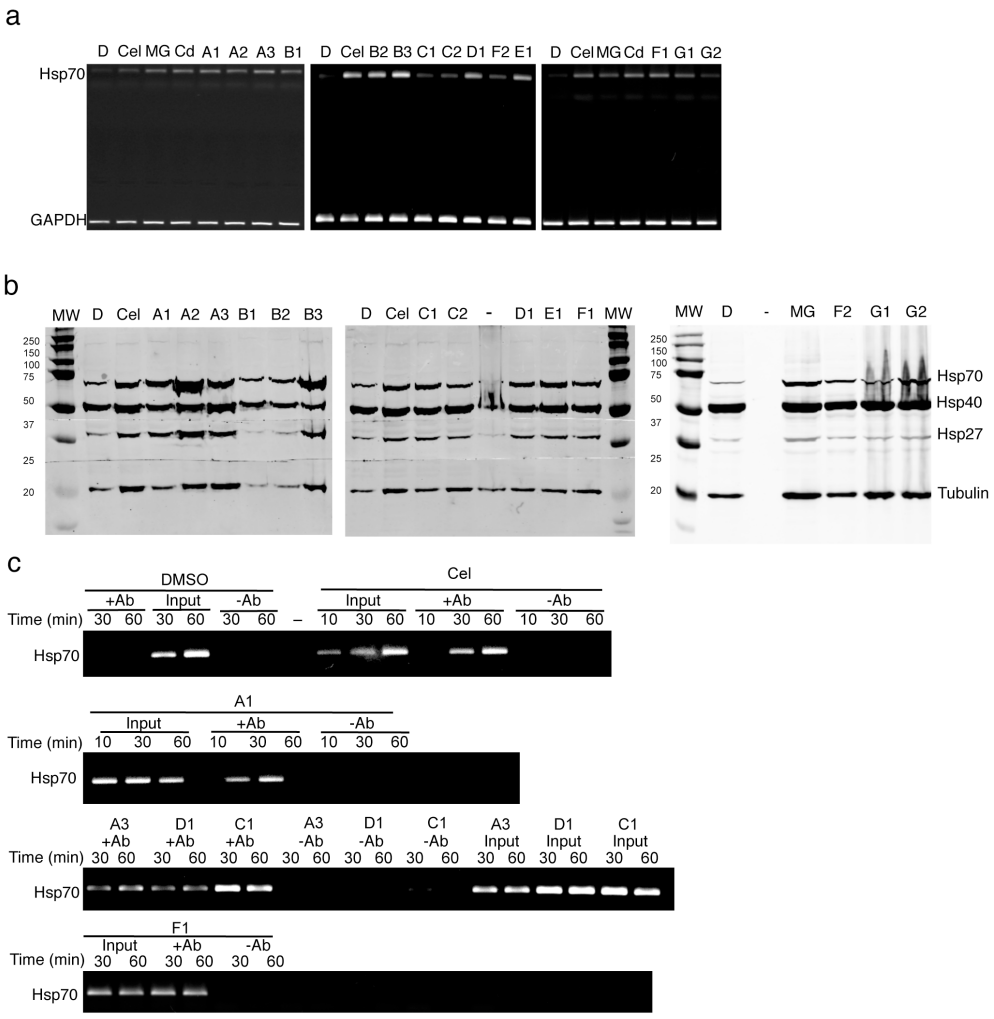

Supplementary Figure 3. Original gel pictures for PCR, western blots and ChIP experiments. (a) RT-PCR results as in Fig. 2a. (b) Western blot analysis of Hsps as in Fig. 2b. (c) ChIP analysis of HSF-1 binding to its promoter as in Fig. 2d.

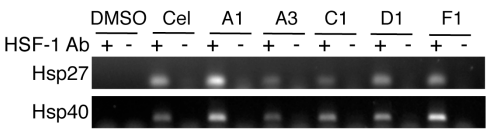

Supplementary Figure 4. Original gel pictures for PCR and western blots experiments. (a) RT-PCR results as in Fig. 3a. (b) Western blot analysis of Hsp90 client protein degradation as in Fig. 7c.

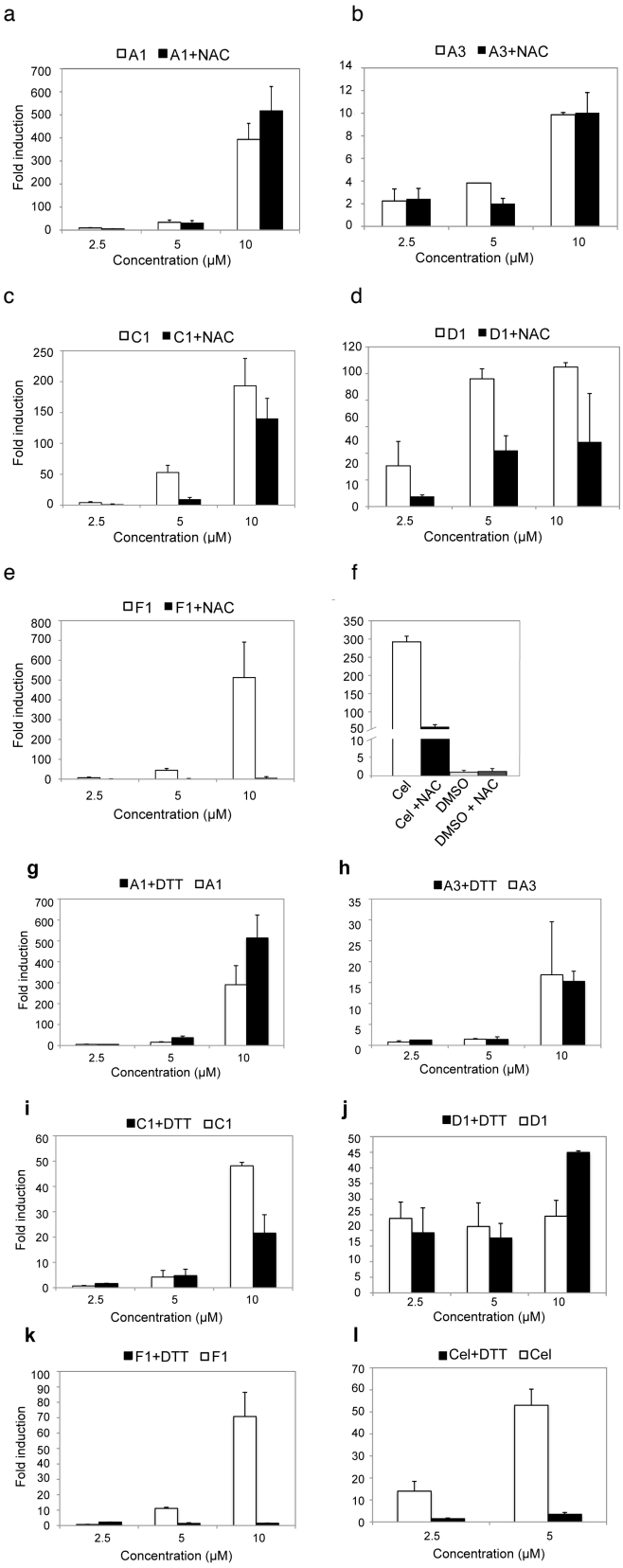

Supplementary Figure 5. The PRs induce HSF-1 binding to the Hsp40 and Hsp27 promoters. Chromatin immunoprecipitation experiments show that both celastrol and selected PRs induce HSF-1 binding to the Hsp40 and Hsp27 promoters *ex vivo*. HeLa cells were treated with DMSO, celastrol (3 μM) and selected PRs (10 μM) for 60 min and then chromatin was cross-linked, harvested, and immunoprecipitated with an antibody specific for HSF-1 (+Ab). The samples were then analyzed by PCR with primers specific for the Hsp40 and Hsp27 promoters. A no antibody control (-Ab) is shown.

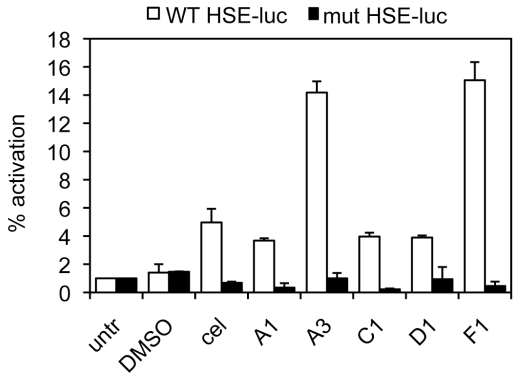

Supplementary Figure 6. Effect of the reducing agents NAC and DTT on the PR activity. HeLa-luc cells were treated with either DMSO, 2.5 μM of celastrol (Cel) or 2.5, 5, and 10 μM selected PRs for 24 h in the absence or presence of either 2 mM NAC (a-f) or 250 μM DTT (g-l). Celastrol and DMSO were used as positive and negative controls, respectively.

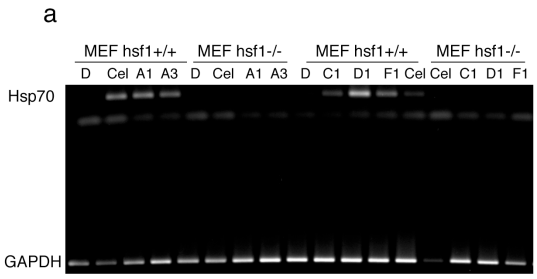

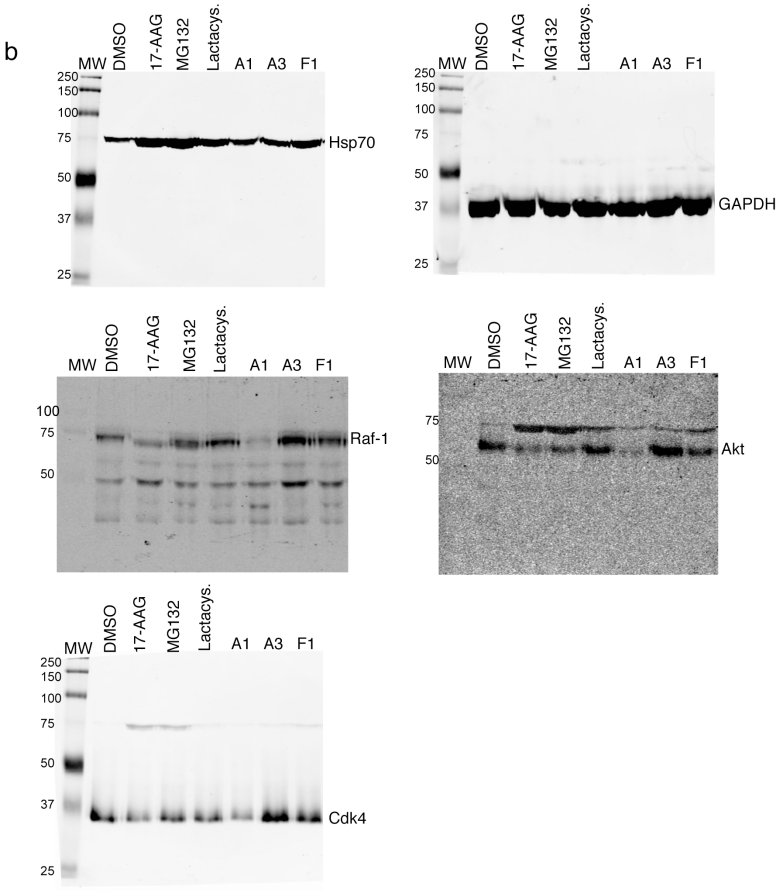

Supplementary Figure 7. The PRs do not activate a reporter gene lacking the correct HSE sequence. HeLa cells were transfected with a luciferase reporter gene fused to either a wild type or mutant HSE promoter. Cells were treated with DMSO (negative control), celastrol (3 μM) or the indicated PRs (10 μM) for 8 h before measuring luminescence. Only cells expressing the wild type promoter were able to induce luciferase expression upon compound treatment.

a

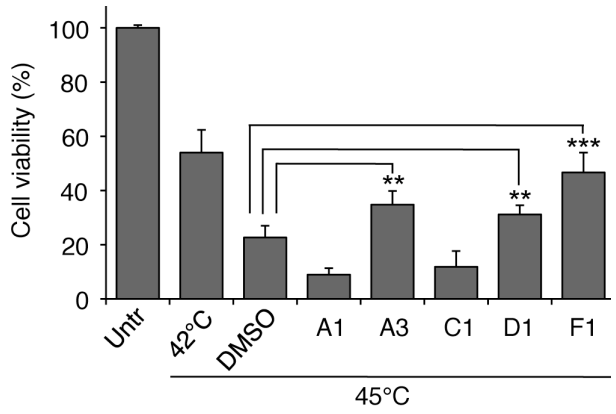

b

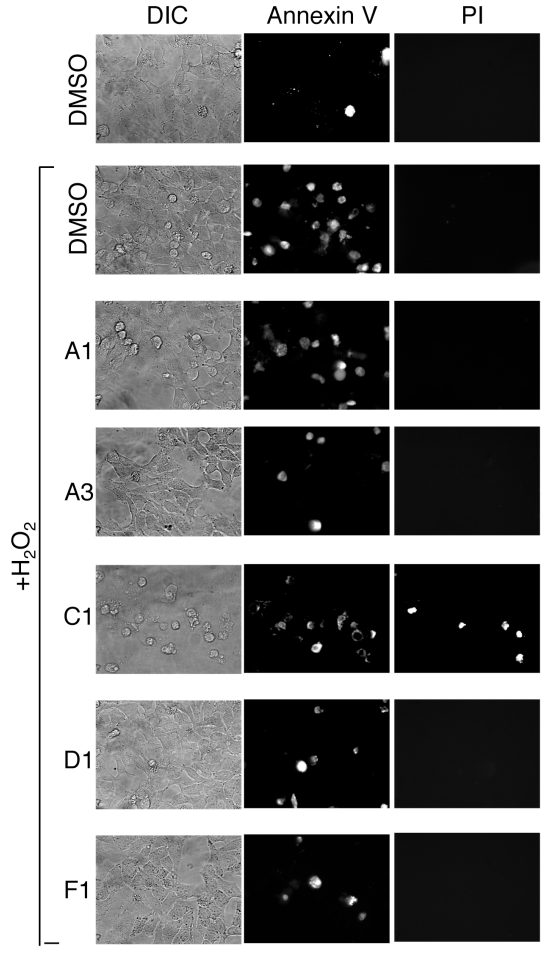

Supplementary Figure 8. The PRs protect cells from stress-induced cell death.
HeLa cells were either left untreated or pretreated with heat shock (42°C) or the indicated PRs for 1 h, washed three times and given fresh medium, and then recovered for 8 h prior to a 35 min 45°C heat shock treatment. 24 h later, the percentage of cell death was determined by Calcein AM assay. The differences in group means were compared by the Student's t test; **p value <0.01; ***p value <0.001.

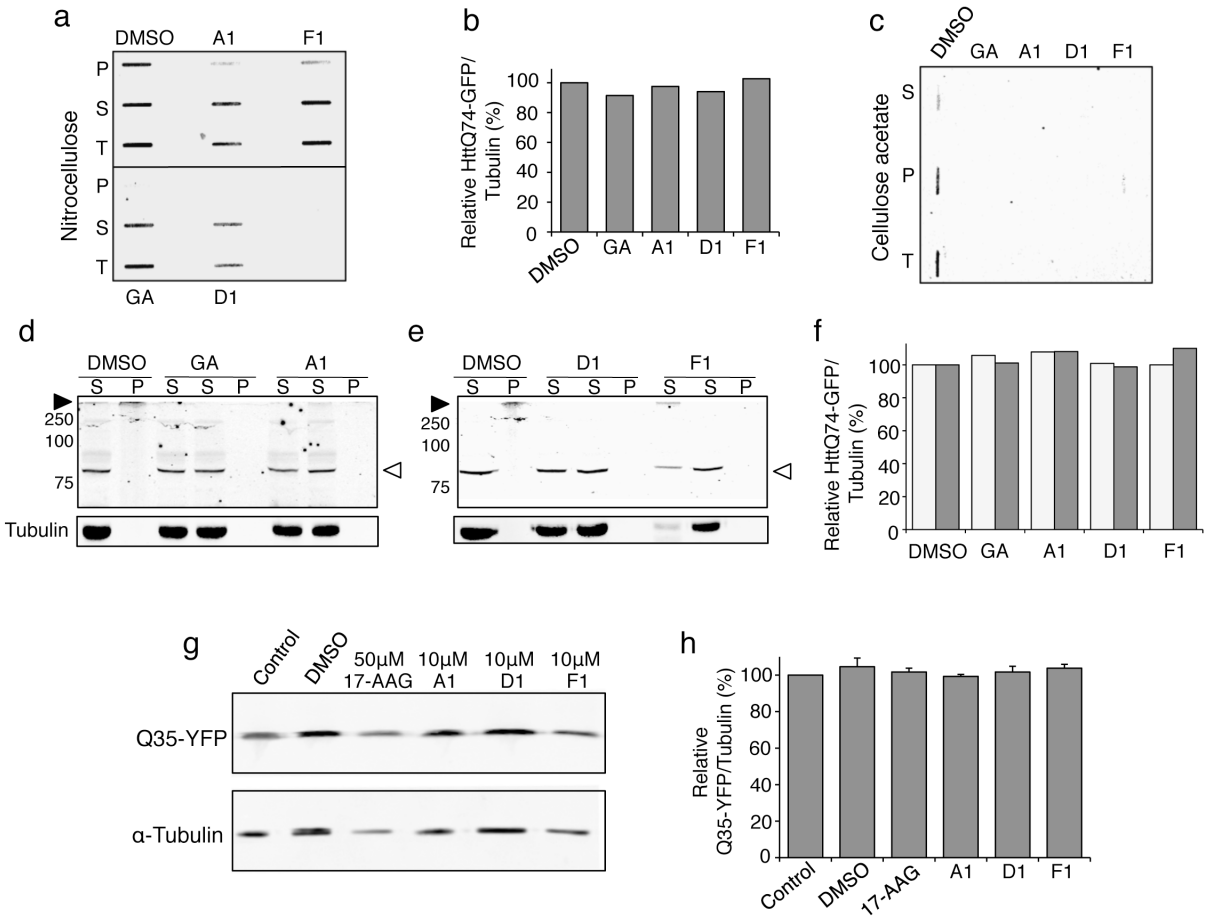

Supplementary Figure 9. The PRs suppress expanded polyQ aggregation without altering the levels of soluble and total protein. (a) Treatment of cells with the indicated PRs for 48 h reduced the insoluble form of the protein compared to the DMSO-treated samples. Nitrocellulose slot-blot was used to detect total (T), soluble (S) and pellet (P) forms of HttQ74-GFP. Equivalent amounts of protein were loaded. (b) Quantification of total HttQ74-GFP protein from (a) with respect to tubulin loading control was done by densiometric analysis. The DMSO-treated samples were arbitrarily set as 100. (c) Insoluble HttQ74-GFP was detected by slot-blot using a cellulose acetate membrane (filter trap assay). (d-e) Soluble (S) and insoluble (P) HttQ74-GFP was detected by western blot. Open and closed arrowheads indicate, respectively soluble and insoluble HttQ74-GFP protein (detected in the stacking gel portion of the western blot). (f) Quantification of soluble HttQ74-GFP protein from (e) with respect to tubulin loading control was done by densiometric analysis. The DMSO-treated samples were arbitrarily set as 100. (g) Western-blot of total polyQ protein from *C. elegans* extracts. (h) Quantification of total polyQ protein from (g) with respect to tubulin loading control was done by densiometric analysis. The control samples were arbitrarily set as 100.

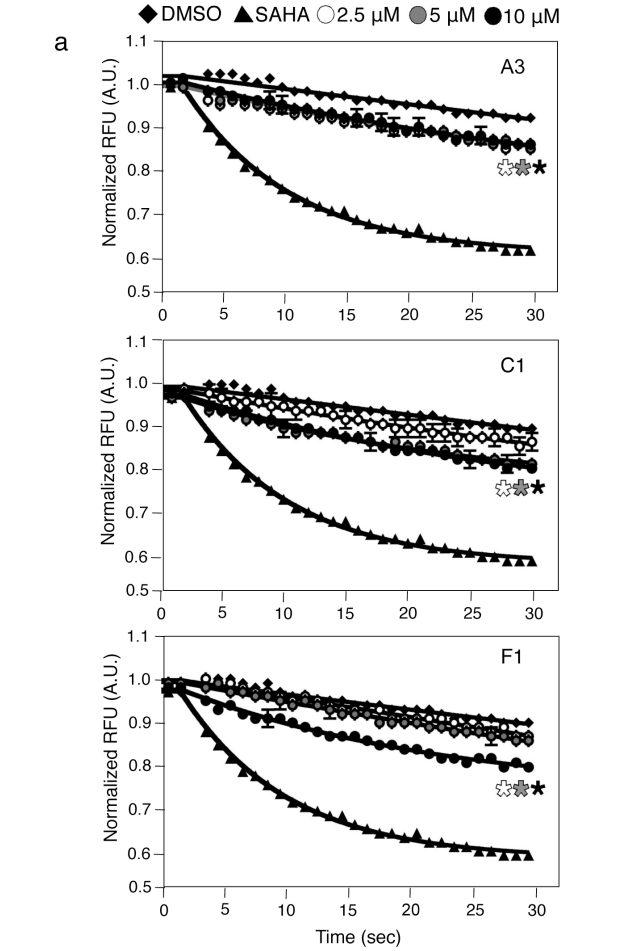

Supplementary Figure 10. Dose-response curve for the PRs A3, C1 and F1 and enzymatic digestion of CFTR Golgi-processed glycoform by Endoglycosidase H. (a) CFBE41o- YFP cells were treated with 0.1% DMSO (diamonds), the positive control 5μM SAHA (triangles) and the indicated PRs at 2.5 (open circles), 5 (grey circles) and 10μM (black circles) for 24 h. Fluorescence quenching is indicative of restored ΔF508- CFTR trafficking (mean ± s.e.m.; n = 3). The open, grey and black asterisks indicate statistically significant differences from DMSO control at the 30s time point. The SAHA treatment yields a significant difference from DMSO (see Figure 5c). (b) Endoglycosidase H resistance assay was used to confirm that band C in the CFTR analysis represents a Golgi modified glycoform. The blot confirms that the ER derived band B glycoform is completely sensitive to EndoH indicated by the appearance of the faster migrating band A, whereas the band C, which is present in all PR treated samples exhibits resistance to endoH.

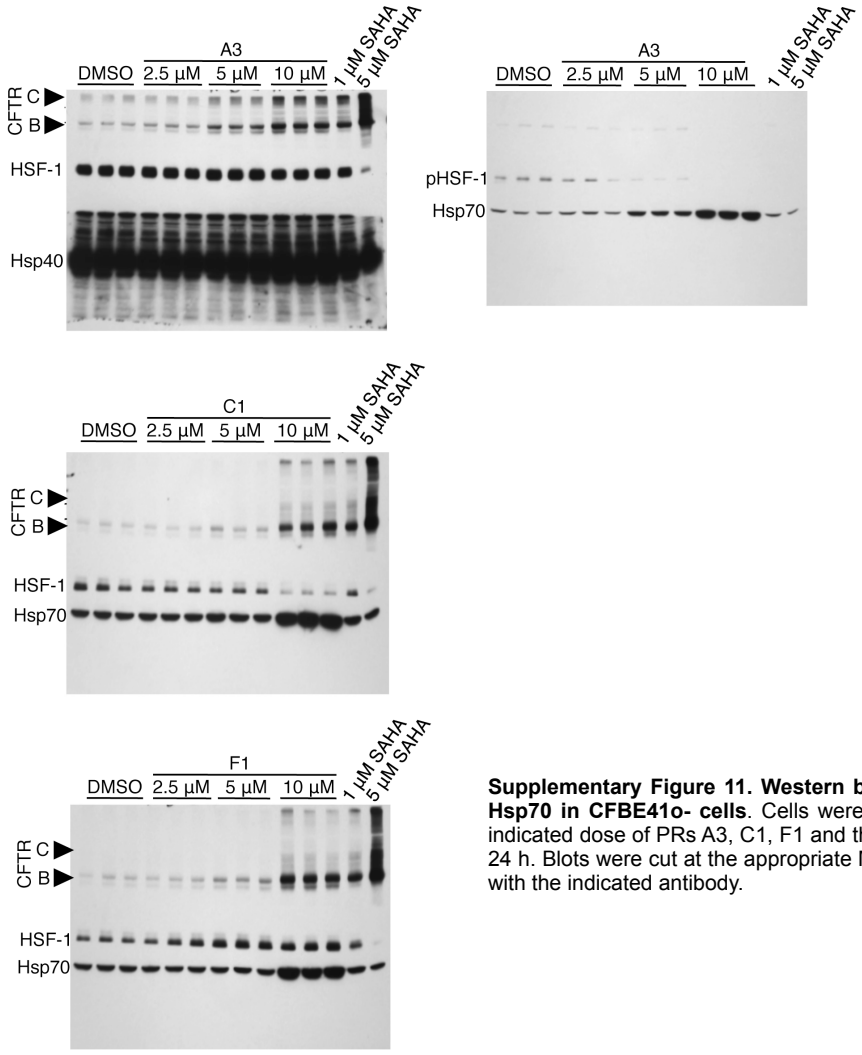

Supplementary Figure 11. Western blot analysis of CFTR and Hsp70 in CFBE41o- cells. Cells were treated with DMSO or the indicated dose of PRs A3, C1, F1 and the positive control SAHA for 24 h. Blots were cut at the appropriate MW and immunoblotted (IB) with the indicated antibody.

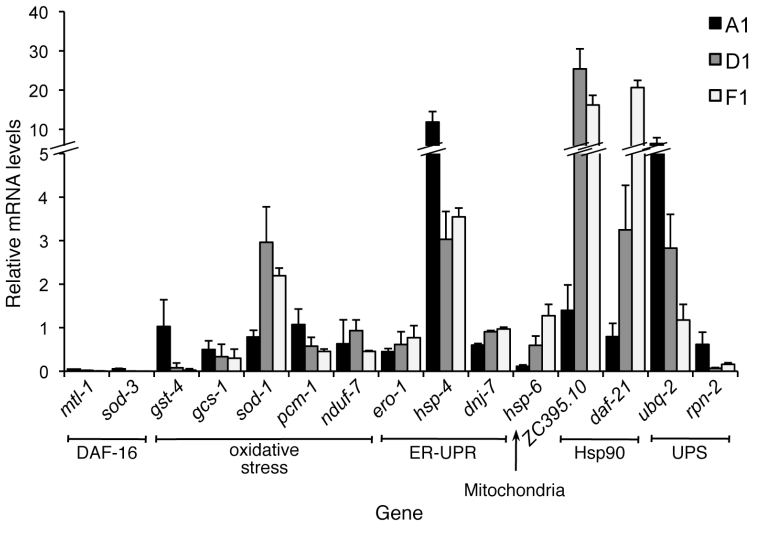

Supplementary Figure 12. Real-time qPCR measurement of stress related gene levels upon treatment with the PRs A1, D1 and F1. Data are relative to the negative control (DMSO). The genes tested are grouped according to stress response or pathway (indicated at the bottom of the figure): DAF-16/FOXO pathway, oxidative stress, ER and mitochondrial UPR, Hsp90 (*daf-21)* chaperone and co-chaperone (*ZC395.10*), and UPS components. Standard deviation in shown.

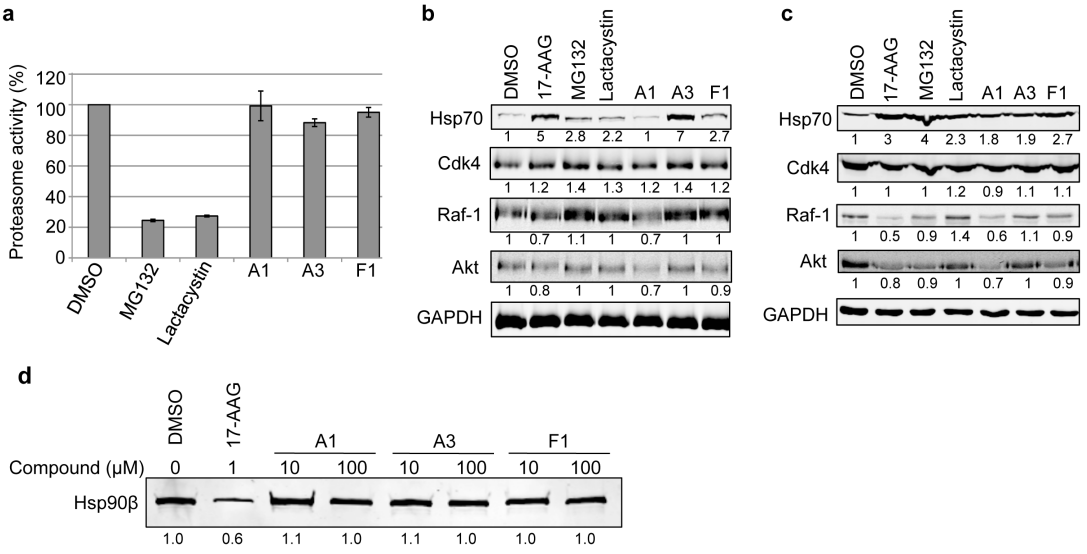

Supplementary Figure 13. (a) HeLa cells were incubated with either DMSO, MG132 (10 μM), lactacystin (6 μM) and the PRs A1, A3 and F1 (10 μM) for 3 h. Proteasome- associated chymotrypsin activity was assessed using the fluorogenic substrate Suc-Leu-Leu-Val-Tyr-7-amido-4-methylcoumarin (suc-LLVY-AMC) as described in Materials and Methods. (b-c) HeLa cells were treated with DMSO, 17-AAG (2 μM), MG132 (10 μM), lactacystin (6 μM) or the PRs A1, A3 and F1 (10 μM) for 6 (b) and 16 h (c). Protein levels of various Hsp90 client proteins (Cdk-4, Raf-1 and Akt) in equal amounts of whole-cell lysates were assessed by western blot analysis. GAPDH was used as loading control. (d) Purified Hsp90β (2 μg) was incubated with either DMSO, 17-AAG (1 μM) or the indicated PRs (10 and 100 μM) for 30 min at 4°C before addition of 1 μM geldanamycin-biotin for 1 h at 4°C. Hsp90 bound to geldanamycin-biotin was captured with neutravidin-agarose beads and analyzed by immunoblotting.

Supplementary Table 1. Assay protocol in 384 and 1,536-well plate formats.

	Order	Step	Condition	Comments
384-well plate format (Southern Res. Inst.)	1	Cell dispensing	20 μL/well	1,875 cells/well
	2	Primary incubation time	16-18 h	37°C, 5%CO_2
	3	Compound addition	50 nL/well in 5 μL medium	Test concentration: 2 μg/mL; final DMSO concentration: 0.2%
	4	Secondary incubation time	24 h	37°C, 5%CO_2
	5	Luciferase detection reagent addition	25 μL/well	
	6	Tertiary incubation	5 min	Room temperature
1,536-well plate format (Scripps)	1	Cell dispensing	5 μL/well	3,750 cells/well
	2	Primary incubation time	4 h	37°C, 5%CO_2
	3	Compound addition	50 nL/well	Test concentration: 10 μM; final DMSO concentration: 1%
	4	Secondary incubation time	16 h	37°C, 5%CO_2
	5	Luciferase detection reagent addition	5 μL/well	
	6	Tertiary incubation	15 min	Room temperature

Supplementary Table 2. Summary of the high-throughput screen results.

Screen details	Scripps Drug Discovery Library	MLPCN Library	NINDS Library
Number of compounds	607,408	196,179	100,000
Compound concentration	10 μM	10 μM	2 μg/ml
Positive control	MG132 (30 μM)	MG132 (30 μM)	$CdCl_2$ (50 μM)
Plate format	1,536 wells	1,536 wells	384 wells
Z' value	0.63	0.62	0.68
Primary hit cut-off (%)	15.86	15.86	5
Primary hit rate (%)	0.11	0.04	0.04
Number of primary hits	677	82	37
Number of confirmed hits	218	12	33

Supplementary Table 3. The PRs contain potentially reactive groups (indicated in red).

Compound structure	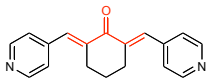	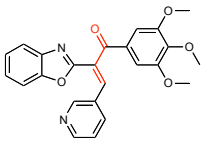	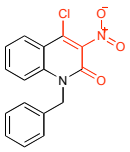	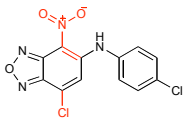	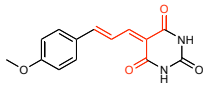
Compound ID	A1	A3	C1	D1	F1

SUPPLEMENTARY METHODS

Compounds. All the compounds were obtained from the commercial vendors indicated below and were used without further purification. A1: (2E,6E)-2,6-Bis(4- pyridinylmethylene)-Cyclohexanone, CAS 871361-88-5, ChemDiv: C151-0032; A2: (3E,5E)-3,5-Bis[(2,4-dimethoxyphenyl)methylene]-1-methyl-4-Piperidinone, CAS 1207456-48-1, Enamine T0514-8318; A3: 2-(2-Benzoxazolyl)-3-(3-pyridinyl)-1-(3,4,5- trimethoxyphenyl)-2-Propen-1-one, CAS 496011-51-9, ChemBridge 7355596; B1: 6- Bromo-2-(4-ethoxy-3-methoxyphenyl)-8-methoxy-3-nitro-2H-1-Benzopyran, CAS 448189-54-6, ChemBridge, 8880788; B2: 1,4-Dimethoxy-2-methyl-5-(2-nitroethenyl)- Benzene, CAS 25505-64-0, ChemBridge 6561455; B3: 2-Ethoxy-6-iodo-4-(2- nitroethenyl)-Phenol, CAS 662160-43-2, ChemBridge 7251856; C1: 4-Chloro-3-nitro-1- (phenylmethyl)-2(1H)-Quinolinone, CAS 385387-83-7, ChemBridge 6935964; C2: 4,5- Dichloro-2-(4,6-dimethyl-2-pyrimidinyl)-3(2H)-Pyridazinone, CAS 78403-59-5, T0507- 9111; D1: 7-Chloro-N-(4-chlorophenyl)-4-nitro-2,1,3-Benzoxadiazol-5-amine, CAS 313966-69-7, ChemBridge 5241454; E1: N-(4,5-Dichloro-2-benzothiazolyl)-5-nitro-2- Furan-carboxamide, CAS 797776-58-0, Asinex BAS 08207501; F1: 5-[3-(4-Methoxyphenyl)-2-propen-1-ylidene]-2,4,6(1H,3H,5H)-Pyrimidinetrione, CAS 100872-83- 1, ChemBridge 5772104; F2: 5-[[5-(3-Bromophenyl)-2-furanyl]methylene]- 2,4,6(1H,3H,5H)-Pyrimidinetrione, CAS 331464-02-9, Asinex BAS 00336306; G1: 2- Cyano-5-(2-nitrophenyl)-N-phenyl-2,4-Pentadienamide, CAS 733044-10-5, Enamine T0516-4089; G2: 2-Cyano-N-cyclohexyl-5-(2-nitrophenyl)-2,4-Pentadienamide, CAS 737819-53-3, Enamine T0516-8259.

Cell Cultures. Mammalian cell lines used in this study were HeLa cells, a stable HeLa cell line containing a heat shock-inducible reporter construct that consist of the Hsp70.1 promoter sequence fused to a luciferase reporter gene (HeLa-luc)[1], WT and hsf-1-/- MEF cells[2], inducible PC12 cells expressing HttQ74-GFP[3] and human bronchial epithelial cells stably expressing the ΔF508-CFTR as well as the H148Q-YFP mutant[4] (CFBE41o- -YFP). HeLa and HeLa-luc cells were maintained in Dulbecco's modified Eagle's medium (DMEM, Invitrogen, Carlsbad, CA) with phenol red buffered with HEPES and supplemented with 10% v/v fetal bovine serum (FBS), 1% L-glutamine, and 100 U/ml penicillin/streptomycin. HeLa-luc cells were also supplemented with 100 µg/ml of G418. WT and hsf-1-/- MEFs were maintained on DMEM supplemented with 10% FBS, 0.1 mM nonessential amino acids, 100 U/ml penicillin/streptomycin, and 55 µM 2-mercaptoethanol. HttQ74-GFP PC12 cells were previously described[3] and were maintained on DMEM supplemented with 5% v/v Tet-approved FBS, 10% v/v horse serum, 100 µg/ml G418, 75 µg/ml hygromycin B, and 100 U/ml penicillin/streptomycin. Cells co-expressing ΔF508-CFTR and CFBE41o- -YFP were grown in α-MEM containing 100 U/ml penicillin/streptomycin, 10% v/v FBS, 2 mM L-glutamine, 2 µg/ml puromycin and 0.75 mg/ml G418. Cells were maintained at 37°C with 5% CO_2 atmosphere until they were ready for passage or harvest.

Cell-based High-throughput Assays. The automated primary screens were performed according to the following steps. For the 100,000 compound library screened at the Southern Research Institute, the assay was optimized for a 384-well plate format and resulted in a Z'-value >0.6 using $CdCl_2$ as positive control (50 µM). HeLa-luc cells were dispensed into white tissue culture treated 384-well plates at a density of 1,875 cells/well in 20 µL assay medium using a WellMate with a small bore cassette head (Matrix Technologies Corp., Thermo Fisher Scientific, Hudson, NH). The assay plates were incubated for 16-18 hours at 37°C and 5% CO_2 before compound addition. Compound addition was performed in a two step process with the positive control added to control wells and an equal volume of medium added to remaining wells with a Biomek FX liquid handling system (Beckman Coulter Inc., Brea, CA). The compounds were then delivered without dilution in 50 nL with 5 µL medium at a concentration of 2 µg/mL using an Echo 550 liquid handler (Labcyte Inc., Sunnyvale, CA). After 24 h incubation with compounds, the assay plates were equilibrated to room temperature before endpoint addition. 25 µl of Bright-Glo Luciferase Assay System (Promega, Madison, WI) was added to the plates using a Multidrop dispenser (Titertek Instruments Inc., Huntsville, AL) and luminescence signal was read using an Envision multi-label plate reader (Perkin Elmer, Waltham, MA). The assay was run in three 107-plate batches run in serial. Every step of the assay process, along with every reagent and instrument used throughout the assay process was tracked using a Uniflow Laboratory Information Management System to ensure consistency between screening runs and to facilitate any trouble shooting that may arise along the way. Following each screening batch, data was imported into IDBS ActivityBase data management system. Because of the low hit rate and the relatively low response elicited by the library compounds when compared to the response to $CdCl_2$, the hit criteria was defined as >5% signal induction of the positive control. Using this criterion, 37 compounds were identified as hits (0.04% hit rate). Dose-response experiments were then performed in triplicate using a 1:2 serial dilution of the hit compounds in DMSO starting from 20 µg/ml. Because of the narrow active concentration range of compounds tested in dose response (data not shown), the list of compounds to be tested in dose response was expanded to 169 based on structural relationships to the hits identified in the primary screen. The majority of the compounds screened in dose response demonstrated very narrow concentration ranges for which they were active. Therefore the criterion for confirmed activity was defined as a compound demonstrating maximum % activation >10% of $CdCl_2$. Using this criterion, 56 compounds (33%) demonstrated confirmed activity in the dose response screen. Of the 56 confirmed active compounds, 33 were hits selected from the primary screen, resulting in a hit confirmation rate of 89%. For the 607,408 Scripps Drug Discovery unique compound library and for the 196,179 compound MLPCN library screened at the SRIMSC, the assay was optimized for a 1,536-well plate format and resulted in a Z' coefficient >0.6 using MG132

(30 μM) as positive control. A detailed description of the protocols used is available on the PubChem website (http://pubchem.ncbi.nlm.nih.gov/; PubChem AIDs 1203 and 1252).

Cytotoxicity Assays. For the hit compounds identified at the Southern Research Institute, the following procedure was used. HeLa cells were plated at a density of 10,000 cells per well in black 96-well plates in 100 μl of DMEM supplemented with 10% FBS and 1% Pen/Strep/Neo. Plates were incubated for 16 hours at 37°C, 5% CO_2 and 95% relative humidity before compound addition. 1 μL of hit compounds in DMSO or DMSO alone were added to the sample or control wells, respectively. Plates were then placed back in the incubator for 24 hours. After incubation, cells were washed 2x with 200 μl of PBS and 200 μl of a solution of 1 μg/ml of calcein AM (Invitrogen, Carlsbad, CA) was added to each well. Cells were then incubated for 45 min at 37°C, 5% CO_2 before fluorescence measurement using an Analyst GT multimode reader (Molecular Devices, Sunnyvale, CA). Percent cytotoxicity was expressed relative to wells containing cells treated with DMSO only (100%). A detailed description of the protocol used at the SRIMSC is available at the PubChem website (http://pubchem.ncbi.nlm.nih.gov/; PubChem AIDs 1259).

Gel Mobility Shift Analysis (EMSA). Electrophoretic mobility shift analysis was performed using a 32P-labeled probe containing the proximal heat shock element from the human Hsp70.1 gene promoter. The whole cell extract-labeled probe mixtures were incubated room temperature for 20 minutes and analyzed by native electrophoresis on 4% polyacrylamide gels. The intensities of the shifted bands were quantified on a PhosphorImager (Molecular Dynamics, Sunnyvale, CA). For competition experiments, a 200-fold molar excess of the same unlabeled double stranded oligonucleotide was used. Supershifts were performed by incubating 1 μl of polyclonal antibodies specific for HSF-1[5] with the whole cell extracts for 20 minutes at room temperature prior to the HSF-1-heat shock element binding reaction.

Chromatin Immunoprecipitation Assays (ChIP). Nuclear cell extracts obtained from about 3 × 107 HeLa cells were used for each tested condition, cross-linked for 10 minutes at room temperature with a 37% formaldehyde solution and sonicated for 30 sec at 4°C. Samples were immunoprecipitated with 10 μl of a rabbit polyclonal HSF-1 #471 at 4°C overnight. Primers used for the human Hsp70.1, Hsp40, Hsp27 and dihydrofolate reductase promoters were the following:
(forward) 5′-GGCGAAACCCCTGGAATATTCCCGA-3′ and (reverse) 5′- AGCCTTGGGACAACGGGAG-3’; (forward) 5′-GTGGTACCCTCCTCCGACCTGTG-3’ and (reverse) 5’-TACTCGAGACCCCCTCCTGCG-3’; (forward) 5′-CTATCTCACACGCGTGTGGTTCC-3′ and (reverse) 5′- TTAAGGAGGACAGAGCCAGACAG-3’.
Primers used for the human dihydrofolate reductase promoter were:
5′-GGCCTCGCCTGCACAAATAGGG-3′ (forward) and 5′- GGGCAGAAATCAGCAACGGGC-3′ (reverse).

Multiplex Gene Expression Analysis. WT and hsf-1-/- MEFs were seeded at a density of 12,000 cells/well in 96-well plates with an overnight incubation at 37°C, 5% CO_2. Cells were treated with serially diluted compounds in a 7-point dose dependent manner. Cell lysis with 50% [v/v] Panomics Lysis Mixture (Lysis Mixture + 10 μl/ml Proteinase K) was performed 6 hours post-compound treatment. Lysed cells were heated at 50°C to ensure appropriate lysing and the plates were then frozen at -80°C. Cell lysates, thawed at room temperature on the day of the assay, were pooled with mouse 8-gene multiplex probe sets and with 8 different sets of magnetic capture beads (Luminex Technology, Austin, TX) in a 100 μl/well volume. Biomek FX was used at every liquid transfer step to reduce variability by human error. The eight plates containing lysate-probe-bead mixtures were incubated at 54°C ± 1°C on a shaking platform for an overnight incubation in the dark (18-20 hours). The following day the hybridization plates were compressed by transferring the hybridized lysates into a single magnetic capture plate. The plate was kept on a magnet to hold the beads and then washed with Panomics Wash Buffer 2.0 on a BioTek ELx405 select plate washer to remove any unbound sample. This step was followed by serial hybridizations and washings of the bDNA pre-amplifier (1 hour, 50°C), bDNA amplifier (1 hour, 50°C), label probe (1 hour, 50°C), and streptavidin-phycoerythrin (SAPE, 30 minutes, room temperature)[6]. The plate was then washed with SAPE wash buffer to remove unbound SAPE and each well was analyzed with the Luminex FlexMap3D (Luminex, Austin, TX). SAPE fluorescence measured from each bead was proportional to the number of mRNA transcripts captured by the beads[7]. Fold changes in gene expression were obtained for each gene per well by normalizing the raw data first to the DMSO control and then to a housekeeping gene (TBP).

HeLa cell transfection with wild type and mutant HSE-luc. HeLa cells were plated in a white 96-well plate and transfected with a wild type and mutant HSE-luc plasmid using FuGENE HD transfection reagent (Roche, Indianapolis, IN). Cells were treated with PRs A1, A3, C1, D1, and F1 (10 μM) and then luciferase activity was measured 24 h later.

Cytoprotection and Apoptosis Analysis. HeLa cells were plated in black 96-well plates at a density of 10,000 cells/well. The cells were treated with DMSO or the PRs A1, A3, C1, D1 and F1 (10 μM) for 1 h and then recovered for 8 h before a 45°C heat shock treatment for 35 min. As a control, the cells were pretreated with a 42°C heat shock for 1 h. Cell death was assessed 24 h later by using the Calcein AM dye. Assessment of apoptotic and necrotic events was performed using the Annexin V- FLUOS/PI Staining Kit (Roche, Indianapolis, IN) accordingly to the manufacturer’s protocol. In brief, cells were washed twice with ice-cold PBS, resuspended in binding buffer, and incubated for 15 min in the dark at room temperature with Annexin V-fluorescein and PI labeling solution. Fluorescence images were

acquired using an Axiovert S100 TV fluorescence microscope (Carl Zeiss, Germany) equipped with a 40x objective and a CoolSNAP HQ camera system (Photometrics, Tucson, AZ). All image processing and analysis was performed using functions in the MetaMorph software (Molecular Devices, Inc., Sunnyvale, CA). For quantification of Annexin V-stained cells, approximately 200 cells were counted for each treatment.

Filter Trap Assay and Immunoblotting. The filter trap assay was performed accordingly to Wanker et al.[8]. In brief, cells were lysed on ice for 30 min in filter trap lysis buffer [50 mM Tris-HCl, pH 8.8; 100 mM NaCl; 5 mM MgCl2; 0.5% (v/v) Nonidet P-40; and 1 mM EDTA] in presence of protease inhibitors. Insoluble material was pelleted by centrifugation and resuspended in 100 µl of 20 mM Tris-HCl, 15 mM MgCl2, 0.5 mg/ml DNase I for 2 h at 37°C. Protein concentration of total, soluble and insoluble fractions was determined by the protein dotMetric assay (G-Biosciences, St. Louis, MO). 20 µg of soluble and insoluble material was diluted into 2% SDS, boiled and added to a 48-well blot apparatus (Bio-Rad Laboratories, Hercules, CA) containing either a nitrocellulose or cellulose acetate membrane. For western blotting, protein samples were electrophoresed by SDS-PAGE and transferred to PVDF membranes using a semi-dry apparatus. Membranes were then blocked in 5% milk for 1 h and then probed with the following primary antibodies: a goat monoclonal anti-GFP IR dye 800 (Rockland Immunochemicals, Gilbertsville, PA) at 1:4,000 and a mouse monoclonal anti-tubulin at 1:5,000 (Sigma, St. Louis, MO). The secondary antibody was an Alexa Fluor 680 goat anti mouse IgG diluted 1:5,000 (Invitrogen, Carlsbad, CA). Western analysis was performed with the Odyssey system (Li-COR, Lincoln, NE).

ΔF508-CFTR YFP Quenching Assay. Human bronchial epithelial cells (CFBE41o-) stably expressing ΔF508-CFTR as well as H148Q/I152L-YFP (CFBE41o- -YFP) were added to a 96-well black walled plate and grown to confluency in growth media (α-MEM containing 100 U/ml penicillin, 100 U/ml streptomycin, 10% v/v FBS, 2mM L-glutamine, 2 µg/ml puromycin and 0.75 µg/ml G418). Cells were treated with the indicated concentration of compounds in complete growth media and incubated at 37°C, 5% CO_2 for 24 h. Cells were subsequently washed three times with 200 µl of PBS pH 7.4 (137 mM NaCl, 2.7 mM KCl, 0.7 mM $CaCl_2$, 1.1 mM $MgCl_2$, 1.5 mM KH_2PO_4, 8.1 mM Na_2HPO_4) and equilibrated in 40 µl of PBS pH 7.4 and maintained at 37°C throughout. Cells were stimulated with a final concentration of 10 µM forskolin (fsk) and 50 µM genistein (gen) for 15 min prior to addition of PBS + NaI (replacement of NaCl with 137 mM NaI). Fluorescence was monitored every second for a total of 30 seconds (3 seconds prior to addition of NaI and 27 seconds after addition of NaI). Data were normalized to the initial fluorescence to account for variations in the overall starting fluorescence. To ensure that the observed H148Q/I152L-YFP fluorescence quenching was the result of ΔF508-CFTR activation and not the action of additional halide channels, the CFTR specific inhibitor (CFInh-172) was used.

ΔF508-CFTR Transport Assay. CFBE41o- cells stably expressing ΔF508-CFTR were plated in 12-well dishes and grown to confluence in growth media (α-MEM containing 100 U/ml penicillin, 100 U/ml streptomycin, 10% v/v FBS, 2 mM L-glutamine and 2 µg/ml puromycin). Cells were treated with the indicated concentration of compound in complete growth media and maintained at 37°C, 5% CO_2 for 24 hrs. Cells were lysed on ice in 50 µl of TBS (50 mM Tris-HCl pH 7.4, 150 mM NaCl) + 1% (v/v) Triton X-100 containing 2 mg/ml of complete protease inhibitor cocktail (Roche, Switzerland) for 30 min. The lysates were harvested and cleared at 20,000xg for 20 min (4°C) and the supernatant was collected for analysis. Equal amount of total protein (15 µg) was separated by SDS-PAGE (8% gel) and transferred to nitrocellulose. The blot was probed overnight at 4oC for CFTR (3G11 rat monoclonal antibody at 1:500 dilution) and indicated chaperone proteins.

***C. elegans* Strains.** Worms were maintained according to standard methods, at 20°C on nematode growth media (NGM) with OP50 E. coli (Brenner 1974). The following strains were obtained from the C. elegans Genetic Center (CGC): wild-type (wt) Bristol strain N2, HSF-1 mutant *hsf-1(sy441)* (PS3551), temperature sensitive strains *unc-52 (e669su250)* and *unc-45(e286*) (HE250 and CB286, respectively). The polyglutamine strain expressing 35 CAG-repeats fused with YFP (Q35::YFP) was described elsewhere (AM140 in CGC)[9].

***C. elegans* Assays for Aggregation and Motility Defects.** The treatment with chemical compounds was performed in a 96-well plate format, in liquid culture[10]. Each well contained a final volume of 60 µL, comprising 20 to 25 L2 (larval 2 stage) age- synchronized animals, compound at the appropriate concentration, and OP50 bacteria to a final OD595nm of 0.8 in the microtiter plate. Animals and bacteria were resuspended in S-medium supplemented with streptomycin, penicillin, and nystatin (Sigma, St. Louis, MO). To obtain the age synchronized population of L2 larvae, gravid adults were bleached with a NaOCl solution [250 mM NaOH and 1:4 (v/v) dilution of commercial bleach] and the eggs were allowed to hatch in M9 buffer overnight at 20°C. The first larval stage (L1) animals were transferred to OP50 plates to allow them to develop into L2 stage (20°C). The animals were then washed with M9 buffer, resuspended in S- medium to the appropriate concentration, and transferred into the 96-well plates. The compounds were dissolved and diluted in 100% DMSO, and the animals were incubated at a maximum concentration of 1.5% DMSO to avoid solvent-specific developmental defects and toxicity. The range of concentrations tested was 0, 1, 5, 10 and 15 µM (final concentration in the well). OP50-only and DMSO-only controls were used. In addition, the compound 17-(allylamino)-17-demethoxygeldanamycin (17-AAG, Biomol, Plymouth Meeting, PA) (at the concentrations 0.5, 1, 5 and 50 µM) was utilized as positive control for induction of the HSR. The plates were incubated at 20°C for 4 days. The animals were scored for changes in aggregation (number of fluorescent foci) using the stereomicroscope Leica

MZ16FA equipped for epifluorescence (Leica Microsystems, Switzerland). Suppression of aggregation was scored positive when ≥50% of the worms had a reduction in fluorescent foci number, without loss of body-wall fluorescence, compared to the DMSO control (experiments done at least in triplicate). Other phenotypes such as thrashing in liquid, body size and progeny number were also taken into account, as indicative of animal health. Simultaneous treatment with RNA interference (RNAi) and compounds was also performed in liquid culture (commercial RNAi library GeneServiceTM, USA). RNAi for *hsf-1* or the empty-vector (EV) control L4440 bacterial cultures were grown overnight in LB-ampicillin 50 μg/ml at 37°C, and induced with 0.7 mM isopropyl β-D-thiogalatoside (IPTG) for 2.5 hours at 37°C. Bacteria was then pelleted and resuspended in supplemented S-medium to a final OD_{595nm} of 0.8 in the microtiter plate. Assay plates were setup as before, with L2 age synchronized animals and 4 days incubation at 20°C. Fluorescent microscopy images were taken using an Axiovert 200 microscope with a Hamamatsu digital camera C4742-98 (Carl Zeiss, Germany). For the motility assay, animals were incubated in liquid culture with the chemical compounds as described above. Six days old animals were transferred from the liquid culture onto a NGM plate seeded with OP50 bacteria (equilibrated at 20°C) and allowed to acclimate for 1 h. At this point the animals' movement was digitally recorded using a Leica M205 FA microscope with a Hamamatsu digital camera C10600-10B (Orca-R2, Leica Microsystems, Switzerland), and the Hamamatsu Simple PCI Imaging software. Movies of 45 sec were captured at 5 frames/s, for each condition, for a minimum of 50 animals, and the experiment was done at least in triplicate (n≥150). Captured frames were merged into *.avi format and were imported directly into ImageJ[11]. Using the LOCI bio-formats plugin and a custom stack deflicker plugin (http://www.loci.wisc.edu/bio- formats/imagej), light average intensity was normalized for each frame. To enhance the definition of the animals in the movies, the difference between each frame and the constant background was calculated, using the Maximum Z stack projection. The resulting movie was converted to binary format using Otsu Thresholding 2. Binary objects representing the animals were tracked using custom ImageJ plugin, wrMTrck (based on "MTrack2" by Nico Stuurman)[12]. The average speed of each animal was calculated by dividing its body length by the duration of each track (body length per second, or BLPS). Motility measurements are given as a percentage of the wild type control strain motility, N2. Statistically significant changes in motility were obtained with **p-value < 0.01 and ***p-value<0.001 (Student's T-test). The wrMTrck plugin and scripts for automated analysis are open-source and publicly available at http://www.phage.dk/plugins.

Semi-quantitative RT-PCR (qPCR). The small molecule treatment, with or without RNAi, was performed at least in triplicate for either N2(wt), Q35 or *hsf-1(sy441)* animals. Animals were collected from the liquid cultures (96-well plates) into eppendorf tubes, washed with M9 buffer, pelleted at 3,000xg (Eppendorf centrifuge 5424, Eppendorf) and re-suspended in Trizol (Invitrogen, Carlsbad, CA). Samples were homogenized by vortexing and incubated on ice for 10 min. 50μl of chloroform were added to each sample, followed by vortexing and centrifugation at 13,500g for 15 min (4°C). A volume of 150μl of 2-propanol was added to each aqueous layer (10 min incubation) and total RNA was spun-down at 18,000g (4°C) for 10 min. The pellets were washed with 75% (v/v) ethanol, air-dried and re-suspended in nuclease free water at 60°C for 10 min. RNA aliquots of 10μg were used for DNase treatment (Applied Biosystems, Carlsbad, CA). 1μg of purified RNA was used for cDNA synthesis (Bio-Rad, Hercules, CA). cDNA samples were diluted to a final volume of 500μl in water and 1.5 μl (~10 ng) were used for real-time PCR amplification. PCR measurements were performed for HSP-70 (*C12C8.1, F44E5.4* and *C30C11.4*), small HSPs (*hsp-16.1* and *hsp-16.49*) mRNA, ER HSP-70 (*hsp-4)*, oxidative stress *sod-1*, HSP-90 chaperone and co-chaperone (*daf-21* and *ZC395.10*) and ubiquitin protein (*ubq-2*) with the following primers:
C12C8.1.fw 5'-ACTCATGTGTCGGTATTTATCA-3'; C12C8.1.rev 5'-ACGGGCTTTCCTTGTTTT-3';
C30C11.4.fw 5'-GCTTCGTACTATTGTGGAATCTC-3'; C30C11.4.rev 5'-GGAGATCTTGCTTGTAGATTCC-3';
F44E5.4.fw 5'-GTCTTCATGCAAAGCTATTGGTATC-3'; F44E5.4.rev 5'-CGTCGTCCAATCAATCCTTTTGCATC-3';
hsp-16.1.fw 5'-ACTTTACCACTATTTCCGTCCAGC-3'; hsp-16.1.rev 5'-GATAATGTATGTCCATCCAAATTA-3';
hsp-16.49 fw 5'-CCATATTGGAGAAATGCTGATCAC-3'; hsp-16.49 rev 5'-CTTCTGGTAGAAGAATCATTTTTG-3';
hsp-4.fw 5'-GCAGATGATCAAGCCCAAAAAG-3' hsp-4.rev 5'-GGAGACGATTGGTTGAACAACAG-3';
sod-1.fw 5'-GGACTTACTCCCGGTCTTCATG-3'; sod-1.rev 5'-GTAAAGCGTGACGAGCGTGTCG-3';
daf-21.fw 5'-CTTGACAAGATTCGCTACCAG-3'; daf-21.rev 5'-GCTTGAAGAGCCTCCATGAAGG-3';
ZC395.10.fw 5'-CTTGTCTATCTGACCATCGAGG-3'; ZC395.10.rev 5'-GGGTCTTCTTCTGAACTGTGATC-3';
ubq-2.fw 5'-GAATCCCACCAGATCAGCAAAG-3'; ubq-2.rev 5'-GTCGCAGTTGTACTTCTGGG-3';
mtl-1 fw 5'-GGCTTGCAAGTGTGACTGCAAAAACAAGC-3'; mtl-1 rev 5'-TTAATGAGCCGCAGCAGTTCCCTGGTGTTGATGG-3'
sod-3 fw 5'-GCTTCAAAGCTTGTTCAACCGGTTGCG-3'; sod-3 rev 5'-CAGCGCTGGTTGGAGAGCAATTGC-3'
gcs-1 fw 5'-GTGCAAGTGTCGACGATCGTAC-3'; gcs-1 rev 5'-GCGAATATGTTTTGCCAGTGGCTC-3'
gst-4 fw 5'-CGACTCCATTTGGCCAGC-3'; gst-4 rev 5'-GATCAGCGTCACTTCTAG-3'
pcm-1 fw 5'-CGGTTTCTGCACCTCACATG-3'; pcm-1 rev 5'-CACGTTCCAATTGTTCACTG-3'
nduf-7 fw 5'-GAG GTT CAA TTT GGC CAC TGA C-3'; nduf-7 rev 5'-CAT ATA TGC GGC GAA GTG CAG-3
dnj-7 fw 5'-GAGCACGGATAGTACGGAC-3'; dnj-7 rev 5'-GAGGCAAGCCATCCAGTC-3'
ero-1 fw 5'-CGACGAAATGCAGTGAATATG-3'; ero-1 rev 5'-GTGTAGCGTTCCGGATTCTTCG-3'
hsp-6 fw 5'-CAGGCCGTTACCAACTCTGC-3'; hsp-6 rev 5'-GCAGTTTCCTTCATCTTCATC-3'
rpn-2 fw 5'-GCC TGC AGA TTT GAC CAT CAA G-3'; rpn-2 rev 5'-CTC GTA ATC GTG TCA GCA GC-3'
As an internal control, we amplified mRNA of *act-1* (actin) with the primers:
act-1.fw 5'-ATCACCGCTCTTGCCCCATC-3'; act-1.rev 5'-GGCCGGACTCGTCGTATTCTTG.

Assay for TS Phenotypes. The temperature sensitive mutant (TS) animals were age-synchronized to L1 stage, and grown in liquid media with or without compounds, as described before[13,14]. Plates were either incubated at the permissive temperature 15°C, or incubated at 15°C until animals reached L4 stage and then transferred to the restrictive temperature, 25°C. TS phenotypes were scored 2 days post-transfer to 25°C [13,14]. For abnormal body shape (or stiff paralysis) in the *unc-52(e669su250)*, partially paralyzed animals with moving heads and stick-like bodies were scored. For the egg laying defect in the *unc-45(e286)* animals were scored for accumulation of eggs in the gonad and enlargement of the animal belly. For control conditions, L1 animals were grown on OP50 bacteria and DMSO at either 15°C or 25°C and scored 2 days later for the TS phenotype. Experiment was performed in triplicate.

Proteasome Inhibition Assay. The assay was essentially performed as described by Kisselev et al.[15]. In brief, HeLa cells were incubated with either DMSO (negative control), the positive controls MG132 (10 μM) and lactacystin (6 μM) or the PRs A1, A3 and F1 for 3 and 6 hours and then harvested. Cells were lysed in homogenization buffer (50 mM Tris-HCl, pH7.5, 250 mM sucrose, 5 mM $MgCl_2$, 2 mM ATP, 1 mM DTT, 0.5 mM EDTA, 0.025% digitonin) for 5 min on ice, and total protein concentration of whole cell extract was determined by Bradford assay. 3 μg of whole cell extracts were combined with assay buffer (50 mM Tris-HCl, pH 7.5, 40 mM KCl, 5 mM $MgCl_2$, 0.5 mM ATP, 1 mM DTT, 0.05 mg/ml BSA) in a black 96-well plate and the reaction was initiated by the addition of a 2x (200 μM) fluorogenic peptide substrate Suc-LLVY-AMC (EMD Chemicals Inc., Gibbstown, NJ). Fluorescence was measured every 10 min using a Synergy H4 multi-mode microplate reader (BioTek, Winooski, VT).

Hsp90 Client Protein Degradation. Analysis of Hsp90 client protein degradation was carried out using HeLa cells that were treated with the indicated compounds for 6, 16 and 24 h. The same procedure described for the Western Blot analysis was followed. The following primary antibodies were used: a mouse monoclonal Cdk-4 (DCS-31, Santa Cruz Biotechnology, Inc., Santa Cruz, CA), a rabbit polyclonal Raf-1 (C-12, Santa Cruz Biotechnology, Inc., Santa Cruz, CA), a rabbit polyclonal Akt (Cell Signaling Technology, Inc., Danvers, MA) and a mouse monoclonal GAPDH (AbCam, Cambridge, MA). The primary antibodies were used at the following dilutions: Cdk-4, 1:200; Raf-1, 1:500; Akt, 1:1,000; and GAPDH, 1:5,000.

Luciferase Renaturation Assay in Rabbit Reticulocyte Lysate. The luciferase renaturation assay was performed essentially as described previously[16,17]. Diluted RRL was pre-incubated with either DMSO (0.2%), 17-AAG (2 μM) or PR A1 (10 μM) for 30 minutes at RT before addition of denatured luciferase.

Geldanamycin Competition Assay. Human recombinant Hsp90β (2 μg) in Hsp90 binding buffer (10 mM Tris, 50 mM KCl, 5 mM $MgCl_2$, 20 mM $NaMoO_4$, 0.01% NP40) was preincubated with either DMSO, 17-AAG (1 μM) or PRs A1, A3 and F1 (10 and 100 μM) for 30 min at 4°C before the addition of 1 μM geldanamycin-biotin (Enzo Life Sciences, Farmingdale, NY). Bound Hsp90 was then captured with neutravidin-agarose beads for 30 min at 4°C. The beads were washed with Hsp90 binding buffer, and Hsp90 was eluted from the beads by incubating in Laemmli sample buffer at 95°C for 5 min.

Supplementary References

1. Westerheide, S.D. et al. Celastrols as inducers of the heat shock response and cytoprotection. *J Biol Chem* **279**, 56053-60 (2004).
2. McMillan, D.R., Xiao, X., Shao, L., Graves, K. & Benjamin, I.J. Targeted disruption of heat shock transcription factor 1 abolishes thermotolerance and protection against heat-inducible apoptosis. *J Biol Chem* **273**, 7523-8 (1998).
3. Wyttenbach, A. et al. Polyglutamine expansions cause decreased CRE-mediated transcription and early gene expression changes prior to cell death in an inducible cell model of Huntington's disease. *Hum Mol Genet* **10**, 1829-45 (2001).
4. Galietta, L.J., Haggie, P.M. & Verkman, A.S. Green fluorescent protein-based halide indicators with improved chloride and iodide affinities. *FEBS Lett* **499**, 220- 4 (2001).
5. Sarge, K.D., Murphy, S.P. & Morimoto, R.I. Activation of heat shock gene transcription by heat shock factor 1 involves oligomerization, acquisition of DNA- binding activity, and nuclear localization and can occur in the absence of stress. *Mol Cell Biol* **13**, 1392-407 (1993).
6. Zhang, A. et al. Small interfering RNA and gene expression analysis using a multiplex branched DNA assay without RNA purification. *J Biomol Screen* **10**, 549-56 (2005).
7. Zheng, Z., Luo, Y. & McMaster, G.K. Sensitive and quantitative measurement of gene expression directly from a small amount of whole blood. *Clin Chem* **52**, 1294-302 (2006).
8. Wanker, E.E. et al. Membrane filter assay for detection of amyloid-like polyglutamine-containing protein aggregates. *Methods Enzymol* **309**, 375-86 (1999).

9. Morley, J.F., Brignull, H.R., Weyers, J.J. & Morimoto, R.I. The threshold for polyglutamine-expansion protein aggregation and cellular toxicity is dynamic and influenced by aging in Caenorhabditis elegans. *Proc Natl Acad Sci U S A* **99**, 10417-22 (2002).
10. Voisine, C. et al. Identification of potential therapeutic drugs for huntington's disease using Caenorhabditis elegans. *PLoS One* **2**, e504 (2007).
11. Collins, T.J. ImageJ for microscopy. *Biotechniques* **43**, 25-30 (2007).
12. Klopfenstein, D.R. & Vale, R.D. The lipid binding pleckstrin homology domain in UNC-104 kinesin is necessary for synaptic vesicle transport in Caenorhabditis elegans. *Mol Biol Cell* **15**, 3729-39 (2004).
13. Gidalevitz, T., Ben-Zvi, A., Ho, K.H., Brignull, H.R. & Morimoto, R.I. Progressive disruption of cellular protein folding in models of polyglutamine diseases. *Science* **311**, 1471-4 (2006).
14. Garcia, S.M., Casanueva, M.O., Silva, M.C., Amaral, M.D. & Morimoto, R.I. Neuronal signaling modulates protein homeostasis in Caenorhabditis elegans post-synaptic muscle cells. *Genes Dev* **21**, 3006-16 (2007).
15. Kisselev, A.F. & Goldberg, A.L. Monitoring activity and inhibition of 26S proteasomes with fluorogenic peptide substrates. *Methods Enzymol* **398**, 364-78 (2005).
16. Nimmesgern, E. & Hartl, F.U. ATP-dependent protein refolding activity in reticulocyte lysate. Evidence for the participation of different chaperone components. *FEBS Lett* **331**, 25-30 (1993).
17. Thulasiraman, V. & Matts, R.L. Luciferase renaturation assays of chaperones and chaperone antagonists. *Methods Mol Biol* **102**, 129-41 (1998).
18. Rowlands, M.G. et al. High-throughput screening assay for inhibitors of heat- shock protein 90 ATPase activity. *Anal Biochem* **327**, 176-83 (2004).

References

REFERENCES

1. Vabulas RM, Raychaudhuri S, Hayer-Hartl M, Hartl FU (2010) Protein folding in the cytoplasm and the heat shock response. Cold Spring Harbor perspectives in biology 2: a004390.
2. Karplus M (2011) Behind the folding funnel diagram. Nature chemical biology 7: 401-404.
3. Wolynes PG, Onuchic JN, Thirumalai D (1995) Navigating the folding routes. Science 267: 1619-1620.
4. Hartl FU, Hayer-Hartl M (2009) Converging concepts of protein folding in vitro and in vivo. Nature structural & molecular biology 16: 574-581.
5. Powers ET, Morimoto RI, Dillin A, Kelly JW, Balch WE (2009) Biological and chemical approaches to diseases of proteostasis deficiency. Annu Rev Biochem 78: 959-991.
6. Dobson CM (2003) Protein folding and misfolding. Nature 426: 884-890.
7. Haass C, Selkoe DJ (2007) Soluble protein oligomers in neurodegeneration: lessons from the Alzheimer's amyloid beta-peptide. Nature reviews Molecular cell biology 8: 101-112.
8. Goldberg AL (2003) Protein degradation and protection against misfolded or damaged proteins. Nature 426: 895-899.
9. Ellgaard L, Helenius A (2003) Quality control in the endoplasmic reticulum. Nature reviews Molecular cell biology 4: 181-191.
10. Voisine C, Orton K, Morimoto RI (2007) Protein Misfolding, Chaperone Networks, and the Heat Shock Response in the Nervous System. Molecular Neurology. pp. 9253-9261.
11. Hartl FU, Hayer-Hartl M (2002) Molecular chaperones in the cytosol: from nascent chain to folded protein. Science 295: 1852-1858.
12. Nathan DF, Vos MH, Lindquist S (1997) In vivo functions of the Saccharomyces cerevisiae Hsp90 chaperone. Proceedings of the National Academy of Sciences of the United States of America 94: 12949-12956.
13. Ben-Zvi AP, Goloubinoff P (2001) Review: mechanisms of disaggregation and refolding of stable protein aggregates by molecular chaperones. Journal of structural biology 135: 84-93.
14. Liberek K, Lewandowska A, Zietkiewicz S (2008) Chaperones in control of protein disaggregation. The EMBO journal 27: 328-335.
15. Tyedmers J, Mogk A, Bukau B (2010) Cellular strategies for controlling protein aggregation. Nature reviews Molecular cell biology 11: 777-788.
16. Ellgaard L, Molinari M, Helenius A (1999) Setting the standards: quality control in the secretory pathway. Science 286: 1882-1888.
17. Kleizen B, Braakman I (2004) Protein folding and quality control in the endoplasmic reticulum. Current opinion in cell biology 16: 343-349.
18. Farinha CM, Amaral MD (2005) Most F508del-CFTR is targeted to degradation at an early folding checkpoint and independently of calnexin. Molecular and cellular biology 25: 5242-5252.
19. Wong E, Cuervo AM (2010) Integration of clearance mechanisms: the proteasome and autophagy. Cold Spring Harbor perspectives in biology 2: a006734.
20. Bence NF, Sampat RM, Kopito RR (2001) Impairment of the ubiquitin-proteasome system by protein aggregation. Science 292: 1552-1555.
21. Kaganovich D, Kopito R, Frydman J (2008) Misfolded proteins partition between two distinct quality control compartments. Nature 454: 1088-1095.
22. Cohen E, Bieschke J, Perciavalle RM, Kelly JW, Dillin A (2006) Opposing activities protect against age-onset proteotoxicity. Science 313: 1604-1610.
23. Johnston JA, Ward CL, Kopito RR (1998) Aggresomes: a cellular response to misfolded proteins. The Journal of cell biology 143: 1883-1898.
24. Ravikumar B, Vacher C, Berger Z, Davies JE, Luo S, et al. (2004) Inhibition of mTOR induces autophagy and reduces toxicity of polyglutamine expansions in fly and mouse models of Huntington disease. Nature genetics 36: 585-595.
25. Ravikumar B, Rubinsztein DC (2004) Can autophagy protect against neurodegeneration caused by aggregate-prone proteins? Neuroreport 15: 2443-2445.
26. Ravikumar B, Duden R, Rubinsztein DC (2002) Aggregate-prone proteins with polyglutamine and polyalanine expansions are degraded by autophagy. Human molecular genetics 11: 1107-1117.
27. Iwata A, Christianson JC, Bucci M, Ellerby LM, Nukina N, et al. (2005) Increased susceptibility of cytoplasmic over nuclear polyglutamine aggregates to autophagic degradation. Proceedings of the National Academy of Sciences of the United States of America 102: 13135-13140.
28. Kourtis N, Tavernarakis N (2011) Cellular stress response pathways and ageing: intricate molecular relationships. The EMBO journal 30: 2520-2531.
29. Yoneda T, Benedetti C, Urano F, Clark SG, Harding HP, et al. (2004) Compartment-specific perturbation of protein handling activates genes encoding mitochondrial chaperones. Journal of cell science 117: 4055-4066.
30. Ritossa F (1996) Discovery of the heat shock response. Cell stress & chaperones 1: 97-98.
31. Morimoto RI (1998) Regulation of the heat shock transcriptional response: cross talk between a family of heat shock factors, molecular chaperones, and negative regulators. Genes & development 12: 3788-3796.

32. Sistonen L, Sarge KD, Phillips B, Abravaya K, Morimoto RI (1992) Activation of heat shock factor 2 during hemin-induced differentiation of human erythroleukemia cells. Molecular and cellular biology 12: 4104-4111.
33. Nakai A, Tanabe M, Kawazoe Y, Inazawa J, Morimoto RI, et al. (1997) HSF4, a new member of the human heat shock factor family which lacks properties of a transcriptional activator. Molecular and cellular biology 17: 469-481.
34. Pirkkala L, Nykanen P, Sistonen L (2001) Roles of the heat shock transcription factors in regulation of the heat shock response and beyond. FASEB J 15: 1118-1131.
35. Akerfelt M, Morimoto RI, Sistonen L (2010) Heat shock factors: integrators of cell stress, development and lifespan. Nat Rev Mol Cell Biol 11: 545-555.
36. Sistonen L, Sarge KD, Morimoto RI (1994) Human heat shock factors 1 and 2 are differentially activated and can synergistically induce hsp70 gene transcription. Molecular and cellular biology 14: 2087-2099.
37. Akerfelt M, Trouillet D, Mezger V, Sistonen L (2007) Heat shock factors at a crossroad between stress and development. Annals of the New York Academy of Sciences 1113: 15-27.
38. Abravaya K, Phillips B, Morimoto RI (1991) Attenuation of the heat shock response in HeLa cells is mediated by the release of bound heat shock transcription factor and is modulated by changes in growth and in heat shock temperatures. Genes & development 5: 2117-2127.
39. Abravaya K, Phillips B, Morimoto RI (1991) Heat shock-induced interactions of heat shock transcription factor and the human hsp70 promoter examined by in vivo footprinting. Molecular and cellular biology 11: 586-592.
40. Abravaya K, Myers MP, Murphy SP, Morimoto RI (1992) The human heat shock protein hsp70 interacts with HSF, the transcription factor that regulates heat shock gene expression. Genes & development 6: 1153-1164.
41. Amin J, Ananthan J, Voellmy R (1988) Key features of heat shock regulatory elements. Molecular and cellular biology 8: 3761-3769.
42. Xiao H, Perisic O, Lis JT (1991) Cooperative binding of Drosophila heat shock factor to arrays of a conserved 5 bp unit. Cell 64: 585-593.
43. Kline MP, Morimoto RI (1997) Repression of the heat shock factor 1 transcriptional activation domain is modulated by constitutive phosphorylation. Molecular and cellular biology 17: 2107-2115.
44. Batulan Z, Shinder GA, Minotti S, He BP, Doroudchi MM, et al. (2003) High threshold for induction of the stress response in motor neurons is associated with failure to activate HSF1. The Journal of neuroscience : the official journal of the Society for Neuroscience 23: 5789-5798.
45. Patil C, Walter P (2001) Intracellular signaling from the endoplasmic reticulum to the nucleus: the unfolded protein response in yeast and mammals. Current opinion in cell biology 13: 349-355.
46. Ron D, Walter P (2007) Signal integration in the endoplasmic reticulum unfolded protein response. Nature reviews Molecular cell biology 8: 519-529.
47. Hetz C, Glimcher LH (2009) Fine-tuning of the unfolded protein response: Assembling the IRE1alpha interactome. Molecular cell 35: 551-561.
48. Wiseman RL, Haynes CM, Ron D (2010) SnapShot: The unfolded protein response. Cell 140: 590-590 e592.
49. Korennykh AV, Egea PF, Korostelev AA, Finer-Moore J, Zhang C, et al. (2009) The unfolded protein response signals through high-order assembly of Ire1. Nature 457: 687-693.
50. Malhotra JD, Kaufman RJ (2007) The endoplasmic reticulum and the unfolded protein response. Seminars in cell & developmental biology 18: 716-731.
51. Finkel T, Holbrook NJ (2000) Oxidants, oxidative stress and the biology of ageing. Nature 408: 239-247.
52. Malhotra JD, Kaufman RJ (2007) Endoplasmic reticulum stress and oxidative stress: a vicious cycle or a double-edged sword? Antioxidants & redox signaling 9: 2277-2293.
53. Tu BP, Weissman JS (2004) Oxidative protein folding in eukaryotes: mechanisms and consequences. The Journal of cell biology 164: 341-346.
54. An JH, Blackwell TK (2003) SKN-1 links C. elegans mesendodermal specification to a conserved oxidative stress response. Genes & development 17: 1882-1893.
55. Oliveira RP, Porter Abate J, Dilks K, Landis J, Ashraf J, et al. (2009) Condition-adapted stress and longevity gene regulation by Caenorhabditis elegans SKN-1/Nrf. Aging cell 8: 524-541.
56. Park SK, Tedesco PM, Johnson TE (2009) Oxidative stress and longevity in Caenorhabditis elegans as mediated by SKN-1. Aging cell 8: 258-269.
57. Yasuda K, Ishii T, Suda H, Akatsuka A, Hartman PS, et al. (2006) Age-related changes of mitochondrial structure and function in Caenorhabditis elegans. Mechanisms of ageing and development 127: 763-770.
58. Balch WE, Morimoto RI, Dillin A, Kelly JW (2008) Adapting proteostasis for disease intervention. Science 319: 916-919.
59. Gidalevitz T, Kikis EA, Morimoto RI (2010) A cellular perspective on conformational disease: the role of genetic background and proteostasis networks. Curr Opin Struct Biol 20: 23-32.
60. Ben-Zvi A, Miller EA, Morimoto RI (2009) Collapse of proteostasis represents an early molecular event in Caenorhabditis elegans aging. Proc Natl Acad Sci U S A 106: 14914-14919.
61. Morimoto RI, Cuervo AM (2009) Protein homeostasis and aging: taking care of proteins from the cradle to the grave. The journals of gerontology Series A, Biological sciences and medical sciences 64: 167-170.
62. Stefani M (2004) Protein misfolding and aggregation: new examples in medicine and biology of the dark side of the protein world. Biochim Biophys Acta 1739: 5-25.
63. Amaral MD, Kunzelmann K (2007) Molecular targeting of CFTR as a therapeutic approach to cystic fibrosis. Trends in pharmacological sciences 28: 334-341.

64. Sadlish H, Skach WR (2004) Biogenesis of CFTR and other polytopic membrane proteins: new roles for the ribosome-translocon complex. The Journal of membrane biology 202: 115-126.
65. Cohen FE, Kelly JW (2003) Therapeutic approaches to protein-misfolding diseases. Nature 426: 905-909.
66. Riordan JR (2005) Assembly of functional CFTR chloride channels. Annual review of physiology 67: 701-718.
67. Wang X, Venable J, LaPointe P, Hutt DM, Koulov AV, et al. (2006) Hsp90 cochaperone Aha1 downregulation rescues misfolding of CFTR in cystic fibrosis. Cell 127: 803-815.
68. Amaral MD (2006) Therapy through chaperones: sense or antisense? Cystic fibrosis as a model disease. Journal of inherited metabolic disease 29: 477-487.
69. Ong DS, Mu TW, Palmer AE, Kelly JW (2010) Endoplasmic reticulum Ca2+ increases enhance mutant glucocerebrosidase proteostasis. Nature chemical biology 6: 424-432.
70. Soto C, Estrada LD (2008) Protein misfolding and neurodegeneration. Arch Neurol 65: 184-189.
71. Ruegg MA, Glass DJ (2011) Molecular mechanisms and treatment options for muscle wasting diseases. Annual review of pharmacology and toxicology 51: 373-395.
72. Taylor JP, Hardy J, Fischbeck KH (2002) Toxic proteins in neurodegenerative disease. Science 296: 1991-1995.
73. Soto C (2003) Unfolding the role of protein misfolding in neurodegenerative diseases. Nat Rev Neurosci 4: 49-60.
74. Auluck PK, Caraveo G, Lindquist S (2010) alpha-Synuclein: membrane interactions and toxicity in Parkinson's disease. Annual review of cell and developmental biology 26: 211-233.
75. Landles C, Bates GP (2004) Huntingtin and the molecular pathogenesis of Huntington's disease. Fourth in molecular medicine review series. EMBO reports 5: 958-963.
76. Rozas JL, Gomez-Sanchez L, Tomas-Zapico C, Lucas JJ, Fernandez-Chacon R (2011) Increased neurotransmitter release at the neuromuscular junction in a mouse model of polyglutamine disease. The Journal of neuroscience : the official journal of the Society for Neuroscience 31: 1106-1113.
77. Treusch S, Cyr DM, Lindquist S (2009) Amyloid deposits: protection against toxic protein species? Cell cycle 8: 1668-1674.
78. Gusella JF, MacDonald ME (2009) Huntington's disease: the case for genetic modifiers. Genome medicine 1: 80.
79. Saunders HM, Bottomley SP (2009) Multi-domain misfolding: understanding the aggregation pathway of polyglutamine proteins. Protein engineering, design & selection : PEDS 22: 447-451.
80. Dion PA, Daoud H, Rouleau GA (2009) Genetics of motor neuron disorders: new insights into pathogenic mechanisms. Nature reviews Genetics 10: 769-782.
81. Strong MJ, Kesavapany S, Pant HC (2005) The pathobiology of amyotrophic lateral sclerosis: a proteinopathy? Journal of neuropathology and experimental neurology 64: 649-664.
82. Hardy J, Selkoe DJ (2002) The amyloid hypothesis of Alzheimer's disease: progress and problems on the road to therapeutics. Science 297: 353-356.
83. Bennett EJ, Bence NF, Jayakumar R, Kopito RR (2005) Global impairment of the ubiquitin-proteasome system by nuclear or cytoplasmic protein aggregates precedes inclusion body formation. Molecular cell 17: 351-365.
84. Holmberg CI, Staniszewski KE, Mensah KN, Matouschek A, Morimoto RI (2004) Inefficient degradation of truncated polyglutamine proteins by the proteasome. The EMBO journal 23: 4307-4318.
85. Kopito RR, Sitia R (2000) Aggresomes and Russell bodies. Symptoms of cellular indigestion? EMBO reports 1: 225-231.
86. Olzscha H, Schermann SM, Woerner AC, Pinkert S, Hecht MH, et al. (2011) Amyloid-like aggregates sequester numerous metastable proteins with essential cellular functions. Cell 144: 67-78.
87. McCampbell A, Taylor JP, Taye AA, Robitschek J, Li M, et al. (2000) CREB-binding protein sequestration by expanded polyglutamine. Human molecular genetics 9: 2197-2202.
88. Nucifora FC, Jr., Sasaki M, Peters MF, Huang H, Cooper JK, et al. (2001) Interference by huntingtin and atrophin-1 with cbp-mediated transcription leading to cellular toxicity. Science 291: 2423-2428.
89. Schaffar G, Breuer P, Boteva R, Behrends C, Tzvetkov N, et al. (2004) Cellular toxicity of polyglutamine expansion proteins: mechanism of transcription factor deactivation. Molecular cell 15: 95-105.
90. Gidalevitz T, Ben-Zvi A, Ho KH, Brignull HR, Morimoto RI (2006) Progressive disruption of cellular protein folding in models of polyglutamine diseases. Science 311: 1471-1474.
91. Gidalevitz T, Krupinski T, Garcia S, Morimoto RI (2009) Destabilizing protein polymorphisms in the genetic background direct phenotypic expression of mutant SOD1 toxicity. PLoS genetics 5: e1000399.
92. Morimoto RI (2008) Proteotoxic stress and inducible chaperone networks in neurodegenerative disease and aging. Genes Dev 22: 1427-1438.
93. Behrends C, Langer CA, Boteva R, Bottcher UM, Stemp MJ, et al. (2006) Chaperonin TRiC promotes the assembly of polyQ expansion proteins into nontoxic oligomers. Mol Cell 23: 887-897.
94. Tam S, Geller R, Spiess C, Frydman J (2006) The chaperonin TRiC controls polyglutamine aggregation and toxicity through subunit-specific interactions. Nature cell biology 8: 1155-1162.
95. Kitamura A, Kubota H, Pack CG, Matsumoto G, Hirayama S, et al. (2006) Cytosolic chaperonin prevents polyglutamine toxicity with altering the aggregation state. Nat Cell Biol 8: 1163-1170.
96. Zoghbi HY, Orr HT (1999) Polyglutamine diseases: protein cleavage and aggregation. Current opinion in neurobiology 9: 566-570.
97. Gutekunst CA, Li SH, Yi H, Mulroy JS, Kuemmerle S, et al. (1999) Nuclear and neuropil aggregates in Huntington's disease: relationship to neuropathology. J Neurosci 19: 2522-2534.
98. Ross CA, Poirier MA (2005) Opinion: What is the role of protein aggregation in neurodegeneration? Nat Rev Mol Cell Biol 6: 891-898.

99. Van Raamsdonk JM, Murphy Z, Slow EJ, Leavitt BR, Hayden MR (2005) Selective degeneration and nuclear localization of mutant huntingtin in the YAC128 mouse model of Huntington disease. Hum Mol Genet 14: 3823-3835.
100. Arrasate M, Mitra S, Schweitzer ES, Segal MR, Finkbeiner S (2004) Inclusion body formation reduces levels of mutant huntingtin and the risk of neuronal death. Nature 431: 805-810.
101. Saudou F, Finkbeiner S, Devys D, Greenberg ME (1998) Huntingtin acts in the nucleus to induce apoptosis but death does not correlate with the formation of intranuclear inclusions. Cell 95: 55-66.
102. Kayed R, Head E, Thompson JL, McIntire TM, Milton SC, et al. (2003) Common structure of soluble amyloid oligomers implies common mechanism of pathogenesis. Science 300: 486-489.
103. Kirkitadze MD, Bitan G, Teplow DB (2002) Paradigm shifts in Alzheimer's disease and other neurodegenerative disorders: the emerging role of oligomeric assemblies. J Neurosci Res 69: 567-577.
104. Klein WL, Krafft GA, Finch CE (2001) Targeting small Abeta oligomers: the solution to an Alzheimer's disease conundrum? Trends Neurosci 24: 219-224.
105. Nagai Y, Inui T, Popiel HA, Fujikake N, Hasegawa K, et al. (2007) A toxic monomeric conformer of the polyglutamine protein. Nat Struct Mol Biol 14: 332-340.
106. Wong SL, Chan WM, Chan HY (2008) Sodium dodecyl sulfate-insoluble oligomers are involved in polyglutamine degeneration. FASEB J.
107. Lambert MP, Barlow AK, Chromy BA, Edwards C, Freed R, et al. (1998) Diffusible, nonfibrillar ligands derived from Abeta1-42 are potent central nervous system neurotoxins. Proc Natl Acad Sci U S A 95: 6448-6453.
108. Lesne S, Koh MT, Kotilinek L, Kayed R, Glabe CG, et al. (2006) A specific amyloid-beta protein assembly in the brain impairs memory. Nature 440: 352-357.
109. Wetzel R (2006) Kinetics and thermodynamics of amyloid fibril assembly. Acc Chem Res 39: 671-679.
110. Legleiter J, Mitchell E, Lotz GP, Sapp E, Ng C, et al. (2010) Mutant huntingtin fragments form oligomers in a polyglutamine length-dependent manner in vitro and in vivo. The Journal of biological chemistry 285: 14777-14790.
111. Kayed R, Glabe CG (2006) Conformation-dependent anti-amyloid oligomer antibodies. Methods Enzymol 413: 326-344.
112. Glabe CG, Kayed R (2006) Common structure and toxic function of amyloid oligomers implies a common mechanism of pathogenesis. Neurology 66: S74-78.
113. Tatar M, Bartke A, Antebi A (2003) The endocrine regulation of aging by insulin-like signals. Science 299: 1346-1351.
114. Kenyon CJ (2010) The genetics of ageing. Nature 464: 504-512.
115. Murphy CT, McCarroll SA, Bargmann CI, Fraser A, Kamath RS, et al. (2003) Genes that act downstream of DAF-16 to influence the lifespan of Caenorhabditis elegans. Nature 424: 277-283.
116. Morley JF, Morimoto RI (2004) Regulation of longevity in Caenorhabditis elegans by heat shock factor and molecular chaperones. Molecular biology of the cell 15: 657-664.
117. Soti C, Csermely P (2007) Aging cellular networks: chaperones as major participants. Experimental gerontology 42: 113-119.
118. Soti C, Csermely P (2007) Protein stress and stress proteins: implications in aging and disease. Journal of biosciences 32: 511-515.
119. Morley JF, Brignull HR, Weyers JJ, Morimoto RI (2002) The threshold for polyglutamine-expansion protein aggregation and cellular toxicity is dynamic and influenced by aging in Caenorhabditis elegans. Proc Natl Acad Sci U S A 99: 10417-10422.
120. Durieux J, Wolff S, Dillin A (2011) The cell-non-autonomous nature of electron transport chain-mediated longevity. Cell 144: 79-91.
121. Brignull HR, Morley JF, Garcia SM, Morimoto RI (2006) Modeling polyglutamine pathogenesis in C. elegans. Methods Enzymol 412: 256-282.
122. Brignull HR, Morley JF, Morimoto RI (2007) The stress of misfolded proteins: C. elegans models for neurodegenerative disease and aging. Adv Exp Med Biol 594: 167-189.
123. Feany MB (2000) Studying human neurodegenerative diseases in flies and worms. J Neuropathol Exp Neurol 59: 847-856.
124. Fernandez-Funez P, Nino-Rosales ML, de Gouyon B, She WC, Luchak JM, et al. (2000) Identification of genes that modify ataxin-1-induced neurodegeneration. Nature 408: 101-106.
125. Ghosh S, Feany MB (2004) Comparison of pathways controlling toxicity in the eye and brain in Drosophila models of human neurodegenerative diseases. Human molecular genetics 13: 2011-2018.
126. Hamamichi S, Rivas RN, Knight AL, Cao S, Caldwell KA, et al. (2008) Hypothesis-based RNAi screening identifies neuroprotective genes in a Parkinson's disease model. Proc Natl Acad Sci U S A 105: 728-733.
127. Kazemi-Esfarjani P, Benzer S (2000) Genetic suppression of polyglutamine toxicity in Drosophila. Science 287: 1837-1840.
128. Kraemer BC, Burgess JK, Chen JH, Thomas JH, Schellenberg GD (2006) Molecular pathways that influence human tau-induced pathology in Caenorhabditis elegans. Hum Mol Genet 15: 1483-1496.
129. Kuwahara T, Koyama A, Koyama S, Yoshina S, Ren CH, et al. (2008) A systematic RNAi screen reveals involvement of endocytic pathway in neuronal dysfunction in alpha-synuclein transgenic C. elegans. Hum Mol Genet 17: 2997-3009.
130. van Ham TJ, Thijssen KL, Breitling R, Hofstra RM, Plasterk RH, et al. (2008) C. elegans model identifies genetic modifiers of alpha-synuclein inclusion formation during aging. PLoS Genet 4: e1000027.
131. Wang J, Farr GW, Hall DH, Li F, Furtak K, et al. (2009) An ALS-linked mutant SOD1 produces a locomotor defect associated with aggregation and synaptic dysfunction when expressed in neurons of Caenorhabditis elegans. PLoS Genet 5: e1000350.

132. Luheshi LM, Crowther DC, Dobson CM (2008) Protein misfolding and disease: from the test tube to the organism. Current opinion in chemical biology 12: 25-31.
133. Marsh JL, Thompson LM (2006) Drosophila in the study of neurodegenerative disease. Neuron 52: 169-178.
134. Culetto E, Sattelle DB (2000) A role for Caenorhabditis elegans in understanding the function and interactions of human disease genes. Human molecular genetics 9: 869-877.
135. Strange K (2003) From genes to integrative physiology: ion channel and transporter biology in Caenorhabditis elegans. Physiological reviews 83: 377-415.
136. Wood WB (1988) Determination of pattern and fate in early embryos of Caenorhabditis elegans. Developmental biology 5: 57-78.
137. Aamodt EJ, Culotti JG (1986) Microtubules and microtubule-associated proteins from the nematode Caenorhabditis elegans: periodic cross-links connect microtubules in vitro. The Journal of cell biology 103: 23-31.
138. Brenner S (1974) The genetics of Caenorhabditis elegans. Genetics 77: 71-94.
139. Link CD (1995) Expression of human beta-amyloid peptide in transgenic Caenorhabditis elegans. Proceedings of the National Academy of Sciences of the United States of America 92: 9368-9372.
140. Faber PW, Alter JR, MacDonald ME, Hart AC (1999) Polyglutamine-mediated dysfunction and apoptotic death of a Caenorhabditis elegans sensory neuron. Proc Natl Acad Sci U S A 96: 179-184.
141. Kraemer BC, Zhang B, Leverenz JB, Thomas JH, Trojanowski JQ, et al. (2003) Neurodegeneration and defective neurotransmission in a Caenorhabditis elegans model of tauopathy. Proceedings of the National Academy of Sciences of the United States of America 100: 9980-9985.
142. Parker JA, Connolly JB, Wellington C, Hayden M, Dausset J, et al. (2001) Expanded polyglutamines in Caenorhabditis elegans cause axonal abnormalities and severe dysfunction of PLM mechanosensory neurons without cell death. Proc Natl Acad Sci U S A 98: 13318-13323.
143. Prahlad V, Morimoto RI (2009) Integrating the stress response: lessons for neurodegenerative diseases from C. elegans. Trends Cell Biol 19: 52-61.
144. Nollen EA, Garcia SM, van Haaften G, Kim S, Chavez A, et al. (2004) Genome-wide RNA interference screen identifies previously undescribed regulators of polyglutamine aggregation. Proc Natl Acad Sci U S A 101: 6403-6408.
145. Tamas I, Hodges E, Dessi P, Johnsen R, Vaz Gomes A (2005) A combined approach exploring gene function based on worm-human orthology. BMC genomics 6: 65.
146. Olsen A, Vantipalli MC, Lithgow GJ (2006) Using Caenorhabditis elegans as a model for aging and age-related diseases. Annals of the New York Academy of Sciences 1067: 120-128.
147. Dillin A, Hsu AL, Arantes-Oliveira N, Lehrer-Graiwer J, Hsin H, et al. (2002) Rates of behavior and aging specified by mitochondrial function during development. Science 298: 2398-2401.
148. Hamilton B, Dong Y, Shindo M, Liu W, Odell I, et al. (2005) A systematic RNAi screen for longevity genes in C. elegans. Genes Dev 19: 1544-1555.
149. Bilen J, Bonini NM (2007) Genome-wide screen for modifiers of ataxin-3 neurodegeneration in Drosophila. PLoS Genet 3: 1950-1964.
150. Giorgini F, Guidetti P, Nguyen Q, Bennett SC, Muchowski PJ (2005) A genomic screen in yeast implicates kynurenine 3-monooxygenase as a therapeutic target for Huntington disease. Nat Genet 37: 526-531.
151. Willingham S, Outeiro TF, DeVit MJ, Lindquist SL, Muchowski PJ (2003) Yeast genes that enhance the toxicity of a mutant huntingtin fragment or alpha-synuclein. Science 302: 1769-1772.
152. Outeiro TF, Lindquist S (2003) Yeast cells provide insight into alpha-synuclein biology and pathobiology. Science 302: 1772-1775.
153. Cooper AA, Gitler AD, Cashikar A, Haynes CM, Hill KJ, et al. (2006) Alpha-synuclein blocks ER-Golgi traffic and Rab1 rescues neuron loss in Parkinson's models. Science 313: 324-328.
154. Kamath RS, Fraser AG, Dong Y, Poulin G, Durbin R, et al. (2003) Systematic functional analysis of the Caenorhabditis elegans genome using RNAi. Nature 421: 231-237.
155. Kamath RS, Ahringer J (2003) Genome-wide RNAi screening in Caenorhabditis elegans. Methods 30: 313-321.
156. Simmer F, Tijsterman M, Parrish S, Koushika SP, Nonet ML, et al. (2002) Loss of the putative RNA-directed RNA polymerase RRF-3 makes C. elegans hypersensitive to RNAi. Current biology : CB 12: 1317-1319.
157. Ahringer J, ed. (2006) Reverse genetics. WormBook, ed The C elegans Research Community, WormBook.
158. Cummings CJ, Mancini MA, Antalffy B, DeFranco DB, Orr HT, et al. (1998) Chaperone suppression of aggregation and altered subcellular proteasome localization imply protein misfolding in SCA1. Nature genetics 19: 148-154.
159. Rubinsztein DC (2006) The roles of intracellular protein-degradation pathways in neurodegeneration. Nature 443: 780-786.
160. Lamitina T, Huang CG, Strange K (2006) Genome-wide RNAi screening identifies protein damage as a regulator of osmoprotective gene expression. Proc Natl Acad Sci U S A 103: 12173-12178.
161. van Ham TJ, Breitling R, Swertz MA, Nollen EA (2009) Neurodegenerative diseases: Lessons from genome-wide screens in small model organisms. EMBO molecular medicine 1: 360-370.
162. Yeger-Lotem E, Riva L, Su LJ, Gitler AD, Cashikar AG, et al. (2009) Bridging high-throughput genetic and transcriptional data reveals cellular responses to alpha-synuclein toxicity. Nature genetics 41: 316-323.
163. Muchowski PJ, Schaffar G, Sittler A, Wanker EE, Hayer-Hartl MK, et al. (2000) Hsp70 and hsp40 chaperones can inhibit self-assembly of polyglutamine proteins into amyloid-like fibrils. Proc Natl Acad Sci U S A 97: 7841-7846.
164. Prahlad V, Cornelius T, Morimoto RI (2008) Regulation of the cellular heat shock response in Caenorhabditis elegans by thermosensory neurons. Science 320: 811-814.

165. Russell SJ, Kahn CR (2007) Endocrine regulation of ageing. Nature reviews Molecular cell biology 8: 681-691.
166. Szewczyk NJ, Hartman JJ, Barmada SJ, Jacobson LA (2000) Genetic defects in acetylcholine signalling promote protein degradation in muscle cells of Caenorhabditis elegans. J Cell Sci 113 (Pt 11): 2003-2010.
167. Garcia SM, Casanueva MO, Silva MC, Amaral MD, Morimoto RI (2007) Neuronal signaling modulates protein homeostasis in Caenorhabditis elegans post-synaptic muscle cells. Genes Dev 21: 3006-3016.
168. Zhang C, Cuervo AM (2008) Restoration of chaperone-mediated autophagy in aging liver improves cellular maintenance and hepatic function. Nature medicine 14: 959-965.
169. Westerheide SD, Morimoto RI (2005) Heat shock response modulators as therapeutic tools for diseases of protein conformation. The Journal of biological chemistry 280: 33097-33100.
170. Westerheide SD, Bosman JD, Mbadugha BN, Kawahara TL, Matsumoto G, et al. (2004) Celastrols as inducers of the heat shock response and cytoprotection. The Journal of biological chemistry 279: 56053-56060.
171. Westerheide SD, Kawahara TL, Orton K, Morimoto RI (2006) Triptolide, an inhibitor of the human heat shock response that enhances stress-induced cell death. The Journal of biological chemistry 281: 9616-9622.
172. Westerheide SD, Anckar J, Stevens SM, Jr., Sistonen L, Morimoto RI (2009) Stress-inducible regulation of heat shock factor 1 by the deacetylase SIRT1. Science 323: 1063-1066.
173. Voisine C, Varma H, Walker N, Bates EA, Stockwell BR, et al. (2007) Identification of potential therapeutic drugs for huntington's disease using Caenorhabditis elegans. PLoS One 2: e504.
174. Klopfenstein DR, Vale RD (2004) The lipid binding pleckstrin homology domain in UNC-104 kinesin is necessary for synaptic vesicle transport in Caenorhabditis elegans. Mol Biol Cell 15: 3729-3739.
175. Brignull HR, Moore FE, Tang SJ, Morimoto RI (2006) Polyglutamine proteins at the pathogenic threshold display neuron-specific aggregation in a pan-neuronal Caenorhabditis elegans model. J Neurosci 26: 7597-7606.
176. Feany MB, Bender WW (2000) A Drosophila model of Parkinson's disease. Nature 404: 394-398.
177. Outeiro TF, Muchowski PJ (2004) Molecular genetics approaches in yeast to study amyloid diseases. J Mol Neurosci 23: 49-60.
178. Van Raamsdonk JM, Warby SC, Hayden MR (2007) Selective degeneration in YAC mouse models of Huntington disease. Brain Res Bull 72: 124-131.
179. Warrick JM, Paulson HL, Gray-Board GL, Bui QT, Fischbeck KH, et al. (1998) Expanded polyglutamine protein forms nuclear inclusions and causes neural degeneration in Drosophila. Cell 93: 939-949.
180. Watson MR, Lagow RD, Xu K, Zhang B, Bonini NM (2008) A Drosophila model for amyotrophic lateral sclerosis reveals motor neuron damage by human SOD1. J Biol Chem 238: 24972-24981.
181. Rayes D, Flamini M, Hernando G, Bouzat C (2007) Activation of single nicotinic receptor channels from Caenorhabditis elegans muscle. Mol Pharmacol 71: 1407-1415.
182. Zhang S, Binari R, Zhou R, Perrimon N (2010) A genomewide RNA interference screen for modifiers of aggregates formation by mutant Huntingtin in Drosophila. Genetics 184: 1165-1179.
183. Gengyo-Ando K, Kagawa H (1991) Single charge change on the helical surface of the paramyosin rod dramatically disrupts thick filament assembly in Caenorhabditis elegans. Journal of molecular biology 219: 429-441.
184. Lee SS, Lee RY, Fraser AG, Kamath RS, Ahringer J, et al. (2003) A systematic RNAi screen identifies a critical role for mitochondria in C. elegans longevity. Nat Genet 33: 40-48.
185. Rea SL, Ventura N, Johnson TE (2007) Relationship between mitochondrial electron transport chain dysfunction, development, and life extension in Caenorhabditis elegans. PLoS Biol 5: e259.
186. Hansen M, Taubert S, Crawford D, Libina N, Lee SJ, et al. (2007) Lifespan extension by conditions that inhibit translation in Caenorhabditis elegans. Aging Cell 6: 95-110.
187. Mattson MP (2008) Dietary factors, hormesis and health. Ageing Res Rev 7: 43-48.
188. Tavernarakis N (2008) Ageing and the regulation of protein synthesis: a balancing act? Trends Cell Biol 18: 228-235.
189. Sakahira H, Breuer P, Hayer-Hartl MK, Hartl FU (2002) Molecular chaperones as modulators of polyglutamine protein aggregation and toxicity. Proc Natl Acad Sci U S A 99 Suppl 4: 16412-16418.
190. Cummings CJ, Sun Y, Opal P, Antalffy B, Mestril R, et al. (2001) Over-expression of inducible HSP70 chaperone suppresses neuropathology and improves motor function in SCA1 mice. Hum Mol Genet 10: 1511-1518.
191. Freeman BC, Toft DO, Morimoto RI (1996) Molecular chaperone machines: chaperone activities of the cyclophilin Cyp-40 and the steroid aporeceptor-associated protein p23. Science 274: 1718-1720.
192. Evans CG, Wisen S, Gestwicki JE (2006) Heat shock proteins 70 and 90 inhibit early stages of amyloid beta-(1-42) aggregation in vitro. J Biol Chem 281: 33182-33191.
193. Wacker JL, Zareie MH, Fong H, Sarikaya M, Muchowski PJ (2004) Hsp70 and Hsp40 attenuate formation of spherical and annular polyglutamine oligomers by partitioning monomer. Nat Struct Mol Biol 11: 1215-1222.
194. Ballinger CA, Connell P, Wu Y, Hu Z, Thompson LJ, et al. (1999) Identification of CHIP, a novel tetratricopeptide repeat-containing protein that interacts with heat shock proteins and negatively regulates chaperone functions. Mol Cell Biol 19: 4535-4545.
195. Nollen EA, Brunsting JF, Song J, Kampinga HH, Morimoto RI (2000) Bag1 functions in vivo as a negative regulator of Hsp70 chaperone activity. Mol Cell Biol 20: 1083-1088.
196. Muchowski PJ, Ning K, D'Souza-Schorey C, Fields S (2002) Requirement of an intact microtubule cytoskeleton for aggregation and inclusion body formation by a mutant huntingtin fragment. Proc Natl Acad Sci U S A 99: 727-732.
197. Miller J, Arrasate M, Shaby BA, Mitra S, Masliah E, et al. (2010) Quantitative relationships between huntingtin levels, polyglutamine length, inclusion body formation, and neuronal death provide novel insight into huntington's disease

molecular pathogenesis. The Journal of neuroscience : the official journal of the Society for Neuroscience 30: 10541-10550.
198. Takahashi Y, Okamoto Y, Popiel HA, Fujikake N, Toda T, et al. (2007) Detection of polyglutamine protein oligomers in cells by fluorescence correlation spectroscopy. J Biol Chem 282: 24039-24048.
199. Thakur AK, Jayaraman M, Mishra R, Thakur M, Chellgren VM, et al. (2009) Polyglutamine disruption of the huntingtin exon 1 N terminus triggers a complex aggregation mechanism. Nat Struct Mol Biol 16: 380-389.
200. Hansen M, Hsu AL, Dillin A, Kenyon C (2005) New genes tied to endocrine, metabolic, and dietary regulation of lifespan from a Caenorhabditis elegans genomic RNAi screen. PLoS Genet 1: 119-128.
201. Gottschalk A, Almedom RB, Schedletzky T, Anderson SD, Yates JR, 3rd, et al. (2005) Identification and characterization of novel nicotinic receptor-associated proteins in Caenorhabditis elegans. EMBO J 24: 2566-2578.
202. Phair RD, Misteli T (2000) High mobility of proteins in the mammalian cell nucleus. Nature 404: 604-609.
203. Liu Y, LeBoeuf B, Garcia LR (2007) G alpha(q)-coupled muscarinic acetylcholine receptors enhance nicotinic acetylcholine receptor signaling in Caenorhabditis elegans mating behavior. The Journal of neuroscience : the official journal of the Society for Neuroscience 27: 1411-1421.
204. Teixeira-Castro A, Ailion M, Jalles A, Brignull HR, Vilaca JL, et al. (2011) Neuron-specific proteotoxicity of mutant ataxin-3 in C. elegans: rescue by the DAF-16 and HSF-1 pathways. Human molecular genetics 20: 2996-3009.
205. Driscoll M, Gerstbrein B (2003) Dying for a cause: invertebrate genetics takes on human neurodegeneration. Nat Rev Genet 4: 181-194.
206. Richmond JE, Jorgensen EM (1999) One GABA and two acetylcholine receptors function at the C. elegans neuromuscular junction. Nat Neurosci 2: 791-797.
207. Tsuboi D, Qadota H, Kasuya K, Amano M, Kaibuchi K (2002) Isolation of the interacting molecules with GEX-3 by a novel functional screening. Biochem Biophys Res Commun 292: 697-701.
208. Niu W, Lu ZJ, Zhong M, Sarov M, Murray JI, et al. (2011) Diverse transcription factor binding features revealed by genome-wide ChIP-seq in C. elegans. Genome research 21: 245-254.
209. Boulin T, Gielen M, Richmond JE, Williams DC, Paoletti P, et al. (2008) Eight genes are required for functional reconstitution of the Caenorhabditis elegans levamisole-sensitive acetylcholine receptor. Proc Natl Acad Sci U S A 105: 18590-18595.
210. Touroutine D, Fox RM, Von Stetina SE, Burdina A, Miller DM, 3rd, et al. (2005) acr-16 encodes an essential subunit of the levamisole-resistant nicotinic receptor at the Caenorhabditis elegans neuromuscular junction. J Biol Chem 280: 27013-27021.
211. Culetto E, Baylis HA, Richmond JE, Jones AK, Fleming JT, et al. (2004) The Caenorhabditis elegans unc-63 gene encodes a levamisole-sensitive nicotinic acetylcholine receptor alpha subunit. The Journal of biological chemistry 279: 42476-42483.
212. Bolz DD, Tenor JL, Aballay A (2010) A conserved PMK-1/p38 MAPK is required in caenorhabditis elegans tissue-specific immune response to Yersinia pestis infection. The Journal of biological chemistry 285: 10832-10840.
213. Qadota H, Inoue M, Hikita T, Koppen M, Hardin JD, et al. (2007) Establishment of a tissue-specific RNAi system in C. elegans. Gene 400: 166-173.
214. Hsu AL, Murphy CT, Kenyon C (2003) Regulation of aging and age-related disease by DAF-16 and heat-shock factor. Science 300: 1142-1145.
215. Sebastiani P, Montano M, Puca A, Solovieff N, Kojima T, et al. (2009) RNA editing genes associated with extreme old age in humans and with lifespan in C. elegans. PloS one 4: e8210.
216. Mosser DD, Theodorakis NG, Morimoto RI (1988) Coordinate changes in heat shock element-binding activity and HSP70 gene transcription rates in human cells. Molecular and cellular biology 8: 4736-4744.
217. Jorgensen EM (2005) Gaba. WormBook : the online review of C elegans biology: 1-13.
218. Rand JB (2007) Acetylcholine. WormBook: 1-21.
219. Jospin M, Qi YB, Stawicki TM, Boulin T, Schuske KR, et al. (2009) A neuronal acetylcholine receptor regulates the balance of muscle excitation and inhibition in Caenorhabditis elegans. PLoS Biol 7: e1000265.
220. Ferayorni AJ, Gunville CF, Grow WA (2004) Nicotine decreases agrin signaling and acetylcholine receptor clustering in C2C12 myotube culture. Journal of neurobiology 60: 51-60.
221. Piguet J, Schreiter C, Segura JM, Vogel H, Hovius R (2011) Acetylcholine receptor organization in membrane domains in muscle cells: evidence for rapsyn-independent and rapsyn-dependent mechanisms. The Journal of biological chemistry 286: 363-369.
222. Lackner MR, Nurrish SJ, Kaplan JM (1999) Facilitation of synaptic transmission by EGL-30 Gqalpha and EGL-8 PLCbeta: DAG binding to UNC-13 is required to stimulate acetylcholine release. Neuron 24: 335-346.
223. Steger KA, Avery L (2004) The GAR-3 muscarinic receptor cooperates with calcium signals to regulate muscle contraction in the Caenorhabditis elegans pharynx. Genetics 167: 633-643.
224. Jospin M, Jacquemond V, Mariol MC, Segalat L, Allard B (2002) The L-type voltage-dependent Ca2+ channel EGL-19 controls body wall muscle function in Caenorhabditis elegans. J Cell Biol 159: 337-348.
225. Lee RY, Lobel L, Hengartner M, Horvitz HR, Avery L (1997) Mutations in the alpha1 subunit of an L-type voltage-activated Ca2+ channel cause myotonia in Caenorhabditis elegans. The EMBO journal 16: 6066-6076.
226. Kwok TC, Ricker N, Fraser R, Chan AW, Burns A, et al. (2006) A small-molecule screen in C. elegans yields a new calcium channel antagonist. Nature 441: 91-95.
227. Adachi R, Kagawa H (2003) Genetic analysis of ryanodine receptor function in Caenorhabditis elegans based on unc-68 revertants. Mol Genet Genomics 269: 797-806.

228. Maryon EB, Saari B, Anderson P (1998) Muscle-specific functions of ryanodine receptor channels in Caenorhabditis elegans. J Cell Sci 111 (Pt 19): 2885-2895.
229. Laporte R, Hui A, Laher I (2004) Pharmacological modulation of sarcoplasmic reticulum function in smooth muscle. Pharmacol Rev 56: 439-513.
230. Robertson AP, Clark CL, Martin RJ (2010) Levamisole and ryanodine receptors. I: A contraction study in Ascaris suum. Mol Biochem Parasitol 171: 1-7.
231. Westerblad H, Andrade FH, Islam MS (1998) Effects of ryanodine receptor agonist 4-chloro-m-cresol on myoplasmic free Ca2+ concentration and force of contraction in mouse skeletal muscle. Cell calcium 24: 105-115.
232. Fruen BR, Mickelson JR, Louis CF (1997) Dantrolene inhibition of sarcoplasmic reticulum Ca2+ release by direct and specific action at skeletal muscle ryanodine receptors. The Journal of biological chemistry 272: 26965-26971.
233. Westerblad H, Allen DG, Bruton JD, Andrade FH, Lannergren J (1998) Mechanisms underlying the reduction of isometric force in skeletal muscle fatigue. Acta physiologica Scandinavica 162: 253-260.
234. Holmberg CI, Hietakangas V, Mikhailov A, Rantanen JO, Kallio M, et al. (2001) Phosphorylation of serine 230 promotes inducible transcriptional activity of heat shock factor 1. EMBO J 20: 3800-3810.
235. Holmberg CI, Roos PM, Lord JM, Eriksson JE, Sistonen L (1998) Conventional and novel PKC isoenzymes modify the heat-induced stress response but are not activated by heat shock. Journal of cell science 111 (Pt 22): 3357-3365.
236. Jorquera G, Juretic N, Jaimovich E, Riveros N (2009) Membrane depolarization induces calcium-dependent upregulation of Hsp70 and Hmox-1 in skeletal muscle cells. Am J Physiol Cell Physiol 297: C581-590.
237. Mosser DD, Kotzbauer PT, Sarge KD, Morimoto RI (1990) In vitro activation of heat shock transcription factor DNA-binding by calcium and biochemical conditions that affect protein conformation. Proceedings of the National Academy of Sciences of the United States of America 87: 3748-3752.
238. Price BD, Calderwood SK (1991) Ca2+ is essential for multistep activation of the heat shock factor in permeabilized cells. Mol Cell Biol 11: 3365-3368.
239. Whitesell L, Lindquist S (2009) Inhibiting the transcription factor HSF1 as an anticancer strategy. Expert Opin Ther Targets 13: 469-478.
240. Liu Q, Hollopeter G, Jorgensen EM (2009) Graded synaptic transmission at the Caenorhabditis elegans neuromuscular junction. Proceedings of the National Academy of Sciences of the United States of America 106: 10823-10828.
241. Glabe CG (2006) Common mechanisms of amyloid oligomer pathogenesis in degenerative disease. Neurobiology of aging 27: 570-575.
242. Rattan SI (2008) Principles and practice of hormetic treatment of aging and age-related diseases. Human & experimental toxicology 27: 151-154.
243. Park HG, Han SI, Oh SY, Kang HS (2005) Cellular responses to mild heat stress. Cellular and molecular life sciences : CMLS 62: 10-23.
244. Shen X, Ellis RE, Sakaki K, Kaufman RJ (2005) Genetic interactions due to constitutive and inducible gene regulation mediated by the unfolded protein response in C. elegans. PLoS genetics 1: e37.
245. Liu Y, Chang A (2008) Heat shock response relieves ER stress. The EMBO journal 27: 1049-1059.
246. Leber JH, Bernales S, Walter P (2004) IRE1-independent gain control of the unfolded protein response. PLoS biology 2: E235.
247. Taldone T, Gozman A, Maharaj R, Chiosis G (2008) Targeting Hsp90: small-molecule inhibitors and their clinical development. Current opinion in pharmacology 8: 370-374.
248. Luo W, Sun W, Taldone T, Rodina A, Chiosis G (2010) Heat shock protein 90 in neurodegenerative diseases. Molecular neurodegeneration 5: 24.
249. Biamonte MA, Van de Water R, Arndt JW, Scannevin RH, Perret D, et al. (2010) Heat shock protein 90: inhibitors in clinical trials. Journal of medicinal chemistry 53: 3-17.
250. Riedel M, Goldbaum O, Schwarz L, Schmitt S, Richter-Landsberg C (2010) 17-AAG induces cytoplasmic alpha-synuclein aggregate clearance by induction of autophagy. PloS one 5: e8753.
251. Stefani M, Dobson CM (2003) Protein aggregation and aggregate toxicity: new insights into protein folding, misfolding diseases and biological evolution. J Mol Med 81: 678-699.
252. Esler WP, Stimson ER, Jennings JM, Vinters HV, Ghilardi JR, et al. (2000) Alzheimer's disease amyloid propagation by a template-dependent dock-lock mechanism. Biochemistry 39: 6288-6295.
253. Esler WP, Felix AM, Stimson ER, Lachenmann MJ, Ghilardi JR, et al. (2000) Activation barriers to structural transition determine deposition rates of Alzheimer's disease a beta amyloid. J Struct Biol 130: 174-183.
254. Tseng BP, Esler WP, Clish CB, Stimson ER, Ghilardi JR, et al. (1999) Deposition of monomeric, not oligomeric, Abeta mediates growth of Alzheimer's disease amyloid plaques in human brain preparations. Biochemistry 38: 10424-10431.
255. Inouye H, Kirschner DA (2000) A beta fibrillogenesis: kinetic parameters for fibril formation from congo red binding. J Struct Biol 130: 123-129.
256. Lomakin A, Teplow DB, Kirschner DA, Benedek GB (1997) Kinetic theory of fibrillogenesis of amyloid beta-protein. Proc Natl Acad Sci U S A 94: 7942-7947.
257. Chen S, Ferrone FA, Wetzel R (2002) Huntington's disease age-of-onset linked to polyglutamine aggregation nucleation. Proc Natl Acad Sci U S A 99: 11884-11889.
258. Wang X, Vitalis A, Wyczalkowski MA, Pappu RV (2006) Characterizing the conformational ensemble of monomeric polyglutamine. Proteins 63: 297-311.
259. Lee CC, Walters RH, Murphy RM (2007) Reconsidering the mechanism of polyglutamine peptide aggregation. Biochemistry 46: 12810-12820.

260. Murphy RM (2002) Peptide aggregation in neurodegenerative disease. Annu Rev Biomed Eng 4: 155-174.
261. Bhattacharyya AM, Thakur AK, Wetzel R (2005) polyglutamine aggregation nucleation: thermodynamics of a highly unfavorable protein folding reaction. Proc Natl Acad Sci U S A 102: 15400-15405.
262. Jarrett JT, Berger EP, Lansbury PT, Jr. (1993) The C-terminus of the beta protein is critical in amyloidogenesis. Ann N Y Acad Sci 695: 144-148.
263. Scherzinger E, Sittler A, Schweiger K, Heiser V, Lurz R, et al. (1999) Self-assembly of polyglutamine-containing huntingtin fragments into amyloid-like fibrils: implications for Huntington's disease pathology. Proc Natl Acad Sci U S A 96: 4604-4609.
264. Snyder SW, Ladror US, Wade WS, Wang GT, Barrett LW, et al. (1994) Amyloid-beta aggregation: selective inhibition of aggregation in mixtures of amyloid with different chain lengths. Biophys J 67: 1216-1228.
265. Tomski SJ, Murphy RM (1992) Kinetics of aggregation of synthetic beta-amyloid peptide. Arch Biochem Biophys 294: 630-638.
266. Kim S, Nollen EA, Kitagawa K, Bindokas VP, Morimoto RI (2002) Polyglutamine protein aggregates are dynamic. Nat Cell Biol 4: 826-831.
267. Lotz GP, Legleiter J, Aron R, Mitchell EJ, Huang SY, et al. (2010) Hsp70 and Hsp40 functionally interact with soluble mutant huntingtin oligomers in a classic ATP-dependent reaction cycle. J Biol Chem 285: 38183-38193.
268. Matsumoto G, Kim S, Morimoto RI (2006) Huntingtin and mutant SOD1 form aggregate structures with distinct molecular properties in human cells. J Biol Chem 281: 4477-4485.
269. Matsumoto G, Stojanovic A, Holmberg CI, Kim S, Morimoto RI (2005) Structural properties and neuronal toxicity of amyotrophic lateral sclerosis-associated Cu/Zn superoxide dismutase 1 aggregates. J Cell Biol 171: 75-85.
270. Magde D, Elson EL, Webb WW (1974) Fluorescence correlation spectroscopy. II. An experimental realization. Biopolymers 13: 29-61.
271. Magde D, Webb WW, Elson E (1972) Thermodynamic Fluctuations in a Reacting System - Measurement by Fluorescence Correlation Spectroscopy. Physical Review Letters 29: 705-&.
272. Elson EL (2004) Quick tour of fluorescence correlation spectroscopy from its inception. J Biomed Opt 9: 857-864.
273. Haustein E, Schwille P (2004) Single-molecule spectroscopic methods. Curr Opin Struct Biol 14: 531-540.
274. Haustein E, Schwille P (2003) Ultrasensitive investigations of biological systems by fluorescence correlation spectroscopy. Methods 29: 153-166.
275. Eigen M, Rigler R (1994) Sorting single molecules: application to diagnostics and evolutionary biotechnology. Proc Natl Acad Sci U S A 91: 5740-5747.
276. Boukari H, Nossal R, Sackett DL (2003) Stability of drug-induced tubulin rings by fluorescence correlation spectroscopy. Biochemistry 42: 1292-1300.
277. Haupts U, Maiti S, Schwille P, Webb WW (1998) Dynamics of fluorescence fluctuations in green fluorescent protein observed by fluorescence correlation spectroscopy. Proc Natl Acad Sci U S A 95: 13573-13578.
278. Kohl T, Schwille P (2005) Fluorescence correlation spectroscopy with autofluorescent proteins. Adv Biochem Eng Biotechnol 95: 107-142.
279. Wachsmuth M, Waldeck W, Langowski J (2000) Anomalous diffusion of fluorescent probes inside living cell nuclei investigated by spatially-resolved fluorescence correlation spectroscopy. J Mol Biol 298: 677-689.
280. Wang Z, Shah JV, Berns MW, Cleveland DW (2006) In vivo quantitative studies of dynamic intracellular processes using fluorescence correlation spectroscopy. Biophys J 91: 343-351.
281. Gerard M, Debyser Z, Desender L, Kahle PJ, Baert J, et al. (2006) The aggregation of alpha-synuclein is stimulated by FK506 binding proteins as shown by fluorescence correlation spectroscopy. Faseb J 20: 524-526.
282. Tjernberg LO, Pramanik A, Bjorling S, Thyberg P, Thyberg J, et al. (1999) Amyloid beta-peptide polymerization studied using fluorescence correlation spectroscopy. Chem Biol 6: 53-62.
283. Ashrafi K, Chang FY, Watts JL, Fraser AG, Kamath RS, et al. (2003) Genome-wide RNAi analysis of Caenorhabditis elegans fat regulatory genes. Nature 421: 268-272.
284. Laurence TA, Kwon Y, Yin E, Hollars CW, Camarero JA, et al. (2007) Correlation spectroscopy of minor fluorescent species: signal purification and distribution analysis. Biophys J 92: 2184-2198.
285. Puchalla J, Krantz K, Austin R, Rye H (2008) Burst analysis spectroscopy: a versatile single-particle approach for studying distributions of protein aggregates and fluorescent assemblies. Proc Natl Acad Sci U S A 105: 14400-14405.
286. Chen S, Berthelier V, Hamilton JB, O'Nuallain B, Wetzel R (2002) Amyloid-like features of polyglutamine aggregates and their assembly kinetics. Biochemistry 41: 7391-7399.
287. Smith AM, Jahn TR, Ashcroft AE, Radford SE (2006) Direct observation of oligomeric species formed in the early stages of amyloid fibril formation using electrospray ionisation mass spectrometry. J Mol Biol 364: 9-19.
288. Herrera F, Tenreiro S, Miller-Fleming L, Outeiro TF (2011) Visualization of cell-to-cell transmission of mutant huntingtin oligomers. PLoS Curr 3: RRN1210.
289. Outeiro TF, Putcha P, Tetzlaff JE, Spoelgen R, Koker M, et al. (2008) Formation of toxic oligomeric alpha-synuclein species in living cells. PLoS ONE 3: e1867.
290. Ramdzan YM, Nisbet RM, Miller J, Finkbeiner S, Hill AF, et al. (2010) Conformation sensors that distinguish monomeric proteins from oligomers in live cells. Chem Biol 17: 371-379.
291. Naidoo N (2009) The endoplasmic reticulum stress response and aging. Reviews in the neurosciences 20: 23-37.
292. Zhang K, Kaufman RJ (2006) Protein folding in the endoplasmic reticulum and the unfolded protein response. Handbook of experimental pharmacology: 69-91.

293. Yoshida H, Haze K, Yanagi H, Yura T, Mori K (1998) Identification of the cis-acting endoplasmic reticulum stress response element responsible for transcriptional induction of mammalian glucose-regulated proteins. Involvement of basic leucine zipper transcription factors. The Journal of biological chemistry 273: 33741-33749.
294. Yoshida H, Matsui T, Yamamoto A, Okada T, Mori K (2001) XBP1 mRNA is induced by ATF6 and spliced by IRE1 in response to ER stress to produce a highly active transcription factor. Cell 107: 881-891.
295. Yoshida Y (2003) A novel role for N-glycans in the ERAD system. Journal of biochemistry 134: 183-190.
296. Henis-Korenblit S, Zhang P, Hansen M, McCormick M, Lee SJ, et al. (2010) Insulin/IGF-1 signaling mutants reprogram ER stress response regulators to promote longevity. Proceedings of the National Academy of Sciences of the United States of America 107: 9730-9735.
297. Zhang K, Shen X, Wu J, Sakaki K, Saunders T, et al. (2006) Endoplasmic reticulum stress activates cleavage of CREBH to induce a systemic inflammatory response. Cell 124: 587-599.
298. Chin KT, Zhou HJ, Wong CM, Lee JM, Chan CP, et al. (2005) The liver-enriched transcription factor CREB-H is a growth suppressor protein underexpressed in hepatocellular carcinoma. Nucleic acids research 33: 1859-1873.
299. Bailey D, Barreca C, O'Hare P (2007) Trafficking of the bZIP transmembrane transcription factor CREB-H into alternate pathways of ERAD and stress-regulated intramembrane proteolysis. Traffic 8: 1796-1814.
300. Danno H, Ishii KA, Nakagawa Y, Mikami M, Yamamoto T, et al. (2010) The liver-enriched transcription factor CREBH is nutritionally regulated and activated by fatty acids and PPARalpha. Biochemical and biophysical research communications 391: 1222-1227.
301. Viswanathan M, Kim SK, Berdichevsky A, Guarente L (2005) A role for SIR-2.1 regulation of ER stress response genes in determining C. elegans life span. Developmental cell 9: 605-615.
302. Haynes CM, Ron D (2010) The mitochondrial UPR - protecting organelle protein homeostasis. Journal of cell science 123: 3849-3855.
303. Lichtlen P, Schaffner W (2001) Putting its fingers on stressful situations: the heavy metal-regulatory transcription factor MTF-1. BioEssays : news and reviews in molecular, cellular and developmental biology 23: 1010-1017.
304. Vargas MR, Johnson JA (2009) The Nrf2-ARE cytoprotective pathway in astrocytes. Expert reviews in molecular medicine 11: e17.
305. Young JC, Agashe VR, Siegers K, Hartl FU (2004) Pathways of chaperone-mediated protein folding in the cytosol. Nature reviews Molecular cell biology 5: 781-791.
306. Fujikake N, Nagai Y, Popiel HA, Okamoto Y, Yamaguchi M, et al. (2008) Heat shock transcription factor 1-activating compounds suppress polyglutamine-induced neurodegeneration through induction of multiple molecular chaperones. The Journal of biological chemistry 283: 26188-26197.
307. Fujimoto M, Takaki E, Hayashi T, Kitaura Y, Tanaka Y, et al. (2005) Active HSF1 significantly suppresses polyglutamine aggregate formation in cellular and mouse models. J Biol Chem 280: 34908-34916.
308. Muchowski PJ, Wacker JL (2005) Modulation of neurodegeneration by molecular chaperones. Nat Rev Neurosci 6: 11-22.
309. Neef DW, Turski ML, Thiele DJ (2010) Modulation of heat shock transcription factor 1 as a therapeutic target for small molecule intervention in neurodegenerative disease. PLoS biology 8: e1000291.
310. Sittler A, Lurz R, Lueder G, Priller J, Lehrach H, et al. (2001) Geldanamycin activates a heat shock response and inhibits huntingtin aggregation in a cell culture model of Huntington's disease. Hum Mol Genet 10: 1307-1315.
311. Vacher C, Garcia-Oroz L, Rubinsztein DC (2005) Overexpression of yeast hsp104 reduces polyglutamine aggregation and prolongs survival of a transgenic mouse model of Huntington's disease. Human molecular genetics 14: 3425-3433.
312. Waza M, Adachi H, Katsuno M, Minamiyama M, Sang C, et al. (2005) 17-AAG, an Hsp90 inhibitor, ameliorates polyglutamine-mediated motor neuron degeneration. Nature medicine 11: 1088-1095.
313. Zhang YQ, Sarge KD (2007) Celastrol inhibits polyglutamine aggregation and toxicity though induction of the heat shock response. Journal of molecular medicine 85: 1421-1428.
314. Solit DB, Osman I, Polsky D, Panageas KS, Daud A, et al. (2008) Phase II trial of 17-allylamino-17-demethoxygeldanamycin in patients with metastatic melanoma. Clinical cancer research : an official journal of the American Association for Cancer Research 14: 8302-8307.
315. Williams GT, Morimoto RI (1990) Maximal stress-induced transcription from the human HSP70 promoter requires interactions with the basal promoter elements independent of rotational alignment. Molecular and cellular biology 10: 3125-3136.
316. Amici C, Sistonen L, Santoro MG, Morimoto RI (1992) Antiproliferative prostaglandins activate heat shock transcription factor. Proceedings of the National Academy of Sciences of the United States of America 89: 6227-6231.
317. Trott A, West JD, Klaic L, Westerheide SD, Silverman RB, et al. (2008) Activation of heat shock and antioxidant responses by the natural product celastrol: transcriptional signatures of a thiol-targeted molecule. Molecular biology of the cell 19: 1104-1112.
318. Li C, Hossieny P, Wu BJ, Qawasmeh A, Beck K, et al. (2007) Pharmacologic induction of heme oxygenase-1. Antioxidants & redox signaling 9: 2227-2239.
319. Wyttenbach A, Swartz J, Kita H, Thykjaer T, Carmichael J, et al. (2001) Polyglutamine expansions cause decreased CRE-mediated transcription and early gene expression changes prior to cell death in an inducible cell model of Huntington's disease. Human molecular genetics 10: 1829-1845.
320. Riordan JR (2008) CFTR function and prospects for therapy. Annual review of biochemistry 77: 701-726.
321. Stringer JR, Bowman MD, Weisblum B, Blackwell HE (2011) Improved small-molecule macroarray platform for the rapid synthesis and discovery of antibacterial chalcones. ACS combinatorial science 13: 175-180.

322. Yadav VR, Prasad S, Sung B, Aggarwal BB (2011) The role of chalcones in suppression of NF-kappaB-mediated inflammation and cancer. International immunopharmacology 11: 295-309.
323. Dinkova-Kostova AT, Holtzclaw WD, Cole RN, Itoh K, Wakabayashi N, et al. (2002) Direct evidence that sulfhydryl groups of Keap1 are the sensors regulating induction of phase 2 enzymes that protect against carcinogens and oxidants. Proceedings of the National Academy of Sciences of the United States of America 99: 11908-11913.
324. Dinkova-Kostova AT, Massiah MA, Bozak RE, Hicks RJ, Talalay P (2001) Potency of Michael reaction acceptors as inducers of enzymes that protect against carcinogenesis depends on their reactivity with sulfhydryl groups. Proceedings of the National Academy of Sciences of the United States of America 98: 3404-3409.
325. Tangallapally RP, Yendapally R, Lee RE, Hevener K, Jones VC, et al. (2004) Synthesis and evaluation of nitrofuranylamides as novel antituberculosis agents. Journal of medicinal chemistry 47: 5276-5283.
326. Roesslein M, Schibilsky D, Muller L, Goebel U, Schwer C, et al. (2008) Thiopental protects human T lymphocytes from apoptosis in vitro via the expression of heat shock protein 70. The Journal of pharmacology and experimental therapeutics 325: 217-225.
327. Yang H, Shelat AA, Guy RK, Gopinath VS, Ma T, et al. (2003) Nanomolar affinity small molecule correctors of defective Delta F508-CFTR chloride channel gating. The Journal of biological chemistry 278: 35079-35085.
328. Yang F, Lim GP, Begum AN, Ubeda OJ, Simmons MR, et al. (2005) Curcumin inhibits formation of amyloid beta oligomers and fibrils, binds plaques, and reduces amyloid in vivo. The Journal of biological chemistry 280: 5892-5901.
329. Teiten MH, Reuter S, Schmucker S, Dicato M, Diederich M (2009) Induction of heat shock response by curcumin in human leukemia cells. Cancer letters 279: 145-154.
330. Gorbatyuk MS, Knox T, LaVail MM, Gorbatyuk OS, Noorwez SM, et al. (2010) Restoration of visual function in P23H rhodopsin transgenic rats by gene delivery of BiP/Grp78. Proceedings of the National Academy of Sciences of the United States of America 107: 5961-5966.
331. Mu TW, Ong DS, Wang YJ, Balch WE, Yates JR, 3rd, et al. (2008) Chemical and biological approaches synergize to ameliorate protein-folding diseases. Cell 134: 769-781.
332. Parenti G (2009) Treating lysosomal storage diseases with pharmacological chaperones: from concept to clinics. EMBO molecular medicine 1: 268-279.
333. Tam LC, Kiang AS, Campbell M, Keaney J, Farrar GJ, et al. (2010) Prevention of autosomal dominant retinitis pigmentosa by systemic drug therapy targeting heat shock protein 90 (Hsp90). Human molecular genetics 19: 4421-4436.
334. Szegezdi E, Logue SE, Gorman AM, Samali A (2006) Mediators of endoplasmic reticulum stress-induced apoptosis. EMBO reports 7: 880-885.